

## Thermonuclear processes in Stars

This book is the added and revised publication of the previous author's book "Thermonuclear processes of the Universe", New-York, NOVA Sci. Publ., 2012, 194p. The first chapter contains the review of thermonuclear processes in the Sun and stars. The second is devoted to the description of the using model and basic calculation methods of some characteristics for bound states and continuum of nuclear particles. In the rest 13th chapters, the radiative capture processes for the  $p^2H$ ,  $p^3H$ ,  $p^6Li$ ,  $p^7Li$ ,  $p^9Be$ ,  $p^{10}B$ ,  $p^{11}B$ ,  $p^{12}C$ ,  $p^{13}C$ ,  $p^{14}C$ ,  $p^{15}N$ , and also  $2H^4He$ ,  $3H^4He$ ,  $3He^4He$ ,  $4He^{12}C$  systems were considered at astrophysical energies. It was shown that using approach allows one to describe available experimental data comparatively well in this energy range. Besides, it was shown that in some cases, for certain nuclear systems, it was possible to predict the behavior of the S-factor at energies lower than 100–200 keV, because these calculations were published in 1995, and new experimental data were appeared only in 1997–2002 years.



S. Dubovichenko - Academician EANS (EU), academician PAAS (RF), academician RANH (RF), academician IIA (RK), doctor of Phys. and Math. Sci. (RK & RF), professor, member of the American Physical Society, member of the European Physical Society, laboratory head "Nuclear astrophysics" at Fessenkov Astrophysical Institute in Almaty, "NCSRT" ASC MID, RK



978-3-639-76478-9

Thermonuclear processes in Stars

Dubovichenko

**Scholars'  
Press**

Sergey Dubovichenko

## Thermonuclear processes in Stars and Universe

**Sergey Dubovichenko**

**Thermonuclear processes in Stars**



**Sergey Dubovichenko**

**Thermonuclear processes in Stars  
and Universe**

**Scholar's Press**

## **Impressum / Imprint**

Bibliografische Information der Deutschen Nationalbibliothek: Die Deutsche Nationalbibliothek verzeichnet diese Publikation in der Deutschen Nationalbibliografie; detaillierte bibliografische Daten sind im Internet über <http://dnb.d-nb.de> abrufbar.

Alle in diesem Buch genannten Marken und Produktnamen unterliegen warenzeichen-, marken- oder patentrechtlichem Schutz bzw. sind Warenzeichen oder eingetragene Warenzeichen der jeweiligen Inhaber. Die Wiedergabe von Marken, Produktnamen, Gebrauchsnamen, Handelsnamen, Warenbezeichnungen u.s.w. in diesem Werk berechtigt auch ohne besondere Kennzeichnung nicht zu der Annahme, dass solche Namen im Sinne der Warenzeichen- und Markenschutzgesetzgebung als frei zu betrachten wären und daher von jedermann benutzt werden dürften.

Bibliographic information published by the Deutsche Nationalbibliothek: The Deutsche Nationalbibliothek lists this publication in the Deutsche Nationalbibliografie; detailed bibliographic data are available in the Internet at <http://dnb.d-nb.de>.

Any brand names and product names mentioned in this book are subject to trademark, brand or patent protection and are trademarks or registered trademarks of their respective holders. The use of brand names, product names, common names, trade names, product descriptions etc. even without a particular marking in this work is in no way to be construed to mean that such names may be regarded as unrestricted in respect of trademark and brand protection legislation and could thus be used by anyone.

Coverbild / Cover image: [www.ingimage.com](http://www.ingimage.com)

Verlag / Publisher:

Scholar's Press

ist ein Imprint der / is a trademark of

OmniScriptum GmbH & Co. KG

Heinrich-Böcking-Str. 6-8, 66121 Saarbrücken, Deutschland / Germany

Email: [info@scholars-press.com](mailto:info@scholars-press.com)

Herstellung: siehe letzte Seite /

Printed at: see last page

**ISBN: 978-3-639-76478-9**

Copyright © 2015 OmniScriptum GmbH & Co. KG

Alle Rechte vorbehalten. / All rights reserved. Saarbrücken 2015

# **TABLE OF CONTENTS**

---

<b>FOREWORD</b>	<b>7</b>
<b>FOREWORD - Author</b>	<b>9</b>
<b>ACKNOWLEDGMENTS</b>	<b>11</b>
<b>SHORT CONTENTS</b>	<b>13</b>
 <b>INTRODUCTION</b>	 <b>19</b>
 <b>1. THERMONUCLEAR PROCESSES</b>	 <b>25</b>
<b>INTRODUCTION</b>	<b>25</b>
1.1 Thermonuclear reactions in the stars	26
1.2 Proton-proton chain	29
1.3 The stellar CNO cycle	33
1.4 Triple alpha process	36
1.5 Another thermonuclear processes in the stars	37
1.6 The dependence of thermonuclear reactions from the star mass	39
1.7 Advances and problems of nuclear astrophysics	42
 <b>2. MODEL AND CALCULATION METHODS</b>	 <b>47</b>
Introduction	47
2.1 Cluster model	50
2.2 Astrophysical S-factors	54
2.3 Potentials and wave functions	57
2.4 Numerical mathematical methods	60
2.5 Classification of cluster states	61
2.6 Methods of phase shift analysis	63
2.7 Generalized matrix eigenvalue problem	64
2.8 Construction of the intercluster potentials	68



<b>3. ASTROPHYSICAL S-FACTOR OF THE PROTON RADIATIVE CAPTURE ON <math>^2\text{H}</math></b>	<b>71</b>
Introduction	71
3.1 Scattering potentials and phase shifts	72
3.2 Astrophysical S-factor	78
Conclusion	83
 <b>4. PROTON RADIATIVE CAPTURE PROCESS ON <math>^3\text{H}</math></b>	 <b>85</b>
Introduction	85
4.1 Scattering potentials and phase shifts	86
4.2 Astrophysical S-factor	92
4.3 Calculation of the astrophysical S-factor	94
Conclusion	119
 <b>5. PROTON RADIATIVE CAPTURE ON <math>^6\text{Li}</math> PROCESS</b>	 <b>121</b>
Introduction	121
5.1. Differential cross sections	122
5.2. Phase shift analysis	123
5.3. Cluster states classification	126
5.4. Potential description of the scattering phase shifts	128
5.5. Astrophysical S-factor	133
Conclusion	135
 <b>6. S-FACTOR OF THE PROTON RADIATIVE CAPTURE ON <math>^7\text{Li}</math></b>	 <b>137</b>
Introduction	137
6.1. Classification of the orbital states	138
6.2. Potential description of the phase shifts of scattering	140
6.3. Astrophysical S-factor	145
Conclusion	148

<b>7. RADIATIVE CAPTURE</b>	
<b>IN THE <math>p^9\text{Be}</math> SYSTEM</b>	<b>149</b>
Introduction	149
7.1 Classification of the orbital states	149
7.2 Potential description of scattering phase shifts	150
7.3 Astrophysical S-factor	156
Conclusion	157
<b>8. PROTON RADIATIVE</b>	
<b>CAPTURE ON <math>^{10}\text{B}</math></b>	<b>159</b>
Introduction	159
8.1 Classification of the cluster states and the level structure of the $p^{10}\text{B}$ system	159
8.2 Construction of the $p^{10}\text{B}$ interaction potentials	162
8.3 Total cross sections of the radiative proton capture on $^{10}\text{B}$	164
Conclusion	167
<b>9. RADIATIVE PROTON</b>	
<b>CAPTURE ON <math>^{11}\text{B}</math></b>	<b>169</b>
Introduction	169
9.1 Structure of cluster states	170
9.2 Interaction potentials	173
9.3 Total cross sections	177
Conclusion	180
<b>10. RADIATIVE PROTON</b>	
<b>CAPTURE ON <math>^{12}\text{C}</math></b>	<b>181</b>
Introduction	181
10.1. Differential cross sections	181
10.2. Control of the computer program	184
10.3. Phase shift analysis of $p^{12}\text{C}$ elastic scattering	186



10.4. Astrophysical S-factor	189
Conclusion	195

## **11. S-FACTORS OF THE PROTON**

### **CAPTURE ON $^{13}\text{C}$**

Introduction	197
11.1 Phase shift analysis and intercluster potentials	197
11.2 Astrophysical S-factor	202
Conclusion	205

## **12. RADIATIVE PROTON**

### **CAPTURE ON $^{14}\text{C}$**

Introduction	207
12.1 Classification of Young tableaux and structure of cluster states	208
12.2 Phase shift analysis of the $p^{14}\text{C}$ elastic scattering	210
12.3 Interaction potentials and total capture cross sections	212
Conclusion	216

## **13. RADIATIVE PROTON**

### **CAPTURE ON $^{15}\text{N}$**

Introduction	217
13.1 Interaction potentials and structure of states	217
13.2 The total proton capture cross sections on $^{15}\text{N}$	222
Conclusion	224

## **14. ASTROPHYSICAL S-FACTORS OF THE RADIATIVE CAPTURE IN THE $^3\text{He}^4\text{He}$ , $^3\text{H}^4\text{He}$ AND $^2\text{H}^4\text{He}$ SYSTEMS**

Introduction	225
14.1 Potentials and scattering phase shifts	226

14.2 New variants of potentials	229
14.3 Results of variational calculations	233
14.4. Astrophysical S-factor	237
14.5. Variation two-body program	241
Conclusion	259
 <b>15. THE <math>^{12}\text{C}(^4\text{He},\gamma)^{16}\text{O}</math> RADIATIVE CAPTURE REACTION</b>	 <b>261</b>
Introduction	261
15.1 Differential cross sections	262
15.2 Phase shift analysis	262
15.3 Description of the scattering phase shifts in the potential model	267
15.4 Astrophysical S-factor	271
Conclusion	274
 <b>CONCLUSION</b>	 <b>275</b>
 <b>APPENDIX 1</b>	 <b>279</b>
<b>APPENDIX 2</b>	<b>291</b>
 <b>REFERENCES</b>	 <b>301</b>

**Sergey B. Dubovichenko**

# ***THERMONUCLEAR PROCESSES IN STARS***

*The second English, enlarged and revised, edition of the book  
"Thermonuclear processes of the Universe," published in New-  
York. NOVA Sci. Publ. 2012. 194p.*

## ***Reviewers***

Professor **Bagrov V.G.** (TSU, Tomsk, Russia),  
professor **Blokhintsev L.D.** (MSU, Moscow, Russia),  
professor **Duisebaev A.D.** (INP, Almaty, Kazakhstan),  
professor **Ishkhanov B.S.** (MSU, Moscow, Russia),  
professor **Strakovsky I.I.** (GWU, Washington, USA)

## ***Editor of English edition***

Asis. prof., PhD **Dzhazairov-Kakhramanov A.V.**  
(Astrophysical Institute, Almaty, Kazakhstan, [albert-i@yandex.kz](mailto:albert-i@yandex.kz))

# FOREWORD

---

This monograph is a fundamental work covering a wide range of questions concerning the structure of nuclei and mechanisms of nuclear reactions, and also use of nuclear methods for the analysis of astrophysical processes in stars. Description is based on numerous original works of the author, published in the prestigious scientific journals. The wide set of nuclear systems is considered in the book, which contain from three ( $p + {}^2\text{H}$ ) to sixteen ( ${}^2\text{He} + {}^{12}\text{C}$ ) nucleons.

Uniqueness of the stated in the book material consists of the fact that theoretical description of all these various systems is based on the unified approach, which can be called the two-body potential cluster model with classification of states according to young tableaux. In spite of the relative simplicity (at the side of other known methods), this approach allows to the author obtain the good description either states of the discrete spectrum (bound states) or states of the continuous spectrum (scattering states) of the considered systems.

Actuality of the book material, to a considerable extent, is determined by the application of the developed approach to the nuclear astrophysics problems that is currently one of the most thriving fields of science. For every considered two-cluster system  $b+c$  the author calculates the astrophysical  $S$ -factor of the radiative capture  $b(c,\gamma)a$ , where  $a$  – bound state of  $b$  and  $c$ . The astrophysical  $S$ -factor is proportional to the cross section of this process and determines the speed of its flowing in the initial regions of stars (including our Sun).

Meanwhile, it should mark out the agreement of theoretical results of the author with the experimental values of the astrophysical  $S$ -factors, measured under laboratory conditions at the experimenter available energies. The problem is that in spite of the progress in the technical equipment of the experiment the direct measurement of their cross sections and astrophysical  $S$ -factors at stellar energies is impossible up to now due to the smallness of the cross sections caused by the Coulomb repulsion for the majority of astrophysical nuclear reaction flowing in stars and determining the prevalence of elements and isotopes of the Universe.

Therefore, there are two possible ways for obtaining the information about the rate of similar reactions in stars:

- 1) Extrapolation of the values of astrophysical  $S$ -factors, measured at higher energies, in the range of astrophysical energies (about units or tens of keV).
- 2) Calculation of the  $S$ -factors at necessary energy range in the frame of some theoretical models.

More reasonable and perspective, at the present time, the second way is seemed, which was chosen by the author.

Reached agreement with the experimental results at higher energies, which is obligatory condition of adequacy of the using approach, allows one to hope for reliability of the obtained results at the interesting for astrophysicists low (stellar) energies. On a number of occasions (for example for systems  $p + {}^2\text{H}$  and  $p + {}^3\text{H}$ ) the calculation results of the author with the good accuracy coincide with the data of the experiment that were appeared much later than these calculations.

The presented book profitably differs from other monographs in the field of nuclear physics and nuclear astrophysics by the wide combination of different types of materials. The physical approaches and obtained on their basis results, also the mathematical and numerical calculation methods and even computer programs are stated in detail in this book.

Obvious advantage of the book is in the availability of the Introduction and Chapter 1, where the fundamentals of physics of thermonuclear processes in the stars (nuclear star cycles, stellar evolution etc) are stated in a condensed form.

The book will be useful undoubtedly for advanced students, postgraduate students (PhD doctoral candidates) and researchers specializing in the field of atomic nuclear physics and nuclear astrophysics.

*Doctor of physical and mathematical sciences,  
Professor and general researcher of the  
Moscow State University **Blokhintsev L.D.***

# FOREWORD

AUTHOR

---

*Nuclear astrophysics is one of the youngest branches of the modern astrophysics, which practically represents the sphere of application of the results obtained in experimental and theoretical physics to the astronomical objects with a view to explain their nature, energy sources, age and chemical composition peculiarities [1].*

Owing to the modern development of astronomy and astrophysics we have a general understanding of the Universe – of its evolution and structure within the distances of the order of 14 billion light years. The observations of the Universe reveal the areas of very compact matter concentration and extremely large distances between them which seem to be “empty”. However, all this “empty” space is filled with gas and dust matter, atoms and various kinds of radiation including neutrino. Furthermore, the modern theories about the Universe involve such concepts as dark matter and dark energy, which determine its mass and characterize its mode of expansion.

The matter which concentrates in the stars and planets of the visible Universe and which forms the gas and dust clouds consists of nuclides, i.e. the atoms of ninety two chemical elements having different numbers of protons and neutrons in their nuclei and ranging from hydrogen to uranium. All the diversity of nuclear composition of the Universe is made up of several hundreds of nuclides and the current level of science – nuclear astrophysics – allows explaining in general the history of their formation and their relative occurrence.

The world around us also consists of various chemical elements and, presently, it is generally recognized that all the elements forming the Earth, the Sun and the whole solar system were produced in the course of the stellar evolution. Our Earth is one of the eight planets of the solar system and our Sun is a common stable star of our galaxy – the Milky Way.

According to the current estimates the Milky Way only comprises several hundred billion stars and even at present time, i.e. 14 billion years after the formation of the visible Universe, which may contain hundred billions of similar galaxies, new stars can be born [1,2].

In this book some methods of analysis certain thermonuclear reactions that flowing in the Sun and stars will be considered: pp-chain, CNO cycle and triple alpha process. Such analysis is based on the modified potential cluster model [3] of light nuclei, which take into account methods of classification of cluster state according to Young tableaux. More particularly the considered here reactions are given in the next chapter, which is titled “Short contents”.



# **ACKNOWLEDGMENTS**

---

The author would like to express a profound gratitude to Prof. Neudatchin V.G. (Institute of Nuclear Physics, Moscow State University, Moscow, Russia), Prof. Igor Strakovsky (G. Washington University, Washington, USA), Prof. Bagrov V.G. (Tomsk State University, Tomsk, Russia), Dr. Uzikov Yu.N. (JIRN, Dubna, Russia), Academician of the National Academy of Sciences of the Republic of Kazakhstan Boos E.G. (Applied-physics Institute, Almaty, Kazakhstan), Prof. Duisebaev A.D. and Prof. Burtebaev N.T. (Institute of nuclear physics of the National Nuclear Centre of the Republic of Kazakhstan, Almaty), Prof. Danaev N.T., Prof. Shmygaleva T.A. (Al-Farabi Kazakh National University, Almaty, Kazakhstan) for the very important discussions of some questions which were considered in the book.

In addition, I would like to express my particular gratefulness to Prof. Ishkhanov B.S. (Institute of Nuclear Physics, Moscow State University, Moscow, Russia) for the possibility to use in the Internet his lectures on thermonuclear physics for students of the Moscow State University and his book “Nucleosynthesis in the Universe”. A part of these materials was used in the Foreword, Introduction and First Chapter of this book.

The author also grateful to Dzhazairov-Kakhramanov A.V. (Fessenkov’s Astrophysical Institute, Almaty, Kazakhstan) and Zazulin D.M. (Al-Farabi Kazakh National University, Almaty, Kazakhstan) for searching and for selecting of the certain part of the experimental material. In addition, the author expresses great thanks to Dzhazairov-Kakhramanov A.V. for reviewing of the second English edition of this book.

I want to mention a special contribution made by science editors Corresponding member of the NAS RK Chechin L.M. (Fessenkov’s Astrophysical Institute, Almaty, Kazakhstan), and Prof. Burkova N.A. (Al Farabi Kazakh National University, Almaty, Kazakhstan) who wrote a number of useful comments, introduced corrections and amendments while editing the book.

Finally, I would like to express my deepest gratitude to Prof.

Blokhintsev L.D. (Institute of Nuclear Physics, Moscow State University, Moscow, Russia). He was more than just a scientific advisor and, subsequently, a reviewer who made some fundamental comments with regard to the contents of the book and wrote the book review placed as a Foreword, he also read thoroughly the manuscript and as a technical editor introduced significant corrections to the initial text.

The work has been partly supported by grants of Program of fundamental researches of the MES RK (the Ministry of Education and Science of the Republic of Kazakhstan) via the Fessenkov V.G. Astrophysical Institute "NCSRT" ASC MID RK.

Thereby, I would like to express a particular gratitude to the President of "NCSRT" ASC MID RK, Corresponding member of the NAS RK, Prof. Zhantaev Zh.Sh. and to the Director of the Fessenkov V.G. Astrophysical Institute Omarov Ch.T. for the assistance and the permanent support of the work with this book and the whole Nuclear Astrophysics themes.

# SHORT CONTENTS

---

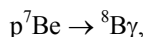
*The progress in studies about the Universe is substantially associated with the achievements in the nuclear and elementary particle physics. It turned out that the laws of microcosm allow understanding what is going on in the Universe. This unity of micro- and macrocosm is a remarkable and edifying example of the unity of Nature [2].*

Before proceeding to the main results we would like to present a summary of the book. In the first chapter we will consider briefly and simply all the major thermonuclear reactions which may take place in the stars at different stages of their formation and evolution. Then we will expand on the analysis of the main thermonuclear processes involving radiative capture – processes in which two colliding particles fuse together to form one particle and emit  $\gamma$ -quantum. They are mediated by electromagnetic interactions which somewhat simplifies their consideration from the theoretical point of view, because the Hamiltonian of this interaction is known exactly. Further on, in addition to the properties of bound states of light atomic nuclei participating in thermonuclear reactions, we will consider the principal characteristics, in particular  $S$ -factors, of radiative capture of protons and other particles by such nuclei at astrophysical energies. The consideration of these reactions is carried out in the frame of the modified potential cluster model (MPCM) with forbidden states (FSs) of light atomic nuclei [3].

Now we are going to give an overview of possible reactions in three major thermonuclear cycles for stable stars of the Main Sequence and then indicate which processes will be considered in this book and which ones will be analyzed in the nearest future.

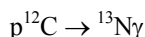
The first cycle is the proton-proton chain, which includes five two-body processes (according to the input channel), mediated by strong or electromagnetic interactions, three of them refer to the radiative capture.

Two such processes will be considered in the present book and the results will be given in chapters 3 and 14. The other five reactions of this cycle (in total there are 10 of them as it was shown further in fig. 1.4 – ch.1) are mediated by weak interactions and these processes will not be consider in this book. Therefore, only the next reaction remains in this cycle

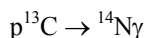


which will be considered in future.

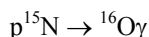
The stellar CNO-cycle consists of 9 similar reactions (13 in total, shown further in tables 1.2–1.4 – ch.1. Four of them are mediated by weak forces), six of them it is radiative capture. The first of these reactions



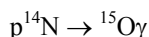
is considered in chapter 10, the second one is the proton capture on  $^{13}\text{C}$



that shown in ch.11, and the results for the third reaction



are given in ch.13. Two last reactions (see tables 1.2–1.4) lead to a formation of  $^{17,18}\text{F}$  nuclei which are not  $p$ -shell nuclei and the possibility of applicability of the modified potential cluster model, which was used for all further calculations, was checked only in the case of neutron capture reaction on  $^{16}\text{O}$  for such cases, described in work [3]. Therefore, in the first place, only one reaction will be considered in future

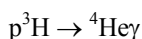


from the remaining processes of the CNO-cycle.

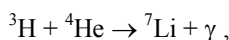
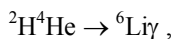
The triple alpha process represents two reactions, one of which involves a two-body radiative capture, which is analyzed on the basis of the

modified potential cluster model in chapter 15. As a result, we have 15 basic thermonuclear reactions with two-body input channels mediated by strong and electromagnetic forces. Ten of them are not the radiative capture processes, six of them are considered in this book. Another two will be considered in future, and two of them, as it was said before, evidently, out of consideration within MPCM. Although this assumption also will be checked in future by the direct calculations.

In addition to the abovementioned processes there are some other radiative capture reactions which supposedly took place at the prestellar stage of evolution of the Universe, i.e., within the first seconds of its existence. They include, for instance [1,2]

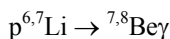


or

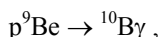


which could take place during the primordial nucleosynthesis [4,5] and the astrophysical *S*-factors of these processes are considered in ch.4 and two last reactions in ch.14.

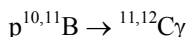
Additionally to the considered above radiative capture in three thermonuclear cycles and reactions of the primordial synthesis the processes of this type were studied



or

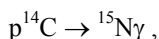


results for them are given further in chapters 5, 6 and 7 and



– proton capture reactions by two stable boron isotopes, results of them are given in chs.8 and 9.

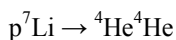
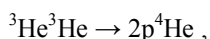
In addition, the reaction



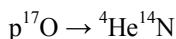
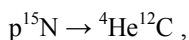
was studied further and it can play a certain role in the processes of the Big Bang – it is considered in ch.12. Altogether, there are ten thermonuclear processes from fifteen considered in these book, which directly take part in different cycles and processes of the primordial nucleosynthesis of our Universe [3].

In conclusion we would like to note that the general title of the book “Thermonuclear processes in the Universe” is chosen so as to account for the future expansion of the book. In the nearest future we are planning to finish the consideration of all possible thermonuclear reactions of radiative capture type on light nuclei. The obtained results will be published in the second edition of this.

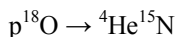
That is, we will consider the remaining thermonuclear processes of proton-proton chain and CNO cycle, which proceed at the expense of strong interactions and are associated with the rearrangement of channels. There are 5 such reactions, in total



for p-p chain and



and



for CNO cycle.

Meanwhile, only first three of them are flowing on  $p$ -shell nuclei, which we will consider in future. It is supposed to carry out the analysis of all these processes on the basis of the modified potential cluster model for light nuclei and classification of orbital states according to Young tableaux, which in some cluster systems leads to the conception of states forbidden by Pauli principle [3].





# ***INTRODUCTION***

---

*The application of the achievements of modern nuclear physics to the study of cosmic phenomena and thermonuclear reactions has allowed to develop a theory of the formation, structure and evolution of stars, a theory of supernova explosion and pulsar production, which are concordant, in qualitative terms, with observations, and to explain the abundance of chemical elements in the Universe [2].*

First, we will consider the background of and conditions required for the initiation of thermonuclear reactions in astronomical objects, specifically in stars with different masses. Explanation of the processes of the star formation and their evolution is one of the most important task of the modern astrophysics on the whole and nuclear astrophysics in particular, since in the known region of the Universe a considerable part of the observable matter is contained exactly in stars at different stages of their progress or in the objects that have already overcome the star stage.

According to the most popular point of view, stars, at the initial stage of their formation, condense under gravity forces from giant gas molecular clouds [4]. These gas clouds mainly consist of molecular hydrogen with a small admixture of deuterium and helium. The last two elements are formed as a result, of primordial nucleosynthesis at the prestellar development stage of the Universe. Stars are formed in this giant gas molecular cloud from separate irregularities or star formation zones [6] and an example of such nebula is given in Figure B1 [7].

The compression of this zone begins from the collapse in its initial part, i.e., from free fall of the matter to the zone centre because of gravity. The compression area gradually moves from the centre to the periphery including completely the whole zone. This is how star formation process begins. The generating cluster in the centre of the collapsing cloud is a protostar or a star at the early stage of its formation [2].



Fig. B1. Star formation nebula in Triangulum Galaxy. ([http://en.wikipedia.org/wiki/H\\_II\\_region](http://en.wikipedia.org/wiki/H_II_region))

known as accretion.

Furthermore, the second stage occurs – rapid compression. At this moment, a protostar is practically non-transparent for visible light but transparent for infrared radiation that carries away excess heat generated during the compression. Therefore, the interior temperature does not rise considerably and the gas pressure does not prevent further collapse. However, the protostar becomes less transparent during compression, because of the growing density of the matter, and this impedes escape of radiation and leads to an increase in gas temperature inside it. At a certain moment, the protostar becomes practically non-transparent for its heat radiation. Temperature increases rapidly along with gas pressure and, together, they can partially compensate gravity and then the protostar compression slows down.

The third stage begins – slow compression. Further rise of temperature causes significant changes of the properties of the matter. Molecules decay to form single atoms at a temperature of several thousands degrees and atoms are ionized at a temperature of about 10,000 Kelvin (K), i.e., their electronic shells break down. These power-intensive processes, as a result, of which the matter turns into plasma, delay the temperature increase for some time, but after all the matter transforms into plasma it recommences. The protostar gradually achieves the state when gravity is practically balanced by internal gas pressure. However, since heat continues to go away and the protostar does not have another energy sources yet, except

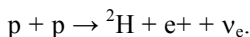
Generally, the protostar evolution can be divided in several stages. The first stage is isolation of a cloud fragment and its densification, which can take place, for example, a result of random fluctuation or under external gravity force. Because of growing weight and gravity, more matter is attracted to the centre of the protostar. The process of the matter falling to protostar from the surrounded external cloud is

compression, its compression gradually continues and its interior temperature continues to grow.

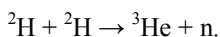
The further development of events depends on sizes and masses of the forming celestial body when the protostar temperature reaches a certain limit. If its mass is not great and equals less than 8% of the mass of the Sun ( $m_{\odot}$ ) then there are no conditions for a stable thermonuclear reaction to begin, which would support its balance. Such formation turns into a state known as Brown Dwarf and then cools with the lapse of time and can become a planet-like object [7].

If the mass of the compressing matter is more than 8% of  $m_{\odot}$ , this is enough for stable thermonuclear reactions to begin to take place inside the protostar under compression and a stable Main Sequence star will form from such cloud (see Appendix 2). When the mass of the most compact part of the cloud approximates, due to accretion, 0.1 of the solar mass, the temperature in the star centre approximates  $10^6$  K and the new stage in the protostar life (the earliest thermonuclear fusion reactions) can begin.

However, these thermonuclear reactions differ, to a significant extent, from reactions taking place in sun-like stationary stars [2]. The point is that the first solar fusion reaction is hydrogen burning (the first reaction of the proton-proton or pp chain)



It requires higher temperature (approximately  $\sim 10^7$  K), while the temperature in the protostar centre equals only  $10^6$  K. The only deuterium fusion reaction can occur effectively at this temperature



Deuterium (the same as  ${}^4\text{He}$ ) is formed at the prestellar evolution stage of the Universe [8] and its content in the protostar substance approximates  $10^{-5}$  of the proton content. However, even such a small amount is enough for the appearance of an effective energy source in the protostar centre, which leads to future temperature rise [2].

The non-transparency of the protostellar matter leads to the fact,

according to Hayashi [6], that convection gas flows begin to appear in protostar. Heated gas regions go from the star centre to the periphery and the cold matter goes down from the surface to the protostar centre, supplying additional deuterium. However, the thermonuclear fusion reactions of deuterium nuclei that have begun produce comparatively low quantities of energy and cannot resist gravitational compression, which still continues at this stage.

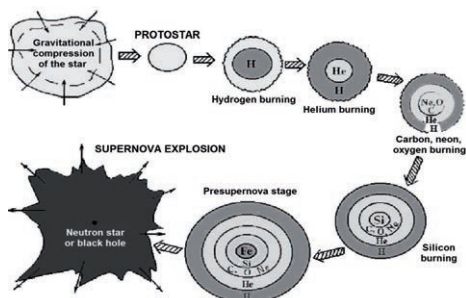


Fig. B2. Basic stages of massive star evolution with the mass  $M > 25 M_{\odot}$  ( $M_{\odot}$  – mass of the Sun) [2]. (<http://nuclphys.sinp.msu.ru/nucsynt/n01.htm>).

Further compression of the stellar matter due to gravity causes a greater temperature rise in the centre of the star, thus creating conditions for the beginning of the helium burning thermonuclear reaction. At this moment, the protostar becomes a stable star since the release of thermonuclear energy can now balance gravity and the star, depending on its mass, takes a certain place in the Hertzsprung-Russell diagram [6] (see Appendix 2).

The scheme of the mechanism of formation, development and death of massive star, which can turn into a supernova [2] in the course of its evolution, is shown in Fig. B2. Star evolution, i.e., the process of its formation, life and transformation into the White Dwarf, is shown in Fig. B3. This is a star with a mass close to the solar mass ([http://en.wikipedia.org/wiki/Stellar\\_evolution](http://en.wikipedia.org/wiki/Stellar_evolution)) [7]. It gradually turns into the Red Giant and the remaining core turns into the White Dwarf after the ejection of the planet nebula (see Appendix 2).

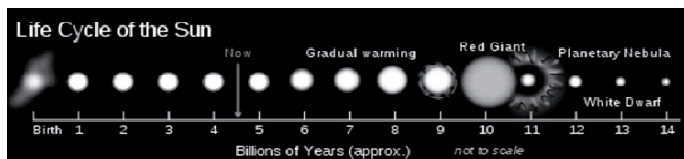


Fig. B3. Development stages of the star like our Sun ( $M \sim M_{\odot}$ ). Numerals show the lifetime in billions of years. ([http://en.wikipedia.org/wiki/Stellar\\_evolution](http://en.wikipedia.org/wiki/Stellar_evolution)).

Meanwhile, we have described in brief the process of the protostar

evolution into an ordinary star, whose stable state is maintained because of the thermonuclear reactions of the pp chain. Obviously, this description is not rigorous and has a quality nature. A rigorous solving of the problem of the star formation from interstellar matter, i.e., molecular gas and the stellar evolution as a whole is hardly possible. It is only possible to develop separate parts of the star formation theory and control them in a continuous fashion through new astronomical observations [6].

We have shown that an astrophysical object turns into a star when stable thermonuclear reactions begin to occur in it and, because of them, the star, depending on its mass, takes a certain place in the Main Sequence. Now let us consider different types of thermonuclear reactions that are a part of three main cycles: pp, CNO, and helium or three-alpha cycle. We will consider the reasons of reactions caused by interaction of atomic nuclei in the stars of different masses at various stages of their development.





# **1. THERMONUCLEAR PROCESSES**

---

## ***Introduction***

Slightly coming back in study of the stellar evolution, we would remind that, when the temperature in the star centre rise up to  $10\div 15$  mln K because of the gravity compression, the value of kinetic energy of scattering hydrogen nuclei is enough for overcoming Coulomb repulsion. The nuclear reaction of hydrogen burning, which is the first reaction of the proton-proton chain [2], begins. Strictly speaking, such explanation of the reaction is not exact, but it is most clear for the followers of classic (not quantum) physics. From the modern quantum point of view, it is more correct to say that the increasing of the kinetic energy leads to the increase in probability of the particles penetration through the potential barrier. In a certain period, it appears that this is enough for initiation of stable thermonuclear reaction of hydrogen fusion. This reaction begins in the bounded central part of the star, but the resulting energy output stops its further gravity compression.

The qualitative change of the energy release mechanism begins at this stage of star development. If the star warming is a result of gravitational compression before the beginning of the nuclear reaction of hydrogen burning, but now the other mechanism is opened – the energy output at the expense of nuclear fusion reactions and that is enough for counteraction against the gravitational forces. As a result, the star acquires stable dimensions and luminosity, which are not changed during billions of years for stars near the solar mass, i.e., all time when the hydrogen burning reaction is going in its centre. Thermonuclear reactions flow differently in stars with various masses, with different rates and approximately continue from tens of millions to tens of billions of years [2].

The small value of the cross section of the hydrogen burning reaction

explains the fact why this stage in the stellar evolution is the most long-continued. The value proportional to the probability of certain interaction process of nuclear particles between each other is named as a cross section in quantum physics. Meanwhile, the small value of the cross section means the small probability of the given process, i.e., the big characteristic time of the reaction flowing.

### ***1.1 Thermonuclear reactions in the stars***

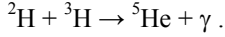
Thermonuclear reaction (fusion reaction, nucleosynthesis or fusion of atomic nuclei) is a variety of nuclear reaction which, as generally regarded, proceeds in stars at energies about  $0.1 \div 100$  keV (1 keV corresponds to the temperature  $10^7$  K according to the  $E = kT$  relation) and leads to the fusion of light atomic nuclei into heavier nuclei [7].

Now, before going to the description of the star thermonuclear processes, we briefly stop on the mechanism of thermonuclear reaction, i.e., on the reason why it is going in plasma (evacuated and ionized gas, generally consisting in atomic nuclei having positive electric charge, and electrons with negative charge). The process of nuclear fusion or thermonuclear reaction goes on if the atomic nuclei, having positive charge, will approach each other at the distance where the strong attractive interaction affects. This distance has the nuclei size order that is approximately equals  $10^{-13}$  cm or 1 fm (1 fermi). It considerably less than atomic size in ordinary and non-ionized state, which has the order of  $10^{-8}$  cm or 1 Å (1 angstrom).

The charges of nuclei and electrons compensate each other at low temperatures and energies if non-ionized atoms exist. But electron shell radii already not exist within distances of the order of 1 fm and can not shade nuclear charges, so they experience strong electrostatic repulsion. The force of this repulsion, in accordance with Coulomb law, varies inversely as the square between the charge distances. The value of the strong interaction, which trend to attract them, begins to rise quickly and becomes much more than Coulomb repulsion at the distances of the order of nuclear size.

Thereby, atomic nuclei have to take the potential Coulomb barrier for enter into a reaction or, be more exact, have enough probability to penetrate

this barrier. For example, the value of this barrier approximately equals  $0.1 \text{ MeV} = 100 \text{ keV} = 10^5 \text{ eV}$  (1 eV is 1 electronvolt) for the radiative capture reaction of deuterium by tritium



Let us provide, for comparison, the required energy for ionization of hydrogen atom, which equals 13 eV only. If to convert the energy equals 0.1 MeV to the temperature, we obtain approximately  $10^9 \text{ K}$ . Such temperature can not be in the majority of stars, for example in the Sun, and it seems that thermonuclear processes are impossible there.

However, at least there are two known nature effects, which are reducing the temperature required for initiation of the thermonuclear reaction. Examine them into detail:

1. Firstly, the temperature characterizes the average kinetic energy of particles in the centre of the star only. There are particles with low and high energy, because it is defined by the Maxwell distribution for gas and plasma. Only a small quantity of nuclei really takes part in thermonuclear reaction. They have energy much more than average – so-called “tail” of the Maxwell distribution [7].

This distribution can be written as a velocity distribution function [2]

$$F(v) = 4\pi v^2 \left( \frac{m}{2\pi kT} \right)^{3/2} \exp \left( -\frac{mv^2}{2kT} \right)$$

or by energies

$$F(E) = 2 \left( \frac{E}{\pi(kT)^3} \right)^{1/2} \exp \left( -\frac{E}{kT} \right) .$$

The form of velocity distribution function, which is absolutely analogous to the energy distribution, is shown in Fig. 1.1.

This distribution has the most probable velocity and energy

$$v_m = \left( \frac{2kT}{m} \right)^{1/2},$$

$$E_m = \frac{mv_m^2}{2} = kT,$$

and root-mean-square velocity  $v_{rms}$  expressing through the average velocity  $\langle v \rangle$  and average energy of the particles

$$v_{\kappa\theta} = \langle v^2 \rangle^{1/2} = \left( \frac{3kT}{m} \right)^{1/2},$$

$$E_{\kappa\theta} = \frac{mv_{\kappa\theta}^2}{2} = \frac{3}{2}kT.$$

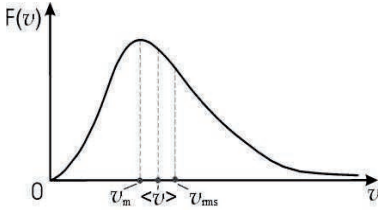


Fig. 1.1. The Maxwell velocity distribution [2]. ([http://fn.bmstu.ru/phys/bib/physbook/tom2/ch5/texthtml/ch5\\_4.htm](http://fn.bmstu.ru/phys/bib/physbook/tom2/ch5/texthtml/ch5_4.htm))

Only small parts of the hydrogen nuclei with a maximum kinetic energy enter into a thermonuclear reaction while the star compression process, because of it the considerable quantity of additional energy emits. The part of this energy is

expended to the increasing of the kinetic energy of some other part of hydrogen nuclei, preparing them to the participation in further nuclear processes. Thereby, the low-energy part of hydrogen nuclei, forming the basic mass of any star, is the energy source for thermonuclear reactions.

2. Secondly, because of effects of quantum physics, atomic nuclei do not need to have the energy more than the value of Coulomb barrier as it was in classic mechanics. These particles can to penetrate through the barrier with certain probability, even through their energy less than this barrier. This phenomenon is called as quantum tunneling effect and is shown graphically below in Fig. 1.2 [9].

It is shown in Fig. 1.2 that this particle has the oscillating wave function (WF)  $\Psi$  outside the barrier ( $r > r_1$ ) determining probability of its existence

in the certain point of space, with the energy  $E_{\text{particle}}$ , which less than barrier's height  $E_{\text{pot}}$ , could penetrate through the barrier.  $\Psi$  is the WF of particle inside the barrier, i.e., at  $r < r_1$  it is not equal to zero and represents itself the function of position with exponentially drooping dependence [8]. In other words, there is certain and completely nonzero probability of particle penetration through the potential Coulomb barrier and its penetration into the region of strong interaction, which leads to the beginning of nuclear rearrangement processes or thermonuclear fusion reactions.

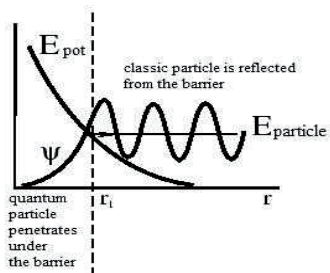


Fig. 1.2. Quantum particle penetration through the potential barrier [8]. (<http://astronet.ru/db/msg/1169513/node36.html>)

on the star, are equivalent and opposite in direction and this star stays in the stationary state in Main Sequence (see later Appendix 2 at the end of the book).

Now we will have detailed consideration of fusion processes of light atomic nuclei, which are possible because of thermonuclear reactions in the centre of the star.

## 1.2 Proton-proton chain

Proton-proton or pp-chain is a set of thermonuclear reactions for the stars of Main Sequence when hydrogen (or exactly, hydrogen atomic nucleus – proton “p”) turns to helium (helium atomic nucleus  ${}^4\text{He}$ ). This cycle can go at lowest energies and it is the main alternative to the CNO cycle, which will be considered next. Evidently, the proton-proton chain dominates in stars with the masses on the order of solar mass, in stable stage of their development. At the same time, the CNO cycle dominates in more massive and hot stars.

The total result of these pp-reactions is the fusion of four protons with the formation of  ${}^4\text{He}$ , with the energy output equivalent to 0.7% of the mass of these protons. Such reaction chain in simplified form goes through the three stages. At first, two protons, having enough energy for penetration through the Coulomb barrier, merge forming of deuteron, positron and electron neutrino. Then the deuteron merges with the positron forming  ${}^3\text{He}$  and  $\gamma$ -quantum and, then, two nuclei of  ${}^3\text{He}$  atom merge forming  ${}^4\text{He}$ ; in this case two protons disengage.

Schematically it is usually identified as [7]

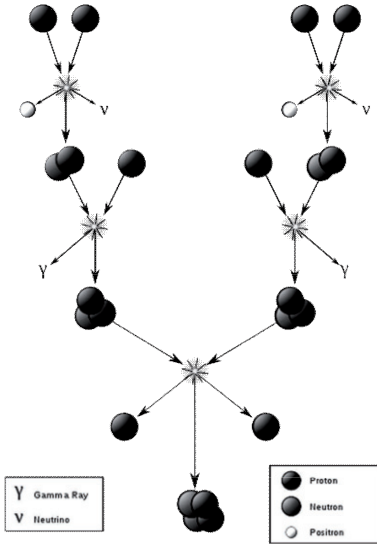
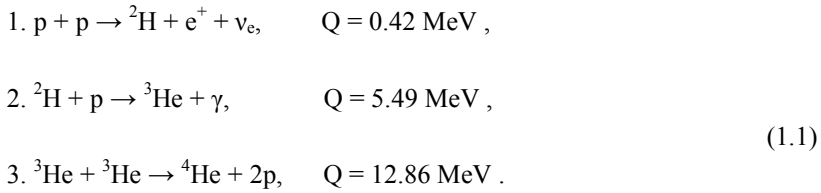


Fig. 1.3. Simplified scheme of the proton-proton chain [7]. (<http://en.wikipedia.org/wiki/File:FusionintheSun.svg>)

Here the  $Q$  value is the energy releasing in the reaction process, which is expressed in the energy units called megaelectronvolt ( $1 \text{ MeV} = 10^6 \text{ eV}$ ). Such reaction chain is shown graphically in Fig. 1.3 [7]. These are only the main reactions of the proton-proton chain, but all other reactions with the designation of channel relative contributions and reaction rates are shown in Fig. 1.4 [2] and Table 1.1 [9].

As it is seen from Table 1.1 and Fig. 1.4, this circle can be finished in three different paths.

The first two reactions have to be realized twice for finishing of the I branch, which was shown above in Fig. 1.3 and (1.1), and gives maximal energy contribution, because of the fact that two  ${}^3\text{He}$  nuclei are needed for the third reaction. Here, it seems,

that it is possible to neglect reaction  $p + p + e^- \rightarrow {}^2\text{H} + \nu$  (see Fig. 1.4), which, like the main process  $p + p \rightarrow {}^2\text{H} + e^- + \nu$ , goes at the expense of weak interactions, but with the probability near three orders less.

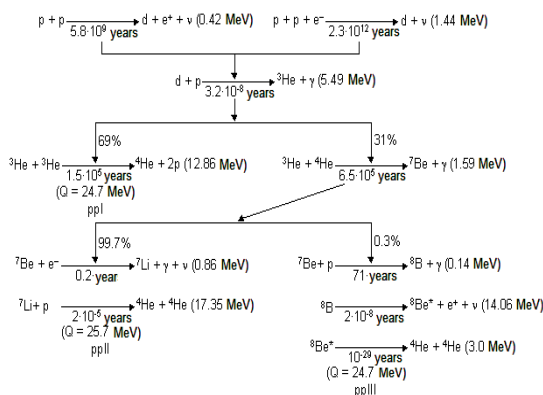


Fig. 1.4. All reactions of the proton-proton chain [2].

(<http://nuclphys.sinp.msu.ru/nuclsynt/n04.htm#docref1>)

so the  ${}^2\text{H}$ ,  ${}^3\text{He}$ ,  ${}^7\text{Be}$ ,  ${}^7\text{Li}$  and  ${}^8\text{B}$  nuclei are not accumulated in the stars in noticeable amounts. Neutrinos are emitted with the extremely high energy for the pp-chain in III branch at the atomic nucleus decay process of the  ${}^8\text{B}$  nucleus with the forming of the unstable beryllium nucleus in the excited state ( ${}^8\text{Be}^*$ ), which almost instantly decays into two  ${}^4\text{He}$  nuclei. These neutrinos from solar thermonuclear reaction products are registered with the different indicators in the Earth [9]. The chain is finished by the I branch in the 70% cases, 30%-the II branch and only the few tenth of percent [2] are related to the III branch, as it is shown in Fig. 1.4.

**Table 1.1. Reactions of proton-proton chain with the designation of energy output  $Q$  and characteristic reaction time  $\tau$  for each process [9],  $X$  is the mass concentration of elements. Reactions of the radiative capture where  $\gamma$ -quantum is generated are marked by italic – just that very type of reactions is considered in this book (from: <http://astronet.ru/db/msg/1190731>)**

No.	Reaction	Q (MeV)	$\tau$ (years)	$\bar{\varepsilon}_\nu$ (MeV); $X$
	$p(p, e^+ \nu) {}^2\text{H}$	0.42	$8.2 \cdot 10^9$	$\bar{\varepsilon}_\nu = 0.26$ ; $\varepsilon_{\nu, \max} = 0.42$
	${}^2\text{H}(p, \gamma) {}^3\text{He}$	5.49	$4.4 \cdot 10^{-8}$	$X({}^2\text{H}) = 2.7 \cdot 10^{-18}$



	${}^3\text{He}({}^3\text{He}, 2p){}^4\text{He}$	12.86	$2.4 \cdot 10^5$	$X({}^3\text{He}) = 1.6 \cdot 10^{-5}$
II	${}^3\text{He}({}^4\text{He}, \gamma){}^7\text{Be}$	1.59	$9.5 \cdot 10^5$	$X({}^7\text{Be}) = 1.2 \cdot 10^{-11}$
	${}^7\text{Be}(e^-, \gamma \nu){}^7\text{Li}$	0.86	0.30	$\varepsilon_\nu = 0.86$ (90%); 0.38 (10%); $\bar{\varepsilon}_\nu = 0.8$
	${}^7\text{Li}(p, {}^4\text{He}){}^4\text{He}$	17.35	$3.8 \cdot 10^{-5}$	$X({}^7\text{Li}) = 1.5 \cdot 10^{-15}$
III	${}^7\text{Be}(p, \gamma){}^8\text{B}$	0.14	$1.0 \cdot 10^2$	$X({}^8\text{B}) = 4 \cdot 10^{-21}$
	${}^8\text{B}(e^+ \nu){}^8\text{Be}^*$	14.06	$3.0 \cdot 10^{-8}$	$\bar{\varepsilon}_\nu = 7.3$ ; $\varepsilon_{\nu, \max} = 14.06$
	${}^8\text{Be}^* \rightarrow 2{}^4\text{He}$	3.0	—	—

The certain main parameters of the proton-proton chain reactions are listed in Table 1.1. Particularly,  $\varepsilon_\nu$  is the energy of emitted neutrinos,  $\bar{\varepsilon}_\nu$  and  $\varepsilon_{\nu, \max}$  are their average and maximum values when neutrinos are emitted in the energy range  $0 < \varepsilon_\nu < \varepsilon_{\nu, \max}$ , also  $X$  is the mass concentration of the intermediate atomic nuclei. The  $\tau$  and  $X$  values are rated for physical conditions closed to expecting in the inner part of the Sun, i.e., for the temperature  $1.5 \cdot 10^7$  K, for the density  $100 \text{ g/cm}^3$  and for equal concentrations of hydrogen and helium by mass ( $X_{\text{H}} = X_{\text{He}} = 0.5$ ). Let us see that the data of characteristic time  $\tau$ , which is given in Fig. 1.4 [2] and in Table 1.1 [9], slightly differ because it is taken from different sources.

Let us note that the hydrogen store in the Sun could be enough for 100 billions of years at the up-to-date rate of its burning by proton-proton chain. However, certain circumstance considerably reduces the hydrogen burning stage. The problem is that hydrogen practically burns only in the inner part of the Sun where the hydrogen stores are enough for 5–6 billions of years, i.e. after this time the Sun, as it follows from the modern star development model, ought to turn into the Red Giant. At this stage, the solar radius approximately will rise in 200 times and the solar outer shell firstly will reach Mercury, then Venus and will come nearer to the Sun, but, it seems, will not affect to its orbit [2].

The core of the more massive than the Sun star begins gradually compress under gravity while hydrogen burning-out. It leads to the pressure and temperature rising and along with proton-proton chain the other thermonuclear process, called CNO cycle, comes into force.

### 1.3 The stellar CNO cycle

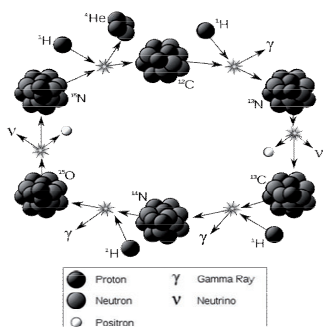


Fig. 1.5. CN cycle reactions [7].  
( [http://en.wikipedia.org/wiki/CNO\\_cycle](http://en.wikipedia.org/wiki/CNO_cycle))

The CNO cycle is the collection of three linked or, more exactly, partly overlapped cycles. The first and most simple of them is the CN cycle (Bethe-cycle or carbon cycle) was suggested by Hans Bethe and, regardless of him, by Carl von Weizsäcker in 1939 year. The main reaction path of the CN cycle is shown in Fig. 1.5 and Table 1.2 [7]. Reactions of the

radiative capture are marked by *italic* in this and the future tables that are considered in this book

The initial nuclei taking part in this reaction are listed in the first column of this and other tables given below – initial reaction channel. The third column reproduces the issue nuclei obtaining in the reaction, in the next – the energy release and in the last – characteristic reaction time [7], which is not noted in the next tables.

**Table 1.2. CN cycle reactions with the designation of energy output and characteristic reaction time [7]. Reactions of the radiative capture are marked by *italic*.**

Fusion	→	Result	Q (MeV)	$\tau$ (years)
<i><math>^{12}\text{C} + p</math></i>	→	<i><math>^{13}\text{N} + \gamma</math></i>	1.95	$1.3 \cdot 10^7$
$^{13}\text{N}$	→	$^{13}\text{C} + e^+ + \nu_e$	1.37	7 min
<i><math>^{13}\text{C} + p</math></i>	→	<i><math>^{14}\text{N} + \gamma</math></i>	7.54	$2.7 \cdot 10^6$
<i><math>^{14}\text{N} + p</math></i>	→	<i><math>^{15}\text{O} + \gamma</math></i>	7.29	$3.2 \cdot 10^8$
$^{15}\text{O}$	→	$^{15}\text{N} + e^+ + \nu_e$	2.76	82 sec
$^{15}\text{N} + p$	→	$^{12}\text{C} + ^4\text{He}$	4.96	$1.1 \cdot 10^5$

The alternative exit channel in the reaction of the proton capture on  $^{15}\text{N}$  is the formation of  $^{16}\text{O}$  with  $\gamma$ -quantum emission. This is initial reaction for the new CNO-I cycle, which has exactly the same structure as the CN cycle and its reactions are represented in Table 1.3 [7]. The CNO-I cycle raises up the energy-release rate of the CN cycle increasing the number of  $^{14}\text{N}$  – catalytic agents for this cycle.

The last reaction, given here, is the interaction of the proton with  $^{17}\text{O}$ , which is also able to have another exit channel creating new, so called, CNO-II cycle listed in Table 1.4 [7]. Thereby, all these CN, CNO-I and CNO-II cycles are formed CNO cycle, which supports the star burning at the next stage after the hydrogen burning cycle.

**Table 1.3. CNO-I cycle reactions with designation of energy output [7].  
Reactions of the radiative capture are marked by italic.**

<b>Fusion</b>	$\rightarrow$	<b>Result</b>	<b>Q (MeV)</b>
<i><math>^{15}\text{N} + p</math></i>	$\rightarrow$	<i><math>^{16}\text{O} + \gamma</math></i>	12.13
<i><math>^{16}\text{O} + p</math></i>	$\rightarrow$	<i><math>^{17}\text{F} + \gamma</math></i>	0.60
$^{17}\text{F}$	$\rightarrow$	$^{17}\text{O} + e^+ + \nu_e$	2.76
$^{17}\text{O} + p$	$\rightarrow$	$^{14}\text{N} + ^4\text{He}$	1.19

**Table 1.4. CNO-II cycle reactions with designation of energy output [7]. Reactions of the radiative capture are marked by italic.**

<b>Fusion</b>	$\rightarrow$	<b>Result</b>	<b>Q (MeV)</b>
<i><math>^{17}\text{O} + p</math></i>	$\rightarrow$	<i><math>^{18}\text{F} + \gamma</math></i>	5.61
$^{18}\text{F}$	$\rightarrow$	$^{18}\text{O} + e^+ + \nu_e$	1.66
$^{18}\text{O} + p$	$\rightarrow$	$^{15}\text{N} + ^4\text{He}$	3.98

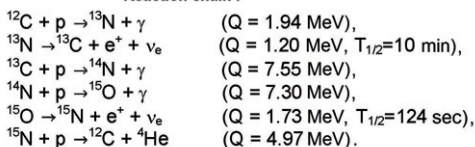
Let us note that there is another and very slow cycle, called OF cycle, but its role in the energy production is negligibly small. However, this cycle is essential for explanation of  $^{19}\text{F}$  nuclei origin in stars. The cycle

follows from the last reaction of the previous cycle going through another channel, and it is shown in Table 1.5 [6].

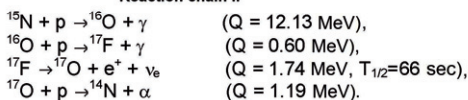
**Table 1.5. OF cycle reactions with designation of energy output [7].**  
**Reactions of the radiative capture are marked by italic.**

Fusion	→	Result	Q (MeV)
$^{18}\text{O} + p$	→	$^{19}\text{F} + \gamma$	7.99
$^{19}\text{F} + p$	→	$^{16}\text{O} + {}^4\text{He}$	8.11
$^{16}\text{O} + p$	→	$^{17}\text{F} + \gamma$	0.60
$^{17}\text{F}$	→	$^{17}\text{O} + e^+ + \nu_e$	2.76

**Reaction chain I**



**Reaction chain II**



**Reaction chain III**

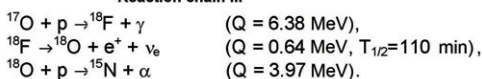


Fig. 1.6. Reactions of CNO cycle [2].

(<http://nuclphys.sinp.msu.ru/nuclysynt/n04.htm#docref2>)

All of main reactions of the triple CNO cycle can be represented in Fig. 1.6, which was taken from another source [2] and where energy values and reaction time ( $T_{1/2}$  half-life) are slightly differed. The proton-proton chain dominates apparently in the stars with masses comparable with the solar mass or less. The CNO cycle is the main source of

energy in more massive stars having higher core temperature [2].

So, the initial stage of fusion thermonuclear reactions consists in the forming of helium nuclei from four hydrogen nuclei, as it was listed in Table 1.1. In addition, helium nuclei along with  $^{12}\text{C}$ ,  $^{14}\text{N}$  and  $^{15}\text{N}$  nuclei are the final products of all three CNO cycles as it was demonstrated in Tables 1.2÷1.4. During the time when hydrogen burning is going in the star's central part, the pp-chain and the CNO cycle going because of hydrogen burning and its reserves are exhausted but helium accumulation is taken

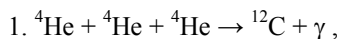
place. So-called helium core is formed in the centre of the star.

The energy release at the expense of the above considered thermonuclear reactions is reduced, when the hydrogen in the centre of the star has burned and the gravitational forces come into force again. In this case, the additional heating will be the result of the compression beginning of the formed helium core of the star. The kinetic energy of the colliding helium nuclei rises up and reaches the sufficient value of probability for overcoming the Coulomb barrier. The next stage of thermonuclear reactions begins – helium burning.

### ***1.4 Triple alpha process***

When the hydrogen in the centre of the star is finished, the stars with the mass less than 40% of solar mass are dying turning into the dim and compact White Dwarfs consisting from the helium [9]. The gravity compression forces, so as the temperature in stars with this mass too, is not enough for the helium reaction ignition.

The central region of the more massive stars is so compressed under the gravity, that the temperature in them comes up to hundreds of millions K. The interaction of helium nuclei is possible at this temperature and the high density of stellar interiors gives the collision of three or even four helium nuclei with the production reaction of carbon or oxygen [9] quite probable:



The first of these reactions is named as “Triple helium reaction” (Triple alpha process) and represents fusion nuclear reaction of three  $^4\text{He}$  atomic nuclei in stellar interiors. It starts at the temperature about  $1.5 \cdot 10^8$  K and at the density of the order of  $5 \cdot 10^7$  kg/m<sup>3</sup>. It is possible that this reaction goes in two stages [9]:

1. Forming of unstable  $^8\text{Be}$  (the half-life is equal to  $10^{-16}$  sec)



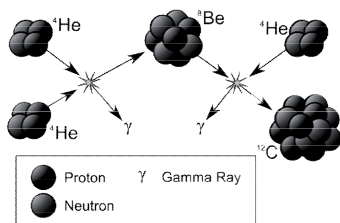
2. Forming of  $^{12}\text{C}$  in one of the excited states

Fig. 1.7. Triple alpha process [6].  
([http://en.wikipedia.org/wiki/Triple-alpha\\_process](http://en.wikipedia.org/wiki/Triple-alpha_process))

This reaction is shown in Fig. 1.7 schematically and leads to the energy output equals 7.28 MeV [7]. The second reaction, given above, is alpha particle capture by carbon nucleus, which can go practically simultaneously with triple  $^4\text{He}$ -process. This reaction leads to the energy output equals 7.16 MeV [8]

and, along with the two-body  $^{12}\text{C}(^4\text{He}, \gamma)^{16}\text{O}$  capture; it can go, apparently, as the reaction of consistent fusion of four helium nuclei with the formation of  $^{16}\text{O}$ .

The stars, with the mass less than  $6\div 8$  of solar mass, have the stage of helium flashing or helium burning (continuing only few percent of hydrogen burning time) de facto is the last period in their life. The certain part of helium and nitrogen forming in the CNO cycle, carbon and oxygen are carried to the star surface. The stellar brightness is increasing; it is blowing and releasing the shell in the form of planet nebula, replenishing the interstellar medium by these elements. The core of this star survives in the form of carbon-oxygen White Dwarf [9].

Thus, one can see from the given reactions that carbon and oxygen are the products of helium burning in the centre of the star, which are formed approximately in equal amounts.

### **1.5 Another thermonuclear processes in the stars**

The central part of the star, generally consisting from carbon and oxygen, loses stability once more and begins compression, which leads to the temperature rising, when the whole helium exhausts (burns) in massive stars, with masses more than  $6\div 8$  solar mass. The temperature also rises in the layer, which adjacent to the star core, consisting of helium. It rises in

the external star layers too, which consist of hydrogen. Therefore, the next script could be real: the helium and hydrogen burning in the quite thin shell around the already inactive carbon-oxygen core. At the same time, the temperature in the core itself is not enough high and, probably, the nuclear reactions with the formation of heavier elements do not take place yet [10].

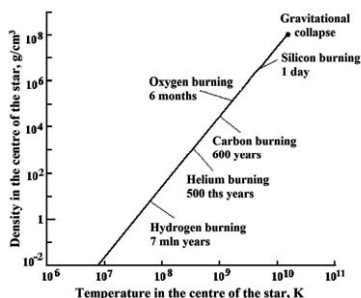
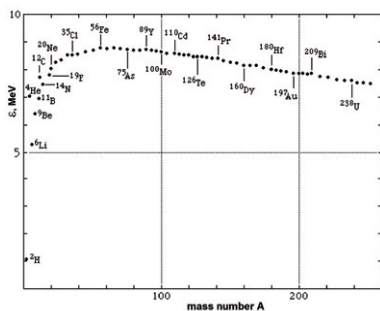


Fig. 1.8. Evolution of the massive star [2]. (<http://nuclphys.sinp.msu.ru/lect/index.html>)



go on till the energy output is possible. The nuclei in the iron zone are formed, as a result, of silicon burning at the final stage of thermonuclear reactions. This is the final stage of all processes of the stellar thermonuclear fusion because the nuclei in the iron zone have the maximal specific binding energy; its diagram is shown in Fig. 1.9 [2].

The thermonuclear reactions with the formation of elements heavier than nuclei in the iron zone cannot occur with the energy output. The energy has to be absorbed in the synthesis of such elements in the reaction process; therefore these processes do not make a contribution to the general energy output of star thermonuclear reactions.

They lose their stability and begin compression to their centre with the rising rate after exhaustion of the material for thermonuclear processes in the massive stars, i.e., after the passing of all possible fusion reactions. If the increasing of internal pressure stops gravity compression, the star central part turns into the superdense neutron star and it can be accompanied by shell ejection and be observed as supernova outburst.

However, if the mass of the neutron star, formed in the previous process after supernova explosion, exceeds the certain limit (Oppenheimer-Volkoff limit which equals  $2\div 3\ m_{\odot}$  [5-7]), then the gravitational collapse goes on till its complete transformation to the black hole [6]. Such process with the final star collapse at temperatures more than  $10^{10}$  K and densities above  $10^8$  g/cm<sup>3</sup> is shown in Fig. 1.8.

### ***1.6 The dependence of thermonuclear reactions from the star mass***

As we have already seen, the nuclear reactions taken place in the thermodynamic equilibrium conditions considerably depend on the star mass. It takes place because the star mass determines the value of the compression gravitational forces that finally determines the maximum temperature, accessible in the star core, where the main thermonuclear reactions occur.

The theoretical calculations results of possible fusion nuclear reactions for stars with different masses [2] are listed in Table 1.6. One can see from the table that the full sequence of fusion nuclear reactions is possible in the massive stars only. The gravitational energy is not



enough for compression and heating of the stellar material to the temperatures that are necessary to the hydrogen burning reactions in stars with the masses about  $M < 0.08 m_{\odot}$ .

**Table 1.6. Theoretical calculation of possible nuclear reactions in stars with different masses [2]**

Stellar mass in $m_{\odot}$ units	Possible nuclear reactions
<0.08	No
0.3	Hydrogen burning
0.7	Hydrogen and helium burning
5.0	Hydrogen, helium and carbon burning
25.0	All fusion reactions with energy output

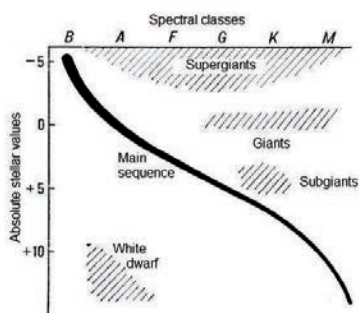


Fig. 1.10. Stellar evolution diagram [9].  
(<http://www.astronet.ru/db/msg/eid/FK86/stars>)

As we said before, the star is in the Main Sequence, which is shown in Fig. 1.10 (see also Appendix 2), till the hydrogen burning reaction occurs in stars with masses on the order of solar mass or more. In the course of time, its central part begins to compress and star temperature rises while the helium nuclei accumulate in this star. The star

layers with ever more distant from the centre can be involved into the process of thermonuclear burning. Expansion and cooling of external star shell is a result of heating, related with this process. Its size increases, and the red color prevails in the radiation spectrum. The star leaves the Main Sequence and moves more to the right, into the Red Giants and Subgiants zone.

Each of described up to now nuclear reactions maintain stellar radiation

at different stages of stellar development. But the iron nuclei are bound strongly than all other atomic nuclei at the last stage, therefore their future transformations can not give the energy output. However, the energy continues to release from its shell at these moments of star life. So such sort of situation can be possible in the issue of silicon burning the iron core of a star will be formed and that is too massive for resistance to action of its own gravity. Its limit mass has been calculated first by S. Chandrasekhar in the range from 1.38 to 1.44 solar masses [7,9] and defines the upper mass limit whereby the star can exist as a White Dwarf. If the star mass is more than this limit, it can turn into neutron star.

Few different processes begin simultaneously when the star mass approaches to the Chandrasekhar limit. These processes cool the star core as much as its inner pressure can not resist to the gravity and it begins catastrophically compress. Such collapse goes on within calculate seconds, but at that energy output is more than the star has released during the whole period of its existence. The main part of this energy releases in the neutrino and gravitational wave forms, but about 1% goes to the heating of external layer of the star and their ejection. For a short time the star becomes comparable in brightness with the whole galaxy, it calls supernova [9] and, as we said, its core can turn into the neutron star.

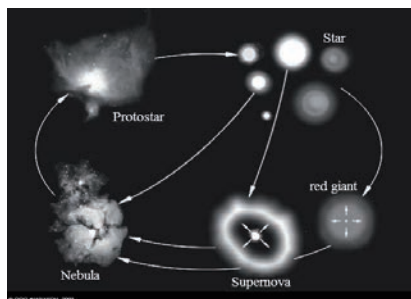


Fig. 1.11. Cycle of matter in the Nature.  
([http://www.gomulina.orc.ru/reterats/nebul\\_5.html](http://www.gomulina.orc.ru/reterats/nebul_5.html))

If the mass of the remain core of such star exceeds the Oppenheimer-Volkoff limit, which estimates as  $2\div3$  solar masses on the modern stage of development of our astrophysical conceptions, then it turns into the black hole [7] and hereon the process of its evolution as astronomical or astrophysical

object called the star is finishing.

In the conclusion of our popular review on thermonuclear reactions we represent the scheme of the cycle of matter in the Nature in Fig. 1.11. It is shown how the protostar is formed in the course of compression of the interstellar gas nebula and then the ordinary star is formed, which meets with a number of transformations depending on its mass and leads to the

production and explosion of supernova and formation of the new nebula. The new protostar, by-turn, can be formed from it and the whole process will repeat again and again.

In the above review, we did not aspire to the detailed description of the formation process of stars with different masses. The aim of this popular description of the stellar evolution is to demonstrate that all star formation stages, independently on their masses, are determined by thermonuclear (per se nuclear) reactions going at ultralow or astrophysical energies and symbolically combined to the different cycles. The possibility of one or another thermonuclear cycle depends on the star mass and wholly determines the stellar evolution process.

### ***1.7 Advances and problems of nuclear astrophysics***

The explanation of ways in the chemical element formation in the stars is one of the significant components of modern nuclear astrophysics. The nuclear doctrine of origin of elements describes the prevalence of different elements in the Universe on the basis of characteristics of these elements, taking into account physical conditions in which they can be formed. In addition, the set of considering nuclear astrophysics processes allows us to interpret, for example, the star luminosity on the different stages of its evolution and to describe, generally, the process of stellar evolution itself. Hereby, the nucleosynthesis questions are closely coupled on the one part with the questions of structure and evolution of the stars and the Universe and on the other part with the nuclear particle interaction properties [2,9].

However, there are a number of complicated and till unsolved problems, which does not allow us to formulate the complete theory of formation and evolution of the objects in the Universe now. Let us give some examples of these up-to-date unsolved problems, directly connected with nuclear astrophysics and nuclear interactions, which are followed from the existing to date nuclear physics problems [2]:

- 1. The insufficiency of experimental data of the nuclear reaction cross sections at low and ultralow, i.e., astrophysical energies.*
- 2. The difficulty of the correct accounting of the reactions going at the*

*expense of weak interactions in describing of the whole set of nuclear reactions, which responsible for element formation in the zone of iron maximum and heavier elements.*

*3. The absence of accurate data for the experimental cross sections of nuclear reactions by the action of neutrons on radioactive nuclei. This problem occurs at the correct description of the prevalence of the elements generated in the  $r$ -process, which is the successive neutron capture in the  $(n,\gamma)$  reactions.*

Furthermore, in this book, we will consider only the questions concerning the first item listed above. This problem consists in the impossibility, at the modern stage of the development of experimental methods, to carry out direct measurements of the cross sections of thermonuclear reactions in the earth's conditions for energies at which they are proceeding in the stars. Furthermore, we will stay at this problem more particularly, but now we will illustrate the main conceptions and representations generally using for the description of the thermonuclear reactions.

It is known that the main characteristic of any thermonuclear reaction are the total reaction cross section or the astrophysical  $S$ -factor, which determines the behavior of the reaction cross section, i.e., the probability of its flowing at vanishing energies. The astrophysical  $S$ -factor can be define experimentally, but it is possible for the majority of interacting nuclei taking place in thermonuclear processes only at the energy range above 100 keV÷1 MeV, meanwhile the errors of its measurement frequently rise up to 100% and more. However, for real astrophysical calculations, for example, for developing and adjustment of the star evolution model, the values of astrophysical  $S$ -factor are required at the energy range about 0.1-100 keV, which corresponds to the temperatures in the star core about  $10^6$  K÷ $10^9$  K.

One of the methods for obtaining the astrophysical  $S$ -factor at zero energy, i.e., the energy of the order of 1 keV and less, is the extrapolation of its values to lower energy range, where it can be determined experimentally. It is the general way which is used, first of all, after carrying out the experimental measurements of cross sections of certain thermonuclear reaction at low energy range.

Let us note that currently, the experimental measurements were done

down to 2.5 keV only for the astrophysical  $S$ -factor of the proton capture on  $^2\text{H}$ , i.e., at the energy range, which can be considered as astrophysical. Similar measurements for all other nuclear systems, which take place in the thermonuclear processes, were reliably carried out, at the best up to 50 keV, for example, as it was done for  $p^3\text{H}$  system.

The second and evidently **most preferable method** consists in theoretical calculations of the  $S$ -factor of some thermonuclear reaction on the basis of certain nuclear models [1; sec. 8]. However, the analysis of all thermonuclear reactions in the frame of unified theoretical point of view is quite labor-consuming problem and therefore, in this book, we will consider only photonuclear processes with  $\gamma$ -quanta, namely the radiative capture of protons and light clusters on certain light nuclei. The processes of the neutron capture on light nuclei are considered in [3].

As for the model choice, one of these models, which we use in present calculations, is the modified potential cluster model of the light atomic nuclei with the classification according to the Young tableaux. The model, in the certain cases, contains the forbidden states (FS) for intercluster interactions and gives a lot of possibilities for carrying out the similar calculations in the simplest form.

We will consider these possibilities more thoroughly in the future, but now we emphasize the general way that leads to the real results in the calculations of the astrophysical  $S$ -factor of certain thermonuclear reaction with  $\gamma$ -quanta; in this case, it is the radiative capture reaction. For carrying out such calculations, it is necessary to have the certain data and execute following steps:

*1. Have at one's own disposal the experimental data of the differential cross sections or excitation functions  $\sigma_{\text{exp}}$  for the elastic scattering of the considering nuclear particles (for example –  $p^2\text{H}$ ) at lowest energies known at the present moment.*

*2. Carry out the phase shift analysis of this data or have the results of the phase shift analysis of the similar data that were done earlier, i.e., know the phase shifts  $\delta_L(E)$  of the elastic scattering depended on the energy  $E$ . It is one of the major parts of the whole calculation procedure of the astrophysical  $S$ -factors in the MPCM with FS, since, on the next step, it allows one to obtain the potentials of the intercluster interaction.*

3. Construct the interaction potentials  $V(r)$  (for example for  $p^2H$  system) according to the discovered phase shifts of scattering. This procedure is called as the potential description of the phase shifts of the elastic scattering in the MPCM with FS and it is necessary to carry out it at lowest energies.

4. It is possible to calculate the total cross sections of the photodisintegration process (for example  $^3He + \gamma \rightarrow p + ^2H$ ) and the total cross sections of the radiative capture ( $p + ^2H \rightarrow ^3He + \gamma$ ) process connected with the previous by the principle of detailed balancing, if we have the intercluster potentials obtained in such a way. As a result you can to calculate the total theoretical cross sections  $\sigma(E)$  of the photonuclear reactions.

5. It is possible to calculate the astrophysical  $S$ -factor of the thermonuclear reaction, for example  $p + ^2H \rightarrow ^3He + \gamma$ , having the total cross sections of the radiative capture only, i.e., the  $S(E)$  value as the function of energy  $E$ , at any lowest energies.

All of these steps can be schematically represented in the next form

$$\sigma_{\text{exp}} \rightarrow \delta_L(E) \rightarrow V(r) \rightarrow \sigma(E) \rightarrow S(E). \quad (1.5)$$

The path, stated above, is identical for all photonuclear reactions and is independent of, for example, reaction energy or some other factors; it is the general under the consideration of any thermonuclear reaction with  $\gamma$ -quanta, if it is analyzed in the frame of the modified potential cluster model with FS. Furthermore, another one method of construction of the intercluster interaction potentials at low energies will be described.

The general sense or goal of using nuclear models and theoretical methods of calculation of thermonuclear reaction characteristics consists in the following. If the certain nuclear model correctly describes the experimental data of the astrophysical  $S$ -factor in that energy range where these data exist, for example 100 keV÷1 MeV, then it is reasonably to assume that this model will describe the form of the  $S$ -factor correctly at the most low energies (about 1 keV) too. This is the certain advantage of the approach stated above over the simple data extrapolation to zero energy, because the using nuclear model has, as a rule, the certain

microscopic justification with a view to the general principles of nuclear physics and quantum mechanics.

Furthermore, we are going over to the immediate description of the concrete results obtained for the astrophysical  $S$ -factors of the radiative capture reactions at the lowest energies in the frame of the modified potential cluster model of light atomic nuclei with the classification of the cluster states according to the Young tableaux, which we will consider more thoroughly in the next chapter. In this book the processes of radiative capture for  $p^2H$ ,  $p^3H$ ,  $p^6Li$ ,  $p^7Li$ ,  $p^9Be$ ,  $p^{10}B$ ,  $p^{11}B$ ,  $p^{12}C$ ,  $p^{13}C$ ,  $p^{14}C$ ,  $p^{15}N$ , as well as  $^2H^4He$ ,  $^3H^4He$ ,  $^3He^4He$  and  $^4He^{12}C$  systems will be considered and it will be shown that this approach gives the possibility to describe the experimental data in the range of ultralow energies comparatively well, when the errors of extracted experimental phase shifts of the elastic scattering have the minimal values. In addition, in cases of certain systems, it is even possible to predict the behavior of the astrophysical  $S$ -factors at the energies lower than 100÷200 keV.

The model representations, i.e., physical models of the atomic nuclear and mathematical calculation methods including numerical methods and algorithms, will be described in detail in the beginning of the next chapter. The certain justification of the cluster model in terms of nuclear shell model will be done; it allows one to obtain good results during the description of the properties of certain light nuclei and gives the mathematical apparatus further used in part in the MPCM with FSs.

## **2. MODEL AND CALCULATION METHODS**

---

### ***Introduction***

The experimental data on cross sections of nuclear reactions are the main source of information on the cluster structure of the nucleus and the properties and mechanisms of interaction between nuclei and their fragments. However, the nuclear-astrophysical experimental studies of reactions are complicated by the fact that the interaction energy of matter in stars is very low, from tenths to tens of kiloelectronvolts. In laboratory conditions, it is practically impossible to perform direct measurements of cross sections of nuclear reactions necessary for astrophysical calculations at such energies, with rare exceptions. Usually cross sections are measured at higher energies and then the obtained results are extrapolated to the energy range of interest for nuclear astrophysics [1].

However, as a rule, the real measurements are related to rather high energy (0.2÷1 MeV) as compared to stellar energy; therefore, simple linear extrapolation of experimental data to the astrophysical energy range is not always justified. Moreover, the interval of experimental errors in measured total radiative capture cross sections or the astrophysical  $S$ -factor at 3÷300 keV in different systems reaches 100%, which highly depreciates results of such extrapolation of experimental data.

Therefore, in many cases only theoretical predictions can fill a gap in experimental information on characteristics of astrophysical fusion reactions [1]. During recent years, due to essential progress in the chiral effective theory of hadron interactions, strict microscopic calculations with realistic nucleon interaction potentials have become possible. At low energies the chiral perturbation theory makes it possible to take into account in a unified way both two-nucleon and multinucleon interactions with controlled accuracy [11], which provides true microscopic calculations of characteristics of few-nucleon systems.



However, due to technical complexity of such calculations the scattering problem is mainly limited by three-nucleon systems, which are considered based on solution of the Faddeev equations [12]. Four-nucleon calculations in the continuous spectrum at low energies based on the Faddeev–Yakubovsky equations [13] in the AGS form [14] with the realistic NN potentials and account of Coulomb interaction were published just in the last years [15,16]. It is expected, in these articles, that the calculation accuracy is as high as for three-nucleon systems, so that the deviation of the theory from experiment can be considered as a critical test for two- and multi-nucleon forces.

Systems with a large number of nucleons in the continuous spectrum are examined based on different microscopic methods, such as the resonating group method (RGM) [17], no-core shell-model [18], and their combinations [19], as well as variational methods (VM) with different bases [20]. Most of these methods are reduced to very cumbersome multichannel calculations, which have an accuracy that cannot always be reliably determined.

In this situation, upon investigation of the astrophysical aspects of nuclear physics, the application of realistic and relatively simple from the practical point of view models, for example the MPCM is quite justified. Usually calculations performed based on model ideas are compared with available low-energy experimental data, and as a result, those approaches that result in the best agreement with experiment are selected.

Furthermore, calculations for astrophysical energies are performed based on the selected approaches and conceptions. Results on astrophysical  $S$ -factors – for example, for reactions of radiative capture – obtained in this case, can be considered as an estimate of corresponding values that is more realistic than simple extrapolation of experimental data. Since, the applied theoretical model, as a rule, has a quite reasonable microscopic justification in terms of nuclear physics.

The knowledge of the wave function of relative motion of nuclear particles taking parts in collisions (scattering processes, reactions) or determines the bound state (BS) of nucleus in two-particle channel is needed in such calculations. These functions can be obtained from the solutions of the Schrödinger equation for each concrete physical problem in discrete or continuous spectrum, if the interaction potential of these

particles is known.

The nuclear interaction potential of particles (in scattering problems, i.e., continuous spectrum or bound states – discrete spectrum) is wittingly unknown and, in principle, its directly determination by currently familiar methods is not seemed to be possible. Therefore, the certain form of its dependence from the distance is chosen (for example Gaussian or exponential), and, by certain nuclear characteristics (usually these are phase shifts of nuclear scattering or binding energy and charge radius for bound states), the parameters of the potential are fixed so that to describe these characteristics. In future, such potential can be used for the calculations of any other nuclear properties, for example, formfactors of the bound states or cross sections of different reactions [21,22].

Thus, practically all range of nuclear physics problems requires the ability to solve the Schrödinger equation with the specified potential and with certain initial and asymptotic conditions. In principle, this is purely mathematical problem in the field of mathematical modeling of physical processes and systems.

One can solve the Schrödinger equations for bound and scattering states using the Runge-Kutt method or finite-difference method [23,24]. Such methods quite allow us to find eigen wave functions and self-energies of quantum system. The obtaining of the wave function is appreciably simplified if one uses the combination suggested by us, of numerical and variational methods with the accuracy control of equation solution with the help of residuals [25] or uses the alternative solution method of the integrated matrix eigenvalue problem. These methods will be briefly stated bellow – see, for example, sec. 2.7 and more detailed description can be found in the book [26].

Consequently, numerous nuclear characteristics are calculated on the basis of obtained solutions, i.e. wave functions of the nucleus, which are the solutions of the initial equations, including phase shifts of scattering and binding energies of atomic nuclei in cluster channels, different characteristics of nuclear and thermonuclear reactions, for example, total cross sections or astrophysical  $S$ -factors etc.

The model, using here, is constructed based on the assumption that the considered nuclei have a two-cluster structure. The choice of this model is determined by the fact that, in many light atomic nuclei, the probability of

formation of nucleon associations (clusters) and the degree of separation from each other are rather high. This is proved by multiple experimental data and theoretical calculations obtained during the last 60 years [21].

For construction of phenomenological potentials of intercluster interaction, the results of phase shift analysis of experimental data on differential cross sections of elastic scattering of corresponding free nuclei are used [27,28]. As a rule, the main contribution in expansion over orbital angular moments for energies below 1 MeV is made by the  $S$ -wave only; therefore, the data on differential cross sections measured at  $8\div 10$  scattering angles, i.e., angular distribution, provides rather complete and accurate phase shift analysis.

The interaction potentials in the framework of the formally two-body scattering problem are chosen from the condition of the best description of obtained phase shifts. In this case, for the considered nucleon system, the many-body character of the problem is taken into account by separation of the single-particle levels of this potential into Pauli-allowed and Pauli-forbidden states. For the lightest atomic nuclei ( $A < 4$ ), the MPCM in which the orbital states are split according to Young tableaux is used. The extended description of this approach you can see in [29,30] and in this section of the book. In the applied model, due to its formally two-body character and potentials obtained on the basis of phase shifts of elastic scattering, it is possible to rather easily calculate the required nuclear characteristics, for example, total cross sections of photonuclear reactions and astrophysical  $S$ -factors practically for any, even the lowest, energies.

## ***2.1 Cluster model***

The considered potential cluster model is rather simple in application, since technically it comes to solution of the two-body problem, or, which is equivalent, to the problem of one body in the field of a force center. Therefore, an objection can be put forward that this model is absolutely inadequate to the many-body problem to which the problem of description of properties of the system consisting of  $A$  nucleons is related.

In this regard, it should be noted that one of the successful models in the theory of atomic nucleus is the model of nuclear shells (SM) that mathematically represents the problem of one body in the field of a force

center. The physical grounds of the potential cluster model considered here trace to the shell model or, more precisely, in a surprising connection between the shell model and the cluster model, which is mentioned in the literature as the nucleon association model (NAM) [6,18].

In the NAM and PCM, the wave function (WF) of the nucleus consisting of two clusters with the numbers of nucleons  $A_1$  and  $A_2$  ( $A = A_1 + A_2$ ) has the form of antisymmetrized product of totally antisymmetric internal wave functions of clusters  $\Psi(1, \dots, A_1) = \Psi(R_1)$  and  $\Psi(A_1 + 1, \dots, A) = \Psi(R_2)$  multiplied by the wave function of their relative motion  $\Phi(R = R_1 - R_2)$

$$\Psi = \hat{A} \{ \Psi(R_1) \Psi(R_2) \Phi(R) \} , \quad (2.1)$$

where  $\hat{A}$  is the operator of antisymmetrization under permutations of nucleons belonging to different clusters,  $R$  is the intercluster distance,  $R_1$  and  $R_2$  are the radius vectors of the position center mass of clusters.

Usually cluster wave functions are chosen in such a way that they correspond to ground states of nuclei consisting of  $A_1$  and  $A_2$  nucleons. These shell wave functions are characterized by specific quantum numbers, including Young tableaux  $\{f\}$ , which determine the permutation symmetry of the orbital part of cluster relative motion WF.

The most important thing, in the model considered in this study, is the rule of calculation of the number of nodes of the wave function of cluster relative motion in the ground state of the nucleus. In the oscillatory shell model for nuclei of  $1p$ -shell in the system of  $A \leq 16$  nucleons there are  $A - 4$  oscillatory excitation quanta [21]. In the total wave function of the nucleus, these oscillatory quanta can be relocated in a random order between states of internal cluster motion (forming excited clusters) and the state of their relative motion. For ground states of clusters in the nucleus interior with the minimal number of excitation quanta compatible with the Pauli principle for the given number of nucleons  $A_1$  or  $A_2$  the number of excitation quanta  $N$  per relative motion is maximal and is determined by the following relation, named as oscillatory rule

$$N = (A - 4) - N_1 - N_2 . \quad (2.2)$$

Here,  $N_1 = A_1 - 4$ , if  $A_1 > 4$ , and  $N_1 = 0$ , if  $A_1 \leq 4$ , and similar  $N_2 = A_2 - 4$ , if  $A_2 > 4$ , and  $N_2 = 0$ , if  $A_2 \leq 4$ . The value of  $N$  determines the number of nodes of the wave function of relative cluster motion and depends on the orbital angular momentum of relative motion  $L$  [21].

The next step is that this oscillatory rule is transferred to the realistic cluster model of the nucleus in which clusters are isolated, i.e., the oscillatory parameters of the clusters  $\hbar\omega_1$  and  $\hbar\omega_2$  do not coincide with the oscillatory parameter of the wave function of relative motion  $\hbar\omega_3$ . However, the cluster isolation that takes place in real cluster nuclei makes it possible to neglect the action of the operator of antisymmetrization in Eq. (2.1) in the first approximation, without rejecting oscillatory rule (2.2) for ground states of clusters.

Assuming this rule for nonoscillatory wave functions, we find that the realistic (nonoscillatory) cluster interaction potential in the corresponding partial wave  $L$  should be sufficiently deep. It is necessary, along with the “ground” (energy lowest) nodeless state and the given state with the number of nodes  $v$  “locate” all levels with a smaller number of nodes upon solution of the Schrödinger equation, i.e., from  $v = -1$  to 1.

This conclusion suggests the idea of Pauli-forbidden states in the cluster model: all levels with a number of nodes smaller than  $v$  that occur in the two-body problem describing cluster relative motion correspond to the number of oscillatory quanta which is smaller than the minimal Pauli-allowed number  $N$ . Therefore, the total wave functions (2.1) with these functions of relative motion vanish in the case of antisymmetrization over all  $A$  nucleons. The ground state of this cluster system, i.e. really existed bound state in this potential, is described by the wave function with nonzero; in the general case, the number of nodes determined from the relation (2.2). But to this effect, in this book, we will use the Young tableau technique, which we will state latter and which will apply at the consideration of different cluster systems, as more general, against (2.2), cluster state classification method.

For preliminary example of utilization of this method, let us consider the classical two-cluster system of the  ${}^6\text{Li}$  nucleus, where the  ${}^4\text{He}$  and  ${}^2\text{H}$  clusters are in the states with Young tableaux  $\{4\}$  and  $\{2\}$ , respectively. The outer product of these Young tableaux yields  $\{4\} \times \{2\} = \{6\} + \{51\} + \{42\}$ . The Young tableaux  $\{6\}$  and  $\{51\}$  correspond to the shell

configurations  $s^6$  and  $s^5p^1$  with orbital moments 0 and 1 are Pauli-forbidden, because it is impossible to be more than four nucleons at the  $s$ -shell [25]. The Young tableau  $\{42\}$  with  $L = 0, 2$  corresponds to the ground state of the nucleus and the allowed configuration  $s^4p^2$ . It contains one forbidden state in the  $S$ -wave, which means that there is one node in the wave function of cluster relative motion at  $L = 0$ .

Thus, the idea of Pauli-forbidden states makes it possible to take into account the many-body character of the problem in terms of interaction potential between clusters. In this case, in practice, the interaction potential is chosen in order to describe the experimental data (scattering phase shifts) on elastic cluster scattering in the corresponding  $L$  partial wave and preferably in the state with one particular Young tableau  $\{f\}$  for the spatial part of the wave function of  $A$  nucleons.

However, the results of the phase shift analysis in the limited energy range, as a rule, prevent unambiguous reconstruction of the interaction potential, especially for nonresonance phase shifts that usually correspond to the BSs of nuclei. Therefore additional requirement for construction of the intercluster BS potential is the demand on its basis the representation of the binding energy of nucleus in the corresponded cluster channel and description of some other static nuclear characteristics. For example, the binding energy, the charge radius, the asymptotic constant etc. are considered; meanwhile, the characteristics of the bound clusters in the nucleus are identified to the characteristics of the corresponded free nuclei [31].

Thereby, the potentials for the BSs of clusters are constructed, in the first place, on the assumption requirement of the description of the basic characteristics of such state. In this case the parameters of these potentials according to known characteristics of the ground states (GSs) of nuclei are fixed quite definitely. However, this additional requirement, obviously, is an idealization of the real situation that exists in the nucleus, since it assumes that in the ground state the nucleus has 100% clusterization. Therefore, the success of this potential model, in description of a system of  $A$  nucleons in the bound state, is determined by the fact how much is the real clusterization of this BS of nucleus in the  $A_1 + A_2$  nucleons.

It is remarkable that the model does not require the knowledge of details of the  $NN$  interaction. In this model, the  $NN$  interaction is

manifested, similarly to the shell model, in creation of the mean nuclear field, and provides clusterization of the nucleus. The remaining “work” on formation of the necessary number of nodes of the wave function of cluster relative motion is executed by the Pauli principle. Therefore, it should be expected that the domain of applicability of the considered model is limited by nuclei with pronounced cluster properties.

However, some nuclear characteristics of particular, even non-cluster, nuclei can be mainly determined by one specific cluster channel and the small contribution of other possible cluster configurations. In this case, the applied single-channel cluster model makes it possible to identify the dominating cluster channel and separate those properties of the cluster system that are determined by this channel [31].

## 2.2 Astrophysical *S*-factors

Astrophysical *S*-factors characterize the behavior of a cross section of nuclear reactions at an energy tending to zero and are determined as follows [32]

$$S(NJ, J_f) = \sigma(NJ, J_f) E_{\text{cm}} \exp \left( \frac{31.335 Z_1 Z_2 \sqrt{\mu}}{\sqrt{E_{\text{cm}}}} \right), \quad (2.3)$$

where  $\sigma$  is the total cross section of the radiative capture process in barn,  $E_{\text{cm}}$  is the particle energy in the center of mass system in kiloelectronvolts,  $\mu$  is the reduced mass of particles in the entrance channel in atomic mass units,  $Z_{1,2}$  are the particle charges in units of elementary charge, and  $N$  are  $E$  or  $M$  transitions with  $J$  multipolarity to the final  $J_f$  state of the nucleus. The numerical coefficient of 31.335 was obtained based on modern values of fundamental constants [33].

The rapidly variable exponential factor specified by the Coulomb barrier is evidently segregated in the given expression for the *S*-factor reaction. Thus, the changing of the *S*-factor value is too slowly than cross section changes, in the case of nonresonance reactions by energy change. Such cross section binary fission

$$\sigma(NJ, J_f) = S(NJ, J_f) P(E)$$

substantially simplifies analysis of the behavior of the astrophysical  $S$ -factor in dependence of energy, even in the resonance region, and usually applies in the range of low and ultralow energies.

The total radiative capture cross sections in the cluster model are given, for example, in [34] or [30] and are written as

$$\sigma(E) = \sum_{J, J_f} \sigma(NJ, J_f) , \quad (2.4)$$

$$\begin{aligned} \sigma_c(NJ, J_f) = & \frac{8\pi K e^2}{\hbar^2 q^3} \frac{\mu}{(2S_i + 1)(2S_2 + 1)} \frac{J + 1}{J[(2J + 1)!!]^2} \times \\ & \times A_J^2(NJ, K) \sum_{L_i, J_i} P_J^2(NJ, J_f, J_i) I_J^2(J_f, J_i) \end{aligned}$$

where for electric orbital  $EJ(L)$  transitions with  $J$  multipolarity the next simple expressions are known [22,34] ( $S_i = S_f = S$ )

$$A_J(EJ, K) = K^J \mu^J \left( \frac{Z_1}{m_1^J} + (-1)^J \frac{Z_2}{m_2^J} \right) , \quad (2.5)$$

$$I_J(J_f, J_i) = \langle \chi_f | R^J | \chi_i \rangle .$$

$$\begin{aligned} P_J^2(EJ, J_f, J_i) = & \delta_{S_i S_f} \left[ (2J + 1)(2L_i + 1)(2J_i + 1)(2J_f + 1) \right] \times \\ & \times (L_i 0 J 0 | L_f 0)^2 \left\{ \begin{matrix} L_i & S & J_i \\ J_f & J & L_f \end{matrix} \right\}^2 \end{aligned}$$

Here,  $q$  is the wave number of particles in the entrance channel;  $L_f, L_i, J_f$  and  $J_i$  are the angular moments of particles in the entrance ( $i$ ) and exit ( $f$ ) channels;  $S_1$  and  $S_2$  are the spins;  $m_1, m_2, Z_1, Z_2$  are the masses and charges of the particles in the entrance channel, respectively;  $K$  and  $J$  are the wave



number and angular moment of  $\gamma$ -quantum in the exit channel; and  $I_J$  is the integral over wave functions of the initial  $\chi_i$  and final  $\chi_f$  states as a function of relative cluster motion with the intercluster distance  $R$ . The above expressions for total cross sections sometimes include the spectroscopic factor  $S_f$  of the final state of the nucleus; however, in the potential cluster model we used it is equal to unity, similarly to [34].

For examination of the magnetic  $M1(S)$  transition caused by the spin part of the magnetic operator using expressions from [35] one can obtain ( $S_i = S_f = S$ ,  $L_i = L_f = L$ ) the form

$$P_1^2(M1, J_f, J_i) = \delta_{S S_f} \delta_{L_i L_f} \left[ S(S+1)(2S+1)(2J_i+1)(2J_f+1) \right] \times$$

$$\times \left\{ \begin{matrix} S & L & J_i \\ J_f & 1 & S \end{matrix} \right\}^2$$

$$A_1(M1, K) = i \frac{\hbar K}{m_0 c} \sqrt{3} \left[ \mu_1 \frac{m_2}{m} - \mu_2 \frac{m_1}{m} \right], \quad (2.6)$$

$$I_J(J_f, J_i) = \langle \chi_f | R^{J-1} | \chi_i \rangle, \quad J = 1.$$

where  $m$  is the mass of the nucleus;  $\mu_1$  and  $\mu_2$  are cluster magnetic moments taken from [36], and, for example, for  $\mu_{2H} = 0.857\mu_0$  and  $\mu_P = 2.793\mu_0$ ;  $\mu_0$  is the nuclear magneton.

The expression in square brackets in (2.6) for  $A_1(M1, K)$  has been obtained on the assumption that, in the general form, for the spin part of the magnetic operator [37]

$$W_{J_m}(S) = i \frac{e\hbar}{m_0 c} K^J \sum_i \mu_i \hat{S}_i \cdot \vec{\nabla}_i (r_i^J Y_{J_m}(\Omega_i))$$

summation by  $r_i$ , i.e., by the center of mass coordinates of clusters, relative to the common center of mass of nucleus, is held before the action of the  $\nabla$ -nabla operator which acts on the expression in brackets ( $r_i^J Y_{J_m}(\Omega_i)$ ) and

leads to decrease of  $r_i$  degree [35]

$$\vec{\nabla}_i(r_i^J Y_{Jm}(\Omega_i)) = \sqrt{J(2J+1)} r_i^{J-1} \vec{\nabla}_i(r_i^{J-1} Y_{Jm}(\Omega_i)) .$$

In this case the coordinates  $r_i$  are  $R_1 = m_2/mR$  and  $R_2 = -m_1/mR$ , where  $R$  is the relative intercluster distance and  $R_1$  and  $R_2$  are the distances from the common center of mass to the centers of mass of each cluster. The operator of electromagnetic transitions for radiation interaction with matter, in electromagnetic processes like radiative capture or photodecay, is well-known [37].

Therefore, there is a fine possibility for clearing the form of two-body strong interaction in the initial channel, when they are in continuous spectrum and in bound states of the same particles in the final channel, i.e., in states in their discrete spectrum.

### **2.3 Potentials and wave functions**

The intercluster interaction potentials for each partial wave, i.e., for the given orbital angular momentum  $L$ , and point-like Coulomb term, were represented as (further, the only nuclear part of potential is given)

$$V(R) = V_0 \exp(-\alpha R^2) + V_1 \exp(-\gamma R) \quad (2.7)$$

or

$$V(R) = V_0 \exp(-\alpha R^2) \quad (2.8)$$

Here, parameters  $V_1$  and  $V_0$  (dim.: MeV),  $\alpha$  and  $\gamma$  (dim.: fm<sup>-2</sup> and fm<sup>-1</sup>, correspondingly) are the potential parameters found from experimental data under the constraint of best description of elastic scattering phase shifts extracted in the course of phase shift analysis from the experimental data of the differential cross sections, i.e. angular distributions or excitation functions.

In some cases, the Coulomb potential includes the Coulomb radius  $R_{\text{Coul}}$  and then the Coulomb potential takes the form

$$V_{\text{Coul}}(r) = \frac{2\mu}{\hbar^2} \begin{cases} \frac{Z_1 Z_2}{r} & r > R_{\text{Coul}} \\ Z_1 Z_2 \left( 3 - \frac{r^2}{R_{\text{Coul}}^2} \right) / 2R_{\text{Coul}} & r < R_{\text{Coul}} \end{cases}.$$

In the variational method, the expansion of wave function of cluster relative motion in non-orthogonal Gaussian basis was used, and independent parameter variation was performed. The wave function itself has the form [22]

$$\Phi_L(R) = \frac{\chi_L(R)}{R} = R^L \sum_i C_i \exp(-\beta_i r^2), \quad (2.9)$$

where  $\beta$  are the variational parameters and  $C$  are the expansion coefficients [26].

The behavior of the wave function of bound states, including ground states of nuclei in cluster channels at large distances, is characterized by the asymptotic constant  $C_W$  determining by the Whittaker constant of the form [38]

$$\chi_L(R) = \sqrt{2k_0} C_W W_{-\eta L+1/2}(2k_0 R), \quad (2.10)$$

where  $\chi_L(R)$  is the numerical wave function of the bound state obtained from the solution of the radial Schrödinger equation and normalized to unity;  $W_{-\eta L+1/2}$  is the Whittaker function of the bound state determining the asymptotic behavior of the wave function which is the solution to the same equation without the nuclear potential; i.e., at large distances  $R$  having the form [26] (see Attachment 1);  $k_0$  is the wave number caused by the channel binding energy of systems;  $\eta$  is the Coulomb parameter; and  $L$  is the orbital angular moment of the bound state.

Asymptotic constant (or asymptotic normalization coefficient) is an important nuclear characteristic. In many cases the knowledge of its value for the  $a$  nucleus in the  $b + c$  channel determines the value of the astrophysical  $S$ -factor of the radiative  $b(c,\gamma)a$  capture process [39]. The asymptotic constant is proportional to the nuclear vertex constant for the

virtual  $a \rightarrow b + c$ , which is the matrix element of this process at the mass surface [40].

The root-mean-square mass radius of the nucleus in the cluster model for the system of two correctly sized clusters was determined as

$$R_m^2 = \frac{m_1}{m} \langle r_m^2 \rangle_1 + \frac{m_2}{m} \langle r_m^2 \rangle_2 + \frac{m_1 m_2}{m^2} I_2 ,$$

where  $\langle r_m^2 \rangle_{1,2}$  are the squared mass radii of clusters, which are taken equal to the radii of corresponding nuclei in the free state and  $I_2$  is the integral of the form

$$I_2 = \langle \chi_L(R) | R^2 | \chi_L(R) \rangle ,$$

for the intercluster distance  $R$  over radial wave functions  $\chi_L(R)$  of relative cluster motion normalized to unity in the ground state of the nucleus with the orbital angular momentum  $L$ .

The root-mean-square charge radius was written as

$$R_z^2 = \frac{Z_1}{Z} \langle r_z^2 \rangle_1 + \frac{Z_2}{Z} \langle r_z^2 \rangle_2 + \frac{(Z_2 m_1^2 + Z_1 m_2^2)}{Z m^2} I_2 ,$$

where  $\langle r_z^2 \rangle_{1,2}$  are the squared charge radii of clusters which are also taken equal to the radii of corresponding nuclei in the free state,  $Z = Z_1 + Z_2$ , and  $I_2$  is the above integral.

The wave function  $\chi_L(R)$  of the relative cluster motion is the solution to the radial Schrödinger equation of the form

$$\chi''_L(R) + [k^2 - V(R) - V_{\text{Coul}}(R) - L(L+1)/R^2] \chi_L(R) = 0 .$$

where  $V(R)$  is intercluster potential (2.7) or (2.8) with the dimension  $\text{fm}^{-2}$ ;  $V_{\text{Coul}}(R)$  is the Coulomb potential; and  $k$  is the wave number determined by the energy  $E$  of particle interaction,  $k^2 = \frac{2\mu E}{\hbar^2}$ .

## **2.4 Numerical mathematical methods**

Finite-difference methods (FDM), which are the modification of methods [40] and take into account Coulomb interactions; variational methods for solution of the Schrödinger equation; and other numerical methods used in these calculations of nuclear characteristics were described in detail in [24]. Therefore, here we mention briefly the main issues connected with general and numerical methods of calculation.

In all calculations using finite-difference and variational methods [22] at the boundary of the region in which the asymptotic constant becomes steady, i.e., approximately  $10\div 20$  fm, the numerical or variational wave function was replaced by Whittaker function (2.10) taking into account the asymptotic constant found earlier. Numerical integration in any matrix elements was performed from 0 to  $25\div 30$  fm. Simpson's method [42] was used; this method yields good results for smooth and weakly oscillating functions provided that several hundred steps per period are given [26].

Computer programs based on the finite-difference method [22,26] were rewritten for these calculations; for calculation of total radiative capture cross sections and characteristics of bound states of nuclei programs were rewritten from TurboBasic to Fortran-90, a more advanced computer language that possesses much broader capabilities. This made it possible to essentially increase the accuracy of all calculations, including the nuclear binding energy in the two-body channel [3]. Now, for example, the accuracy of calculation of Coulomb wave functions for scattering processes controlled by the value of Wronskian (see Attachment 1) and the accuracy of finding the root of the determinant in finite-difference method [26] that determines the accuracy of finding the binding energy are of the order of  $10^{-14}\div 10^{-20}$  and the real absolute accuracy of determination of binding energy in the finite-difference method for different two-body systems was  $10^{-6}\div 10^{-8}$  MeV. The rapidly converging continued fraction representation [43], described in Attachment 1, has been used for calculation of Coulomb wave functions; this representation makes it possible to obtain the values of the functions with high accuracy in a wide range of variables taking modest computing time [44].

The variational program for finding variational wave functions and

binding energies of nuclei in cluster channels has been rewritten in Fortran-90, which made it possible to essentially increase the rate of seeking the minimum of the multiparametric functional determining the binding energy of two-body systems in all considered nuclei [3]. This program, as before, applies the multiparametric variational method with expansion of WF in non-orthogonal Gaussian basis and independent parameter variation. Similar programs, based on multiparametric variational method, were also modified for phase shift analysis in which differential cross sections of elastic scattering of nuclear particles have been used [3].

Exact values of particle masses [36] were determined in all calculations, if there are no special reserves, and the constant  $\hbar^2/m_0$  was taken equal to 41.4686 MeV fm<sup>2</sup>. The Coulomb parameter  $\eta = \mu \cdot Z_1 \cdot Z_2 \cdot e^2 / (q \cdot \hbar^2)$  was represented as  $\eta = 3.44476 \cdot 10^{-2} \cdot Z_1 \cdot Z_2 \cdot \mu / q$ , where  $q$  is the wave number determined by the energy of interacting particles in the entrance channel in fm<sup>-1</sup>. The Coulomb potential for  $R_{\text{Coul}} = 0$  was written as  $V_{\text{Coul}}(\text{MeV}) = 1.439975 \cdot Z_1 \cdot Z_2 / R$ , where  $R$  is the distance between particles in the entrance channel in fermi.

## 2.5 Classification of cluster states

States with minimal spin in the processes of scattering of some light atomic nuclei turn out to be mixed according to Young orbital tableaux, for example, the doublet state p<sup>2</sup>H [29] is mixed according to tableaux {3} and {21}. On the other hand, these states considered as bound ones, for example, the doublet p<sup>2</sup>H channel of <sup>3</sup>He is pure with tableau {3} [29]. Let us put the classification of states of, for example, the p<sup>2</sup>H system according to orbital and spin-isospin Young tableaux and demonstrate how to obtain these results.

In the general case, the possible orbital Young tableau  $\{f\}$  of some nucleus  $A(\{f\})$  consisting of two parts  $A_1(\{f_1\}) + A_2(\{f_2\})$  is the direct outer product of orbital Young tableaux of these parts  $\{f\}_L = \{f_1\}_L \times \{f_2\}_L$  and is determined using the Littlewood's theorem [29]. Therefore, the possible orbital Young tableaux of the p<sup>2</sup>H system, in which tableau {2} is used for <sup>2</sup>H, are the symmetries {3}<sub>L</sub> and {21}<sub>L</sub>.

Spin-isospin tableaux are the direct inner product of spin and isospin

Young tableaux of the nucleus of  $A$  nucleons  $\{f\}_{ST} = \{f\}_S \otimes \{f\}_T$  and for the system with the number of particles not larger than eight are given in [45]. For any of these moments (spin and isospin), the corresponding tableau of the nucleus consisting of  $A$  nucleons, each of which has an angular moment equals  $1/2$ , is constructed as follows: in the cells of the first row, the number of nucleons with the moments pointing in one direction, for example, upward, is indicated. In cells of the second row, if it is required, the number of nucleons with the moments directed in the opposite direction, for example, downward, is indicated. The total number of cells in both rows is equal to the number of nucleons in the nucleus. Moments of nucleons in the first row which have a pair in the second row with the oppositely directed moment are compensated and yield zero total moment. The sum of moments of nucleons of the first row, which are not compensated by moments of nucleons of the second row, yields the total moment of the whole system.

In this case for the  $p^2H$  system and the isospin  $T = 1/2$ , we have  $\{21\}_T$ ; for the spin state with  $S = 1/2$ , we also obtain  $\{21\}_S$ ; and for  $S$  or  $T = 3/2$ , the tableau of the form  $\{3\}_{ST}$ . Upon construction of the spin-isospin Young tableau for the quartet spin state of the  $p^2H$  system with  $T = 1/2$ , we have  $\{3\}_S \otimes \{21\}_T = \{21\}_{ST}$ , and for the doublet state  $\{21\}_S \otimes \{21\}_T = \{111\}_{ST} + \{21\}_{ST} + \{3\}_{ST}$  [45].

The total Young tableau of the nucleus is determined in a similar way as the direct inner product of the orbital and spin-isospin tableau  $\{f\} = \{f\}_L \otimes \{f\}_{ST}$ . The total wave function of the system in the case of antisymmetrization does not identically vanish only if it does not contain the antisymmetric component  $\{1^N\}$ , which is realized upon multiplication of conjugated  $\{f\}_L$  and  $\{f\}_{ST}$ . Therefore, the tableaux  $\{f\}_L$  conjugated to  $\{f\}_{ST}$  are allowed in this channel and all other symmetries are forbidden, since they result in zero total wave function of the system of particles after its antisymmetrization.

This yields that, for the  $p^2H$  system in the quartet channel, only the orbital wave function with the symmetry  $\{21\}_L$  is allowed and the function with  $\{3\}_L$  turns out to be forbidden, since the product  $\{21\}_{ST} \otimes \{3\}_L$  does not result in an antisymmetric component of the wave function. At the same time, in the doublet channel, we have  $\{111\}_{ST} \otimes \{3\}_L = \{111\}$  and

$\{21\}_{ST} \otimes \{21\}_L \sim \{111\}$  [45], and in both cases we obtain the antisymmetric tableau. Therefore, the doublet spin state turns out mixed according to Young orbital tableaux.

In [29] the method for separation of such states according to Young tableaux was proposed and it was shown that the mixed scattering phase shifts can be represented in the form of the half-sum of pure phase shifts  $\{f_1\}$  and  $\{f_2\}$

$$\delta^{\{f_1\}+\{f_2\}} = 1/2(\delta^{\{f_1\}} + \delta^{\{f_2\}}) . \quad (2.11)$$

In this case it is assumed that  $\{f_1\} = \{21\}$  and  $\{f_2\} = \{3\}$  and the doublet phase shifts extracted from the experiment are mixed according to these two tableaux. Then it is assumed that the quartet scattering phase shifts, pure according to orbital Young tableau  $\{21\}$ , can be identified with the pure doublet scattering phase shift  $p^2H$  corresponding to the same Young tableau. Then Eq. (2.11) allows to find the pure doublet  $p^2H$  phase shift with tableau  $\{3\}$  and then construct the pure interaction potential according to Young tableaux that can be used for description of characteristics of the bound state. Similar relations exist for a number of other lightest nuclear systems, for example,  $p^3H$ ,  $^2H^2H$ ,  $^2H^3He$ ,  $p^6Li$ , etc. which are mixed according to Young tableaux and (or) isospin [22], and some of them will be considered in this book later.

## 2.6 Methods of phase shift analysis

If the experimental differential cross sections of elastic scattering are known, certain set of parameters called the scattering phase shifts  $\delta'_{sL}$  can be found, which makes it possible to describe the behavior of these cross sections with a reasonable accuracy. The quality of description of experimental data based on certain theoretical function (functional of several variables) can be estimated using the  $\chi^2$  method represented in [46]

$$\chi^2 = \frac{1}{N} \sum_{i=1}^N \left[ \frac{\sigma'_i(\theta) - \sigma^e_i(\theta)}{\Delta \sigma^e_i(\theta)} \right]^2 = \frac{1}{N} \sum_{i=1}^N \chi_i^2 , \quad (2.12)$$



where  $\sigma^e$  and  $\sigma'$  are the experimental and theoretical, i.e., calculated for some given values of scattering phase shifts  $\delta_{s,L}'$ , elastic scattering cross sections of nuclear particles for the  $i^{\text{th}}$  scattering angle;  $\Delta\sigma^e$  is the error of the experimental cross sections for this angle; and  $N$  is the number of measurements.

The expressions describing differential cross sections are the expansion of some functional  $d\sigma(\theta)/d\Omega$  in a numerical series containing variational parameters. The expansion parameters  $\delta_{s,L}'$  have to be found from the constraint of the best description of the expansion. Since, the expressions for differential cross sections are usually accurate [46], then, if the number of expansion terms  $L$  increases to infinity, the value of  $\chi^2$  should tends to zero. This criterion was used for choosing the specified set of phase shifts resulting in the minimum of  $\chi^2$ , which may be the global minimum of the given multiparametric variational problem [47].

Thus, for example, in the  $p^6\text{Li}$  system, the procedure of minimization of the functional  $\chi^2$  as a function of  $2L + 2$  variables, each being the phase shift  $\delta_L$  of the particular partial wave without spin-orbital splitting, was performed for searching of scattering phase shifts using experimental cross sections. To solve this problem, the minimum of  $\chi^2$  in certain bounded range of values of the variables is sought. However, even in this range, many local minima of  $\chi^2$  with a magnitude of the order of unity can be found. The choice of the lowest of them makes it possible to hope that it will correspond to the global minimum that is the solution to the variational problem under given orbital moment  $L$ . Moreover, the value of this minimum should relatively smoothly decrease with increasing number of partial waves  $L$ .

We used the criteria and methods presented above for phase shift analysis in  $p^6\text{Li}$ ,  $p^{12}\text{C}$ ,  $p^{13}\text{C}$ ,  $p^{14}\text{C}$ , and  $^4\text{He}^{12}\text{C}$  systems at low energies, which are important for astrophysical calculations. The expressions for finding differential cross sections require for carrying out phase shift analysis for the systems mentioned above are presented in the corresponding sections of the book and in work [46].

## **2.7 Generalized matrix eigenvalue problem**

Let us consider, at first, the standard method for solution of the

generalized matrix problem for the Schrödinger equation, which occurs if the non-orthogonal variational method is used in nuclear physics or nuclear astrophysics, and then examine its modification appropriate for solution of this problem in numerical calculations at the up-to-date computer [3,26,48]. For determination of the energy eigenvalue spectrum and eigen wave functions in the variational method upon expansion of wave function in the non-orthogonal Gaussian basis [49], the generalized matrix eigenvalue problem of the next form [50]

$$(H - EL)C = 0, \quad (2.13)$$

where  $H$  is the symmetric Hamiltonian matrix;  $L$  is the matrix of overlapping integrals, which is transformed into the identity matrix  $I$  in the case of using orthogonal basis;  $E$  are the energy eigenvalues; and  $C$  are the eigenvectors of the problem.

Representing the matrix  $L$  in the form of the product of the lower  $N$  and upper  $V$  triangular matrices [50], after simple transformations, we obtain the common eigenvalue problem

$$H'C = EIC', \quad (2.14)$$

where

$$\begin{aligned} H' &= N^{-1}HN^{-1}, \\ C' &= VC, \end{aligned}$$

and  $V^{-1}$  and  $N^{-1}$  inversed to the  $V$  and  $N$  matrices, respectively.

Furthermore, we find the matrices  $N$  and  $V$ , performing triangularization of the symmetric matrix  $L$  [51], for example, using the Khaletskii method [50]. Then we determine the inverse matrices  $N^{-1}$  and  $V^{-1}$ , for example, using the Gauss method, and calculate the elements of the matrix  $H' = N^{-1}HN^{-1}$ . We find the complete diagonal with respect to the  $E$  matrix  $(H' - EI)$  and calculate its determinant  $\det(H' - EI)$  for some energy  $E$ . The energy resulting in the zero determinant is the eigen energy of the problem, and the corresponding vectors  $C'$  are the eigenvectors (2.14). If  $C'$  are known, it is easy to find the eigenvectors of the initial problem  $C$

(2.13), since the matrix  $V^{-1}$  is already known. The described method of reduction of the generalized matrix problem to the common matrix problem is called the Schmidt orthogonalization method [52].

In two-body problems for light atomic nuclei with one variational parameter  $\beta_i$  in variational wave function (2.9), this method is rather stable and makes it possible to obtain reasonable results. However, in the three-body nuclear system, when the variational wave function is represented in the form [22]

$$\Phi_{l,\lambda}(r, R) = r^\lambda R^l \sum_i C_i \exp(-\delta_i r^2 - \beta_i R^2) = \sum_i C_i \Phi_i, \quad (2.15)$$

for some values of two variational parameters  $\delta_i$  and  $\beta_i$ , the method for finding inverse matrices sometimes results in instability and overflow upon running the computer program [53], which is a certain trouble for solution of tasks of this type.

Therefore, an alternative method for numerical solution of the generalized matrix eigenvalue problem free from the difficulties indicated above with enhanced computer performance can be proposed. That is to say that initial matrix Eq. (2.13) is the homogeneous system of linear equations and has nontrivial solutions only if its determinant  $\det(H - EL)$  is equal to zero. For computer numerical methods, it is not necessary to expand the matrix  $L$  into triangular matrices and find the new matrix  $H'$  and new vectors  $C'$  by determining inverse matrices, as was described above using the standard method.

It is possible to expand the nondiagonal symmetric matrix  $(H - EL)$  into triangular matrices and seek energies resulting in zero determinant, i.e. eigen energies, using numerical methods in the given domain. In the real physical problem it is not necessary to seek all eigenvalues and eigen energies, but only one or two eigenvalues for the system energy and corresponding wave functions have to be found.

Therefore, the initial matrix  $(H - EL)$  can be expanded into two triangular matrices using, for example, the Khaletskii method, in such a way that the main diagonal of the upper triangular matrix  $V$  contains units,

$$A = H - EL = NV$$

the determinant of this matrix for  $\det(V) = 1$  [50] is calculated

$$D(E) = \det(A) = \det(N) \det(V) = \det(N) = \prod_{i=1}^m n_{ii}$$

and the zero of this determinant is used to find the required energy eigenvalue. Here,  $m$  is the order of the matrices and the determinant of the triangular matrix  $N$  is equal to the product of its diagonal elements.

Thus, we obtain a rather simple problem of finding the zero of a functional of one variable

$$D(E) = 0 ,$$

the solution of this problem does not present great difficulty and can be found to any accuracy, for example, using dichotomy method (method of division in halves).

As a result we eliminate the necessity of finding both inverse to  $V$  and  $N$  matrices, and performing several matrix multiplications in order to first obtain the new matrix  $H'$  and then the finite matrix of eigenvectors  $C$ . Absence of such operations, especially inverse matrices searching, appreciably increase the computer count rate, independently of program language [54].

For estimation of the accuracy of solution, i.e., the accuracy of expansion of the initial matrix into two triangular matrices, residuals [54] for matrix elements can be used. After expansion the matrix  $A$  into two triangular matrices  $NV$ , the residue matrix is calculated

$$T = A - S ,$$

i.e., the difference over all elements of the initial matrix  $A$  and the approximate matrix

$$S = NV ,$$

where  $V$  and  $N$  are the preliminarily found numerical triangular matrices.

As a result, the residue matrix  $T$  yields the deviation of the approximate

quantity  $S$  found numerically from the true value of each element of the initial matrix  $A$ . The method described in this book is used practically in all variational calculations presented below, and the maximal value of any element of the matrix  $T$  does not exceed  $10^{-10}$ .

This method, which seems quite obvious in numerical implementation, made it possible to obtain good stability of the algorithm for solution of the considered problem; it does not result in overflow in the course of running the computer program, since it does not require determination of inverse to  $V$  and  $N$  matrices [56].

Hereby, the introduced alternative method of finding eigenvalues of the generalized matrix problem, considered on the basis of the Schrödinger equation solution using the non-orthogonal variational basis, delivers us from the instabilities appearing during the use of normal solution methods of such mathematical problem, i.e., usual Schmidt orthogonalization method [3,26].

## ***2.8 Construction of the intercluster potentials***

Dwell more thoroughly on the procedure of construction of the intercluster partial potentials used here at the given orbital moment  $L$ , estimating criteria and sequence of parameter finding and pointing to their errors and ambiguities. The parameters of the BS potentials are found in the first place, if they at the given number of the allowed and forbidden states in this partial wave are fixed quite unambiguously according to binding energy, nuclear radius and asymptotic constant in the considered channel [3].

The accuracy of the obtained BS potential parameters is connected, in the first place, with the AC accuracy, which is usually equal to 10÷20%, because the accuracy of the experimental determination of the charged radius usually much higher – 3÷5%. There are no other ambiguities in this potential, because the classification of states according to Young tableaux allows one unambiguously to fix the number of BSs, FSs, or ASs in this partial wave, which completely determine its depth, and the potential width depends wholly from the AC value. The principles of determination the number of FSs and ASs for given partial wave are cited in the previous paragraphs of this section and in work [3].

It is necessary to note here that calculations of the charged radius in any model have model errors, i.e., errors that caused by the accuracy of the model itself. In the MPCM the value of this radius depends from the integral over the model WFs, i.e., the model errors of such functions simply sum. The AC values are determined by the asymptotics of model WFs in one point at their asymptotics and, evidently, have appreciably lower error. Therefore, the BS potentials must be constructed so that, in the first place, maximally agree with the AC values that were obtained on the basis of independent methods, which allow one to extract AC from the experimental data [39].

The intercluster potential of the nonresonance scattering process obtained according to the scattering phase shifts at the given number of BSs, ASs, and FSs in the considered partial wave also constructs quite unambiguously. The accuracy of the determination of this potential connects with, in the first place, the accuracy of phase shift extraction scattering phases from experimental data and can reach 20÷30%. And here this potential does not have ambiguities, because the classification of the states according to Young tableaux allows one unambiguously to fix the number of the BSs, which absolutely determines its depth, and the width of the potential at the given depth is determined by the shape of the scattering phase shift.

At the construction of the nonresonance scattering potential according to data on nuclear spectra in the certain channel, it is difficult to estimate the accuracy of determination of its parameters even at the given number of BSs, though it is possible, evidently, to hope that it a little higher the error in the previous case. This potential, as it is usually supposed for the energy range down to 1 MeV, has to lead to the scattering phase shift approximate to zero or gives the taper shape of the phase shift, because there are no resonance levels in the spectrum of nucleus.

At the analysis of the resonance scattering, when in the considered partial wave at energies down to 1 MeV there is a rather sharp resonance with the width of 10÷50 keV, at the given number of BSs, the potential also constructs completely unambiguously. At the given number of BSs its depth fixes unambiguously according to the resonance energy of the level, and the width is completely determined by the width of such resonance. The error of its parameters usually not exceed the error of width

determination of this level and equals approximately 3÷5%. Meanwhile this applies to the construction of the partial potential according to the scattering phases and to the determination of its parameters by the resonance in nuclear spectra.

Consequently, all potentials have not ambiguities and allow one to describe total cross sections of the radiative capture processes, without involvement of such notation as the spectroscopic factor  $S_f$ , i.e., its value simply to take equal to unit, as it was done in work [34]. In other words, at the consideration of the capture reaction in the MPCM for the potentials matched in the continuous spectrum with the characteristics of scattering process which take into account the resonance shape of the phase shifts and with the characteristics of discrete spectrum describing the basic properties of the BS of nucleus, so there is no necessity to introduce additional term  $S_f$  [34]. Evidently, all available effects in this reaction, including the possibility of the cluster configuration are taking into account at the construction of the interaction potentials.

It becomes possible because the potentials are constructed taking into account the structure of the FSs and on the basis of description observable, i.e., experimental characteristics of interacting clusters in the initial channel and formed in the final state some nucleus, which describing by the cluster structure that consists with initial particles. Thus, the presence of the  $S_f$ , takes into account into the BS cluster wave functions, which become clear on the basis of such potentials by solving the Schrödinger equation.

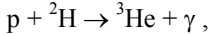
In conclusion we note that at the construction of partial interaction potentials it is taken into consideration that they depend not only from orbital moment  $L$ , but from total spin  $S$  and total moment  $J$  of the cluster system. In other words, we will have different parameter values for different moments  $L, S, J$ . Since, usually the  $E1$  and the  $M1$  transitions between different states  $^{(2S+1)}L_J$  in continuous and discrete spectra are considered, so the potentials of these states will be different [3].

# **3. ASTROPHYSICAL S-FACTOR OF THE PROTON RADIATIVE CAPTURE ON $^2\text{H}$**

---

## ***Introduction***

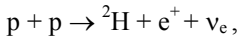
Let us start the immediate consideration of thermonuclear reactions from the radiative capture process



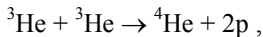
which is the first nuclear reaction of the proton-proton or pp-chain mediating due to the electromagnetic interactions, since  $\gamma$ -quantum takes part in it [57]. This reaction process makes essential contribution into the energy yield of the fusion reactions [58] that, as usually considered, determine the burning of the Sun and stars of our Universe.

Since, interacting nuclear particles of the proton-proton chain have a minimal potential barrier, so the pp-chain is the first chain of nuclear reactions which can take place at lowest energies and, consequently, at stellar temperatures, and there is in all stable stars of the Main Sequence.

As we already say in the first section: the process of the proton radiative capture on  $^2\text{H}$  in the pp-chain is the basic one for the transition from the primordial proton fusion



which takes place due to the weak interactions with the participation of electron neutrino  $\nu_e$ , to one of the final in pp-chain reaction of capture of two nuclei  ${}^3\text{He}$  [59]





which progresses due to the strong nuclear interactions [57].

A detailed study of the reaction of the proton radiative capture on  $^2\text{H}$  from the theoretical and experimental points of view is of fundamental interest not only for nuclear astrophysics, but for the whole nuclear physics of ultralow energies and the lightest atomic nuclei [60]. Therefore, experimental studies of this process are continuing and already at the beginning of 2000<sup>th</sup> year, due to the European project LUNA, new experimental data of the proton radiative capture on  $^2\text{H}$  at energies down to 2.5 keV has appeared. These energies may take place in fusion reactions in the Sun and many stable stars [6]. These experimental results, along with earlier results at greater energies will be used by us in future and will examine more thoroughly in the next paragraphs of this section.

It should be noted that the lightest nuclei with  $A \leq 4$ , strictly speaking, are neither shell nor cluster ones. This follows from microscopic calculations of these nuclei with realistic  $NN$  potentials (see, for example, [61]). For example, in  $^3\text{He}$  along with the  $p^2\text{H}$  cluster configuration, the configuration  $p^2\text{H}^*$  is also present, where  $^2\text{H}^*$  is the spin-singlet deuteron (np pair in  $^1S_0$  state), and spectroscopic factors for common and singlet deuterons are approximately equal to  $S = 1.5$  [62,63]. The channel with singlet deuteron is clearly manifested in the elastic  $p^3\text{He}$  backward scattering both in purely nucleon scattering mechanism [62] and in processes with production of virtual  $\pi$  meson [63].

However, at low energies and low momentum transfers, it is reasonable to apply the considered two-cluster approach to few-nucleon systems with  $A = 3$  and 4, at least to compare results obtained in the frame of the MPCM with multi-body calculations and the MPCM results for systems with  $A > 4$ . In this regard, the using of this approach to such systems, especially for low-energy process analysis, seems quite reasonable.

### ***3.1 Scattering potentials and phase shifts***

Total cross sections of photoprocesses for the lightest  $^3\text{He}$  and  $^3\text{H}$  nuclei in the potential cluster model with FS were considered earlier in [30]. In these calculations for photodisintegration of  $^3\text{He}$  and  $^3\text{H}$  in the  $p^2\text{H}$  and  $n^2\text{H}$

channels,  $E1$  transitions due to the orbital part of the electric operator  $Q_{jm}(L)$  [22] were taken into account. Cross sections of  $E2$  processes and cross sections depending on the spin part of electric operator turned out to be lower by several orders of magnitude. Then it was assumed that electric  $E1$  transitions in the  $N^2H$  system are possible between ground pure according to Young tableau  $\{3\}$  doublet  $^2S$  state of  $^3H$  and  $^3He$  nuclei and doublet  $^2P$  scattering states mixed according to Young tableaux  $\{3\} + \{21\}$ . Such transition is quite possible since the quantum number, connected with Young tableaux, evidently is not saved in electromagnetic processes [29].

Furthermore, for calculation of photonuclear processes in  $p^2H$  and  $n^2H$  systems [3], the nuclear part of the intercluster interaction potential was represented in form (2.7) with the point-like Coulomb term, Gaussian attractive  $V_0$ , and exponential repulsive  $V_1$  parts. The potential of each partial wave was constructed in order to correctly describe the corresponding partial elastic scattering phase [64]. Using these representations the potentials of the  $p^2H$  interaction for scattering processes were obtained; the parameters of these potentials are given in [22,30,65] and in the second and third row of Table 3.1. Then in the doublet channel, mixed according to Young tableaux  $\{3\}$  and  $\{21\}$  [29], as it was shown in the previous section, pure phase shifts (2.11) were separated and based on these phase shifts the pure  $^2S$  potential of the bound state with Young tableau  $\{3\}$  for  $^3He$  in  $p^2H$  channel was constructed [30,65].

Calculations of the  $E1$  transition showed [30] that best results for description of total photodisintegration cross sections for  $^3He$  in the region of  $\gamma$ -quantum energies of  $6\div 28$  MeV, including the maximum value at  $E_\gamma = 10\div 13$  MeV. For this the potential of the  $^2P$  wave for the  $p^2H$  scattering with peripheral repulsion given in Table 3.1 is used. In this case it is assumed that the  $^2S$  interaction in the bound state is pure according to Young tableau  $\{3\}$  and has the Gaussian form with the parameters  $V_0 = -34.75$  MeV,  $\alpha = 0.15$  fm $^{-2}$ . These parameters were obtained based on a correct description of the binding energy (with an accuracy of several kiloelectronvolts) and charge radius of  $^3He$ .

These potentials were used to calculate total radiative cross sections of the proton radiative capture on  $^2H$  and the astrophysical  $S$ -factor at energies down to 10 keV [22,30], although at that time experimental data on the  $S$ -factor for energies above  $150\div 200$  keV only was known [66]. New

experimental data on the  $S$ -factor of the proton radiative capture on  $^2\text{H}$  at energies down to 2.5 keV appeared not long ago [67-69]. Therefore, it is interesting to elucidate whether the potential cluster model based on  $E1$  and  $M1$  transitions is capable of describing new data using the  $^2P$  scattering interaction obtained earlier, the mixed  $^2S$  potential of the bound  $p^2\text{H}$  state from Table 3.1 and the pure, according Young tableaux,  $^2S$  potential of the bound  $p^2\text{H}$  state specified here in the first row of Table 3.1.

**Table 3.1. Potentials of the  $p^2\text{H}$  [30,65] interaction for spin  $S = 1/2$**

$^{2S+1}L, \{f\}$	$V_0$ (MeV)	$\alpha$ (fm <sup>-2</sup> )	$V_1$ (MeV)	$\gamma$ (fm <sup>-1</sup> )
$^2S, \{3\}$	-34.76170133	0.15	—	—
$^2S, \{3\} + \{21\}$	-55.0	0.2	—	—
$^2P, \{3\} + \{21\}$	-10.0	0.16	+0.6	0.1

Our preliminary results [70] showed that the accuracy of calculation of the binding energy for the  $p^2\text{H}$  system of  $^3\text{He}$ , which was at a level of  $1 \div 2$  keV [30], should be substantially increased for calculating the  $S$ -factor at energies about 1 keV. More stringent control of the behavior of the “tail” of the wave function of the bound state at large distances is needed. Moreover, it is necessary to increase the accuracy of calculation of the Coulomb wave functions [26] determining the behavior of asymptotics of the scattering wave scattering functions in the  $^2P$  wave.

Using the capabilities of improved computer programs [3] for more correct description of experimental binding energy of  $^3\text{He}$  in the  $p^2\text{H}$  channel, the parameters of a pure with Young tableau  $\{3\}$  the doublet  $^2S$  potential were specified. This potential (see Table 3.1) became somewhat deeper than that used in [29]; now it results in complete agreement of the experimental ( $-5.4934230$  MeV) [71] binding energy and calculated ( $-5.4934230$  MeV) binding energy obtained with exact values of particle masses [36]. The difference between the potentials given in [30] and Table 3.1 is, first of all, due to the application of the exact masses of particles and more accurate description of binding energy of  $^3\text{He}$  in the  $p^2\text{H}$  channel. For all of these calculations, the absolute accuracy of calculation of the binding energy in our computer program in language Fortran-90 using the finite-difference method

was set on a level of  $10^{-8}$  MeV [3,26].

The charge radius of  $^3\text{He}$  with this potential turns out to be equal to 2.28 fm, which is somewhat larger than experimental data given in Table 3.2 [36,71,72]. It follows from this data that the radius of deuteron cluster is larger than the radius of  $^3\text{He}$ . Therefore, if the deuteron is inside  $^3\text{He}$  as a cluster, for correct description of the  $^3\text{He}$  radius, it should be compressed by approximately 20÷30% of its size in the free state [22,49,73].

**Table 3.2. Experimental masses and charge radii of light nuclei used in these calculations [36,71,72]**

Nucleus	Radius (fm)	Mass (amu)
$^1\text{H}$	0.8768(69)	1.00727646677
$^2\text{H}$	2.1402(28)	2.013553212724
$^3\text{H}$	1.63(3); 1.76(4); 1.81(5) Average 1.73	3.0155007134
$^3\text{He}$	1.976(15); 1.93(3); 1.877(19); 1.935(30) Average 1.93	3.0149322473
$^4\text{He}$	1.671(14)	4.001506179127

In order to control the behavior of wave functions of bound states at large distances, the asymptotic constant  $C_W$  with the asymptotics of the wave function in the form of Whittaker function (2.10) was calculated; the value of this constant in an interval of 5÷20 fm is  $C_W = 2.33(3)$ . The error shown here is determined by averaging the constant over the interval indicated above.

The determination of this constant from experimental data yields values in an interval of 1.76÷1.97 [74-76], which is somewhat lower than the value obtained here. The results of three-body calculations [77] should also be mentioned; in these calculations, good agreement with experiment [78] for the ratio of asymptotic constants of the  $^2S$  and  $^2D$  waves was obtained and the following value was found for the constant  $C_W = 1.878$ . However, in work [38], which was published later than [74-76], the value 2.26(9) is

presented, which agrees quite with our calculations. It can be seen from the data presented in these works that experimental results on asymptotic constants obtained at different times and by different authors scatter considerably. This data is in the range from 1.76 to 2.35 with the mean value of 2.06.

In the cluster two-cluster model, the value of  $C_W$  and charge radius strongly depends on the width of the potential well. Other parameters of the  $^2S$  potential of ground states can always be found, for example,

$$V_0 = -48.04680730 \text{ MeV}, \quad \alpha = 0.25 \text{ fm}^{-2}, \quad (3.1)$$

$$V_0 = -41.55562462 \text{ MeV}, \quad \alpha = 0.2 \text{ fm}^{-2}, \quad (3.2)$$

$$V_0 = -31.20426327 \text{ MeV}, \quad \alpha = 0.125 \text{ fm}^{-2}, \quad (3.3)$$

which yield the same binding energy for  $^3\text{He}$  in the  $p^2\text{H}$  channel. The first of them at an interval of  $5 \div 20$  fm results in the asymptotic constant  $C_W = 1.945(3)$  and the charge radius  $R_{ch} = 2.18$  fm, the second yields the constant  $C_W = 2.095(5)$  and  $R_{ch} = 2.22$  fm, and the third  $C_W = 2.519(3)$  and  $R_{ch} = 2.33$  fm. The cluster radii from Table 3.2 are used in the calculations of charge radii.

It can be seen from these results that potential (3.1) makes it possible to obtain the charge radius that is the closest to experiment value. Further reduction of the potential width may result in correct description of its value; however, it will be shown below that it will not make it possible to reproduce the  $S$ -factor of the proton radiative capture on  $^2\text{H}$ . In this sense potential (3.2), which is characterized by somewhat larger width, has the minimal admissible width of the potential well for which it is possible to obtain an asymptotic constant practically equal to its experimental average value of 2.06 and acceptably describe the behavior of the astrophysical  $S$ -factor in the broadest energy region.

For a complementary check of the determination of the binding energy in two-body channels, the variational method with the expansion of WFs by nonorthogonal Gaussian basis (2.9) and independent parameter variation [26] has been used; this method already made it possible to obtain a binding energy of  $-5.4934228$  MeV

for a grid with a dimensionality of 10 for the pure, according Young tableaux, potential from Table 3.1. The asymptotic constant  $C_w$  of the variational wave function at distances of  $5\div 20$  fm in these calculations was on a level of  $2.34(1)$ , and the residual did not exceed  $10^{-12}$  [26]. The parameters and coefficients of expansion of the radial wave function for this potential of form (2.9) are given in Table 3.3. Under the search of the WF expansion coefficients (2.9)  $C_i$  they determine so that lead to the WF normalization equals 1 [26]. The normalization coefficient  $N$ , shown in this table, determines, per se, the accuracy of search such coefficients in the VM, i.e., the accuracy of normalization of WF to unit.

**Table 3.3. Variational parameters and expansion coefficients of radial wave function of the  $p^2H$  bound state system for potential from Table 3.1. Normalization of function with these coefficients on an interval of  $0\div 25$  fm is  $N = 0.999999997$**

$i$	$\beta_i$	$C_i$
1	2.682914012452794E-001	-1.139939646617903E-001
2	1.506898472480031E-002	-3.928173077162038E-003
3	8.150892061325998E-003	-2.596386495718163E-004
4	4.699184204753572E-002	-5.359449556198755E-002
5	2.664477374725231E-002	-1.863994304088623E-002
6	4.4687619986542310E+001	1.098799639286601E-003
7	8.482112461789261E-002	-1.172712856304303E-001
8	1.541789664414691E-001	-1.925839668633162E-001
9	1.527248552219977E-000	3.969648696293301E-003
10	6.691341326208045E-000	2.097266548250023E-003

The variant of potential (3.2) was also considered in the framework of the variational method; the same binding energy,  $-5.4934228$  MeV, has been obtained for this potential. The variational parameters and coefficients of expansion of the radial wave function are given in Table 3.4.

The asymptotic constant in a range of  $5\div 20$  fm turned out to be equal to  $2.09(1)$ , and the residual was of an order of  $10^{-13}$ . Since the

variational energy decreases with increasing dimensionality of the basis and yields the upper boundary of the true binding energy [79], and the finite-difference energy increases with decreasing step and increasing number of steps [26], an average value of  $-5.4934229(1)$  MeV can be taken as a realistic estimate of the binding energy in this potential. Thus, it may be considered that the error of determination of the binding energy of the  $p^2H$  system in  $^3He$  using two methods based on two different computer programs is  $\pm 0.1$  eV in the given potential.

**Table 3.4. Variational parameters and expansion coefficients of radial wave function of the  $p^2H$  bound state system for potential (3.2). Normalization of function with these coefficients on an interval of  $0 \div 25$  fm is  $N = 0.999999998$**

$i$	$\beta_i$	$C_i$
1	3.485070088054969E-001	-1.178894628072507E-001
2	1.739943603152822E-002	-6.168137382276252E-003
3	8.973931554450264E-003	-4.319325351926516E-004
4	5.977571392609325E-002	-7.078243409099880E-002
5	3.245586616581442E-002	-2.743665993408441E-002
6	5.8379917320454490E+001	1.102401456221556E-003
7	1.100441373510820E-001	-1.384847981550261E-001
8	2.005318455817479E-001	-2.114723533577409E-001
9	1.995655373133832E-000	3.955231655325594E-003
10	8.741651544040529E-000	2.101576342365150E-003

### 3.2 Astrophysical $S$ -factor

In our calculations of the astrophysical  $S$ -factor [60], the energy region of the proton radiative capture on  $^2H$  from 1 keV to 10 MeV was considered and also the  $E1$  transition from the  $^2P$  wave of scattering to the ground  $^2S$  state with  $\{3\}$  and potential parameters listed in Table 3.1. For the  $S(E1)$ -factor for 1 keV, a value of 0.165 eV b was obtained, which is in a quite agreement with the known data including the separation of  $S(0)$ -factor into  $S_s$  and  $S_p$  parts due to  $M1$  and  $E1$  transitions. This

separation was made in [68], where it was obtained that  $S_s(0) = 0.109(10)$  and  $S_p(0) = 0.073(7)$  eV b, which for the total  $S$ -factor should yield  $0.182(17)$  eV b. On the other hand, in the expression for linear interpolation of the total  $S$ -factor, the authors give the following values [68]:  $S_0 = 0.166(5)$  and  $S_1 = 0.0071(4)$  eV b keV<sup>-1</sup>

$$S(E_{\text{cm}}) = S_0 + E_{\text{cm}} S_1 . \quad (3.4)$$

Here  $E_{\text{cm}}$  – energy in the center of mass system (c.m.) and for  $S(0)$  a value of  $0.166(14)$  keV b was given; this value is determined with all possible errors taken into account from the experiment and its extrapolation.

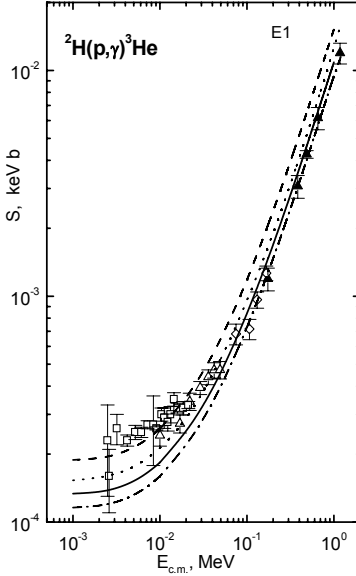
The results obtained with separation of the  $S$ -factor into  $M1$  and  $E1$  parts were given in one of the first papers [66] devoted to astrophysical factors, wherein it was obtained that  $S_s(0) = 0.12(3)$  and  $S_p(0) = 0.127(13)$  eV b for a total  $S$ -factor of  $0.25(4)$  eV b. This data of  $S_s(0)$  value quite coordinate with data given in [68]. Experimental data [69] yield the total astrophysical factor  $S(0) = 0.216(10)$  eV b; this means that the contributions of  $M1$  and  $E1$  differ from the above values [68]. In this paper the following parameters of linear extrapolation (3.4) are given:  $S_0 = 0.216(6)$  eV b and  $S_1 = 0.0059(4)$  eV b keV<sup>-1</sup>, which noticeably differ from the data of [68].

The other known results for the  $S$ -factor obtained from experimental data without separation into  $M1$  and  $E1$  parts yield for zero energy  $0.165(14)$  eV b [80]. Previous results of the same authors yield  $0.121(12)$  eV b [81], and in theoretical calculations [82] the following values were obtained for different models:  $S_s(0) = 0.105$  and  $S_p(0) = 0.08 \div 0.0865$  eV b and the total  $S$ -factor equals to  $0.185 \div 0.192$  eV b. It follows from the given above results that there exists a great ambiguity in the data obtained during the last 10÷15 years. These results make it possible to conclude that, most probably, the value of the total  $S$ -factor at zero energy is in an interval from  $0.109$  eV b [81] to  $0.226$  eV b [69].

The average of these values yields an  $S$ -factor equal to  $0.167(59)$  eV b, which quite agrees with that obtained here based on  $E1$  transition. Our calculations of the  $S$ -factor of the proton radiative capture on  $^2\text{H}$  for the

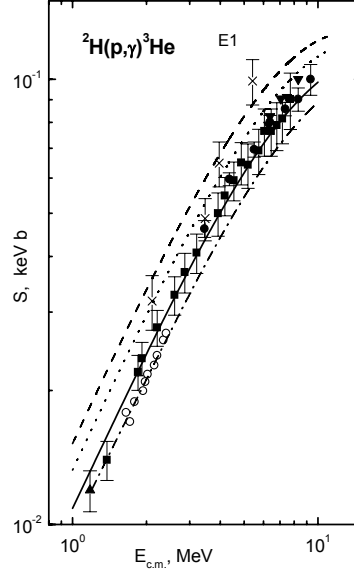


potential given in Table 3.1 at energies from 1 keV to 10 MeV are shown in Figs. 3.1 and 3.2 with dotted lines. The obtained  $S$ -factor rather well reproduces new experimental data at energies of 10÷50 keV [68], and at lower energies the calculated curve is within the interval of experimental errors of [69].



With kind permission of the European Physical Journal (EPJ)

Fig. 3.1. Astrophysical  $S$ -factor of the proton radiative capture on  $^2\text{H}$  in a range of 1 keV÷1 MeV for  $E1$  transition. Curves show calculations with potentials given in the text. Triangles show experiment [66], open rhombs [67], open triangles [68], and open squares [69].



With kind permission of the European Physical Journal (EPJ)

Fig. 3.2. Astrophysical  $S$ -factor of the proton radiative capture on  $^2\text{H}$  in a range of 1÷10 MeV for  $E1$  transition. Curves show calculations with potentials given in the text. Upward triangles show experiment [66], squares [83], points [84], crosses [85], downward triangles [86], and circles [87].

The solid lines in Figs. 3.1 and 3.2 show the results for potential (3.2), which reproduces the behavior of the  $S$ -factor at energies of 50 keV÷10 MeV somewhat better and for 1 keV yields  $S_p = 0.135$  eV b. For 20÷50 keV, the calculated curve follows the lower boundary of errors [68], and below 10 keV it falls into the interval of experimental errors of the project LUNA obtained most recently [69]. The value of the

$S$ -factor obtained at zero energy with this potential agrees well with data [66] for electric  $E1$  transition  $S_p(0)$ .

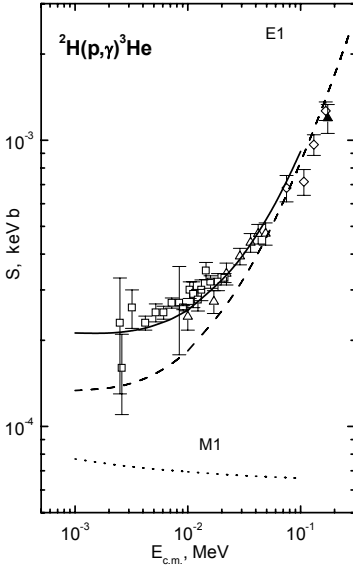


Fig. 3.3. Astrophysical  $S$ -factor of the proton radiative capture on  $^2\text{H}$  in a range of  $1\text{ keV} \div 0.3\text{ MeV}$  for  $E1$  and  $M1$  transitions. Curves show calculations with potentials given in the text. Triangles show experiment [66], open rhombs [67], open triangles [68], and open squares [69].

comes to no more than  $0.005\text{ eV b}$ ; this quantity can be assumed for the error of determination of the calculated  $S$ -factor for zero energy and accept that it equals  $0.135(5)\text{ eV b}$ .

At low energies, the  $M1$  transition from the  $^2S$  scattering state mixed according to Young tableaux to the bound  $^2S$  state of  $^3\text{He}$  in the  $p^2\text{H}$  channel, pure for orbital symmetry can give contribution to the total astrophysical  $S$ -factor. For these calculations we used expressions (2.4) and (2.6), the doublet  $^2S$  potential of scattering states with parameters given in Table 3.1 [22,65,88] and the ground state  $^2S$  potential (3.2).

The results of calculations of the  $M1$  process at  $1 \div 100\text{ keV}$  are shown in Fig. 3.3 by the dotted line at the bottom of the figure and the results of the  $E1$  transition for the GS potential with the parameters (3.2) are presented by the dashed curve, which shown in Fig. 3.1 by the solid line.

The dashed lines in Figs. 3.1 and 3.2 show the results for potential (3.3), and the dash-dotted line, for potential (3.1). It can be assumed based on these calculations that the best results are obtained for bound state potential (3.2), which describes experimental data in the broadest energy interval. It provides a certain compromise in description of the asymptotic constant, charge radius, and astrophysical  $S$ -factor of the proton radiative capture on  $^2\text{H}$ . It can be seen in Fig. 3.1 that, at low energies of about  $1 \div 3\text{ keV}$ , the  $S_p$ -factor is practically independent of the energy; thus, the determination of this factor at zero energy yields approximately the same value as at  $1\text{ keV}$ . Therefore, the difference of  $S$ -factor at 0 and  $1\text{ keV}$  probably

The total  $S$ -factor is shown by the solid line, which demonstrates a small contribution of  $M1$   $S_s$ -factor at the energies above 100 keV and its significant influence to the energy range of the order of  $1\div 10$  keV.

The total  $S$ -factor dependence on energy in the range of  $2.5\div 50$  keV is in complete accordance with the findings of works [68,69] and for the  $S_s$ -factor of the  $M1$  transition at 1 keV we obtained the value of 0.077 eV b, which leads to the value of 0.212(5) eV b for the total  $S$ -factor and which is in a good agreement with the new measurements data from LUNA project [69]. And as it can be seen from Fig. 3.3, at the energies of  $1\div 3$  keV the value of the total  $S$ -factor is more stable than it was for the  $E1$  transition and we consider it to be absolutely reasonable to write the result as 0.212 eV b with the error of 0.005.

If expression (3.4) will be used for the  $S$ -factor parametrization, then it is possible to describe the solid line in Fig. 3.3 by the parameters  $S_0 = 0.1909$  eV b and  $S_1 = 0.006912$  eV b keV<sup>-1</sup> in the energy range of 1-100 keV, with the average  $\chi^2 = 0.055$ .

If we use the quadric form of the  $S$ -factor parametrization

$$S(E_{\text{cm}}) = S_0 + E_{\text{cm}} S_1 + E_{\text{cm}}^2 S_2 \quad (3.5)$$

The next values were obtained for the parameters:  $S_0=0.1957$  eV b,  $S_1=0.006055$  eV b keV<sup>-1</sup> and  $S_2=0.00001179$  eV b keV<sup>-2</sup>, with the average  $\chi^2=0.017$  in the energy range 1-100 keV. The 10% errors of the calculated  $S$ -factor values are used for determination of  $\chi^2$ .

The approximation of the calculation results, by the analytical function of certain type with the performing of  $\chi^2$  minimization, is actually done here and further, therefore the  $S_0$  and  $S(0)$  values are slightly differ, but this difference usually not more than 10%. Meanwhile, the quadratic form (3.5) reproduces the behavior of the calculated  $S$ -factor a bit better, as one can see.

There is another method of the  $S$ -factor parametrization: when the value  $S_0$ , determining its behavior at zero energy, is predetermined. In this case, these values are obtained for the parameters of the form (3.5):  $S_0=0.2120$  eV b,  $S_1=4.5366\cdot 10^{-3}$  eV b keV<sup>-1</sup> and  $S_2=2.8622\cdot 10^{-5}$  eV b keV<sup>-2</sup> with the average  $\chi^2=0.124$ , at the same energy range and for 10% errors.

Furthermore, it is necessary to note that we are unable to build the

scattering  $^2S$ -potential uniquely because of the ambiguities in the results of phase shift analysis of  $p^2H$  scattering. For example, the other variant of this potential with parameters  $V_0 = -35.0$  MeV,  $\alpha = 0.1$  fm $^{-2}$  [21,65,88], which also describes well the doublet  $S$  phase shift of scattering, leads at these energies to  $S$ -factor of the  $M1$  process several times lower than in the previous case. Such a big ambiguity in parameters of the  $^2S$  potential of scattering, associated with errors of phase shifts extracted from the experimental data of phase shifts of scattering, does not allow us to make certain conclusions about the contribution of the  $M1$  process in the proton radiative capture on  $^2H$ , probably because of neglecting of spin-orbital splitting in such analysis, which can influence to the value of the  $^2S$  phase shift. But the first of described variants conforms to the latest measurements [68,69].

If the GS potentials are defined by the bound energy, asymptotic constant and charge radius quite uniquely and by an additional criterion – usage of the scattering phase shifts which are "pure" in accordance with Young tableau, but the situation with the construction of scattering potentials is not so unambiguous. Then, in the case of scattering processes, it is necessary to carry out a more accurate phase shift analysis, particularly for the  $^2S$  wave, and to take into account the spin-orbital splitting of the  $^2P$  phase shifts at low energies, as it was done for the elastic  $p^{12}C$  scattering at energies  $0.2 \div 1.2$  MeV [89]. Carrying out of this additional analysis will allow us to adjust the potential parameters used in the calculations of the proton radiative capture on  $^2H$  in the modified potential cluster model, thereby increasing the accuracy of the calculation results.

## **Conclusion**

Thus, the  $S$ -factor calculations of the proton radiative capture on  $^2H$  for the  $E1$  transition at the energy range down to 10 keV, which we carried out about 20 years ago [30], when the experimental data above  $150 \div 200$  keV [66] was only known, are in a good agreement with the new data of works [67,68] in the energy range from  $10 \div 20$  to  $150 \div 200$  keV. Moreover, this is true about the GS potential from Table 3.1 and the interaction with parameters from (3.2). The results of the  $S_p$ -factors for two considered potentials at the energies lower than 10 keV (Fig. 3.1) practically fall

within the error band of work [69] and show that the  $S$ -factor tends to remain constant at energies  $1\div 3$  keV.

In spite of the uncertainty of the  $M1$  contribution to the process, which results from the errors and ambiguity of the  $^2S$  scattering phases, the scattering potential (set forth in Table 3.1) with mixed Young tableaux in the  $^2S$  wave allows obtaining a reasonable value for the astrophysical  $S_s$ -factor of the magnetic transition in the range of low energies. At the same time, the value of the total  $S$ -factor is in a good agreement with all known experimental measurements [67-69] at energies from 2.5 keV to 10 MeV (Figs 3.2 and 3.3).

As a result, the MPCM based on the intercluster potentials adjusted for the elastic scattering phase shifts and GS characteristics, for which the FS structure is determined by the classification of BSs according to Young orbital tableaux and parameters suggested as early as 20 years ago [30], allows describing correctly the astrophysical  $S$ -factor for the whole range of energies under consideration. Intrinsically, the behavior of the  $S$ -factor of the radiative capture was predicted in our calculations of twenty-year remoteness [30] for the reaction  $p^2H \rightarrow ^3He\gamma$  in the range from  $10\div 20$  to  $150\div 200$  keV, the value of which at these energies is basically determined by the  $E1$  transition [90,91].

## 4. PROTON RADIATIVE CAPTURE PROCESS ON $^3\text{H}$

---

### *Introduction*

In a continuation of the investigation of fusion reactions [60] based on the modified potential cluster model with separation of orbital states according to Young tableaux [92], we consider the possibility of description of the astrophysical  $S$ -factor of the proton radiative capture on  $^3\text{H}$  at energies as low as 1 keV. This reaction is of certain interest from the theoretical and experimental points of view for understanding the dynamics of photonuclear processes with the lightest atomic nuclei at low energies. Therefore, experimental studies of this reaction continue, and new data for the total cross section of the proton radiative capture on  $^3\text{H}$  and the astrophysical  $S$ -factor in the energy range from 50 keV to 5 MeV and at 12 and 39 keV (center of mass system) has been obtained.

Probably, this reaction took a certain role at the prestellar stage of evolution of the Universe [2], when at the temperature about  $10^9$  K the next reactions (primordial nucleosynthesis) became possible

1.  $p + n \rightarrow ^2\text{H} + \gamma$ ,
2.  $^2\text{H} + p \rightarrow ^3\text{He} + \gamma$ ,
3.  $^2\text{H} + n \rightarrow ^3\text{H} + \gamma$ ,
4.  $^2\text{H} + ^2\text{H} \rightarrow ^3\text{He} + n$ ,
5.  $^2\text{H} + ^2\text{H} \rightarrow ^3\text{H} + p$ ,
6.  $^2\text{H} + ^2\text{H} \rightarrow ^4\text{He} + \gamma$ ,
7.  $^3\text{H} + p \rightarrow ^3\text{He} + n$ ,
8.  $^3\text{He} + n \rightarrow ^3\text{H} + p$ ,
9.  $^3\text{H} + p \rightarrow ^4\text{He} + \gamma$ ,
10.  $^3\text{He} + n \rightarrow ^4\text{He} + \gamma$ ,
11.  $^2\text{H} + ^3\text{H} \rightarrow ^4\text{He} + n$ .

This situation could realize at the live time of the Universe about  $10^2$  sec, when the number of protons and neutrons was comparable – approximately 0.2 neutrons from the proton number [2,4,8,9]. The last reaction No.10 mediates with comparatively small probability, since the  $E1$  process is forbidden by the isospin selection rules, which leads to the factor  $\left( \frac{Z_1}{m_1^J} + (-1)^J \frac{Z_2}{m_2^J} \right)$  at  $J = 1$  that evaluated expressions (2.5), and, in general, the probability of the  $E2$  transitions is near  $1.5 \div 2.0$  orders less [37]. The epoch of primordial nucleosynthesis [4] is finished approximately at 200 sec; practically all neutrons are bound into  ${}^4\text{He}$  nuclei, the number of which is about 25% relative to  ${}^1\text{H}$  nuclei. The relative content of  ${}^2\text{H}$  and  ${}^3\text{He}$  is about at the level  $10^{-5}$  from  ${}^1\text{H}$  [4].

Let us go now to the direct consideration of the astrophysical  $S$ -factor of the proton radiative capture on  ${}^3\text{H}$  in the potential cluster model at lowest energies. At the beginning we will construct the intercluster interaction potentials for the elastic scattering and bound states and will carry out their classification according to Young tableaux.

#### 4.1 Scattering potentials and phase shifts

The  $p^3\text{H}$  system is mixed with respect to isospin, since for  $T_z = 0$  the following values are possible:  $T = 0$  and 1. Hence, both triplet and singlet phase shifts and, therefore, potentials effectively depend on two isospin values. Due to the Pauli exclusion principle, mixing with respect to isospin results in mixing according to Young tableaux. In particular, in the singlet spin state, two orbital Young tableaux,  $\{31\}$  and  $\{4\}$ , are allowed [92]. Then it was shown in [92,93] that singlet phase shifts of the  $p^3\text{H}$  scattering mixed with respect to isospin can be represented in the form of the half-sum of pure with respect to isospin singlet phase shifts

$$\delta^{\{T=1\}+\{T=0\}} = 1/2[\delta^{\{T=1\}} + \delta^{\{T=0\}}], \quad (4.1)$$

this is equivalent to the following expression for the scattering phase shifts in terms of Young tableaux

$$\delta^{\{4\}+\{31\}} = 1/2\delta^{\{31\}} + 1/2\delta^{\{4\}}.$$

Pure phases correspond to Young tableaux  $\{31\}$  and  $T = 1$  for the  $p^3\text{He}$  system and  $\{4\}$  and  $T = 0$  for the  $p^3\text{H}$  system. Since the  $p^3\text{He}$  system at  $T_z = 1$  is pure according to isospin, then from the equation (4.1) based on known pure scattering phases with  $T = 1$  in the  $p^3\text{He}$  system [94-99] and mixed phases in the  $p^3\text{H}$  system with isospin  $T = 0$  and 1 [100-102] yields pure with respect to isospin phases of the  $p^3\text{H}$  scattering with  $T = 0$  and corresponding pure potentials of the  $p^3\text{H}$  interaction are constructed based on these scattering phases [92,93]. It is supposed in this approach that pure phase shifts with isospin  $T = 1$  in the  $p^3\text{H}$  system can be compared to phase shifts with  $T = 1$  in the  $p^3\text{He}$  channel.

The nuclear part of the intercluster potential of the  $p^3\text{H}$  and the  $p^3\text{He}$  interactions is represented in the form (2.7) with the point-like Coulomb term for performing calculations of the photonuclear processes in the considered system. The potential of the each partial wave, as for the previous  $p^2\text{H}$  system, is constructed for a correct description of the applicable partial wave of the elastic scattering [103].

**Table 4.1. Singlet potentials of the form (2.7) for the  $p^3\text{He}$  scattering, pure with respect to isospin of  $T = 1$  [92,93]**

<i>System</i>	$^{2S+1}L$	$V_0$ (MeV)	$\alpha$ (fm <sup>-2</sup> )	$V_1$ (MeV)	$\gamma$ (fm <sup>-1</sup> )
$p^3\text{He}$	$^1S$	-110.0	0.37	+45.0	0.67
	$^1P$	-15.0	0.1	—	—

Consequently, the potentials of the  $p^3\text{He}$  interactions for the elastic scattering processes and pure with respect to isospin of  $T = 1$  were obtained, their parameters are listed in Table 4.1 [92,93]. The singlet and pure with respect to isospin  $S$  phase shift of the  $p^3\text{He}$  elastic scattering, using in future in order to receive the singlet  $p^3\text{H}$  phase shifts with isospin  $T = 0$ , is shown by the solid line in Fig. 4.1a together with the experimental data from the works [94-96].

Parameters of the potential for the singlet  $^1P_1$  and the triplet  $^3P_1$  waves given in the Table 4.1 are chosen in order to receive a certain compromise



between different results, so far as there are few different variants of the phase shift analyses of the elastic  $p^3\text{He}$  scattering, for example [94-96]. The singlet  $^1P_1$  phase shift of the elastic  $p^3\text{He}$  scattering with  $T=1$  used in our calculations of the  $E1$  transition to the ground state of  $^4\text{He}$  in the  $p^3\text{H}$  channel with  $T=0$  is shown in Fig. 4.1b by solid line and the experimental data of works [94-99] are given in this figure too.

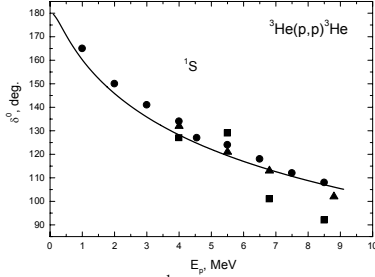


Fig. 4.1a. Singlet  $^1S$  phase shift of the elastic  $p^3\text{He}$  scattering. Experimental data: points [94], squares [95], and triangles [96].

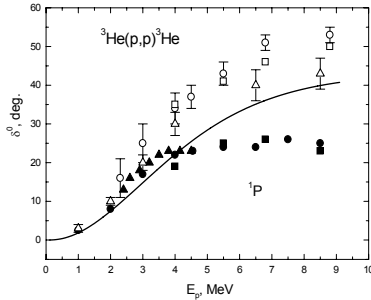


Fig. 4.1b. Singlet  $^1P$  phase shift of the elastic  $p^3\text{He}$  scattering. Experimental data: points [94], squares [95], triangles [97], circles [98], open squares [96], and open triangles [99].

scattering (dotted line) and the results of calculation of this phase with potential (4.2) (solid line). Thus-obtained pure (according to Young tableau) interactions can be used for calculation of different characteristics of the bound ground state  $^4\text{He}$  in the  $p^3\text{H}$  channel. The degree of agreement of the results obtained in this case with experiment now depends on the degree of clusterization of this nucleus in the considered channel only.

The interaction potential (4.2) obtained in [93] on the whole

The singlet and mixed according to isospin and Young tableaux  $S$  phase shift of the elastic  $p^3\text{H}$  scattering, determining from the experimental differential cross sections and used further for the obtaining of the pure  $p^3\text{H}$  phase shifts for potential of form (2.8) with parameters  $V_0 = -50$  MeV,  $\alpha = 0.2$  fm $^{-2}$ , is shown in Fig. 4.2 by the solid line together with the experimental data of works [100-102].

Then, using expression (4.1), for the pure  $p^3\text{H}$  potential with  $T=0$  (2.8) in the  $^1S$  wave, the following parameters have been found

$$V_0 = -63.1 \text{ MeV}, \quad \alpha = 0.17 \text{ fm}^{-2}.$$

Fig. 4.3 shows the pure according to Young tableau singlet  $^1S$  phase of the elastic  $p^3\text{H}$

correctly describe the channel binding energy of the  $p^3\text{H}$  system (to several kiloelectronvolts) and the root-mean-square radius of  $^4\text{He}$  [93]. These potentials were used to calculate differential [92] and total [93] cross sections of the proton radiative capture on  $^3\text{H}$  and the astrophysical  $S$ -factors at energies down to 10 keV. It should be noted that, at that time, experimental data for the  $S$ -factor only was known in the energy region above 700÷800 keV [104].

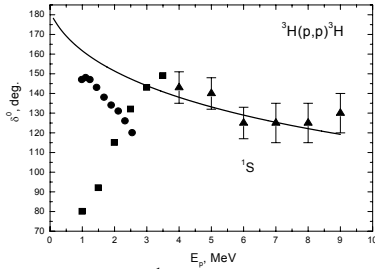


Fig. 4.2. Singlet  $^1S$  phase shift of the elastic  $p^3\text{H}$  scattering. Experimental data: points [100], squares [101], and triangles [102].

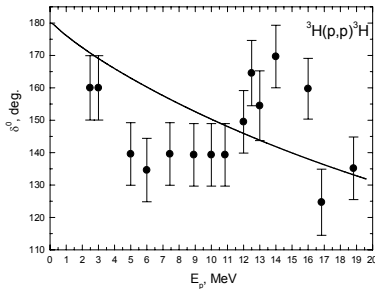


Fig. 4.3. Singlet pure according to Young tableau  $^1S$  phase shift of the elastic  $p^3\text{H}$  scattering.

modified programs were used here in order to refine parameters of the potential of the ground state for the  $p^3\text{H}$  system of  $^4\text{He}$  (see Table 4.2), which differ from those presented in [93] by approximately 0.2 MeV.

This difference is mainly connected with the application in new calculations of more accurate values of masses of  $p$  and  $^3\text{H}$  particles [36] and more accurate description of the binding energy of  $^4\text{He}$  in the  $p^3\text{H}$  channel. For this energy based on more accurate values of particle masses [36], a value of  $-19.813810$  MeV was obtained; the calculation with the potential considered here yields  $-19.81381000$  MeV. The accuracy of

New experimental data at energies from 50 keV to 5 MeV [105] and at 12 and 36 keV [106] was obtained not long ago. Therefore, it is of interest to elucidate whether the potential cluster model with the singlet  $^1P$  potential obtained earlier and refined interaction of the ground  $^1S$  state of  $^4\text{He}$  is capable of describing this new, more accurate, data.

Our preliminary results [107] have shown that, for calculation of the  $S$ -factor at energies of the order of 1 keV, the same conditions as in the  $p^2\text{H}$  system [70] discussed in the previous section should be satisfied – first of all, the accuracy of finding the binding energy of  $^4\text{He}$  in the  $p^3\text{H}$  channel should be increased. New

modified programs were used here in order to refine parameters of the potential of the ground state for the  $p^3\text{H}$  system of  $^4\text{He}$  (see Table 4.2), which differ from those presented in [93] by approximately 0.2 MeV.

determination of the energy value in this potential using our program based on the finite-difference method [26] is  $10^{-8}$  MeV.

**Table 4.2. Pure with respect to isospin of  $T = 0$  potentials of the form (2.8) for the  $p^3H$  interactions [93] in a singlet channel. Here,  $E_{BS}$  is the calculated bound state energy and  $E_{exp}$  is the experimental value of this energy [72]**

<i>System</i>	$^{2S+1}L$	$V_0$ (MeV)	$\alpha$ (fm <sup>-2</sup> )	$E_{BS}$ (MeV)	$E_{exp}$ (MeV)
$p^3H$	$^1S$	-	0.17	-19.81381000	-19.813810
	$^1P$	+8.0	0.03	—	—

The behavior of the “tail” of the wave function of the bound state of  $p^3H$  system at large distances was verified using asymptotic constant (2.10) [38,108], which turned out to be equal to  $C_W = 4.52(1)$  at an interval of  $5 \div 10$  fm. As before, the given error of the asymptotic constant becomes clear by its averaging over the range referred above. Known results on extraction of the asymptotic constant from experimental data yield a value of  $5.16(13)$  for the  $p^3H$  channel [38]. For the asymptotic constant of the  $n^3He$  system in [38], a value of  $5.1(4)$  has been obtained that is very close to the parameter of the  $p^3H$  channel. On the other hand, in [108] a value of  $4.1$  was given for the constant of the  $n^3He$  system, a value of  $4.0$  for  $p^3H$ . The average value between these constants is in a quite agreement with our results. Again, a considerable difference between the data on asymptotic constants can be seen. For the  $n^3He$  system, the constant is in the interval of  $4.1 \div 5.5$ , whereas for the  $p^3H$  channel it may assume values from  $4.0$  to  $5.3$ .

For the charge radius of  $^4He$  with this potential, a value of  $1.73$  fm has been obtained by taking the tritium radius of  $1.63$  fm [71] and the proton radius of  $0.877$  fm [36]. Note that the experimental value of the  $^4He$  radius equals  $1.671(14)$  fm [72] (see Table 3.2).

For complementary control of the accuracy in determining the binding energy in the  $S$  BS potential from Table 4.2, the variational method with expansion of the wave function over a non-orthogonal Gaussian basis has been used; this method for a dimensionality of  $10$  and independent parameter variation [26] made it possible to increase the binding energy to

19.81380998 MeV. Asymptotic constant  $C_W$  (2.10) of the variational wave function at distances of  $5 \div 10$  fm was on the level of 4.52(2), and the residual did not exceed  $10^{-11}$  [26]. The variational parameters and coefficients of expansion of the radial wave function of form (2.9) are given in Table 4.3.

**Table 4.3. Variational parameters and expansion coefficients of radial wave function of the  $p^3H$  bound state system for the  $^1S$  potential given in Table 4.2. Normalization of the function with these coefficients in an interval of  $0 \div 25$  fm is  $N = 0.9999999998$**

$i$	$\beta_i$	$C_i$
1	3.775399682294165E-002	-3.553662130779118E-003
2	7.390030511120065E-002	-4.689092850709087E-002
3	1.377393687979590E-001	-1.893147614352133E-001
4	2.427238748079469E-001	-3.619752356073335E-001
5	4.021993911220914E-001	-1.988757841748206E-001
6	1.780153251456691E+000	5.556224701527299E-003
7	5.459871888661887E+000	3.092889292994009E-003
8	1.921317723809205E+001	1.819890982631486E-003
9	8.416117121198026E+001	1.040709526875803E-003
10	5.603939880318445E+002	5.559240350868498E-004

It has been mentioned in the previous section that the variational energy decreases with increasing dimensionality of the basis and yields the upper limit for the true binding energy, while the finite-difference energy increases with decreasing step and increasing number of steps [24]. Therefore, for the actual binding energy in this potential, an average value of -19.81380999(1) MeV can be taken. In this case the error of determination of the binding energy using the two methods presented above and based on two different computer programs is  $\pm 0.01$  eV  $\pm 10$  meV or  $\pm 10^{-8}$  MeV. Meanwhile it coincides with the initially given accuracy of the FDM, equals  $10^{-8}$  MeV [26].

It can be seen from these results that the simple two-cluster  $p^3H$  model with classification of orbital states according to Young tableaux makes it

possible to obtain a quite reasonable value for such characteristics of the bound state of the  $^4\text{He}$  nucleus as charge radii and asymptotic constants. These results can testify in favor of a relatively high degree of clusterization of this nucleus in the  $p^3\text{H}$  channel. Therefore, such model is completely able to bring us to reasonable results at the calculations of the astrophysical  $S$ -factors at low energy range, and now we are going over to their consideration.

## 4.2 Astrophysical $S$ -factor

Earlier in [93], based on the modified potential cluster model, the total cross sections and the astrophysical  $S$ -factor of the proton radiative capture process on  $^3\text{H}$  were calculated and it was assumed that the main contribution into the cross sections of  $E1$  photodisintegration of  $^4\text{He}$  in the  $p^3\text{H}$  channel, or into the proton radiative capture on  $^3\text{H}$ , was due to the isospin-flip transitions for which  $\Delta T = 1$  [109]. Therefore, the  $^1P_1$  potential for the  $p^3\text{He}$  scattering in the pure with respect to isospin ( $T = 1$ ) singlet state of this system and the  $^1S$  potential for the ground pure with respect to the isospin  $T = 0$  bound state of the  $^4\text{He}$  nucleus in the  $p^3\text{H}$  channel [93] should be used in calculations. These ideas were used for calculation new the  $E1$  transition with refined potential of the ground state of  $^4\text{He}$  (see Table 4.2) [110]. The results of calculation of the astrophysical  $S$ -factor at energies as low as 1 keV are shown in Figs. 4.4a and 4.4b with a solid line. At energies as low as 10 keV, the obtained results practically do not differ from our previous results given in [93].

New experimental data was taken from [105,106], and additional data from [111] not known to us earlier was also used. It can be seen from these figures that the calculations we carried out about 20 years ago well reproduce the new data on the  $S$ -factor obtained in [105] at energies from 50 keV to 5 MeV (center of mass system).

This data possess noticeably lower ambiguity at energies above 1 MeV than do earlier results [104,112-114] and more accurately determine the general behavior of the  $S$ -factor at low energies, practically coinciding with early data [111] in an energy range of 80÷600 keV. The energy region above 1÷2 MeV has been studied in

many papers; therefore, for comparison, we are shown these earlier results in Fig. 4.4b, demonstrated a large ambiguity of experimental measurements which was done in different time and works: circles [112], open squares [113], crosses (×) [114], and downward open triangles [104].

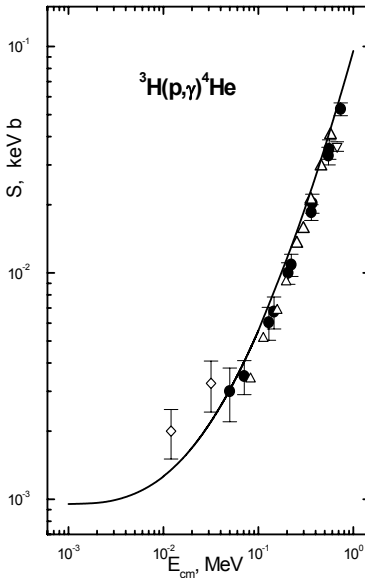


Fig. 4.4a. Astrophysical  $S$ -factor of the proton radiative capture on  $^3\text{H}$  in a range of 1 keV–1 MeV. Solid line shows calculation with the potential given in the text. Points show recalculation of total capture cross sections [105] from [106], upward open triangles [111], rhombs [106], downward open triangles [104].

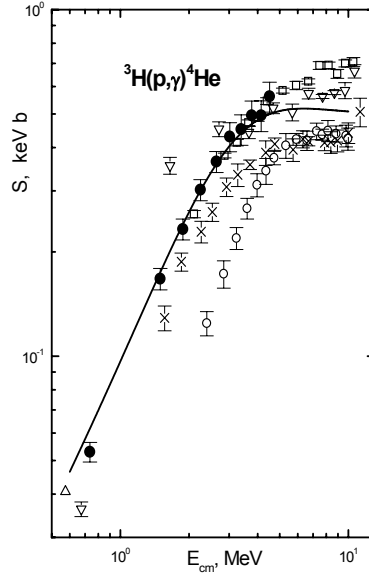


Fig. 4.4b Astrophysical  $S$ -factor of the proton radiative capture on  $^3\text{H}$  in a range of 1–10 MeV. Solid line shows calculation with the potential given in the text. Points show recalculation of total capture cross sections [105] from [106], upward open triangles [111], circles [112], open squares [113], crosses [114], and downward open triangles [104].

At energy of 1 keV, the value of the  $S$ -factor turned out to be equal to 0.96 eV b, and the results of calculation at energies below 50 keV are somewhat lower than the data of [106], where a value of 2.0(2) eV b was obtained for  $S(0)$ . Note that simple extrapolation of the available experimental data to 1 keV over the last three points of [105,111] results in a value of approximately 0.6(3) eV b, i.e., that is lower by a factor of 3 than the value obtained in [106]. The data of work [106] has the large

error and, it seems, ought to be improved in future. It can be seen from Fig. 6a that, at the lowest energies, approximately in a range of 1÷3 keV, the  $S$ -factor is almost independent of energy. This gives grounds to assume

that its value at zero energy practically does not differ from the value at 1 keV. Therefore, the difference of the  $S$ -factor at 0 and 1 keV probably is not more than 0.05 eV b, and this value may be considered as the error in determining the calculated  $S$ -factor at zero energy.

If for the  $S$ -factor parametrization one can use quadric form (3.5), then the next values were obtained for the parameters:  $S_0 = 9.5301\text{E-}01$  eV b,  $S_1 = 3.5123\text{E-}02$  eV b keV<sup>-1</sup> and  $S_2 = 1.1907\text{E-}04$  eV b keV<sup>-2</sup>, with the average  $\chi^2 = 0.05$  at the energy range 1÷100 keV. In this case this form slightly worse do for the interpolation of the  $S$ -factor, therefore it has slightly other form at low energies, than the  $S$ -factor for the proton radiative capture on <sup>2</sup>H.

### **4.3 Calculation of the astrophysical $S$ -factor**

Let us give the text of the computer program for calculation of the astrophysical  $S$ -factor, radiative capture cross section and photodisintegration of <sup>4</sup>He into the p<sup>3</sup>H channel and the binding energy in the two-body system. The program is based on the finite-difference method, described in detail in [26]. Here we will give these methods of the search of binding energy and WFs for the bound states and scattering processes only in a brief form.

The Schrodinger equation [41] for central potentials

$$u''_L + [k^2 - V(r)] u_L = 0$$

with such and such boundary condition at  $k^2 < 0$  makes the Sturm-Liouville boundary-value problem and at the transition from the second derivation to the finite differences [23-25]

$$u'' = [u_{n+1} - 2u_n + u_{n-1}]/h^2, \quad u = u(r_n)$$

turns to the closed loop system of linear algebraic equations. The condition of the equality to zero its determinant  $D_N$ , achieving at certain  $k_0$

$$D_N = \begin{pmatrix} \theta_1 & 1 & 0 & . & . & . & 0 \\ \alpha_2 & \theta_2 & 1 & 0 & . & . & 0 \\ 0 & \alpha_3 & \theta_3 & 1 & 0 & . & 0 \\ . & . & . & . & . & . & . \\ . & . & . & . & . & . & . \\ 0 & . & 0 & 0 & \alpha_{N-1} & \theta_{N-1} & 1 \\ 0 & . & 0 & 0 & 0 & \alpha_N & \theta_N \end{pmatrix} = 0 ,$$

allows one to determine the binding energy of the system of two particles  $k_0$

Here  $N$  is the number of equations,  $h = \Delta r/N$  is the step of finite-difference mesh,  $\Delta r$  is an interval of the system solution, and

$$\alpha_n = 1 , \quad \alpha_N = 2 , \quad \theta_n = k^2 h^2 - 2 - V_n h^2 ,$$

$$\theta_N = k^2 h^2 - 2 - V_n h^2 + 2hf(\eta, L, Z_n) , \quad Z_n = 2k r_n ,$$

$$r_n = nh , \quad n = 1, 2, \dots, N , \quad k = \sqrt{|k^2|} ,$$

$$f(\eta, L, Z_n) = -k - 2k\eta/Z_n - 2k(L - \eta)/Z_n^2 ,$$

where  $V_n = V(r_n)$  is the potential of the cluster interaction in the point  $r_n$ .

Such notation of the boundary conditions  $f(\eta, L, Z_n)$  allows approximately take into account the Coulomb interaction, i.e., effects, which gives accounting into the WF asymptotic the Whittaker function (see Attachment 1)

The view of logarithmic derivative of the WF in the exterior domain can be obtained from the integral expression of the Whittaker function [52]

$$f(\eta, L, Z) = -k - \frac{2k\eta}{Z} - \frac{2k(L - \eta)}{Z^2} S ,$$



where

$$S = \frac{\int_0^{\infty} t^{L+\eta+1} (1+t/z)^{L-\eta-1} e^{-t} dt}{\int_0^{\infty} t^{L+\eta} (1+t/z)^{L-\eta} e^{-t} dt} .$$

The calculations show that the value  $S$  does not exceed 1.05, and its influence to the binding energy of two-body system is negligible.

The calculation of  $D_N$  is carried out by recurrence formulae of the form

$$D_{-1} = 0 , \quad D_0 = 1 ,$$

$$D_n = \theta_n D_{n-1} - \alpha_n D_{n-2} ,$$

$$n = 1 \dots N .$$

Another recurrent process is used for finding of the form of bound state wave functions

$$u_0 = 0 , \quad u_1 = \text{const} ,$$

$$u_n = \theta_{n-1} u_{n-1} + \alpha_{n-1} u_{n-2} ,$$

$$n = 2 \dots N ,$$

where const is the arbitrary number, usually given in the range  $0.001 \div 0.1$ .

Thus, it is possible to find determinant and wave function of the bound state. The energy leading to the null of determinant

$$D_N(k_0) = 0$$

is considered the self-energy of the system, and the wave function at this energy is the eigenfunction of the problem.

The last recurrent relation uses for searching WFs too in the case of

continuous spectrum of eigenvalues, i.e., at the a priori given energy ( $k^2 > 0$ ) of scattering particles [26].

Let us give of the computer program written on the language Fortran-90. Explanation of the parameters, given values, for example, potentials and titles of calculation blocks are given directly in the text of the program.

### **PROGRAM p3T\_S**

! THE CALCULATION PROGRAMM OF THE ASTROPHYSICAL S-  
!FACTOR OF THE P<sup>3</sup>H CAPTURE

USE MSIMSL

IMPLICIT REAL(8) (A-Z)

INTEGER III,L,N,N3,I,NN,NV,NH,L1,L2,N1,N2,IFUN,N5, MINI, IFAZ  
DIMENSION EEE(0:1000)

COMMON /M/ V(0:10240000),U1(0:10240000),U(0:10240000)

COMMON /BB/ A2,R0,AK1,RCU

COMMON /AA/ SKS,L,GK,R,SSS,AKK,CC

COMMON /CC/ HK,IFUN,MINI,IFAZ

COMMON /DD/ SS,AAK,GAM

! \* \* \* \* \* CALCULATION PARAMETERS \* \* \* \* \* \* \* \* \* \*

WFUN=0

RAD=1

FOTO=1

IFUN=0; ! If = 0 then FDM, If = 1 then RK

IFAZ=1; ! If = 0 the phase shift simply = 0, If = 1 - the phase shift is  
calculated

MINI=0; ! If = 0 the phase shift is calculated at the bottom of the range, If  
= 1 the search of the phase shift according to given accuracy is done

IF (IFAZ==0)THEN

MINI=0

PRINT \*, 'ASSIMPTOTIC AT R ONLY !'

END IF

! \* \* \* \* \* MASSES AND CHARGES \* \* \* \* \* \* \* \* \* \*

Z1=1.0D-000

Z2=1.0D-000

Z=Z1+Z2

AM1=1.00727646677D-000; ! MACCA P

```

AM2=3.0155007134D-000; ! MACCA T
AM=AM1+AM2
RK11=0.877D-000; ! P
RM11=0.877D-000; ! P
RK22=1.63D-000; ! T
RM22=1.72D-000; ! T
PI=4.0D-000*DATAN(1.0D-000)
PM=AM1*AM2/AM
A1=41.4686D-000
B1=2.0D-000*PM/A1
AK1=1.439975D-000*Z1*Z2*B1
GK=3.44476D-002*Z1*Z2*PM
! ***** CALCULATION PARAMETERS *****
N=1000; N3=N
RR=30.0D-000 ! Distance in fm for the determination of the WF
H=RR/N; H1=H; HK=H*H
SKN=-22.0D-000; HC=0.1D-000; SKV=1.0D-000
SKN=SKN*B1; SKV=SKV*B1; HC=HC*B1
NN=0; NH=1
NV=100 ! The number of the energy steps at the S-factor calculation
EH=1.0D-003 ! The energy step at the S-factor calculation
EN=1.0D-003 ! The initial energy at the S-factor calculation
EP=1.0D-015; ! The absolute accuracy of search of the determinant zero
and Coulomb functions
EP1=1.D-008; ! The absolute accuracy of search of the binding energy
EP2=1.0D-003; ! The accuracy of search of the asymptotic constant in
the relative units
EP3=1.0D-003; ! The accuracy of search of the scattering phase shifts in
the relative units
! ***** POTENTIALS *****
V0=62.906841138D-000; ! P3H FOR RCU=0. R=1.73 C=4.51(1)
R0=0.17D-000
V1=0.0D-000
R1=1.0D-000
L=0
A2=-V0*B1

```

```

A33=V1*B1
VP=15.0D-000
RP=0.1D-000
L1=1
VD=V0
RD=R0
L2=2
AP=-VP*B1
AD=-VD*B1
RCU=0.0D-000
! * * * * * SEARCH OF THE MINIMUM * * * * *
III=1
CALL
MIN(EP,B1,SKN,SKV,HC,H,N,L,A2,R0,AK1,RCU,GK,ESS,SKS,A33,R1
)
PRINT *, '      E      N      DEL-E'
EEE(III)=ESS
111 N=2*N
H=H/2.0D-000
III=III+1
CALL
MIN(EP,B1,SKN,SKV,HC,H,N,L,A2,R0,AK1,RCU,GK,ESS1,SKS,A33,R
1)
EEE(III)=ESS1
EEPP=ABS(EEE(III))-ABS(EEE(III-1))
PRINT *,EEE(III),N,EEPP
IF (ABS(EEPP)>EP1) GOTO 111
ESS=ESS1
PRINT *,EEE(III),N,EEPP
12 FORMAT(1X,E19.12,2X,I10,2X,3(E10.3,2X))
OPEN (25,FILE='E.DAT')
WRITE(25,*) ESS,SKS,N,H
CLOSE(25)
SK=SKS
SSS=DSQRT(ABS(SKS))
SS=SSS

```

```

AKK=GK/SSS
AAK=AKK
HK=H*H
ZZ=1.0D-000+AAK+L
GAM=DGAMMA(ZZ)
! * * * * * CALCULATION OF THE WF * * * * *
* * * *
333 CONTINUE
IF (IFUN==0) THEN
N1=N/4
ELSE
N1=N/8
END IF
N1=N
IF (IFUN==0) THEN
CALL FUN(U,H,N1,A2,R0,A33,R1,L,RCU,AK1,SK)
ELSE
CALL FUNRK(U,N1,H,L,SK,A2,R0)
END IF
! * * * * * NORMALIZATION OF THE WF * * * * *
* *
N2=1
N5=N1
N1=1
CALL ASSIM(U,H,N5,C0,CW0,CW,N1,EP2)
DO I=0,N1
V(I)=U(I)*U(I)
ENDDO
CALL SIMP(V,H,N1,SII)
HN=1.0D-000/DSQRT(SII)
OPEN (24,FILE='FUN-WWW.DAT')
DO I=0,N1
X=I*H
U(I)=U(I)*HN
ENDDO
CLOSE(24)

```

```

! * * * * ASYMPTOTIC CONSTANTS * * * * *
CALL ASSIM(U,H,N1,C0,CW0,CW,N1,EP2)
1 FORMAT(1X,4(E13.6,2X))
! * * * RENORMALIZATION OF THE WF'S TAIL * * * *
SQQ=DSQRT(2.0D-000*SS)
DO I=N1+1,N,N2
R=I*H
CC=2.0D-000*R*SS
CALL WHI(R,WWW)
U(I)=CW*WWW*SQQ
ENDDO
1122 CONTINUE
! * * * * * REPEAT NORMALIZATION OF THE WF * * * * *
DO I=1,N1
V(I)=U(I)*U(I)
ENDDO
DO I=N1+1,N,N2
V(I)=U(I)*U(I)
ENDDO
CALL SIMP(V,H,N,SIM)
HN=SIM
HN=1.0D-000/DSQRT(HN)
DO I=1,N1
U(I)=U(I)*HN
ENDDO
DO I=N1+1,N,N2
U(I)=U(I)*HN
ENDDO
! * * * ASYMPTOTIC CONSTANTS * * * * * CALL
ASSIM(U,H,N,C0,CW0,CW,N,EP2)
! * * * * * PRINTING OF THE WF * * * * *
IF (WFUN==0) GOTO 2233
OPEN (24,FILE='FUN.DAT')
WRITE(24,*) '      R      U'
PRINT *, '      R      U'
DO I=0,N

```

```

X=H*I
PRINT 2,X,U(I)
WRITE(24,2) X,U(I)
ENDDO
CLOSE(24)
2233 CONTINUE
! * * * * * RADIUS * * * * *
666 IF (RAD==0) GOTO 7733
OPEN (23,FILE='RAD.DAT')
WRITE(23,*) ' E      SQRT(RM**2)      SQRT(RZ**2)'
DO I=0,N
X=I*H
V(I)=X*X*U(I)*U(I)
ENDDO
CALL SIMP(V,H,N,RKV)
RM=AM1/AM*RM11**2      +      AM2/AM*RM22**2      +
((AM1*AM2)/AM**2)*RKV
RZ=Z1/Z*RK11**2      +      Z2/Z*RK22**2      +
(((Z1*AM2**2+Z2*AM1**2)/AM**2)/Z)*RKV
PRINT *,'(RM^2)^1/2= ',DSQRT(RM)
PRINT *,'(RZ^2)^1/2= ',DSQRT(RZ)
PRINT *,'(RKV^2)^1/2= ',DSQRT(RKV)
WRITE(23,2) DSQRT(RM),DSQRT(RZ)
2 FORMAT(1X,2(E16.8,2X))
CLOSE(23)
7733 CONTINUE
! * * * * * CALCULATION OF THE S-FACTORS
* * * * *
PRINT *,'CALCULATE CROSS SECTION ?'
READ *
IF (FOTO==0) GOTO 9988
CALL
SFAC(EN,EH,NN,NV,NH,B1,ESS,H,N,L1,L2,RCU,AD,AK1,AP,PI,Z1,Z
2,AM1,AM2,PM,RD,RP,GK,EP,EP3,N2)
9988 CONTINUE
END

```

```

SUBROUTINE ASSIM(U,H,N,C0,CW0,CW,I,EP)
! Subroutine for the calculation of the asymptotic constant
IMPLICIT REAL(8) (A-Z)
INTEGER I,L,N,J,N2
DIMENSION U(0:10240000)
COMMON /AA/ SKS,L,GK,R,SS,GGG,CC
N2=10
OPEN (22,FILE='ASIMP.DAT')
WRITE(22,*) '      R      C0      CW0      CW'
SQQ=DSQRT(2.0D-000*SS)
PRINT *, '      R      C0      CW0      CW'
IF (I==N) THEN
DO J=N/16,N,N/16
R=J*H
CC=2.0D-000*R*SS
C0=U(J)/DEXP(-SS*R)/SQQ
CW0=C0*CC**GGG
CALL WHI(R,WWW)
CW=U(J)/WWW/SQQ
PRINT 1,R,C0,CW0,CW,I
WRITE(22,1) R,C0,CW0,CW
ENDDO
ELSE
I=N
R=I*H
CC=2.0D-000*R*SS
CALL WHI(R,WWW)
CW1=U(I)/WWW/SQQ
12 I=I-N2
IF (I<=0) THEN
PRINT *, 'NO STABLE ASSIMPTOTIC FW'
STOP
END IF
R=I*H
CC=2.0D-000*R*SS
CALL WHI(R,WWW)

```



```

CW=U(I)/WWW/SQQ
IF (ABS(CW1-CW)/ABS(CW)>EP .OR. CW==0.0D-000) THEN
CW1=CW
GOTO 12
END IF
PRINT *,'      R      C0      CW0      CW'
PRINT 1,R,C0,CW0,CW,I
WRITE(22,1) R,C0,CW0,CW
END IF
CLOSE(22)
1 FORMAT(1X,4(E13.6,2X),3X,I8)
END
FUNCTION F(X)
! Subroutine for the calculation of the integrand values for the Whittaker
function
IMPLICIT REAL(8) (A-Z)
INTEGER L
COMMON /AA/ SKS,L,GK,R,SS,AA,CC
F=X**(AA+L)*(1.0D-000+X/CC)**(L-AA)*DEXP(-X)
END
SUBROUTINE WHI(R,WH)
! Subroutine for the calculation of the Whittaker function
USE MSIMSL
IMPLICIT REAL(8) (A-Z)
REAL(8) F
EXTERNAL F
COMMON /DD/ SS,AAK,GAM
CC=2.0D-000*R*SS
Z=CC**AAK
CALL      DQDAG      (F,0.0D-000,25.0D-000,0.0010D-000,0.0010D-
000,1,RES,ER)
WH=RES*DEXP(-CC/2.0D-000)/(Z*GAM)
END
SUBROUTINE
MIN(EP,B1,PN,PV,HC,HH,N3,L,A22,R0,AK1,RCU,GK,EN,COR,A33
,R1)

```

! Subroutine for the calculation of the binding energy values

IMPLICIT REAL(8) (A-Z)

INTEGER I,N3,L,LL

HK=HH\*\*2; LL=L\*(L+1)

IF(PN>PV) THEN

PNN=PV; PV=PN; PN=PNN

ENDIF

A=PN; H=HC

1 CONTINUE

CALL DET(A,GK,N3,A22,R0,L,LL,AK1,RCU,HH,HK,D1,A33,R1)

B=A+H

2 CONTINUE

CALL DET(B,GK,N3,A22,R0,L,LL,AK1,RCU,HH,HK,D2,A33,R1)

IF (D1\*D2>0.0D-000) THEN

B=B+H; D1=D2

IF (B<=PV .AND. B>=PN) GOTO 2

I=0; RETURN; ELSE

A=B-H; H=H\*1.0D-001

IF(ABS(D2)<EP .OR. ABS(H)<EP) GOTO 3

B=A+H; GOTO 1

ENDIF

3 I=1; COR=B; D=D2; EN=COR/B1;

**END**

**SUBROUTINE**

**DET(DK,GK,N,A2,R0,L,LL,AK,RCU,H,HK,DD,A3,R1)**

! Subroutine for the calculation of the determinant value

IMPLICIT REAL(8) (A-Z)

INTEGER(4) L,N,II,LL

S1=DSQRT(ABS(DK))

G2=GK/S1

D1=0.0D-000

D=1.0D-000

DO II=1,N

X=II\*H

XX=X\*X

F=A2\*DEXP(-XX\*R0)+A3\*DEXP(-XX\*R1)+LL/XX

```

IF (X>RCU) GOTO 67
F=F+(AK/(2.0D-000*RCU))*(3.0D-000-(X/RCU)**2)
GOTO 66
67 F=F+AK/X
66 IF (II==N) GOTO 111
D2=D1
D1=D
OM=DK*HK-F*HK-2.0D-000
D=OM*D1-D2
ENDDO
111 Z=2.0D-000*X*S1
OM=DK*HK-F*HK-2.0D-000
W=-S1-2.0D-000*S1*G2/Z-2.0D-000*S1*(L-G2)/(Z*Z)
OM=OM+2.0D-000*H*W
DD=OM*D-2.0D-000*D1
END
SUBROUTINE FUN(U,H,N,A2,R0,A3,R1,L,RCU,AK,SK)
! Subroutine for the calculation of the values for potentials
IMPLICIT REAL(8) (A-Z)
DIMENSION U(0:10240000)
INTEGER N,L,K,IFUN,MIN,IFAZ
COMMON /CC/ HK,IFUN,MIN,IFAZ
U(0)=0.0D-000
U(1)=0.1D-000
DO K=1,N-1
X=K*H
XX=X*X
Q1=A2*DEXP(-R0*XX)+A3*DEXP(-R1*XX)+L*(L+1)/XX
IF (X>RCU) GOTO 1571
Q1=Q1+(3.0D-000-(X/RCU)**2)*AK/(2.0D-000*RCU)
GOTO 1581
1571 Q1=Q1+AK/X
1581 Q2=-Q1*HK-2.0D-000+SK*HK
U(K+1)=-Q2*U(K)-U(K-1)
ENDDO
END

```

**SUBROUTINE SIMP(V,H,N,S)**

! Subroutine for the calculation of the integral the Simpson method

IMPLICIT REAL(8) (A-Z)

DIMENSION V(0:10240000)

INTEGER N,II,JJ

A=0.0D-000; B=0.0D-000

A111: DO II=1,N-1,2

B=B+V(II)

ENDDO A111

B111: DO JJ=2,N-2,2

A=A+V(JJ)

END DO B111

S=H\*(V(0)+V(N)+2.0D-000\*A+4.0D-000\*B)/3.0D-000

**END****SUBROUTINE CULFUN(LM,R,Q,F,G,W,EP)**

! Subroutine for the calculation of the Coulomb functions

IMPLICIT REAL(8) (A-Z)

INTEGER L,K,LL,LM

EP=1.0D-020

L=0

F0=1.0D-000

GK=Q\*Q

GR=Q\*R

RK=R\*R

B01=(L+1)/R+Q/(L+1)

K=1

BK=(2\*L+3)\*((L+1)\*(L+2)+GR)

AK=-R\*((L+1)\*\*2+GK)/(L+1)\*(L+2)

DK=1.0D-000/BK

DEHK=AK\*DK

S=B01+DEHK

15 K=K+1

AK=-RK\*((L+K)\*\*2-1)\*((L+K)\*\*2+GK)

BK=(2\*L+2\*K+1)\*((L+K)\*(L+K+1)+GR)

DK=1.D-000/(DK\*AK+BK)

IF (DK&gt;0.0D-000) GOTO 35

```

25 F0=-F0
35 DEHK=(BK*DK-1.0D-000)*DEHK
S=S+DEHK
IF (ABS(DEHK)>EP) GOTO 15
FL=S
K=1
RMG=R-Q
LL=L*(L+1)
CK=-GK-LL
DK=Q
GKK=2.0D-000*RMG
HK=2.0D-000
AA1=GKK*GKK+HK*HK
PBK=GKK/AA1
RBK=-HK/AA1
AOMEK=CK*PBK-DK*RBK
EPSK=CK*RBK+DK*PBK
PB=RMG+AOMEK
QB=EPSK
52 K=K+1
CK=-GK-LL+K*(K-1)
DK=Q*(2*K-1)
HK=2.0D-000*K
FI=CK*PBK-DK*RBK+GKK
PSI=PBK*DK+RBK*CK+HK
AA2=FI*FI+PSI*PSI
PBK=FI/AA2
RBK=-PSI/AA2
VK=GKK*PBK-HK*RBK
WK=GKK*RBK+HK*PBK
OM=AOMEK
EPK=EPSK
AOMEK=VK*OM-WK*EPK-OM
EPSK=VK*EPK+WK*OM-EPK
PB=PB+AOMEK
QB=QB+EPSK

```

```

IF ((ABS(AOMEK)+ABS(EPSK))>EP) GOTO 52
PL=-QB/R
QL=PB/R
G0=(FL-PL)*F0/QL
G0P=(PL*(FL-PL)/QL-QL)*F0
F0P=FL*F0
ALFA=1.0D-000/DSQRT(ABS(F0P*G0-F0*G0P))
G=ALFA*G0
GP=ALFA*G0P
F=ALFA*F0
FP=ALFA*F0P
W=1.0D-000-FP*G+F*GP
IF (LM==0) GOTO 123
AA=DSQRT(1.0D-000+Q**2)
BB=1.0D-000/R+Q
F1=(BB*F-FP)/AA
G1=(BB*G-GP)/AA
WW1=F*G1-F1*G-1.0D-000/DSQRT(Q**2+1.0D-000)
IF (LM==1) GOTO 234
DO L=1,LM-1
AA=DSQRT((L+1)**2+Q**2)
BB=(L+1)**2/R+Q
CC=(2*L+1)*(Q+L*(L+1)/R)
DD=(L+1)*DSQRT(L**2+Q**2)
F2=(CC*F1-DD*F)/L/AA
G2=(CC*G1-DD*G)/L/AA
WW2=F1*G2-F2*G1-(L+1)/DSQRT(Q**2+(L+1)**2)
F=F1; G=G1; F1=F2; G1=G2
ENDDO
234 F=F1; G=G1
123 END
SUBROUTINE
SFAC(EN,EH,NN,NV,NH,B1,ES,H,N4,L1,L2,RCU,AD,AK1,AP,PI,Z1,
Z2,AM1,AM2,PM,RD,RP,GK,EP,EP2,N2)
! Subroutine for the calculation of the S-factor
! and capture cross section

```

```

IMPLICIT REAL(8) (A-Z)
INTEGER(4)
L1,L2,N3,NN,NV,NH,II,KK,ID,IP,N2,N4,IFUN,MIN,I,IFAZ
COMMON /M/ V(0:10240000),U1(0:10240000),U(0:10240000)
DIMENSION FA1(0:1000),EG(0:1000),ECM(0:1000), FA2(0:1000),
SZ2(0:1000),SR2(0:1000),SZ1(0:1000),
SR1(0:1000),SR(0:1000),SZ(0:1000),EL(0:1000),SF(0:1000)
COMMON /CC/ HK,IFUN,MIN,IFAZ
! CALCULATION OF THE SCATTERING PHASE SHIFTS
FUNCTIONS
! AND MATRIX ELEMENTS OF THE S_FACTORS
N3=N4; N2=4
A33=0.0D-000
R1=0.0D-000
OPEN (1,FILE='SFAC.DAT')
WRITE (1,*) ' ECM(I) EG(I) SR1(I) SR2(I)
SR(I) SZ1(I) SZ2(I) SZ(I) SF(I)
F'
PRINT *, ' EG ECM SR1 SR2 SR
SZ1 SZ2 SZ SF F'
A1: DO I=NN,NV,NH
ECM(I)=EN+I*EH
EG(I)=ECM(I)+ABS(ES)
SK=ECM(I)*B1
SS1=SK**0.5
G=GK/SS1
! CALCULATION OF THE COULOMB D-FUNCTIONS
X1=H*SS1*(N3-4)
X2=H*SS1*(N3)
CALL CULFUN(L2,X1,G,F11,G11,W0,EP)
CALL CULFUN(L2,X2,G,F22,G22,W0,EP)
! * * * CALCULATION OF THE D SCATTERING FUNCTIONS * * *
*
IF (IFUN==0) THEN
CALL FUN(U1,H,N3,AD,RD,A33,R1,L2,RCU,AK1,SK)
ELSE

```

```

CALL FUNRK(U1,N3,H,L2,SK,AD,RD)
END IF
! *****          CALCULATION OF THE D PHASE SHIFTS
*****

F1=F11
G1=G11
F2=F22
G2=G22
CALL FAZ(N3,F1,F2,G1,G2,U1,FA1,I,XH2)
IF (MIN==0) GOTO 543
IF ((FA1(I) == 0.D-000)) GOTO 543
II=N3
135 II=II-N2
IF (II<=4) THEN
PRINT *,'NO DEFINITION D-FAZA'
GOTO 555
END IF
X1=H*SS1*(II-4)
X2=H*SS1*(II)
CALL CULFUN(L2,X1,G,F11,G11,W0,EP)
CALL CULFUN(L2,X2,G,F22,G22,W0,EP)
F1=F11
G1=G11
F2=F22
G2=G22
CALL FAZ(II,F1,F2,G1,G2,U1,FA2,I,XH2)
IF ( ABS ( FA1(I) - FA2(I) ) > ABS(EP2*FA2(I)) ) THEN
FA1(I)=FA2(I)
GOTO 135
END IF
ID=II
DO J=ID,N4
X=H*SS1*J
CALL CULFUN(L2,X,G,F1,G1,W0,EP)
U1(J)=(DCOS(FA2(I))*F1+DSIN(FA2(I))*G1)
ENDDO

```



```

! ** CALCULATION OF THE E2 MATRIX ELEMENTS *****
543 CONTINUE
D1: DO J=0,N4
X=H*J
V(J)=U1(J)*X*X*U(J)
ENDDO D1
CALL SIMP(V,H,N4,AID1)
AID=AID1
! **** CALCULATION OF THE P SCATTERING FUNCTIONS ****
555 IF (IFUN==0) THEN
CALL FUN(U1,H,N3,AP,RP,A33,R1,L1,RCU,AK1,SK)
ELSE
CALL FUNRK(U1,N3,H,L1,SK,AP,RP)
END IF
! **** CALCULATION OF THE COULOMB P-FUNCTIONS ***
X1=H*SS1*(N3-4)
X2=H*SS1*(N3)
CALL CULFUN(L1,X1,G,F11,G11,W0,EP)
CALL CULFUN(L1,X2,G,F22,G22,W0,EP)
! ***** CALCULATION OF THE P PHASE SHIFTS
*****\
F1=F11
G1=G11
F2=F22
G2=G22
CALL FAZ(N3,F1,F2,G1,G2,U1,FA1,I,XH2)
IF (MIN==0) GOTO 545
IF ( (FA1(I) == 0.D-000)) GOTO 545
KK=N3
134 KK=KK-N2
IF (KK<=4) THEN
PRINT *, 'NO DEFINITION P-FAZA'
GOTO 1122
END IF
X1=H*SS1*(KK-4)
X2=H*SS1*(KK)

```

```

CALL CULFUN(L1,X1,G,F11,G11,W0,EP)
CALL CULFUN(L1,X2,G,F22,G22,W0,EP)
F1=F11
G1=G11
F2=F22
G2=G22
CALL FAZ(KK,F1,F2,G1,G2,U1,FA2,I,XH)
IF (ABS ( FA1(I) - FA2(I) ) > ABS(EP2*FA2(I)) ) THEN
FA1(I)=FA2(I)
GOTO 134
END IF
IP=KK
DO J=IP,N4
X=H*SS1*J
CALL CULFUN(L2,X,G,F1,G1,W0,EP)
U1(J)=(DCOS(FA2(I))*F2+DSIN(FA2(I))*G2)
ENDDO
! ***  CALCULATION OF THE E1 MATRIX ELEMENTS  ***
545 CONTINUE
CC1:DO J=0,N4
X=H*J
V(J)=U1(J)*X*U(J)
ENDDO CC1
CALL SIMP(V,H,N4,BIP)
AIP=BIP
! *****  CALCULATION OF THE CROSS SECTIONS
*****
AMEP=3.0D-000*AIP**2
AMED=5.0D-000*AID**2
AKP=SS1
AKG=(EG(I))/197.331D-000
BBBB=344.46D-000*8.0D-000*PI*3.0D-000/2.0D-000/9.0D-000/25.0D-
000/2.0D-000/2.0D-000*PM**5*(Z1/AM1**2+Z2/AM2**2)**2
SZ2(I)=BBBB*(AKG/AKP)**5*AMED*AKP**2
SR2(I)=SZ2(I)*2.0D-000*2.0D-000/2.0D-000*(AKP/AKG)**2
BBB=344.46D-000*8.0D-000*PI*2.0D-000/9.0D-000/2.0D-000/2.0D-

```

```

000*PM**3*(Z1/AM1-Z2/AM2)**2
SZ1(I)=BBB*(AKG/AKP)**3.*AMEP
SR1(I)=SZ1(I)*2.0D-000*2.0D-000/2.0D-000*(AKP/AKG)**2
SR(I)=SR1(I)+SR2(I)
SZ(I)=SZ1(I)+SZ2(I)
EL(I)=ECM(I)*AM1/PM
SSS=DEXP(Z1*Z2*31.335D-
000*DSQRT(PM)/DSQRT(ECM(I)*1.0D+003))
SF(I)=SZ(I)*1.0D-006*ECM(I)*1.0D+003*SSS
PRINT                                                    2,
ECM(I),EG(I),SR1(I),SR2(I),SR(I),SZ1(I),SZ2(I),SZ(I),SF(I),FA1(I)*180./
PI
WRITE                                                    (1,2)
ECM(I),EG(I),SR1(I),SR2(I),SR(I),SZ1(I),SZ2(I),SZ(I),SF(I),FA1(I)*180./
PI
1122 ENDDO A1
CLOSE (1)
2 FORMAT(1X,11(E13.6,1X))
END
SUBROUTINE FAZ(N,F1,F2,G1,G2,V,F,I,H2)
! SUBROUTINE FOR CALCULATION OF THE SCATTERING PHASE
SHIFTS
IMPLICIT REAL(8) (A-Z)
INTEGER I,J,N,MIN,IFUN,IFAZ
DIMENSION V(0:10240000),F(0:1000)
COMMON /CC/ HK,IFUN,MIN,IFAZ
U1=V(N-4)
U2=V(N)
IF (IFAZ==0) THEN
FA=0.0D-000
ELSE
AF=-((F1*(1-(F2/F1)*(U1/U2)))/(G1*(1-(G2/G1)*(U1/U2))))
FA=DATAN(AF)
END IF
IF (FA<1.0D-008) THEN
FA=0.0D-000

```

```

ENDIF
H2=(DCOS(FA)*F2+DSIN(FA)*G2)/U2
F(I)=FA
DO J=0,N
V(J)=V(J)*H2
ENDDO
END
SUBROUTINE FUNRK(V,N,H,L,SK,A22,R00)
! ***** SOLVING OF THE SCHRÖDINGER EQUATION
! BY THE RUNGE-KUTT ! METHOD IN THE WHOLE RANGE
! OF VARIABLES *****
IMPLICIT REAL(8) (A-Z)
INTEGER I,N,L
DIMENSION V(0:10240000)
VA1=0.0D-000; ! VA1 - Value of the function in zero
PA1=1.0D-003 ! PA1 - Value of the derivative in zero
DO I=0,N-1
X=H*I+1.0D-015
CALL RRUN(VB1,PB1,VA1,PA1,H,X,L,SK,A22,R00)
VA1=VB1
PA1=PB1
V(I+1)=VA1
ENDDO
END
SUBROUTINE RRUN(VB1,PB1,VA1,PA1,H,X,L,SK,A,R)
! **** SOLVING OF THE SCHRÖDINGER EQUATION BY THE
RUNGE-KUTT ! METHOD AT ONE STEP *****
IMPLICIT REAL(8) (A-Z)
INTEGER L
X0=X
Y1=VA1
CALL FA(X0,Y1,FK1,L,SK,A,R)
FK1=FK1*H
FM1=H*PA1
X0=X+H/2.0D-000
Y2=VA1+FM1/2.0D-000

```

```

CALL FA(X0,Y2,FK2,L,SK,A,R)
FK2=FK2*H
FM2=H*(PA1+FK1/2.0D-000)
Y3=VA1+FM2/2.0D-000
CALL FA(X0,Y3,FK3,L,SK,A,R)
FK3=FK3*H
FM3=H*(PA1+FK2/2.0D-000)
X0=X+H
Y4=VA1+FM3
CALL FA(X0,Y4,FK4,L,SK,A,R)
FK4=FK4*H
FM4=H*(PA1+FK3)
PB1=PA1+(FK1+2.0D-000*FK2+2.0D-000*FK3+FK4)/6.0D-000
VB1=VA1+(FM1+2.0D-000*FM2+2.0D-000*FM3+FM4)/6.0D-000
END
SUBROUTINE FA(X,Y,FF,L,SK,A,R)
! * CALCULATION OF THE FUNCTION F(X,Y) BY THE RUNGE-
KUTT ! METHOD *
IMPLICIT REAL(8) (A-Z)
INTEGER L
COMMON /BB/ A2,R0,AK,RCU
VC=A*DEXP(-R*X*X)
IF (X>RCU) GOTO 1
VK=(3.0D-000-(X/RCU)**2)*AK/(2.0D-000*RCU)
GOTO 2
1 VK=AK/X
2 FF=-(SK-VK-VC-L*(L+1)/(X*X))*Y
END

```

Furthermore, the results of the check calculation on this program are given. The first printing shows the process of convergence of the binding energy  $E$  for the  $p^3H$  system with the BS potential given in Table 4.2 in accordance with the current accuracy  $\delta E$  and with the given step number  $N$ , which provides such accuracy

$E$	$N$	$\delta E$
-19.814143936616980	2000	-1.001912862701460E-003
-19.813893481090760	4000	-2.504555262170527E-004
-19.813830868619080	8000	-6.261247168382056E-005
-19.813815215615060	16000	-1.565300401296099E-005
-19.813811302282760	32000	-3.913332307092787E-006
-19.813810324242950	64000	-9.780398002590118E-007
-19.813810079038370	128000	-2.452045890777299E-007
-19.813810018177860	256000	-6.086050419185085E-008
-19.813810005390660	512000	-1.278720418440571E-008
-19.813810000116750	1024000	-5.273907532910016E-009

Furthermore, the calculation of the asymptotic constant  $C_w$  (so as  $C_0$  and  $C_{w0}$  [26]) was carried out according to the intercluster distance  $R$  and determine the range of such distances where constant practically does not change

$R$	$C_0$	$C_{w0}$	$C_w$
.595547E+00	.553644E+00	.553842E+00	.564169E+00
.119109E+01	.143211E+01	.146335E+01	.147985E+01
.178664E+01	.240107E+01	.248411E+01	.250441E+01
.238219E+01	.320668E+01	.334693E+01	.336846E+01
.297773E+01	.373762E+01	.392783E+01	.394870E+01
.357328E+01	.402419E+01	.425267E+01	.427192E+01
.416883E+01	.415189E+01	.440837E+01	.442577E+01
.476438E+01	.419640E+01	.447389E+01	.448954E+01
.535992E+01	.420445E+01	.449867E+01	.451280E+01
.595547E+01	.419907E+01	.450743E+01	.452029E+01
.655102E+01	.418981E+01	.451063E+01	.452241E+01
.714656E+01	.418003E+01	.451211E+01	.452298E+01
.774211E+01	.417082E+01	.451321E+01	.452330E+01
.833766E+01	.416264E+01	.451460E+01	.452401E+01
.893320E+01	.415628E+01	.451723E+01	.452605E+01
.952875E+01	.415383E+01	.452350E+01	.453180E+01

The screen output is finished at the distance 9.5287 fm, and it means

that at the next step, for example at 10 fm, the constant difference will be equal to  $EP2$ , i.e., the stabilization range of the AC was found.

The calculation results of the charge  $\langle R_z^2 \rangle^{1/2}$  and mass  $\langle R_m^2 \rangle^{1/2}$  radii [26] of  $^4\text{He}$  in the  $p^3\text{H}$  channel in fm are given next

$$\langle R_m^2 \rangle^{1/2} = 1.784, \quad \langle R_z^2 \rangle^{1/2} = 1.731$$

And finally, the calculation results of the astrophysical  $S$ -factor in keV b are given, because they are given in the final channel at the energies  $1 \div 10$  keV. Only results for the  $E1$  and  $E2$  capture cross sections and their sum  $S_Z(I)$  and the total  $S$ -factor  $SF(I)$  were shown here

$E_{CM}(I)$	$S_{Z1}(I)$	$S_{Z2}(I)$	$S_Z(I)$	$SF(I)$
.100000E-02	.144176E-08	.471624E-14	.144177E-08	.963835E-03
.200000E-02	.211076E-05	.812620E-11	.211077E-05	.970699E-03
.300000E-02	.495617E-04	.219483E-09	.495619E-04	.998845E-03
.400000E-02	.316038E-03	.158231E-08	.316040E-03	.103361E-02
.500000E-02	.110298E-02	.615998E-08	.110298E-02	.107124E-02
.600000E-02	.275390E-02	.169655E-07	.275392E-02	.111092E-02
.700000E-02	.558004E-02	.375959E-07	.558008E-02	.115135E-02
.800000E-02	.982865E-02	.718952E-07	.982872E-02	.119232E-02
.900000E-02	.156780E-01	.123729E-06	.156781E-01	.123378E-02
.100000E-01	.232458E-01	.196850E-06	.232460E-01	.127578E-02

As one can see, at the energy 1 keV (at the printout the energy is given in MeV) the values of  $0.964 \cdot 10^{-3}$  keV b or 0.964 eV b were obtained for the  $S$ -factor.

This variant of the program works at the parameter value  $MINI = 0$ , which determines the search mode of the scattering phase shift at the integration domain boundary, in this case it equals  $RR = 30$  fm. If the parameter  $MINI = 1$ , then the phase shift at each energy will calculate from 30 fm, towards the lesser distances. Consequently, the range of its stabilization at the given  $EP3 = 10^{-3}$ , which is usually equals  $10 \div 20$  fm, was obtained.

The given above results were obtained by using the finite-difference method [26] for search of the scattering WF. It achieves with the value, at

the beginning of the program, parameter  $IFUN = 0$ , and now let us give the result at  $IFUN = 1$ , when the Runge-Kutt (RK) method is used for search these WFs – here parameter  $MINI = 0$

$E_{CM}(I)$	$S_{Z1}(I)$	$S_{Z2}(I)$	$S_Z(I)$	$SF(I)$
.100000E-02	.144159E-08	.471344E-14	.144159E-08	.963717E-03
.200000E-02	.211039E-05	.812107E-11	.211040E-05	.970529E-03
.300000E-02	.495546E-04	.219350E-09	.495549E-04	.998703E-03
.400000E-02	.315976E-03	.158129E-08	.315978E-03	.103340E-02
.500000E-02	.110280E-02	.615615E-08	.110280E-02	.107107E-02
.600000E-02	.275358E-02	.169553E-07	.275360E-02	.111079E-02
.700000E-02	.557894E-02	.375720E-07	.557898E-02	.115113E-02
.800000E-02	.982720E-02	.718512E-07	.982728E-02	.119215E-02
.900000E-02	.156765E-01	.123657E-06	.156766E-01	.123366E-02
.100000E-01	.232417E-01	.196727E-06	.232419E-01	.127555E-02

Hence, it is obviously that the  $S$ -factor at 1 keV equals approximately the value  $10^{-4}$  eV b or 0.01%, which can be considered as the error of the WF calculation method.

## **Conclusion**

Thus, in the framework of the considered cluster model based on the  $E1$  transition only, it was possible to predict the general behavior of the  $S$ -factor of the  $p^3H$  capture at energies from 50 to 700 keV. Indeed, based on the analysis of experimental data above 700 keV about 20 years ago, we made predictions of the behavior of the  $S$ -factor for energies as low as 10 keV [93]. It can be seen now that the results of these calculations well reproduce new data on the  $S$ -factor obtained in [105] (points in Figs. 4.4a, 4.4b) at energies from 50 keV to 5 MeV [115].

So, the using two-body model, which are based on intercluster potentials describing phase shifts of elastic scattering and characteristics of the bound state, with parameters suggested about 20 years ago [88,93], allows correctly describe the astrophysical  $S$ -factor on the base of the  $E1$  transition in the whole energy range. The structure of FSs of such potentials is defined on the base of cluster state classification according to Young



tableau.

# 5. PROTON RADIATIVE CAPTURE ON ${}^6\text{Li}$ PROCESS

---

## *Introduction*

New measurement of the differential cross sections of the elastic  $p{}^6\text{Li}$  scattering at energies from 350 keV to 1.15 MeV in laboratory system (l.s.) with 10% error has been performed for improvement of the available experimental data in [27,116]. The data [27] considered in this section was obtained for five energies: 593 keV for 13 scattering angles in an interval of  $57^\circ\div 172^\circ$ , 746.7 and 866.8 keV for 11 scattering angles in an interval of  $45^\circ\div 170^\circ$ , and 976.5 and 1136.6 keV for 15 scattering angles in an interval of  $30^\circ\div 170^\circ$ .

We performed the phase shift analysis and obtained the  ${}^2_4S$  and  ${}^2P$  scattering phase shifts based on measurements [27,116] and differential cross sections of the elastic scattering at energy of 500 keV from an earlier paper [117]. The found phase shifts were used to construct the potentials for  $L = 0$  in the  $p{}^6\text{Li}$  interactions at low energies without taking into account spin-orbital splitting, and then the astrophysical  $S$ -factor was calculated for energies beginning from 10 keV.

Though, it seems, that the reaction of the proton radiative capture on  ${}^6\text{Li}$  may be of certain interest for nuclear astrophysics [118], it has not been experimentally studied sufficiently well. There are comparatively few works devoted to measurements of the total cross sections and determination of the astrophysical  $S$ -factor [34] performed in the energy range from 35 keV to 1.2 MeV. However, it seems to us that it is of interest to consider the possibility of description of the  $S$ -factor in the astrophysical energy region where experimental data is available using the potential cluster model with classification of bound states according to orbital Young's tableaux [119,120].

### 5.1. Differential cross sections

At the examination of scattering processes in the system of particles with spins 1/2 and 1 without taking into account spin-orbital splitting of phase shifts, the cross section of the elastic scattering is represented in the simplest form [46]

$$\frac{d\sigma(\theta)}{d\Omega} = \frac{2}{6} \frac{d\sigma_d(\theta)}{d\Omega} + \frac{4}{6} \frac{d\sigma_k(\theta)}{d\Omega} , \quad (5.1)$$

where the indices  $d$  and  $k$  are related to the doublet (with a total spin 1/2) and quartet (with a total spin 3/2) states of the  $p^6\text{Li}$  scattering and the cross sections themselves are expressed in terms of scattering amplitudes

$$\begin{aligned} \frac{d\sigma_d(\theta)}{d\Omega} &= |f_d(\theta)|^2 , \\ \frac{d\sigma_k(\theta)}{d\Omega} &= |f_k(\theta)|^2 , \end{aligned} \quad (5.2)$$

which are written in the form

$$f_{d,k}(\theta) = f_c(\theta) + f_{d,k}^N(\theta) , \quad (5.3)$$

where

$$\begin{aligned} f_c(\theta) &= - \left( \frac{\eta}{2k \sin^2(\theta/2)} \right) \exp \{ i\eta \ln[\sin^{-2}(\theta/2)] + 2i\sigma_0 \} , \\ f_d^N(\theta) &= \frac{1}{2ik} \sum_L (2L+1) \exp(2i\sigma_L) [S_L^d - 1] P_L(\cos\theta) , \\ f_k^N(\theta) &= \frac{1}{2ik} \sum_L (2L+1) \exp(2i\sigma_L) [S_L^k - 1] P_L(\cos\theta) , \end{aligned} \quad (5.4)$$

and  $S_L^{d,k} = \eta_L^{d,k} \exp[2i\delta_L^{d,k}(k)]$  is the scattering matrix in the doublet and quartet spin state [46].

The possibility of application of simple expressions (5.1–5.4) for calculation of elastic scattering cross sections is due to the fact that, in the low-energy region, the spin-orbital splitting of phase shifts is relatively small, which is proved by the results of phase shift analysis performed in [121], in which spin-orbital splitting of scattering phase shifts was taken into account.

## 5.2. Phase shift analysis

Earlier phase shift analysis of differential cross sections and excitation functions for the elastic  $p^6\text{Li}$  scattering without taking into account the doublet  $^2P$  wave has been performed in [121]. Our phase shift analysis is performed at lower energies important for nuclear astrophysics and takes into account all lower partial waves, including the doublet  $^2P$  wave. The analysis is based on the differential cross sections given in [27,116] and [117].

At an energy of 500 keV, based on data from [117], we found the  $^2S$  and  $^4S$  scattering phase shifts given in Table 5.1 numbered 1. The obtained results of calculation of cross sections quite agree with experimental data for the averaged over all points  $\chi^2 = 0.15$ . The error of differential cross sections of this data was assumed equal to 10%. The account of the doublet  $^2P$  and quartet  $^4P$  phase shifts showed that their numerical values are smaller than  $0.1^\circ$ .

The next five energies correspond to new results of measurement of differential cross sections performed in [27,116]. The first of them, 593 keV, provides the possibility of finding the  $^{2,4}S$  phase shifts, which slightly differ from phase shifts at the previous energy, possess the same  $\chi^2$ , and are given in Table 5.1 numbered 2; the phase shifts for  $^{2,4}P$  waves also tend toward zero.

At an energy of 746.7 keV, we find the  $^{2,4}S$  phase shifts (Table 5.1, No. 3-1), which make it possible to describe the cross sections with the accuracy  $\chi^2 = 0.23$ . In spite of the smallness of  $\chi^2$ , the attempt to take into account the  $^{2,4}P$  phase shifts has been made. First it was assumed that the

quartet  $^4P$  phase shift is negligible, which follows from the results of [121], in which the account began from 1.0÷1.5 MeV.

**Table 5.1. Results of phase shift analysis of elastic  $p^6\text{Li}$  scattering**

No.	$E$ (keV)	$^2S$ (deg)	$^4S$ (deg)	$^2P$ (deg)	$^4P$ (deg)	$\chi^2$
1	500.0	176.2	178.7	—	—	0.15
2	593.0	174.2	178.8	—	—	0.15
3-1	746.4	170.1	180.0	—	—	0.23
3-2	746.4	172.5	179.9	1.7	—	0.16
4-1	866.8	157.8	180.0	—	—	0.39
4-2	866.8	170.2	174.9	3.9	—	0.22
4-3	866.8	169.6	175.0	3.5	0.1	0.23
5-1	976.5	160.0	178.5	—	—	0.12
5-2	976.5	167.0	174.5	1.1	—	0.12
6-1	1136.3	144.9	180.0	—	—	0.58
6-2	1136.3	164.7	171.1	5.8	—	0.32
6-3	1136.3	166.4	169.9	5.5	0.1	0.32

The results of our analysis taking into account the  $^2P$  phase shift only are shown in Table 5.1 numbered 3.2. It can be seen that taking into account the small doublet  $^2P$  phase shift somewhat changes the value of the doublet  $^2S$  phase shift, increasing its value, and decreases  $\chi^2 = 0.16$ . Taking into account the quartet  $^4P$  phase shift yielded a negligible value, smaller than  $0.1^\circ$ , which completely agrees with the results of [121] and our results for energy of 866.8 keV.

The result of a phase shift search for energy of 866.8 keV taking into account the  $^2^4S$  waves only is given in Table 5.1 No.4-1 for  $\chi^2 = 0.39$ . It can be seen that the value of the  $^2S$  phase shift sharply drops as compared with the previous energy. The account of the  $^2P$  wave noticeably increases its value (Table 5.1 No.4-2) and decreases the value of  $\chi^2$  by practically a factor of 2. The attempt to take into account the quartet  $^4P$  phase shift resulted in a value no higher than  $0.1^\circ$  (Table 5.1 No.4-3), which indicates

a small contribution of this phase shift at this energy. Any increase of the  $^4P$  wave, including for other values of the other phase shifts, resulted in the growth of  $\chi^2$ . For this energy, as well as all other considered energies from [26,113], it is impossible to find any variant for nonzero quartet phase shift if  $\chi^2$  tends to minimum.

For the next energy of 976.5 keV, the values of the  $^2S$  and  $^4S$  phase shifts were found without considering the  $^2,4P$  waves (see Table 5.1 No.5-1). The subsequent account of the  $^2P$  wave noticeably increases the value of the  $^2S$  phase shift if the  $^4P$  wave is neglected, as can be seen from Table 5.1 No.5-2 for  $\chi^2 = 0.12$ . If the quartet  $^4P$  wave is included in the analysis, it tends toward zero with decreasing  $\chi^2$ .

The last from the considered energies equals of 1.1363 MeV from [27,116], even when one takes into account the  $^2,4S$  waves only results to the relatively low  $\chi^2$  equals 0.58 (see Table 5.1 No.6-1). In this case taking into account the  $^2P$  wave results in a noticeable increase of the  $^2S$  phase shift. The corresponding results of the cross section calculation are shown in Table 5.1 No.6-2. The process of taking into account the quartet  $^4P$  wave, at this energy, leads it to the value about  $0.1^\circ$ , as it is shown in Table 5.1 No.6-3.

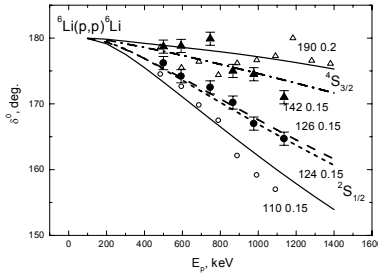


Fig. 5.1a. Doublet and quartet  $S$  phase shifts of the elastic  $p^6\text{Li}$  scattering at low energies. Doublet and quartet  $S$  phase shifts in the presence of the  $^2P$  wave are given when the  $^4P$  phase shift was equal to zero. The  $^2S$  (points) and the  $^4S$  (triangles) phase shifts were obtained according to data [27,116,117]. Upward open triangles and open circles show results of phase shift analysis [121] for comparison. Lines show results of calculation with different potentials.

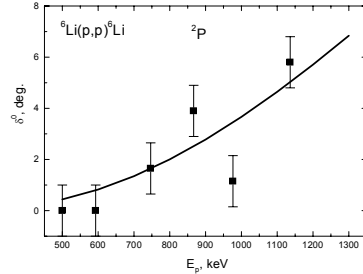


Fig. 5.1b. Doublet  $^2P$  phase shifts of the elastic  $p^6\text{Li}$  scattering at low energies. Squares show the results of our phase shift analysis at  $^4P = 0$ . The solid line shows the result of calculation with the found potential.

Thus, for description of all experimental data from [27,116], it is not necessary to take into account the quartet  $^4P$  waves in this energy region, i.e., their value is equal to or smaller than  $0.1^\circ$ . On the whole, this agrees with the results of [121]; however, the doublet  $^2P$  phase shift reaches almost  $5.5^\circ \div 6^\circ$  and cannot be neglected. The general form of the  $^2S$  and  $^4S$  scattering phase shifts are shown in Fig. 5.1a, and the doublet  $^2P$  phase shifts are shown in Fig. 5.1b. In spite of the rather large spread of results for the  $^4S$  phase shifts, the doublet  $^2S$  phase shift has a certain tendency toward a smaller magnitude, but this takes place much more slowly than it follows from results of analysis [121], in which the  $^2P$  wave was not taken into account. If the doublet  $^2P$  wave is not taken into account in our analysis, results very close to the results of phase shift analysis from [121] are obtained for the  $^2S$  scattering phase shift.

The errors of the elastic scattering phase shifts are determined by the ambiguity of the phase shift analysis, namely, for virtually the same value of  $\chi^2$ , which can be differ by  $5 \div 10\%$ , it is possible to obtain somewhat different magnitudes of scattering phase shifts. We estimate this ambiguity on the level of  $1^\circ \div 1.5^\circ$ ; this is shown for the  $^2,4S$  and the  $^2P$  phase shifts in Figs. 5.1a and 5.1b.

### 5.3. Cluster states classification

The possible orbital Young tableaux in the  $p^6\text{Li}$  system turn out to be forbidden, if the tableau  $\{6\}$  forbidden for the  $^2\text{H}^4\text{He}$  channel in  $^6\text{Li}$  is used. They correspond to the forbidden states with  $\{7\}$  and  $\{61\}$  configurations and the moment of relative movement  $L = 0$  and 1, which evaluates by the Elliot rule [123]. The forbidding of such diagrams for wave functions follows from requirement of the Littlewood's theorem that it can not be more than four cells in one row of Young tableau for nuclei of  $p$ -shell [123].

When the allowed tableau  $\{42\}$  in the  $^2\text{H}^4\text{He}$  cluster channel of  $^6\text{Li}$  is accepted, then, for the complete system  $p^6\text{Li}$ , with spin  $S = 1/2$  there is the forbidden level with the tableau  $\{52\}$  and moments one and two, and there are forbidden states with  $\{43\}$  and  $\{421\}$  configurations for  $L = 1$ . Thus, the  $p^6\text{Li}$  potentials ought to have forbidden bound  $\{52\}$  state in the  $S$  wave and allowed bound level in the  $P$  wave with two Young tableaux  $\{43\}$  and  $\{421\}$ . Only one tableau  $\{421\}$  is allowed in the quartet spin state of this

system, as it was shown in Table 5.2. The table was obtained on the basis of the results given in [45].

**Table 5.2. Classification of the orbital states in the  $p^6\text{Li}$  and the  $n^6\text{Li}$  systems.**

System	$T$	$S$	$\{f\}_T$	$\{f\}_S$	$\{f\}_{ST} = \{f\}_S \otimes \{f\}_T$	$\{f\}_L$	$L$	$\{f\}_{AS}$	$\{f\}_{FS}$
$n^6\text{Li}$ $p^6\text{Li}$	1/2	1/2	{43}	{43}	$\{7\} + \{61\} + \{52\}$	$\{7\}$	0	—	$\{7\}$
					+	$\{61\}$	1	—	$\{61\}$
					$+ \{511\} + \{43\} +$	$\{52\}$	0,2	—	$\{52\}$
					$+ \{421\} + \{4111\} +$	$\{43\}$	1,3	{43}	—
					$\{322\} ++ \{3211\} +$	$\{421\}$	1,2	{421}	—
	3/2	3/2	{43}	{52}	$\{2221\} + \{331\}$				
					$\{61\} + \{52\} +$	$\{7\}$	0	—	$\{7\}$
					$\{511\} ++ \{43\} +$	$\{61\}$	1	—	$\{61\}$
					$2\{421\} +$	$\{52\}$	0,2	—	$\{52\}$
					$+ \{331\} + \{322\} +$	$\{43\}$	1,3	—	$\{43\}$
					$+ \{3211\}$	$\{421\}$	1,2	{421}	—

It is possible that it is more correctly to consider both acceptable tableaux  $\{6\}$  and  $\{42\}$  for the bound states of  $^6\text{Li}$ , since both of them are included to the number of forbidden and allowed states of the  $^2\text{He}^4\text{He}$  configuration. Then the level classification will be slightly different, the number of forbidden states will increase, and additional forbidden bound level will be added in the each partial wave with  $L = 0$  and 1. This, more complete, tableau of states also listed in Table 5.2, and intrinsically it is the sum of first and second cases, considered above. In Table 5.2 the complete spin  $\{f\}_S$  and isospin  $\{f\}_T$  Young tableaux of  $^7\text{Be}$  in the  $p^6\text{Li}$  channel, their production  $\{f\}_{ST}$ , and all possible orbital  $\{f\}_L$  symmetries of the  $p^6\text{Li}$  system, which are divided into allowed  $\{f\}_{AS}$  and forbidden  $\{f\}_{FS}$  tableaux with the orbital moments  $L$ .

The next notations were used in Table 5.2:  $T$ ,  $S$  and  $L$  are, respectively, the isospin, spin and orbital moment of particles in the  $p^6\text{Li}$  system;  $\{f\}_S$ ,  $\{f\}_T$ ,  $\{f\}_{ST}$  and  $\{f\}_L$  are, respectively, the spin, isospin, spin-isospin and possible orbital Young tableaux;  $\{f\}_{AS}$  and  $\{f\}_{FS}$  are the Young tableaux of allowed and forbidden states, respectively. The conjugate Young tableaux



$\{f\}_{ST}$  and  $\{f\}_L$  are shown in boldface italic font

As it is seen from this table, there are two allowed tableaux  $\{43\}$  and  $\{421\}$  in the doublet spin state of the  $p^6\text{Li}$  system and then scattering states are mixed according to orbital symmetries. At the same time, one generally consider that for the doublet GS of  $^7\text{Be}$  in the  $p^6\text{Li}$  channel with  $J = 3/2^-$  и  $L = 1$  corresponds only one allowed tableau  $\{43\}$  [119]. The considered  $p^6\text{Li}$  system is completely analogous to the  $p^2\text{H}$  channel of  $^3\text{He}$ , which doublet state is also mixed according to the Young tableaux  $\{3\}$  and  $\{21\}$ . Therefore, the potentials, which are constructed on the base of the phase shifts of the elastic scattering description in the  $p^6\text{Li}$  system can not use for the description of the GS of  $^7\text{Be}$  in the  $p^6\text{Li}$  channel.

In this case, the phase shifts of the  $p^6\text{Li}$  elastic scattering so as the  $p^2\text{H}$  system (2.11), is presented as a halfsum of the pure phase shifts [21,22]

$$\delta_L^{\{43\}+\{421\}} = 1/2\delta_L^{\{43\}} + 1/2\delta_L^{\{421\}}.$$

The mixed phase shifts are determined as a result of the phase shift analysis of the experimental data, which is, generally, differential cross sections of the elastic scattering or excited functions. Then, it is supposed [21,22] that it is possible to use the phase shifts, of the same symmetry from the quartet channel, as the  $\{421\}$  pure phase shifts of the doublet channel. As a result, it is possible to find the  $\{43\}$  pure doublet phase shifts of the  $p^6\text{Li}$  scattering and use these phase shifts for the construction the pure interaction, which ought to correspond to the potential of the bound state of the  $p^6\text{Li}$  system in  $^7\text{Be}$  [21,22].

#### **5.4. Potential description of the scattering phase shifts**

For obtaining the partial intercluster  $p^6\text{Li}$  interactions according to available scattering phase shifts, we use the common Gaussian potential with a point-like Coulomb term that can be represented in form (2.8). The following potential parameters were obtained for description of the results of phase shift analysis from [121]

$$^2S: V_0 = -110 \text{ MeV}, \quad \alpha = 0.15 \text{ fm}^{-2},$$

$$^4S: V_0 = -190 \text{ MeV}, \quad \alpha = 0.2 \text{ fm}^{-2}.$$

The obtained potentials contain two forbidden bound states corresponding to Young tableaux  $\{52\}$  and  $\{7\}$  [22,119]. The results of phase shift calculation for these potentials are shown in Fig. 5.1a by solid lines together with the results of phase shift analysis from work [121] which shown by circles and open triangles.

For the description of the obtained scattering phase shifts, the potentials with the next parameters are more preferred

$$^2S: V_0 = -126 \text{ MeV}, \quad \alpha = 0.15 \text{ fm}^{-2},$$

$$^4S: V_0 = -142 \text{ MeV}, \quad \alpha = 0.15 \text{ fm}^{-2}.$$

These potentials also contain two forbidden bound states with Young tableaux  $\{52\}$  and  $\{7\}$ . The phase shifts calculated using these potentials are shown in Fig. 5.1 by the dashed and the dot-dashed lines, in comparison with the results of our phase shift analysis shown by points and triangles.

The potential for the doublet  $^2P$  wave of the elastic  $p^6\text{Li}$  scattering can be represented, for example, by the following parameters

$$^2P: V_0 = -68.0 \text{ MeV}, \quad \alpha = 0.1 \text{ fm}^{-2}.$$

The solid line in Fig. 5.1b shows the results of the calculation of phase shifts with this potential, which has one forbidden bound state with the Young tableau  $\{61\}$  and allowed state with Young tableaux  $\{43\}$  and  $\{421\}$ .

This potential wrongly represents the binding energy of  $^7\text{Be}$  in the  $p^6\text{Li}$  channel because this allowed state turns out to be mixed with respect to the two above symmetries, while the ground bound state corresponds only to the tableau  $\{43\}$  [119,120]. Even if the methods, for obtaining the pure phase shifts presented in [119,120], are used it is impossible to obtain a potential of the ground state that is pure according to Young tableaux. This is probably due to low clusterization probability of  $^7\text{Be}$  in the  $p^6\text{Li}$  channel, which value has the essential role using the abovementioned methods.

Therefore, a the  $^2P_{3/2}$  wave potential of the ground state of  $^7\text{Be}$  that was

pure according to orbital symmetries with Young tableau  $\{43\}$  was constructed in such a way that the channel energy, i.e., the binding energy of the ground state of the nucleus with  $J = 3/2^-$  as  $p^6\text{Li}$  system and its root-mean-square radius, were described well. The thus-obtained parameters of the pure  ${}^2P_{3/2}^{\{43\}}$ -potential are as follows

$${}^2P_{3/2}: V_0 = -252.914744 \text{ MeV}, \quad \alpha_P = 0.25 \text{ fm}^{-2}. \quad (5.5)$$

This potential in the framework of the finite-difference method yields the binding energy of an allowed state with the Young tableau  $\{43\}$  equal to  $-5.605800 \text{ MeV}$  for an experimental value of  $-5.6058 \text{ MeV}$  [124] and has one forbidden state corresponding to Young tableau  $\{61\}$ . The root-mean-square charge radius turns out to be equal to  $2.63 \text{ fm}$ , which on the whole agrees with the data of [124], and the constant  $C_W$  from (2.10) in an interval of  $5 \div 13 \text{ fm}$  is equal to  $2.66(1)$ . The AC value of  $2.85(4) \text{ fm}^{-1/2}$  was obtained in [125] that is after the recalculation to the dimensionless value at  $\sqrt{2k} = 0.983$  gives  $2.90(5)$ . It is quite agree with the obtained above value.

For the parameters of  ${}^2P_{1/2}^{\{43\}}$  potential of the first excited state of  ${}^7\text{Be}$  with  $J = 1/2^-$ , the following values were obtained

$${}^2P_{1/2}: V_0 = -251.029127 \text{ MeV}, \quad \alpha_P = 0.25 \text{ fm}^{-2}. \quad (5.6)$$

This potential results in a binding energy of  $-5.176700 \text{ MeV}$  for an experimental value of  $-5.1767 \text{ MeV}$  [124] and contains the forbidden state with tableau  $\{61\}$ . Asymptotic constant (2.10) in an interval of  $5 \div 13 \text{ fm}$  is equal to  $2.53(1)$ , and the root-mean-square charge radius is equal to  $2.64 \text{ fm}$ . The absolute accuracy of finding the energy of the bound levels for the  $p^6\text{Li}$  system in  ${}^7\text{Be}$  for our new programs specified to be equal to  $10^{-6} \text{ MeV}$  [26]. The parameters of potentials of bound states obtained here somewhat differ from our previous results [119]. This is connected with the use of precise values of particle masses and more accurate description of the experimental values of energy levels [124].

The variational method, used for controlling of the accuracy of determination of the binding energy, yielded a value of  $-5.605797 \text{ MeV}$

for the energy of the ground state, and as we said in section three, for this potential the mean binding energy obtained by two methods is – 5.6057985(15) MeV. Therefore, the accuracy of calculation of the binding energy, obtained by two different methods and by two different programs, is equal to  $\pm 1.5$  eV. The asymptotic constant in the interval of 5÷13 fm turned out to be relatively stable and equals 2.67(2), and the root-mean-square charge radius coincided with the results of the finite-difference method. The variational wave function of form (2.9) for the ground state of  ${}^7\text{Be}$  in the  $p^7\text{Li}$  channel with potential (5.5) is given in Table 5.3, and the residual WF value does not exceed  $10^{-12}$ .

**Table 5.3. Variational parameters and expansion coefficients of the radial wave function of the ground bound state for the  $p^6\text{Li}$  system of  ${}^7\text{Be}$  for  ${}^2P_{3/2}$  potential (5.5). Normalization of the function with these coefficients in an interval of 0÷25 fm is  $N = 0.999999999999895$**

$i$	$\beta_i$	$C_i$
1	2.477181344627947E-002	1.315463702527344E-003
2	5.874061769072439E-002	1.819913407984276E-002
3	1.277190608958812E-001	9.837541674753882E-002
4	2.556552559403827E-001	3.090018297080802E-001
5	6.962545656024610E-001	-1.195304944694753
6	87.215179556255360	3.237908749007494E-003
7	20.660304078047520	5.006096657700867E-003
8	1.037788131786810	-6.280751485496025E-001
9	2.768782138965186	1.282309968994793E-002
10	6.753591325944827	8.152343478073063E-003

The variational method yielded an energy of –5.176697 MeV for the first excited level; therefore, the average energy is equal to –5.1766985(15) MeV with the same accuracy for both methods as for the ground state. The asymptotic constant in an interval of 5÷13 fm is about 2.53(2), the residual is no larger than  $10^{-12}$ , and the root-mean-square charge radius almost does not differ from the corresponding value for the ground state. The parameters of the wave function (2.9) of the excited state of  ${}^7\text{Be}$  in the  $p^6\text{Li}$

channel for potential (5.6) are given in Table 5.4.

**Table 5.4. Variational parameters and expansion coefficients of the radial wave function of the first excited bound state for the  $p^6\text{Li}$  system of  ${}^7\text{Be}$  for  ${}^2P_{1/2}$  potential (5.6). Normalization of the function with these coefficients on an interval of  $0\div 25$  fm is  $N = 0.9999999999999462$**

$i$	$\beta_i$	$C_i$
1	2.337027900191992E-002	1.218101547601343E-003
2	5.560733180673633E-002	1.653319276756672E-002
3	1.214721917930904E-001	9.009619752334307E-002
4	2.474544878067495E-001	3.003291466882630E-001
5	7.132725465249825E-001	-1.332325501226168
6	84.896023494945160	3.273725679869025E-003
7	1.162854732120233	-5.340018423135894E-001
8	1.574203000936825	9.367648737801053E-002
9	5.779896847077723	1.033713941440747E-002
10	19.422905786572090	5.314592946045428E-003

Let us give potential parameters, which describe the quartet  ${}^4P$  elastic scattering phase shifts from work [121]

$${}^4P_{1/2}: V_0 = -802.0 \text{ MeV}, \quad \alpha = 0.5 \text{ fm}^{-2},$$

$${}^4P_{3/2}: V_0 = -4476.0 \text{ MeV}, \quad \alpha = 2.65 \text{ fm}^{-2},$$

$${}^4P_{5/2}: V_0 = -1959.0 \text{ MeV}, \quad \alpha = 1.15 \text{ fm}^{-2}.$$

The quality of phase shift description using these potentials is illustrated in Figs. 5.2a and 5.2b. The potentials contain two forbidden bound states, which correspond to the forbidden, in the quartet spin channel, Young tableaux  $\{61\}$  and  $\{43\}$ .

It should be noted that, based on the results for the doublet  ${}^2P$  scattering phase shift shown in Fig. 5.1b obtained in this phase shift analysis, it is impossible to construct an unambiguous  ${}^2P$  potential. For this purpose,

results of the analysis at higher energies are necessary and they should be obtained taking into account the  $^2P$  wave and spin-orbital splitting of phase shifts.

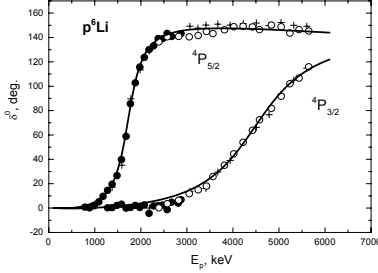


Fig. 5.2a. Quartet  $^4P$  phase shifts of the elastic  $p^6\text{Li}$  scattering. Points, circles, and crosses show the results of phase shift analysis [121]. Solid lines show the results of calculation with the obtained potentials.

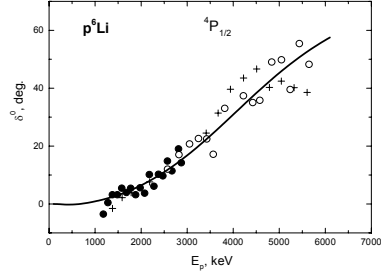


Fig. 5.2b. Quartet  $^4P$  phase shifts of the elastic  $p^6\text{Li}$  scattering. Points, circles, and crosses show the results of phase shift analysis [121]. The solid line shows the result of calculation with the found potential.

### 5.5. Astrophysical $S$ -factor

Upon examination of the astrophysical  $S$ -factor, the  $E1$  transitions from the  $^2S$  and the  $^2D$  scattering states to the ground  $^2P_{3/2}$  and the first excited  $^2P_{1/2}$  bound states of  $^7\text{Be}$  in the  $p^6\text{Li}$  channel have been taken into account. The wave function of the  $^2D$  scattering state without account being taken of spin-orbital splitting has been calculated based on the  $^2S$  potential with the orbital angular momentum  $L = 2$ . The results of calculations showed that the above  $^2S$  scattering potential based on phase shift analysis [121] with a depth of 110 MeV strongly underestimates the astrophysical  $S$ -factor. At the same time, the doublet  $^2S$  potential with a depth of 126 MeV following from our results correctly reproduces the general behavior of the experimental  $S$ -factor. The obtained results are shown in Fig. 5.4. The dashed line shows the result for the transition from the  $^2S$  and the  $^2D$  scattering waves to the ground state of the  $^7\text{Be}$  nucleus, the dotted line shows the results for the transitions to the first excited state, and the solid line shows the total  $S$ -factor. Points, triangles, and circles show experimental data from [126] given in [127].

The calculated  $S$ -factor for 10 keV has the values  $S(3/2^-) = 76$  eV b

and  $S(1/2^-) = 38$  eV b for a total value of 114 eV b. The obtained  $S(1/2^-)$ -factor quite well describes the experimental data for transition to the first excited state of  ${}^7\text{Be}$  at low energies (circles in the left and at the bottom of Fig. 5.3). For comparison of the calculated  $S$ -factor at zero energy (an energy of 10 keV is taken as zero), we present the known results for the total  $S(0)$  factor: 79(18) [128], 105 (at 10 keV) [127], and 106 eV b [129]. For the  $S$ -factor in the case of transition to the ground state, a value of 39 eV b is given in [130], and for transition to the first excited state, 26 eV b; therefore, the total  $S$ -factor is equal to 65 eV b. It can be seen that there exists a rather large difference in the data and our results, on the whole, agree with the available data.

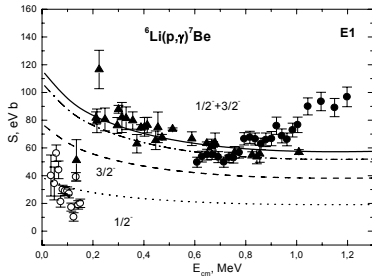


Fig. 5.3. Astrophysical  $S$ -factor of the proton radiative capture on  ${}^6\text{Li}$ . Points, triangles, and circles show experimental data [126] given in [127]. The dashed line shows the result for transitions from the  ${}^2S$  and  ${}^2D$  scattering waves to the ground state of  ${}^7\text{Be}$  and the dotted line for transitions to the first excited state. The solid line shows the total  $S$ -factor.

this potential is shown in Fig. 5.3 by a dash-dotted line, which agrees within error with the experimental data at energies below 1 MeV.

It should be noted that, if potentials without forbidden states or with another number of these states are used in  $S$  or  $P$  waves, the calculated value of the  $S$ -factor turns out to be essentially smaller than the values obtained earlier. For example, the  ${}^2S$  potential with one forbidden state and the parameters of 25 MeV and  $0.15 \text{ fm}^{-2}$ , which quite well describes scattering phase shifts, and the potential of the ground state presented above yield for 10 keV an  $S$ -factor approximately equal to 1 eV b.

The dot-dashed line in Fig. 5.3 at the range of 1÷200 keV at the average value of  $\chi^2 = 0.0048$  and at the errors of 10% for the calculated

Moreover, a slight change of the depth of the  ${}^2S$  scattering potential, which virtually has no impact on the behavior of calculated phases, rather strongly influences the  $S$ -factor. For example, for the potential depth equal to 124 MeV, the phases are shown in Fig. 5.1a by short-dashed lines, and for energy of 10 keV we obtain 105 eV b for the  $S$ -factor, that is in a good agreement with the latest experimental data [127,128]. The total  $S$ -factor with

value can be parametrized by the expression

$$S(E_{\text{cm}}) = S_0 + E_{\text{cm}}^{1/2} S_1, \quad (5.7)$$

with parameters  $S_0 = 109.58 \text{ eV b}$  and  $S_1 = -2.3992 \text{ eV b keV}^{-1/2}$ . Meanwhile, the experimental value of the  $S$ -factor at zero energy of  $106 \text{ eV b}$  [129] was used for 1 keV. At the second method of parametrization, considered in paragraph 3.2, we obtain:  $S_0 = 106.00 \text{ eV b}$  and  $S_1 = -2.0647 \text{ eV b keV}^{-1/2}$  at  $\chi^2 = 0.0230$ .

## **Conclusion**

Thereby, the phase shift analysis of new experimental data of the elastic  $p^6\text{Li}$  scattering was done for obtaining of intercluster potentials. Then, the potentials of intercluster interaction for continuous spectrum were constructed on the basis of the obtained scattering phase shifts. These potentials are mixed according to Young tableaux and contain forbidden states, in what connection each partial wave is described by its own potential of the Gaussian form with certain parameters. The potentials pure according to Young tableaux were used for the description of the bound states of  $^7\text{Be}$ ; they describe its main characteristics and, in the first place, the binding energy. Thus, the doublet  $^2S$  phase shifts obtained in our phase shift analysis that take into account the doublet  $^2P$  phase shift result in a potential that, unlike interaction constructed based on the results of analysis [121], provides a description of the experimental  $S$ -factor at energies below 1 MeV. Similarly to in the case of lighter nuclei [110], the applied potential cluster model with the above potentials makes it possible to obtain quite reasonable results in description of process of the proton radiative capture on  $^6\text{Li}$  in the astrophysical energy region [131,132].

However, it must be noted that in work [3] for the  $n^6\text{Li}$  system the variant of the classification of orbital states was considered, when only the Young tableau  $\{42\}$  is used for  $^6\text{Li}$ . It is quite enough for the correct description of the available data on the proton capture on  $^6\text{Li}$  at astrophysical energies. Therefore, it is impossible to give specified preference of one of these variants of classification of states in this system.



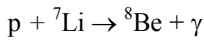


## **6. S-FACTOR OF THE PROTON RADIATIVE CAPTURE ON ${}^7\text{Li}$**

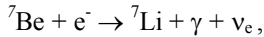
---

### ***Introduction***

Reaction of the radiative capture



at ultralow energies resulting in formation of unstable  ${}^8\text{Be}$ , which decays into two  $\alpha$ -particles may take place along with the weak process



as one of the final reactions of the proton-proton chain [2]. Therefore, the in-depth study of this reaction, in particular of the form and energy dependence of the astrophysical  $S$ -factor, is of a certain interest for the nuclear astrophysics.

To calculate the astrophysical  $S$ -factor of the proton radiative capture on  ${}^7\text{Li}$  in the modified potential cluster model [3,22] which we usually use for such calculations [110,115,133,134] it is necessary to know partial potentials of the  $p$ - ${}^7\text{Li}$  interaction in the continuous and discrete spectra. We will again assume that such potentials should follow the classification of cluster states by orbital symmetries [21] as it was assumed in our earlier works [48,60,122] and in previous sections of this book, for other nuclear systems.

Let us note, that in the using approach, the potentials of scattering processes are usually constructed on the basis of description of elastic scattering phase shifts obtained from experimental data while the interactions in bound states are determined by the requirement to reproduce the main characteristics of the bound state of the nucleus assuming that it is mainly due to cluster channel consisting of the initial particles of the

considering reaction.

For example, in the radiative capture process  ${}^2\text{H}$  and  ${}^4\text{He}$  particles colliding at low energies form  ${}^6\text{Li}$  in the ground state, and the remaining energy are released as a  $\gamma$ -quantum. Since there is no restructuring in such reactions we can consider potentials of one and the same nuclear system of particles that is the  ${}^2\text{H}{}^4\text{He}$  system in continuous and discrete spectra. In the latter case it is assumed that the ground state of  ${}^6\text{Li}$  is very likely caused by the  ${}^2\text{H}{}^4\text{He}$  cluster configuration. Such approach leads to quite reasonable results of the description of the astrophysical  $S$ -factors of this and some other reactions of radiative capture [134].

It seems that in this case  ${}^8\text{Be}$  does not consist of the  $p{}^7\text{Li}$  cluster system and most probably is determined by the  ${}^4\text{He}{}^4\text{He}$  configuration into which it decays. However, it is possible that  ${}^8\text{Be}$  will be in the bound state of the  $p{}^7\text{Li}$  channel for a while just after of the reaction of the proton radiative capture on  ${}^7\text{Li}$  and only after this it changes to the state defined by the bound  ${}^4\text{He}{}^4\text{He}$  system, which disintegrates to this channel. Such an assumption makes it possible to consider  ${}^8\text{Be}$  as the  $p{}^7\text{Li}$  cluster system and use the MPCM methods, at least at the initial stage of its formation in the reaction  $p + {}^7\text{Li} \rightarrow {}^8\text{Be} + \gamma$  [135].

### **6.1. Classification of the orbital states**

First, we would like to note that the  $p{}^7\text{Li}$  system has the  $T_z = 0$  isospin projection and it is possible for two values of total isospin  $T = 1$  and  $0$  [136], therefore the  $p{}^7\text{Li}$  channel is mixed by isospin as the  $p{}^3\text{H}$  system [110], even though as it will be shown later both of isospin states ( $T = 1, 0$ ), in contrast to the  $p{}^3\text{H}$  system, in the triplet spin state correspond to the allowed Young tableau  $\{431\}$  [21]. The cluster  $p{}^7\text{Be}$  and  $n{}^7\text{Li}$  channels with  $T_z = \pm 1$  and  $T = 1$  are pure by isospin in a complete analogy with the  $p{}^3\text{He}$  and  $n{}^3\text{H}$  systems [110].

The spin-isospin Young tableaux of  ${}^8\text{Be}$  for the  $p{}^7\text{Li}$  channel are the product of spin and isospin parts of the WF. Particularly, under consideration of any of these moments ( $S$  or  $T$ ) we will have  $\{44\}$  tableau at the ground state of  ${}^8\text{Be}$  with the zero moment, tableau  $\{53\}$  for a certain state with moment equals one and for the state with moment equals two –

$\{62\}$  symmetry form. In the first case, moments of four nucleons are directed to the opposite side to other four nucleons and the total moment of the system of eight nucleons is equal to zero. In the second case, moments of five nucleons are directed to the one side but three nucleons to another, as a result two nucleons remain not compensated and their total moment equals one. The last variant presents moments of six nucleons directed to one side and two nucleons to other side, four nucleons are not compensated and the total moment equals two.

**Table 6.1. The classification of the orbital states in the  $p^7\text{Li}$  ( $n^7\text{Be}$ ) systems for isospin  $T = 0$  and 1.**

Here:  $T$ ,  $S$  and  $L$  are, respectively, the isospin, spin and orbital moment of  $p^7\text{Li}$  system;  $\{f\}_S$ ,  $\{f\}_T$ ,  $\{f\}_{ST}$  and  $\{f\}_L$  are, respectively, the spin, isospin, spin-isospin and possible orbital Young tableaux;  $\{f\}_{AS}$  and  $\{f\}_{FS}$  are the Young tableaux of, respectively, allowed and forbidden states. The conjugate tableaux are shown in boldface italic font

System	$T$	$S$	$\{f\}_T$	$\{f\}_S$	$\{f\}_{ST} = \{f\}_S \otimes \{f\}_T$	$\{f\}_L$	$L$	$\{f\}_{AS}$	$\{f\}_{FS}$
$p^7\text{Li}$ $n^7\text{Be}$	0	1	$\{44\}$	$\{53\}$	$\{71\} + \{611\} + \{53\} +$ $+ \{521\} + \{431\} +$ $+ \{4211\} + \{332\} +$ $+ \{3221\}$	$\{8\}$	0	—	$\{8\}$
						$\{71\}$	1	—	$\{71\}$
	0	1	$\{44\}$	$\{53\}$	$\{71\} + \{611\} + \{53\} +$ $+ \{521\} + \{431\} +$ $+ \{4211\} + \{332\} +$ $+ \{3221\}$	$\{53\}$	1,3	—	$\{53\}$
						$\{44\}$	0,2,4	—	$\{44\}$
$p^7\text{Li}$ $n^7\text{Be}$	0	1	$\{44\}$	$\{53\}$	$\{71\} + \{611\} + \{53\} +$ $+ \{521\} + \{431\} +$ $+ \{4211\} + \{332\} +$ $+ \{3221\}$	$\{44\}$	0,2,4	—	$\{44\}$
						<b><i><math>\{431\}</math></i></b>	1,2,3	$\{431\}$	—
	0	1	$\{44\}$	$\{62\}$	$\{62\} + \{521\} + 44\} +$ $+ \{431\} + \{422\} +$ $+ \{3311\}$	$\{8\}$	0	—	$\{8\}$
						$\{71\}$	1	—	$\{71\}$
$p^7\text{Li}$ $n^7\text{Be}$	1	1	$\{53\}$	$\{53\}$	$\{8\} + 2\{62\} + \{71\} +$ $+ \{611\} + \{53\} +$ $2\{521\} + \{5111\} +$ $\{44\} + \{332\} +$ $+ 2\{431\} + 2\{422\} +$ $+ \{4211\} + \{3311\} +$ $+ \{3221\}$	$\{53\}$	1,3	—	$\{53\}$
						$\{44\}$	0,2,4	—	$\{44\}$
	1	1	$\{53\}$	$\{53\}$	$\{8\} + 2\{62\} + \{71\} +$ $+ \{611\} + \{53\} +$ $2\{521\} + \{5111\} +$ $\{44\} + \{332\} +$ $+ 2\{431\} + 2\{422\} +$ $+ \{4211\} + \{3311\} +$ $+ \{3221\}$	<b><i><math>\{431\}</math></i></b>	1,2,3	$\{431\}$	—
						$\{44\}$	0,2,4	—	$\{44\}$

	2	{53}	{62}	{71} + {62} + {611} + + 2{53} + 2{521} + + 2{431} + {422} + + {4211} + {332}	{8} {71} {53} {44} {431}	0 1 1,3 0,2,4 1,2,3	– – – – –	{8} {71} {53} {44} {431}
--	---	------	------	---	--------------------------------------	---------------------------------	-----------------------	--------------------------------------

If the tableau {7} is used for  ${}^7\text{Li}$  then possible Young tableaux of the  $p^7\text{Li}$  system turn out to be forbidden, because of the rule that there can not be more than four cells in a row [120,123], and they correspond to forbidden states with configurations {8} and {71} and relative motion moments (orbital angular moment)  $L = 0$  and 1, which is determined by the Elliot rule [123].

The  $p^7\text{Li}$  system, in the triplet spin state, contains forbidden states with the tableau {53} in the  $P_1$  wave and {44} in the  $S_1$  wave and allowed state with the configuration {431} at  $L = 1$  when the tableau {431} is accepted for  ${}^7\text{Li}$ . Thus, the  $p^7\text{Li}$  potentials in the different partial waves should have the forbidden bound state {44} in the  $S_1$  wave and forbidden and allowed bound levels in the  $P_1$  wave with tableaux {53} and {431}, respectively.

The considered classification is true for any isospin state of the  $p^7\text{Li}$  system ( $T = 0$  or 1) in the triplet spin channel. Allowed symmetries are absent for spin  $S = 2$  and all Young tableaux listed above correspond to forbidden states, as it was shown in Table 6.1.

Probably, as it was in a previous case for the  $p^6\text{Li}$  system, it is more correctly to consider both allowed tableaux {7} and {43} for bound states of  ${}^7\text{Li}$ , because of the fact that they exist in FSs and ASs of this nucleus in the  ${}^3\text{H}^4\text{He}$  configuration [134]. Then the level classification will be slightly different, the number of forbidden states will increase and an extra forbidden state will appear in each partial wave. Such more complete scheme of FSs and ASs, per se, is a sum of the first and the second cases considered above is listed in Table 6.1.

## 6.2. Potential description of the phase shifts of scattering

Because of the isospin mixing phase shifts of the  $p^7\text{Li}$  elastic scattering are represented as a half-sum of the isospin pure phase shifts (4.1) [20,25]

$$\delta^{\{T=1\}+\{T=0\}} = 1/2[\delta^{\{T=1\}} + \delta^{\{T=0\}}]$$

in complete analogy with the  $p^3\text{H}$  system. The phase shifts with  $T=1,0$  mixed by isospin are usually determined as a result of the phase shift analysis of the experimental data of differential cross sections of the elastic scattering or excitation function. The pure phase shifts with isospin  $T=1$  are determined from the phase shift analysis of the  $p^7\text{Be}$  or  $n^7\text{Li}$  elastic scattering. As a result it is possible to find the pure  $p^7\text{Li}$  scattering phase shifts with  $T=0$  and construct the interaction model using these results which have to correspond to the potential of the ground bound state for the  $p^7\text{Li}$  system of  $^8\text{Be}$  [21]. Just the same method of the phase shift separation was used for the  $p^3\text{H}$  system [22] and its absolute validity was shown [110,115].

However, we failed to find experimental data of differential cross sections or phase shifts of the  $p^7\text{Be}$  or  $n^7\text{Li}$  elastic scattering at astrophysical energies [137], so here we will consider only isospin-mixed potentials of the elastic scattering processes in the  $p^7\text{Li}$  system and pure potentials of the bound state with  $T=0$  which are constructed on the base of description BS characteristics and are chosen in the Gaussian form with point-like Coulomb term (2.8).

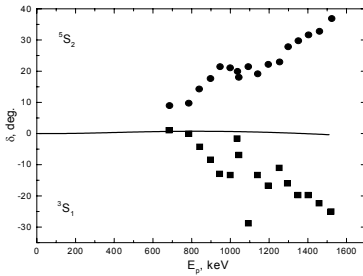


Fig. 6.1.  $^3S_1$  and  $^5S_2$  phase shifts of the elastic  $p^7\text{Li}$  scattering at low energies. Points and squares – phase shifts received from the experimental data in work [139]. Line – calculations with the Gaussian potential based on parameters given in the text.

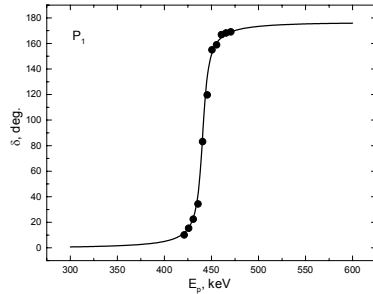


Fig. 6.2.  $^5P_1$  phase shift, which mixed with the  $^3P_1$  phase shift, for the elastic  $p^7\text{Li}$  scattering at low energies. Points – phase shifts received from the experimental data in work [139]. Line – calculations with the Gaussian potential based on parameters given in the text.

The phase shifts of the  $p^7\text{Li}$  elastic scattering obtained from the phase

shift analysis of the experimental data of excitation functions [138] taking into account spin-orbital splitting at the energies down to 2.5 MeV are given in work [139]. These phases, which are shown by points and squares in Figs. 6.1 and 6.2, we will use further for the intercluster potential construction for the  $p^7\text{Li}$  elastic scattering in the  $S_1$  and  $P_1$  waves.

One can see in Fig. 6.1 that the  $S_1$  phase shift practically equals zero in the range from 0 to 800 keV, then it sharply drops and at 1500 keV approximately equals  $-25^\circ$ . Since later we will consider the low and astrophysical energy range only, and then we will limit the energy range from 0 keV to 800 keV. Practically zero phase shift at these energies is received with the potential of the form (2.8) and parameters

$$V_0 = -147 \text{ MeV}, \quad \alpha = 0.15 \text{ fm}^{-2}.$$

Such potential contains two FSs with {8} and {44} as it follows from the state classification given in Table 6.1, and the calculation results of the  $S_1$  phase shift are shown in Fig. 6.1 by the solid line. Of course, the  $S_1$  phase shift at about zero one can obtain from the other variants of potential parameters with two FS. In this regard it is not possible to fix its parameters unambiguously and the other combinations of  $V_0$  and  $\alpha$  are possible. However, this potential, as the above potential, should have comparatively large width, which gives small change of the phase shift when the energy changes in the range from 0 to 800 keV.

There is an over-threshold level in the  $P_1$  scattering wave with the energy 17.640 MeV and  $J^\pi T = 1^+ 1$  or 0.441 MeV (l.s.) which is above the threshold of the cluster  $p^7\text{Li}$  channel in  $^8\text{Be}$ , with the binding energy of this channel of  $-17.2551$  MeV [136]. The level of 0.441 MeV has very small width equals only 12.2(5) keV [136] for the  $p^7\text{Li} \rightarrow ^8\text{Be}\gamma$  radiative capture reaction and the  $p^7\text{Li}$  elastic scattering. Such a narrow level leads to the sharp rise of the  $P_1$  elastic scattering phase shift, which should be mixed by spin states  $^5P_1$  and  $^3P_1$  [139] for the total moment  $J = 1$ . For determinacy we will note further that the main contribution to the considered processes gives the triplet spin state and the contribution of the state at  $S = 2$  is relatively small. Note that the  $^3P_0$ ,  $^3P_1$  and  $^3P_2$  phases there are in the triplet state, and the spin quartet leads to the  $^5P_1$ ,  $^5P_2$  and  $^5P_3$  states.

The phase shift, which is shown with points in Fig. 6.2 [139], can be described by the Gaussian potential (2.8) with parameters

$$V_0 = -5862.43 \text{ MeV}, \quad \alpha = 3.5 \text{ fm}^{-2}.$$

This potential, mixed in isospin  $T=0$  and 1, has two FS with  $\{71\}$  and  $\{53\}$  according to Table 6.1 and the calculation results of the  $P_1$ -phase shift of the elastic scattering are shown in Fig. 6.2 with a solid line. The potential parameters that describe the  $P_1$  scattering phase shift are fixed quite unambiguously at the interval of sharp increase obtained from the experimental data and the potential itself should have very small width, which should determine the width of the resonance.

It can be deemed that both of the potentials received above give a good description of the results of the phase shift analysis for two considered partial waves in this energy range [139], since furthermore we will consider the astrophysical  $S$ -factor only at the energies from 0 to 800 keV.

The following parameters of the potential of the bound  $^3P_0$  state of the  $p^7\text{Li}$  system corresponding to the ground state of  $^8\text{Be}$  in the examined cluster channel are obtained

$$V_0 = -433.937674 \text{ MeV}, \quad \alpha = 0.2 \text{ fm}^{-2}.$$

The bound energy  $-17.255100 \text{ MeV}$  with the accuracy of  $10^{-6} \text{ MeV}$  [26], the root-mean-square radius is equal to 2.5 fm and the asymptotic constant, calculated with the help of Whittaker functions (2.10), equals  $C_w = 12.4(1)$  were obtained with such a potential. The error of the constant is estimated by its averaging in the range  $6 \div 10 \text{ fm}$  where the asymptotic constant is practically stable. In addition to the allowed BS with  $\{431\}$  corresponding to the ground state of  $^8\text{Be}$ , this  $P_0$  potential has two FSs with  $\{71\}$  and  $\{53\}$  in total correspondence with the classification of orbital cluster states given in Table 6.1.

It seems that the root-mean-square radius of  $^8\text{Be}$  in the  $p^7\text{Li}$  cluster channel should not differ a lot from the  $^7\text{Li}$  radius which equals 2.35(10) fm [124], since the nucleus is in a strongly bound ( $\sim -17 \text{ MeV}$ ) i.e. compact state. Moreover, at such binding energy,  $^7\text{Li}$  itself can be in deformed, compressed form as it is for deuteron cluster inside  $^3\text{He}$  nucleus



[110]. Therefore, the value of the root-mean-square radius for the  $p^7\text{Li}$  channel in the GS of  $^8\text{Be}$  received above has quite a reasonable value.

The variational method with the expansion of the cluster wave function of the  $p^7\text{Li}$  system in non-orthogonal Gaussian basis [22] is used for an additional control of the accuracy of bound energy calculations and the energy  $-17.255098$  MeV with  $N = 10$  order of matrix were obtained for this potential which differ from the above finite-difference value by 2 eV only. Residuals [26] are of the order of  $10^{-11}$ , asymptotic constant at the range  $5 \div 10$  fm equals 12.3(2); the charge radius does not differ from previous results. Expansion parameters of the received variational GS radial wave function of  $^8\text{Be}$  in the  $p^7\text{Li}$  cluster channel are listed in Table 6.2.

**Table 6.2. Variational parameters and expansion coefficients of the radial wave function in the form (2.9) of the ground state of  $^8\text{Be}$  in the  $p^7\text{Li}$  channel in non-orthogonal Gaussian basis [22,26]. Normalization of the function with these coefficients on an interval of  $0 \div 25$  fm is  $N = 1.000000000000001$**

$i$	$\beta_i$	$C_i$
1	1.140370098659333E-001	-9.035361688615057E-002
2	5.441057961629589E-002	-5.552214961281388E-003
3	2.200385338662954E-001	-4.776382639167991E-001
4	5.657244883872561E-001	3.790054587274382
5	9.613849915820404E-001	-2.409004172680931
6	1.216602174819119	-3.280156202364487
7	4.797601726001004	2.475815245412750E-002
8	14.137444509612200	1.070215776034501E-002
9	45.160915627598030	6.119172187062497E-003
10	191.081716320368200	3.950399055271339E-003

As it was told before, the variational energy decreases as the dimension of the basis increases and gives the upper limit of the true bound energy, but the finite-difference energy increases as the size of steps decreases and the number of steps increases [26], therefore it is possible to use the average value  $-17.255099(1)$  MeV for the real bound energy in this

potential. Thus, the calculation error of the bound energy of  ${}^8\text{Be}$  in the cluster  $p{}^7\text{Li}$  channel using two different methods is about  $\pm 1$  eV.

Our computer program, based on the finite-difference method [26], was changed for carrying out these calculations, as it was in other cases, for earlier considered cluster systems. This program has been rewritten in Fortran-90, which made it possible to essentially increase the rate and accuracy of all calculations, for example, for determining the binding energy in two-body channel [3]. Now, the absolute accuracy of finding the energy of bound states of the  $p{}^7\text{Li}$  system in  ${}^8\text{Be}$  is equal to  $10^{-6}$  MeV. The accuracy of finding the root of the determinant equals  $10^{-14}$  and the value of Wronskian of Coulomb wave functions for continuous spectrum, determined the accuracy of finding of the phase shifts of scattering, is not worse than  $10^{-15}$ .

### 6.3. Astrophysical *S*-factor

While considering electromagnetic transitions in the proton capture reaction on  ${}^7\text{Li}$  we will take into account the  $E1$  process from the scattering  ${}^3S_1$  wave (see Fig. 6.1) to the ground bound state of  ${}^8\text{Be}$  in the cluster  $p{}^7\text{Li}$  channel with  $J^P T = 0^+ 0$  and the  $M1$  transition from the scattering  $P_1$  wave (see Fig. 6.2) also to the GS of nucleus. Cross sections of the  $E1$  transition from the scattering  ${}^3D_1$  wave (with potential for the  ${}^3S_1$  wave at  $L = 2$ ) to the GS of  ${}^8\text{Be}$  are by  $2\div 4$  orders lower than from the  ${}^3S_1$ -wave transition at the energy range  $0\div 800$  keV. Furthermore, we will consider only the  $S$ -factor for the transition to the ground state of  ${}^8\text{Be}$ , i.e.,  ${}^7\text{Li}(p, \gamma_0){}^8\text{Be}$  reaction. One of the last experimental measurements of the  $S$ -factor of this reaction in the energy range from 100 keV to 1.5 MeV was made in work [135].

The standard expressions (2.4)÷(2.6) are used for the  $S$ -factor calculations. Values:  $\mu_p = 2.792847$  [35] and  $\mu({}^7\text{Li}) = 3.256427$  [141] are accepted for magnetic moment of proton and  ${}^7\text{Li}$ . The expression in square brackets (2.6) for  $A_1(M1, K)$  is obtained in assumption that the summation by  $r_i$  is done in the general form for spin part of magnetic operator [37], i.e., by coordinates of mass centre of clusters, before operating to the expression in parentheses  $(r_i^l Y_{jm}(\Omega_i))$  by  $\nabla$  operator, which leads to the

reduction of  $r_1$  power [35]. If, at first, we use  $\nabla$  operation towards the expression in these brackets, then as a character  $A_1(M1, K)$  for  $M1$  we obtain

$$A(K) = \frac{e\hbar}{m_0 c} K \sqrt{3} [\mu_1 + \mu_2] . \quad (6.1)$$

Since the astrophysical  $S$ -factor of the considered reaction at the resonance energy completely depends on the value of the  $M1$  transition, which cross section is three orders of magnitude more than  $E1$ , so this reaction may be a certain test for correctness of expressions (2.6) or (6.1).

The calculation results for the astrophysical  $S$ -factor with the above potentials at the energy range  $5 \div 800$  keV (l.s.) are shown in Fig. 6.3. The  $E1$  transition is shown by the dashed line, dotted line – the  $M1$  process, solid line – the sum of these processes. The shown results, obtained on the base of the expression (2.6), argue in favor of this approach, although the performed conclusions will be absolutely correct only in the case of 100% clusterization of  ${}^8\text{Be}$  into the cluster  $p{}^7\text{Li}$  channel. In the considered reaction the  $M1$  transition like the  $E1$  transition in the  $p{}^3\text{H}$  system [110] goes with change of the isospin  $\Delta T = 1$ , since the ground state of  ${}^8\text{Be}$  has  $T = 0$  and resonance isospin in the  $P_1$  wave of scattering equals 1.

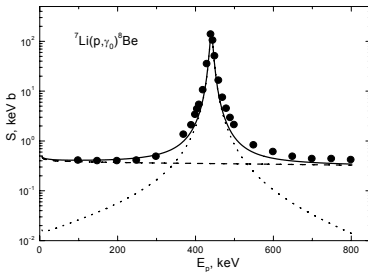


Fig. 6.3. Astrophysical  $S$ -factor of the proton radiative capture on  ${}^7\text{Li}$  reaction. Dots – experimental data from [140]. Lines – calculation results for different electromagnetic transitions with the potentials mentioned in the text.

The value of 0.50 keV b was obtained for the astrophysical  $S$ -factor at 5 keV (cm) for the transition to GS of  ${}^8\text{Be}$ , where the  $E1$  process gives the value of 0.48 keV b, which is in a good agreement with the data from [140]. The calculated and experimental  $S$ -factor values [140] at the energy range  $5 \div 300$  keV (l.s.) are given in Table 6.3. As it can be seen from Fig. 6.3 and

Table 6.3, the value of the theoretical  $S$ -factor at the energy range  $30 \div 200$  keV is almost constant and approximately equal to  $0.41 \div 0.43$  keV b, which agrees with data of the work [140] for the energy range  $100 \div 200$  keV

practically within the experimental errors.

**Table 6.3. Calculated astrophysical  $S$ -factor of the proton radiative capture on  ${}^7\text{Li}$  reaction at low energies and its comparison with the experimental data [140]**

$E_{ls.}$ (keV)	$S_{exp}$ (keV b) [140]	$S_{EI}$ (keV b)	$S_{MI}$ (keV b)	$S_{EI+MI}$ (keV b)
5.7	—	0.48	0.02	0.50
29.7	—	0.41	0.02	0.43
60.6	—	0.39	0.02	0.41
98.3	0.41(3)	0.39	0.03	0.42
198.3	0.40(2)	0.37	0.06	0.43
298.6	0.49(2)	0.36	0.16	0.52

Let us compare some extrapolation results of the different experimental data to zero energy. The value 0.25(5) keV b was obtained in [130] and the value 0.40(3) keV b in [142] on the basis of data [140]. Then in work [143] on the basis of new measurements of the total cross sections of the  ${}^7\text{Li}(p,\gamma_0){}^8\text{Be}$  reaction at the energy range 40÷100 keV the value 0.50(7) keV b was suggested which is in a good agreement with the obtained above value at the energy 5 keV.

It is interesting to look at the chronology of different works for determination of the astrophysical  $S$ -factor of  ${}^7\text{Li}(p,\gamma_0){}^8\text{Be}$  reaction. It was believed in 1992 that its value equals 0.25(5) keV b [130], the value of 0.40(3) keV b [142] was obtained in 1997 on the basis of measurements made in 1995 [140] and the measurements in 1999 at lower energies led to the value of 0.50(7) keV b [143]. This chronology demonstrates well the constant increase (notably double) in the value obtained for the astrophysical  $S$ -factor of  ${}^7\text{Li}(p,\gamma_0){}^8\text{Be}$  reaction (two fold increase) as the energy of experimental measurements decreased, and it seems that this value can undergo a visible change in the earlier future.

In order to correctly describe the calculated  $S$ -factor, shown in Fig. 6.3 by the solid line, it is necessary to use quadric parametrization of the form (3.5). The next values are obtained for parameters  $S_0 = 0.47218$  keV b,  $S_1 = -$

$1.1996 \cdot 10^{-3}$  keV b keV<sup>-1</sup>,  $S_2 = 5.3407 \cdot 10^{-6}$  keV b keV<sup>-2</sup> in this case at the average  $\chi^2 = 0.072$  in the range 1÷200 keV. 10%-errors in the calculated values of the  $S$ -factor are used for determination of the  $\chi^2$ , the  $S$ -factor value of 0.5 keV b obtained at the zero energy [143] was used at 1 keV. At the second method of parametrization considered in the paragraph 3.2 we obtain:  $S_0 = 0.5$  keV b,  $S_1 = -1.7973 \cdot 10^{-3}$  keV b keV<sup>-1</sup> and  $S_2 = 8.0259 \cdot 10^{-6}$  keV b keV<sup>-2</sup> at  $\chi^2 = 0.118$ .

### **Conclusion**

Thus, the  $E1$  and the  $M1$  transitions from the  $^3S_1$  and the  $^{3-5}P_1$  scattering waves to the ground bound state in the  $p^7\text{Li}$  channel of  $^8\text{Be}$  were considered in the modified potential cluster model. It is possible to completely describe available experimental data for the astrophysical  $S$ -factor at the energies up to 800 keV taking into account certain assumptions concerning calculation methods of magnetic transition and rearrangement of channels in  $^8\text{Be}$  and to obtain its value for zero (5 keV) energy [115], which is in a good agreement with the latest experimental measurements [143].

Note that in work [3] for the  $n^7\text{Li}$  system, the variant of classification of orbital states was considered, when only one tableau {43} was used for  $^7\text{Li}$ . In this case it is quite succeeded correctly describe the available data on the neutron radiative capture on  $^7\text{Li}$  at astrophysical energies. Therefore, it is not possible to choose, unambiguously, one of these variants of classification of states in the  $n^7\text{Li}$  or  $p^7\text{Li}$  systems.

# **7. RADIATIVE CAPTURE IN THE $p^9\text{Be}$ SYSTEM**

---

## ***Introduction***

Let us consider the  $p^9\text{Be} \rightarrow {}^{10}\text{B}\gamma$  reaction in the astrophysical energy range in the modified potential cluster model with splitting of orbital states according to Young tableaux and, in some cases, with forbidden states. We should note that we managed to find only one work devoted to a detailed experimental measurement of the cross sections and the astrophysical  $S$ -factor for this reaction [144] at low energies. We will use the results of this work furthermore for comparison with our model calculations.

The knowledge of the  $p^9\text{Be}$  interaction potentials in continuous and discrete spectrum is required for the calculation of the astrophysical  $S$ -factor of the proton radiative capture on  ${}^9\text{Be}$  in the MPCM [3,22] which we usually used for the analysis of similar reactions [110,132,133]. Again we will consider that such potentials should correspond to the classification of cluster states according to orbital symmetries [3,21,22], as it was assumed earlier for other light nuclear systems.

### **7.1 Classification of the orbital states**

First, we will define the orbital Young tableaux of  ${}^9\text{Be}$ , for example, in the  $p^8\text{Li}$  or in the  $n^8\text{Be}$  channels. If we assume that it is possible to use tableaux  $\{44\} + \{1\}$  in the  $8 + 1$  system, then two possible symmetries:  $\{54\} + \{441\}$  are obtained for this system. The first of them is forbidden because it contains five cells in one matrix row [123]. We note, promptly, that the given classification of orbital states according to Young tableaux has qualitative character, because there is no table of Young tableaux products for the system with  $A = 9, 10$  particles, though they exist for all systems with  $A < 9$  [45] and they are used for the analysis of the number of allowed and forbidden states in wave functions of different cluster systems [88].

Furthermore, if the tableau  $\{54\}$  is used for  ${}^9\text{Be}$  then, possible, Young tableaux of the  $p^9\text{Be}$  system turn out to be forbidden, because of the rule that it can not be more than four cells in one row [123,145]. They are corresponded to forbidden states with configurations  $\{64\}$ ,  $\{55\}$  and relative motion moments  $L = 0$  and  $1$ , which is determined by the Elliot rule [123]. Another forbidden tableau  $\{541\}$  is present in this product as in the examined case too and correspond to  $L = 1$ .

When the tableau  $\{441\}$  is accepted for  ${}^9\text{Be}$ , the  $p^9\text{Be}$  system contains forbidden states with the  $\{541\}$  tableau in the  $P$ -wave and, evidently, with the  $\{442\}$  in the  $S$ -wave and AS configuration  $\{4411\}$  with  $L = 1, 3$ . Thus, the  $p^9\text{Be}$  potentials in different partial waves should have forbidden bound  $\{442\}$  state in the  $S$ -wave and forbidden and allowed bound levels in the  $P$ -wave with  $\{541\}$  and  $\{4411\}$  Young tableaux, respectively.

We can examine the case when for  ${}^9\text{Be}$  both possible orbital Young tableaux  $\{54\}$  and  $\{441\}$  are used. The same approach was quite successfully used earlier for consideration of the  $p^6\text{Li}$  [116] and the  $p^7\text{Li}$  [135] systems. Then the level classification will be slightly different – the number of forbidden states will increase and an additional forbidden bound level will appear in every partial wave with  $L = 0$  and  $1$ . Such a more complete tableau of states, which we will use later, equals the sum of the first and the second cases considered above and there are two FSs in the  $S$  and  $P$  waves with allowed states in the  $P$  wave. One of them – the  ${}^5P_3$  state – can correspond to the ground state of  ${}^{10}\text{Be}$  in the  $p^9\text{Be}$  channel.

## ***7.2 Potential description of scattering phase shifts***

The considered  $p^9\text{Be}$  channel in  ${}^{10}\text{Be}$  has the isospin projection equal to  $T_z = 0$ , which is possible with two values of the total isospin  $T = 1$  and  $0$  [136], therefore the  $p^9\text{Be}$  system, as well as  $p^3\text{H}$  [110], turns out to be isospin-mixed. In this case the  $p^9\text{Be}$  and  $n^9\text{Be}$  cluster channels with  $T_z = \pm 1$  and  $T = 1$  are isospin-pure in a complete analogy with the  $p^3\text{He}$  and  $n^3\text{H}$  systems [110]. The phase shifts of the elastic  $p^9\text{Be}$  scattering are represented as a half-sum of pure isospin phase shifts [21,22] because this system is isospin-mixed, as it was given above in (4.1).

The isospin-mixed phase shifts with  $T = 1, 0$  are derived from the phase shift analysis of experimental data, which are usually the differential cross sections of the  $p^9\text{Be}$  elastic scattering. The pure phase shifts with the isospin  $T = 1$  are obtained from the phase shift analysis of the  $p^9\text{Be}$  or  $n^9\text{Be}$  elastic scattering. Consequently, one can find pure  $T = 0$  phase shifts for the  $p^9\text{Be}$  scattering and construct the interaction potential which should correspond to the potential of the bound state of the  $p^9\text{Be}$  system in  $^{10}\text{Be}$  [136]. Just the same method of splitting of phase shifts and potentials was used for the  $p^3\text{H}$  system [92,110] and has demonstrated its total availability.

However, we have not found the data on phase shifts for the  $n^9\text{Be}$ ,  $p^9\text{B}$  and  $p^9\text{Be}$  elastic scattering at astrophysical energies [137], therefore, here we will consider only isospin-mixed potentials of the scattering processes in the  $p^9\text{Be}$  system and pure potentials for bound states with  $T = 0$ , which, as earlier, are constructed on the basis of the description of the BS characteristics – binding energy, charge radius and asymptotic constant. Exactly the same approach we used earlier for the  $p^6\text{Li}$  and  $p^7\text{Li}$  systems and the potential is selected in a simple Gaussian form with a point-like Coulomb term (2.8).

Since we don't have the phases of the  $p^9\text{Be}$  elastic scattering obtained from the phase shift analysis of experimental data, we will only rely on the purely qualitative views about their behavior as an energy function. It is known, in particular, that there is  $J = 1^-$  over threshold level with  $T = 0+1$ , energy 0.319(5) MeV (l.s.) and 133 keV (l.s.) width [136,146]. This resonance state can be formed by the  $^3S_1$  configuration in the  $p^9\text{Be}$  channel of  $^{10}\text{B}$  because  $J(^9\text{Be}) = 3/2^-$  and  $J(p) = 1/2^+$ . The presence of such a level leads to the resonance of the phase shift which equals  $90^\circ$  at this energy.

However, the resonance of the  $S$ -factor measured in [144] is observed at the energy of 299 keV (l.s.) which is listed in Table 1 and Fig. 4 of work [144]. At the same time the value of 0.380(30) MeV (l.s.) with the width of 330(30) keV (l.s.) is given for the resonance energy in Table 2 of work [144]. Both of these values do not correspond to the well-known data [136,146]. That is why an additional analysis of the experimental results was carried out in later works [147,148] and the values of 328÷329 keV (l.s.) with the width of 155÷161 keV were obtained for the energy of this level, which slightly differs from data of [136,146].



Since there is a large difference between various data, we slightly varied parameters of this potential for receiving the best description of the  $S$ -factor resonance location given in work [144]. Consequently, the potential of the  $^3S_1$ -wave of scattering was obtained, which leads to the resonance of the  $90^\circ$  phase shift at 333 keV (l.s.) and has the following parameters

$$V_0 = -69.5 \text{ MeV}, \quad \alpha = 0.058 \text{ fm}^{-2}.$$

The triplet  $^3S_1$  phase shift of this potential is shown in Fig. 7.1 by the solid line and has a resonance nature, while the potential itself contains two FSs in accordance with the last variant of the given above classification.

If we use the expression for calculation of the level width using  $\delta$  phase shift of scattering [79]

$$\Gamma_{l.s.} = 2(d\delta/dE_{l.s.})^{-1},$$

then the width of such resonance approximately equals 150(3) keV (l.s.), which is in a complete agreement with the results of works [147,148].

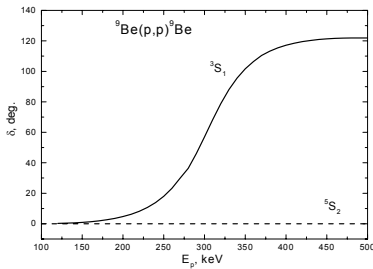


Fig. 7.1.  $S$  phase shifts of the elastic  $p^9\text{Be}$  scattering at low energies. Lines – results obtained using Gaussian potentials with parameters that are given in the text.

Furthermore, we assume that the  $^5S_2$  phase shift almost vanishes to zero at the energy range up to 600 keV which will be considered here because there are no such levels at  $^{10}\text{B}$  spectra comparable to this partial wave at these energies [136,146]. Practically zero phase shift is obtained with the Gaussian potential and parameters

$$V_0 = -283.5 \text{ MeV}, \quad \alpha = 0.3 \text{ fm}^{-2}.$$

It contains two FS as it follows from the classification of orbital states given earlier. The phase shift of scattering is shown in Fig. 7.1 by the dashed line. Of course, it is possible to obtain the  $^5S_2$  phase shift in the vicinity of zero by using some other variants of potential parameters with

two forbidden states. In this regard it is not possible to fix its parameters definitely and other combinations of  $V_0$  and  $\alpha$  are possible. However, additional calculations of the  $E1$  transition from the elastic  ${}^5S_2$  wave to the bound  ${}^5P_3$  state have shown the weak dependence of the  $S$ -factor of the proton radiative capture on  ${}^9\text{Be}$  by the parameters of this potential. Only the zero values of the scattering phase shifts play the main role here.

The following parameters of the potential of the bound  ${}^5P_3$  state of the  $\text{p}^9\text{Be}$  system corresponding to the GS of  ${}^{10}\text{B}$  in the cluster channel under consideration were obtained

$$V_0 = -719.565645 \text{ MeV}, \quad \alpha = 0.4 \text{ fm}^{-2}.$$

With this potential we have obtained the binding energy of  $-6.585900$  MeV with the accuracy of  $10^{-6}$  MeV [26], the root-mean-square radius is equal to  $2.58$  fm while the experimental value is  $2.58(10)$  fm [136] and the asymptotic constant calculated by Whittaker functions is equal to  $C_W = 2.94(1)$ . Values  $R_p = 0.8768(69)$  fm [36] and  $R_{Be} = 2.519(12)$  fm [136] were used for cluster radii. The asymptotic constants  $C_W$  error is estimated by its averaging at the range of  $5 \div 15$  fm where the asymptotic constant is practically stable. In addition to the allowed BS corresponding to the GS of  ${}^{10}\text{B}$  such the  $P$  potential has two FSs in complete correspondence with the classification of orbital cluster states which was given above.

For the purposes of comparison, we give the results of work [149] for the AC where its value equals  $C_W = 2.37(2) \text{ fm}^{-1/2}$ . It is necessary to note, that in this work we use this expression for the determination of the asymptotic constant

$$\chi_L(R) = C_W W_{-\eta, L+1/2}(2k_0 R),$$

which differs from our definition (2.10) for  $\sqrt{2k_0}$  value. To bring these constants to a unified dimensionless form the results should be divided by  $\sqrt{2k_0}$ , where  $k_0 = 0.536 \text{ fm}^{-1}$  for the  $\text{p}^9\text{Be}$  system. Then we receive for AC in our definition the value of  $2.29$ , which substantially differs from the above result. However, if we take AC value received in work, the charge

radius of  $^{10}\text{B}$  will be somewhat underestimated because the “tail” of the wave function decreases more sharply.

The following parameters for the potentials of the first three excited but not bound states in the  $p^9\text{Be}$  channel with  $J^P T = 1^+0, 0^+1$  and  $1^+0$  at energies 0.71835, 1.74015 and 2.1543 MeV [136] were received

$$V_0(0.718350) = -715.162918 \text{ MeV}, \quad \alpha = 0.4 \text{ fm}^{-2},$$

$$V_0(1.740150) = -708.661430 \text{ MeV}, \quad \alpha = 0.4 \text{ fm}^{-2},$$

$$V_0(2.154300) = -705.935443 \text{ MeV}, \quad \alpha = 0.4 \text{ fm}^{-2}.$$

They describe precisely the values of the given above energy levels and shown, which, relative to the  $p^9\text{Be}$  channel threshold, are equal to  $-5.867550, -4.845700$  and  $-4.431600$  MeV. They properly lead to charge radii of 2.59, 2.60 and 2.61 fm, asymptotic constant of 2.74(1), 2.46(1) and 2.35(1) at the range from  $4\div 5$  fm to  $11\div 13$  fm and have two FSs and one AS.

The variational method with the expansion of the cluster wave function of the  $p^9\text{Be}$  system in non-orthogonal Gaussian basis (2.9) is used for an additional control of the accuracy of the binding energy calculations [26]. The ground state energy equals  $-6.585896$  MeV was obtained for this potential with the order of matrix  $N = 10$  which differs from the above finite-difference value [26] by 4 eV only. Residuals have  $10^{-11}$  order, asymptotic constant at the range  $5\div 10$  fm equals 2.95(3), and the charge radius does not differ from the previous results. Expansion parameters of the received variational GS radial wave function of  $^{10}\text{B}$  in the  $p^9\text{Be}$  cluster channel are listed above in Table 7.1.

As we repeatedly noted that the variational energy decreases as the dimension of the basis increases and gives the upper limit of the true binding energy, but the finite-difference energy increases as the size of steps decreases and the number of steps increases [26]. Therefore, it is possible to use the average value of  $-6.585898(2)$  MeV for the real binding energy in this potential. Meanwhile, the calculation error of finding the binding energy of  $^{10}\text{B}$  in the  $p^9\text{Be}$  cluster channel using two different

methods is about  $\pm 2$  eV.

**Table 7.1. The variational coefficients and expansion parameters of the  $^{10}\text{B}$  ground state radial WF for the  $\text{p}^9\text{Be}$  channel in non-orthogonal Gaussian basis [26]. The normalization coefficient of the wave function in the range  $0 \div 25$  fm equals  $N = 1.000000000000002$**

$i$	$\beta_i$	$C_i$
1	7.715930101739352E-002	-2.802002694398972E-002
2	3.224286905853033E-002	-2.092599791641983E-003
3	1.677117157858407E-001	-1.481060223206524E-001
4	3.388993785610822E-001	-5.049291144131660E-001
5	9.389553670123860E-001	4.713342588832875
6	1.999427899506135	-7.632712971301209
7	2.988529100669578	-5.267741895838846E-001
8	6.878703971128334	6.022748751134505E-002
9	23.149662023260950	2.252725100117285E-002
10	100.917699526293000	1.285655220977827E-002

**Table 7.2. Variational parameters and expansion coefficients of the  $0^{+1}$  state WF for the  $^{10}\text{B}$  nucleus at the energy of 1.74015 MeV in non-orthogonal Gaussian basis [26]. The normalization coefficient of the wave function in the range  $0 \div 25$  fm equals  $N = 9.99999999999970\text{E}-001$**

$i$	$\beta_i$	$C_i$
1	6.669876139241313E-002	-2.347210794847986E-002
2	2.667656102033708E-002	-1.775040363036249E-003
3	1.517176918481825E-001	-1.283117981223353E-001
4	3.212149403864399E-001	-4.601647158129205E-001
5	9.260148198737874E-001	4.396116518097601
6	1.968143319382518	-7.091171845894630

7	2.891825315028276	-6.237051439471658E-001
8	6.205147839342107	6.217503950196968E-002
9	20.141061492467640	2.305215376077275E-002
10	86.640072856521640	1.321899076244325E-002

In the frames of the VM we obtained that the value of energy equals – 4.845692 MeV, the charge radius of 2.61 fm and the AC is equal to 2.48(2) in the range 5÷12 fm for the potential of the second excited state. The expansion parameters of the WF in non-orthogonal Gaussian basis are listed in Table 7.2. The average energy value –4.845696(4) MeV is obtained for this level using two different methods and two different computer programs and residuals are of the order of  $10^{-13}$ .

### 7.3 Astrophysical *S*-factor

While considering electromagnetic transitions we will take into account the *E1* process, denote it as the *E1*(BS), from the resonance  $^3S_1$  wave of scattering to three excited, but bound states in the  $p^9\text{Be}$  cluster channel of  $^{10}\text{B}$  with  $J^P T = 1^+0, 0^+1$  and  $1^+0$  [136] denoting them as the  $^3P$  states. As well as the *E1* transition from the  $^5S_2$ -wave of scattering with zero phase shift to the ground bound  $^5P_3$  state of this nucleus denoting it as *E1* (GS).

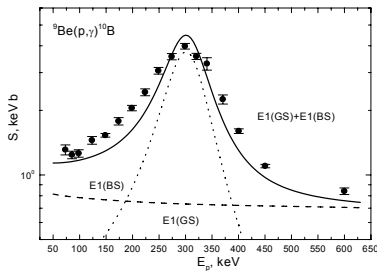


Fig. 7.2. Astrophysical *S*-factor of the proton radiative capture on  $^9\text{Be}$  reaction. Dots – experimental data from work [144]. Lines – calculation results for different electromagnetic transitions with the potentials mentioned in the text.

The calculation results and experimental data for the *S*-factor at the energy range 50÷600 keV (l.s.) from work [144] are shown in Fig. 7.2 by the solid line. Obviously, the value of the total calculated *S*-factor at the energy range 50÷100 keV remains almost constant and equals 1.15(2) keV b, which is in quite a good agreement with the data of work [144], where the average of the first three experimental points at the energy 70÷100 keV equals 1.27(4) keV b.

The transition to the  $^5P_3$  GS of  $^{10}\text{B}$  from the  $^5S_2$  scattering wave leads to the value of 0.81 keV b for the calculated  $S$ -factor at the energy 50 keV (dashed line in Fig. 7.2). Line extrapolation of the received result to zero energy gives approximately 0.90 keV b. The sum of transitions from the  $^3S_1$  scattering wave to the three bound  $^3P$  levels is shown in Fig. 7.2 by the dotted line.

For comparison we will give some extrapolation results to zero energy for different experimental data. For instance, the value 0.92 keV b was obtained in work [130] for the  $S$ -factor with transition to the GS, which is in complete agreement with the value of 0.90 keV b received above. However, the values 1.4 keV b, 1.4 keV b and 0.47 keV b are given for the transitions to the three excited levels considered above with  $J^P T = 1^+0$ ,  $0^+1$  and  $1^+0$  respectively [130] and their sum evidently exceeds our result and data from work [144]. Furthermore, the value 0.96(2) keV b for the total  $S$ -factor was received in the later work [147] and the value from 0.96(6) to 1.00(6) keV b was found in one of the latest works [148] devoted to this reaction. Both of these values are in good agreement with the values obtained above.

## **Conclusion**

Thus, the  $E1$  transitions from the  $^5S_2$  and  $^3S_1$  waves of scattering to the ground bound  $^5P_3$  state in the  $p^9\text{Be}$  channel of  $^{10}\text{B}$  and its three excited states  $1^+0$ ,  $0^+1$  and  $1^+0$  also bound in this channel are considered in the modified potential cluster model. Having made certain assumptions of common character about interactions in the  $p^9\text{Be}$  channel of  $^{10}\text{B}$  it is possible to describe well the existing experimental data of the astrophysical  $S$ -factor at the energy range down to 600 keV and to receive its value for zero (50 keV) energy which is in complete agreement with the latest experimental data [144,147,148]. The  $S(0)$ -factor at zero energy for the transition to the GS of  $^{10}\text{B}$  is obtained generally good.

However, the scattering potentials are constructed on the basis of some qualitative conceptions because of the absence of the data for the phase shift analysis of the  $p^9\text{Be}$  elastic scattering and three BS potentials are obtained only approximately, because of the absence of data on the radii and the AC of  $^{10}\text{B}$  in these excited states. Therefore, these results should be

considered only as a preliminary estimate of the possibility to describe the astrophysical  $S$ -factor of the reaction under consideration on the basis of the MPCM with FSs. But it is possible to obtain quite acceptable results for the astrophysical  $S$ -factor in spite of approximate consideration of the  $p^9\text{Be} \rightarrow ^{10}\text{B}\gamma$  radiative capture process.

In conclusion, it should be mentioned that the available  $S$ -factor experimental data for this reaction differs significantly from each other and it seems that more accurate study of the  $p^9\text{Be} \rightarrow ^{10}\text{B}\gamma$  radiative capture at astrophysical energy and more precise definition of the location of the resonance and its width in the  $^3S_1$  scattering wave [150] are required.

We should note that in work [3] the variant of classification of orbital states was considered for the  $n^9\text{Be}$  system, when the Young tableau  $\{441\}$  was used for  $^9\text{Be}$ . Consequently, the correct description of the available data of the neutron radiative capture on  $^9\text{Be}$  at astrophysical energies was obtained. Therefore, it is impossible to give the certain preference to one of these variants of state classifications in the  $n^9\text{Be}$  system. However, furthermore we will use for nuclei only the Young tableaux, which concern to their GS, i.e., without taking into account tableaux of FS in these nuclei. For example, the Young tableaux  $\{4411\}$  or  $\{442\}$  will be used for  $^{10}\text{B}$ , since, because of the absence of tables of Young tableau products, it is impossible to unambiguously believe that the last of them is forbidden.

# **8. PROTON RADIATIVE CAPTURE ON $^{10}\text{B}$**

---

## ***Introduction***

In this chapter the results in the field of study of thermonuclear proton capture reaction on  $^{10}\text{B}$  at ultralow, i.e., astrophysical energies will be presented. This reaction does not take part of thermonuclear cycles evidently, but up to now, evidently, was not considered on the basis of any model. In this case, as it was before, the MPCM is used as a nuclear model, which allows one to consider some thermonuclear processes, notably, radiative capture reactions of neutrons and protons on light nuclei, on the basis of unified views, criteria and methods [31,91,151,152].

### ***8.1 Classification of the cluster states and the level structure of the $p^{10}\text{B}$ system***

Furthermore we will assume that it will be possible to accept the orbital Young tableau in the form  $\{442\}$  for  $^{10}\text{B}$ . Therefore, we have  $\{1\} \times \{442\} = \{542\} + \{443\} + \{4421\}$  [123]. The first from the obtained tableaux is compatible with the orbital moments  $L = 0, 2, 3, 4$  and is forbidden, because in the nuclear  $s$ -shell should not be five nucleons. The second tableau is allowed and is compatible with the orbital moment  $L = 1, 2, 3, 4$ , and the third, is also allowed and is compatible with  $L = 1, 2, 3$  [123].

As it was said, the absence of product tables of Young tableaux for particle numbers 10 and 11 makes impossible the accurate classification of cluster states in the considered system of particles. However, even so qualitative estimation of the orbital symmetries allows one to determine existence of FSs in the  $S$  and  $D$  waves and the absence of FSs for the  $P$  waves. Exactly this structure of the FSs and the ASs in different partial waves will be used further for construction of the intercluster interaction potentials that are necessary for calculation of the total cross sections of the



considered radiative capture reaction at low energies.

Thus, limiting only according to the lowest partial waves with the orbital moment  $L = 0, 1$  it can be said that only the allowed state is in the potentials of the  $P$  waves for the  $p^{10}\text{B}$  system, but in the  $S$  waves there is only forbidden state. Meanwhile, the  $P$  wave corresponds to two allowed Young tableaux  $\{443\}$  and  $\{4421\}$ . This situation is analogous, evidently, to the  $\text{N}^2\text{H}$  system that was described in the paragraph 3.1, when potentials for the scattering processes depend from two Young tableaux, but for BS only from one. Therefore, here we will consider that the GS potential corresponds to only one tableau  $\{443\}$  – it determines the lowest allowed level for BS in the given partial potential with  $L = 1$  [3]. Consequently, the BS potentials and the scattering potentials are different, because they depend on the other sets of Young tableaux [21]. Therefore, to fix the idea, we will consider that for the discrete spectrum the allowed states in the  $P$  waves, which correspond to the GS and to the BS of  $^{11}\text{C}$ , are the bound, but for the scattering processes they are not bound. The forbidden state for the  $S$  scattering waves in the  $p^{10}\text{B}$  system is the bound state.

Note that in the previous chapter the orbital Young tableau in the form  $\{4411\}$  was obtained for  $^{10}\text{B}$ . Therefore, for the  $p^{10}\text{B}$  system, limiting only by the nuclei of  $1p$  shell, we have  $\{1\} \times \{4411\} = \{5411\} + \{4421\}$  [123]. The first from the obtained tableaux compatible with the orbital moments  $L = 1, 3$  and is forbidden because in the nuclear  $s$  shell could not be five nucleons. The second one is allowed and compatible with the orbital moments  $L = 1, 2, 3$  [123]. This implies that limiting the orbital moments  $L = 0, 1$  it can be said that for the  $p^{10}\text{B}$  system in the potentials of the  $P$  waves there is the FS with tableau  $\{5411\}$  and the AS with tableau  $\{4421\}$ , which corresponds to the GS of  $^{11}\text{C}$ , and in the  $S$  waves the BSs are absent. The results for potentials for the capture total cross sections of this variant of classification will be considered in future, but already in the next chapter for the  $p^{11}\text{B}$  system the Young tableaux  $\{443\}$  and  $\{4421\}$  were used for the GS of  $^{11}\text{B}$ .

Revert to the first variant of classification let us note that the bound allowed  $p^{10}\text{B}$  state in the  $^6P_{3/2}$  wave corresponds to the GS of  $^{11}\text{C}$  with  $J^\pi, T = 3/2^-, 1/2$  and  $\{443\}$  and locate at the binding energy for the  $p^{10}\text{B}$  system of  $-8.6894$  MeV [153] (it will be recalled that for  $^{10}\text{B}$   $J^\pi, T = 3^+, 0$  [153]). Some of the  $p^{10}\text{B}$  scattering states and BSs can be mixed by spin

with  $S = 5/2$  ( $2S+1 = 6$ ) and  $S = 7/2$  ( $2S+1 = 8$ ), but so long as here we consider only transitions to the  ${}^6P_{3/2}$  GS, then in the future calculations only partial waves at spin  $S = 5/2$  will be used.

Let us consider the whole spectrum of resonance levels of  ${}^{11}\text{C}$  in the  $p^{10}\text{B}$  channel – at the energy lower 1.0 MeV it has three states (see, for example, Table 11.41 in review [153]):

1. The resonance at the energy of 0.010(2) MeV (l.s.) with the moment  $J = 5/2^+$  and the width of 16(1) keV (l.s.). It corresponds to the level of  ${}^{11}\text{C}$  at 8.699(10) MeV.

2. The state at the positive energy 0.56(6) MeV (l.s.) with the moment  $J = 5/2^+$  and the width of 550(100) keV (l.s.). – it is the level of  ${}^{11}\text{C}$  at the energy of 9.200(50) MeV.

3. The third resonance at 1.050(60) MeV (l.s.) with the moment  $J = 3/2^-$  and the width of 230(50) keV (l.s.). – it is the level of  ${}^{11}\text{C}$  at the energy of 9.640(50) MeV.

The first and the second from these resonances can be the  ${}^6S_{5/2}$  state of the  $p^{10}\text{B}$  system, and the third is the  ${}^6P_{3/2}$  resonance.

At the low energies the transitions are possible generally from the  $S$  scattering waves, therefore at the considering of the  $E1$  transitions they are possible only to the  $P$  bound states. For example, such transitions are possible to the  ${}^6P_{3/2}$  GS. In addition, the  $M1$  processes to the GS from the  $P$  waves of the continuous spectrum are probable. Particularly, the  $E1$  transition from the  ${}^6S_{5/2}$  scattering wave to the  ${}^6P_{3/2}$  GS is possible:

$$1. {}^6S_{5/2} \rightarrow {}^6P_{3/2}^I .$$

In addition, the  $M1$  transition from two  ${}^6P_{3/2}$  and  ${}^6P_{5/2}$  scattering waves to the GS of  ${}^{11}\text{C}$ :

$$2. {}^6P_{3/2} + {}^6P_{5/2} \rightarrow {}^6P_{3/2} .$$

The first of these waves have the resonance at 1.05 MeV and leads to the resonance transition, but as it can be seen from the results of work [34]

where the total cross sections of the proton radiative capture on  $^{10}\text{B}$  are given, its contribution is too small. In addition, on the basis of the form of the  $S$ -factor of the proton capture on  $^{10}\text{B}$  the resonance at 0.56 MeV [34] in the  $^6S_{5/2}$  wave is also practically invisible due to its big width, which is equal, per se, to the energy of this resonance. Thus, besides the  $E1$  transition from the  $^6S_{5/2}$  scattering wave to the GS, the  $M1$  transition from the  $^6P_{3/2}$  and  $^6P_{5/2}$  scattering waves to the ground state will be considered, meanwhile the resonance at 1.05 MeV does not take into account.

In all given calculations for the mass of proton we use the value of  $m_p = 1.00727646677$  amu [36], and the mass of  $^{10}\text{B}$  equals  $m(^{10}\text{B}) = 10.012936$  amu [137].

## 8.2 Construction of the $p^{10}\text{B}$ interaction potentials

We will use the Gaussian form of interaction (2.8) with the point-like Coulomb term for construction of the central intercluster potentials. Since, furthermore in the first place the transitions from certain scattering waves to the  $^6P_{3/2}$  GS of  $^{11}\text{C}$  in the  $p^{10}\text{B}$  channel will be considered, we will obtain firstly the potential of this state. As it was said the ground state lies at the binding energy of -8.6894 MeV in the  $p^{10}\text{B}$  channel and has the moment  $3/2^-$ , that is pure by spin  $S = 5/2$  the  $^6P_{3/2}$  level [153]. Since, we have not find data on the charge radius  $^{11}\text{C}$ , it will be reasonable to consider that there is not big difference between it and the radius of  $^{11}\text{B}$  equals of 2.43(11) fm [153]. The radius of  $^{10}\text{B}$  is known and is equal to 2.4277(499) fm [137], and the proton radius has the value of 0.8775(51) fm [36].

Consequently, the parameters of the  $^6P_{3/2}$  GS without FS were obtained, as it is followed from the given above classification of FSs and ASs according to Young tableaux for the  $p^{10}\text{B}$  system

$$V_{\text{g.s.}} = -337.1459 \text{ MeV}, \quad \alpha_{\text{g.s.}} = 1.0 \text{ fm}^{-2}. \quad (8.1)$$

It leads to the charge radius of 2.32 fm, the binding energy of -8.6894 MeV at accuracy of  $10^{-4}$  MeV [154], and the AC equals 1.16 at the range of  $2 \div 10$  fm. The scattering phase shift of this potential smoothly drops from  $180^\circ$  at zero energy to  $179^\circ$  at 1.0 MeV. As usual, we use the dimensionless AC value that is determined through the

Whittaker function (1.2.3). In the work [155] the value  $8.9(8) \text{ fm}^{-1}$  is given for square of the dimensional AC of the GS, which has the factor “6” connected with the permutation of nucleons [40]. So as for the dimensional AC we obtain  $1.22(5) \text{ fm}^{-1/2}$ . Since  $\sqrt{2k_0} = 1.11$ , then for the dimensionless AC we have  $1.10(5)$  value that is in a good agreement with the obtained above value.

Furthermore, it will be possible to construct the potential for the  ${}^6S_{5/2}$  resonance, which lies at  $0.010(2) \text{ MeV}$  with the moment  $J = 5/2^+$  at the width  $16(1) \text{ keV}$  and corresponds to the level  $8.699 \text{ MeV}$  of  ${}^{11}\text{C}$  [153]. This potential can have the parameters

$$V_{S52} = -49.8 \text{ MeV}, \quad \alpha_{S52} = 0.088 \text{ fm}^{-2}. \quad (8.2)$$

It contains the FS and, as it will be seen further, reproduces the resonance location in the total cross sections of the proton radiative capture on  ${}^{10}\text{B}$  [156,157] at lowest energies practically correct.

The next  ${}^6S_{5/2}$  potential for the resonance at  $0.56(60) \text{ MeV}$  (l.s.) with the moment  $J = 5/2^+$  and the width  $550(100) \text{ keV}$  can have the parameters

$$V_{S52} = -18.293 \text{ MeV}, \quad \alpha_{S52} = 0.033 \text{ fm}^{-2},$$

has the bound FS and correctly reproduce the resonance energy of  $560(1) \text{ keV}$  at the width of  $570(5) \text{ keV}$ , and its phase shift is shown in Fig. 8.1 by the solid line. The scattering phase shift value at the resonance energy is equal to  $90.0^\circ(5)$ .

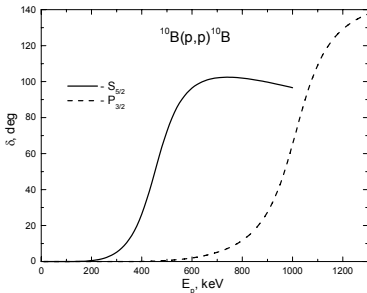


Fig. 8.1. The  $S_{5/2}$  and  $P_{3/2}$  phase shifts of the  $p^{10}\text{B}$  elastic scattering at low energies, obtained with the potentials given in the text.

It is possible to give the potential parameters without FSs for the  ${}^6P_{3/2}$  resonance at  $1.05(6) \text{ MeV}$  with the width of  $230(50) \text{ keV}$ , though we shall not use it in future calculations for a while

$$V_{P32} = -31.5 \text{ MeV}, \quad \alpha_{P32} = 0.1 \text{ fm}^{-2}.$$

This potential leads to the resonance

at 1050(1) keV with the width of 250(5) keV and with the phase shift value of 90(1)°, and its phase shift is shown in Fig. 8.1 by the dashed line.

Since, in the region up to 1.0 MeV that we consider, the  ${}^6P_{3/2}$  and  ${}^6P_{5/2}$  scattering waves have not resonances, we will consider their phase shifts close to zero, and because they does not contain FSs, then the depth of such potentials, for the first variant, can be equalized to zero. In the capacity of the second variant it is possible to consider that this potential has to have parameters leading to the scattering phase shifts that close, but not exactly equals zero.

### 8.3 Total cross sections of the radiative proton capture on ${}^{10}\text{B}$

We would remind one that the experimental data for the total cross sections the astrophysical  $S$ -factors of the radiative proton capture on  ${}^{10}\text{B}$  are given in works [156,157]. Meanwhile, the numerical values of the  $S$ -factor, obtained in work [157], were taken from the data base EXFOR, given in the MSU site [137], and the numerical values of the  $S$ -factor for the transition to the GS, obtained in work [156] were taken from figures of this work.

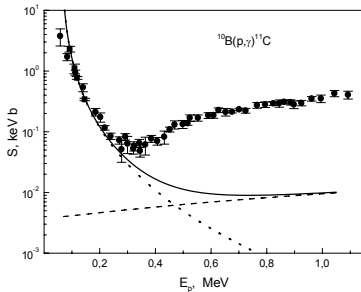


Fig. 8.2. Astrophysical  $S$ -factor of the radiative proton capture on  ${}^{10}\text{B}$  to the GS. Experiment: points (●) – numerical data on the  $S$ -factor are from figures of work [156], squares (■) – numerical data on the  $S$ -factor obtained in [157] – were taken from data base EXFOR, given in the MSU site [137].

Consider now the astrophysical  $S$ -factor of the radiative proton capture on  ${}^{10}\text{B}$  to the GS of  ${}^{11}\text{C}$  with the potential (8.1), which shape is shown in Fig. 8.2 by points and squares [156,157]. The astrophysical  $S$ -factor does not contain evident resonances at energies 560 keV and 1050 keV, where the resonance states are observed in the elastic  $p^{10}\text{B}$  scattering and resonances in spectra of  ${}^{11}\text{C}$  [153]. There is only the resonance in the range of zero energy, which corresponds to the

resonance in the  ${}^6S_{5/2}$  scattering wave at 10 keV. Therefore the potential of this state was constructed only on the basis of the correct description of the

resonance in the capture  $S$ -factor. Consequently, the potential parameters (8.2) were obtained, and the form of the calculated  $S$ -factor of the radiative proton capture on  $^{10}\text{B}$  for the  $E1$  transition from the  $^6S_{5/2}$  scattering wave to the  $^6P_{3/2}$  ground state, i.e., the process No. 1 from the chapter 8.1 is given in Fig. 8.2 and Fig. 8.3 by the dotted line at low energies.

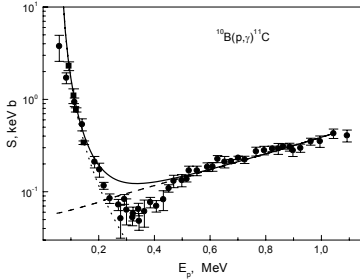


Fig. 8.3. Astrophysical  $S$ -factor of the radiative proton capture on  $^{10}\text{B}$  to the GS. Points and squares – experiment as in Fig. 8.2.

nonresonance  $M1$  transitions from the  $^6P_{3/2}$  and  $^6P_{5/2}$  scattering waves to the  $^6P_{3/2}$  GS – the calculated results are shown in Fig. 8.2 by the dashed line. The first variant of the potential with the zero depth was used for both scattering waves, because such states haven't resonances at low energies and forbidden states, and therefore the potential should lead to the phase shifts that close or equal to zero.

The summed cross section of two considered above processes that describes the  $S$ -factor only in the energy range  $0.25 \div 0.30$  MeV is shown by the solid line in Fig. 8.2, meanwhile only at the expense of the resonance transition to the GS at 10 keV. We have not considered here the resonance processes like  $M1$  from the  $^6P_{3/2}$  scattering wave at 1.05 MeV or the  $E1$  transition from the resonance  $^6S_{5/2}$  wave at 560 keV to the GS of  $^{11}\text{C}$  because they lead to the resonances in the calculated cross sections that are not observing in the available measurements of the total cross sections and the astrophysical  $S$ -factor of the proton radiative capture reaction on  $^{10}\text{B}$  at low energies.

Since, the results of the phase shift analysis for the  $p^{10}\text{B}$  elastic scattering are absent and there are not accurate data of the phase shifts, then it might be supposed that the  $^6P_{3/2}$  and  $^6P_{5/2}$  phase shifts in the energy range less than 1.0 MeV do not need to be equal to zero exactly. They can well be

close to zero, i.e., to have the value in order of magnitude of  $1 \div 2$  degrees. Therefore, let us try to clear one question: can the nonresonance  $M1$  transition for certain  ${}^6P_{3/2}$  and  ${}^6P_{5/2}$  potentials of the elastic scattering allow one to correctly reproduce the general shape of the  $S$ -factor of the proton radiative capture on  ${}^{10}\text{B}$  above  $0.25 \div 0.30$  MeV and have the phase shifts close to zero? It was found that the potential parameters the same for both  ${}^6P_{3/2}$  and  ${}^6P_{5/2}$  scattering waves without bound FSs can be represented in the next form

$$V_p = -291 \text{ MeV}, \quad \alpha_p = 1.0 \text{ fm}^{-2}, \quad (8.3)$$

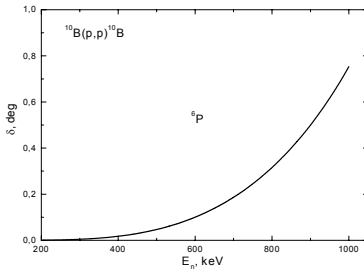


Fig. 8.4. The  ${}^6P$  phase shift of the  $p^{10}\text{B}$  elastic scattering for the potential (8.3).

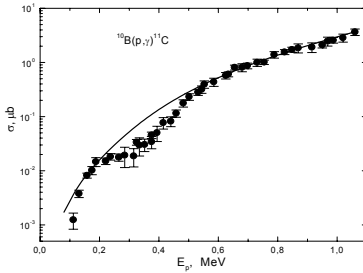


Fig. 8.5. Total cross sections of the radiative proton capture on  ${}^{10}\text{B}$  to the GS.

Experiment: points (●) – numerical cross section values, obtained in [156], which were taken from the data base EXFOR, given in the MSU site [137].

capture on  ${}^{10}\text{B}$  at energies up to 1.0 MeV.

Furthermore, the total cross section of the radiative proton capture on  ${}^{10}\text{B}$  is shown in Fig. 8.5 by the solid line, which corresponds to the astrophysical  $S$ -factor that shown in Fig. 8.3. Only the experimental data of

which allow, in general, correctly describe the available experimental data on the  $S$ -factor [156] at the energies from  $0.25 \div 0.30$  MeV to, approximately, 1.0 MeV, as it was shown below in Fig. 8.3 by the dashed line. The solid line, as before, shows the summation total cross section for the considered  $M1$  and  $E1$  transitions (processes No. 1 and No. 7 from the paragraph 8.1). The scattering phase shift of this potential at 1.0 MeV reaches 0.8 degree and is shown in Fig. 8.4. This result quite corresponds to the conception about the closeness of the phase shift to zero and allows one to acceptably reproduce the behavior of total cross sections of the proton

the work [156] are shown in Fig. 8.5, and the calculated  $S$ -factor at lowest energies, as it was seen from Figs. 8.2 and 8.3, evidently, better coincide with data of work [157]. Generally, the total calculated cross sections are in well agreement with the available experimental data [156] at energies more than 400 keV, though the range 200÷400 keV is reproduced slightly worse.

Thereby, it is seen that at the accounting of two  $E1$  and  $M1$  transitions it is possible, in general, to describe experimental data on the astrophysical  $S$ -factor or on the total cross sections of the radiative proton capture on  $^{10}\text{B}$  at energies up to 1.0 MeV. And in this system on the basis on more or less simple assumption about the FS and AS structure in the wave function of intercluster interaction in the frame of MPCM with FSs it is quite succeeded to reproduce the known experimental measurements [158].

However, the shape of the astrophysical  $S$ -factor at energies in the range of the first resonance 10 keV did not determined completely at the experimental measurements. The cross section did not measured at the resonance energy; therefore it is prematurely to speak about the correct description of the  $S$ -factor in the whole range of low energies. At the same cause it is impossible to propose new variant of approximation of the calculated  $S$ -factor at low energies.

## **Conclusion**

Thus, the methods of obtaining the shape and the depth of the intercluster interactions for scattering and bound states that used here allow to get rid of the discrete and continuous ambiguity of its parameters [29,154], which are inherent to the optical model [46] and observing in the usual approaches at the construction of the intercluster potentials in the continuous and discrete spectrum of the two-body system. Furthermore, the obtained by the same way potentials can be used in any calculations connected with the solution of nuclear-physical and astrophysical problems of low, lowest and thermal interaction energies [21,29,154,158].





## 9. RADIATIVE PROTON CAPTURE ON $^{11}\text{B}$

---

### *Introduction*

Continuing to study the processes of the radiative capture [31,91,151,152], which usually take part of different thermonuclear cycles [1], we consider the  $p^{11}\text{B} \rightarrow \gamma^{12}\text{C}$  reaction in the frame of the MPCM at astrophysical energies. In this case, because of absence of the results of the phase shift analysis, the potentials of the intercluster interactions for the scattering processes are constructed in terms of the description of the structure of spectra of resonance states of the  $p^{11}\text{B}$  system in  $^{12}\text{C}$ . For BSs or GSs of nuclei that are forming as a result of the capture reaction in the cluster channel, which coincides with the initial particles, the intercluster potential usually are constructed on the basis of reproduction of the binding energy of these particles in the final nucleus. And also some basic characteristics of such states as, for example, charge and/or mass radiuses and asymptotic constant [91,151,152].

Let us note that usually supposed [159] that the proton capture reaction on  $^{11}\text{B}$  at the astrophysical energies ( $E_p < 100$  keV) leads to the small cross sections of the formation of  $^{12}\text{C}$ , because of the large Coulomb barrier. The proton capture reaction on  $^{11}\text{B}$  is also neglected in the primordial nucleosynthesis and formation of  $^{12}\text{C}$  at the neutron capture on  $^{11}\text{B}$  with the following beta decay of  $^{12}\text{B}$  to  $^{12}\text{C}$  is supposed. The density of  $^4\text{He}$  nuclei in the star nucleosynthesis, produced in the p-p chain, is sufficiently large and namely triple alpha process is responsible for synthesis of  $^{12}\text{C}$ . However, as it is known in the last time, it is impossible to neglect by the neutron capture on  $^{11}\text{B}$  in full [159].

One of the last measurements of the reaction rate for  $^{11}\text{B}(p, \gamma)$  process at low energies, generally, were focused in the narrow resonance range at  $E_p = 163$  keV with small width [159,160]. Study of this resonance with the help of the capture  $^{11}\text{B}(p, \gamma_{0+1})$  reaction to the GS and the first excited state

(FES) allows one to obtain the width of  $\Gamma = 6.7$  keV and the cross section of  $\sigma_\gamma = 125$   $\mu\text{b}$  in the resonance range, which differ from the assumed values [161] ( $\Gamma = 5.3$  keV and  $\sigma_\gamma = 158$   $\mu\text{b}$ ) more than by 20%. The values of  $\Gamma = 5.4$  keV and  $\sigma_\gamma = 130$   $\mu\text{b}$  were obtained relatively recently in [162], and was drawn the conclusion that this resonance plays the key role in the determination of the reaction rate for the  $^{11}\text{B}(p,\gamma)$  process at low and astrophysical energies. Therefore, this reaction can play the certain role in different thermonuclear processes in the Universe at synthesis of  $^{12}\text{C}$  [159,160,162].

### 9.1 Structure of cluster states

In view of absence of the complete tables for products of Young tableaux for systems with a number of nucleons more than eight, [31,91,151,152] the presented below results might be consider as the qualitative estimation of the possible orbital symmetries in the ground state of  $^{12}\text{C}$  in the  $p^{11}\text{B}$  cluster channel. At the same time, just basing on such classification we succeeded to reproduce, and, what is more important, to explain available experimental data on the radiative nucleon capture reactions in the channels  $p^{12}\text{C}$  [31,91], and also  $n^{12}\text{C}$  and  $n^{13}\text{C}$  [3,151,152].

So, it is reasonable to use similar classification of the cluster states according to orbital symmetries, which leads us to a certain number of FSs and ASs in the intercluster wave functions for the given orbital moment. It means that the WF of the cluster relative motion for the bound or scattering state has a certain number of nodes – in present case the proton and the  $^{11}\text{B}$  system are taken as clusters.

Let us assume the  $\{443\}$  orbital Young tableau for the GS of  $^{11}\text{B}$  with moments  $J^\pi, T = 3/2^-, 1/2^-$  [161], therefore for the  $p^{11}\text{B}$  system one has  $\{1\} \times \{443\} \rightarrow \{543\} + \{444\} + \{4431\}$  [123]. The first tableau in this product is compatible with the orbital momenta of  $L = 1, 2, 3, 4$ , it is forbidden, as no more than four nucleons may be on  $s$ -shell. The second tableau is allowed and compatible with the orbital momenta of  $L = 0, 2, 4$ , as for the third one also allowed the corresponding momenta of  $L = 1, 2, 3$  [16].

Therefore, just restricting by the lowest partial waves with orbital

angular moments  $L = 0$  and  $1$  one may state that for the  $p^{11}\text{B}$  system in the potential of the  $^3S_1$  state there is only the allowed state. This state may be not bound and lay in continuous spectrum, as far as the bound and forbidden state is absent here. Each of  $^3P$  waves has bound forbidden and allowed state. One of them, notably  $^3P_0$ , corresponds to the GS of  $^{12}\text{C}$  with quantum moment  $J^\pi, T = 0^+, 0$  which is at the binding energy of the  $p^{11}\text{B}$  system of  $-15.9572$  MeV [161]. Others triplet  $^3P$  states have bound FS, but may also have AS in continuous spectrum. Another one bound state in the  $^3P_2$  wave corresponds to the FES of  $^{12}\text{C}$  with  $J^\pi, T = 2^+, 0$ . The  $^3P$  scattering waves contain bound FSs, but can have ASs in the continuous spectrum, i.e., allowed state will not be bound for scattering potentials.

Here, it must be noted that, in principle, the other variant of such state classification is possible, if the  $\{4421\}$  orbital Young tableau will assume for the GS of  $^{11}\text{B}$ . Then within the  $1p$ -shell treating of the  $p^{11}\text{B}$  system one has  $\{1\} + \{4421\} \rightarrow \{5421\} + \{4431\}$ . The first tableau in this product is forbidden – it compatible with the orbital momenta  $L = 1, 2, 3$ , it is forbidden. The second tableau is allowed and compatible with the orbital momenta  $L = 1, 2, 3$ . Thus, considering only waves with the orbital moment  $L = 0$  and  $1$  may be thought that for the  $p^{11}\text{B}$  system there are forbidden and allowed states, the last of them can be not bound for the discrete spectrum. Since, only  $S$  scattering waves are considered further, then, in this case, the presence and number of the bound ASs and FSs in these two partial waves stay as before.

In addition, some  $p^{11}\text{B}$  scattering states and bound states can be mixed by spin for  $S = 1$  and  $2$ . However here we assume that all states have spin  $S = 1$ , i.e., are pyre triplet. It allows to determine a certain minimal set of transitions that allow one to consider the capture processes, as to the GS and to the first excited state [161], the cross sections for which are given in works [159,163,164,165].

Furthermore, let us treat two resonance states in the  $p^{11}\text{B}$  system at positive energies:

1. First resonance state of  $^{12}\text{C}$  in the  $p^{11}\text{B}$  channel appears at  $162$  keV (l.s.) or  $148.6(4)$  keV in c.m. and has a total width less than  $5.3(2)$  keV in c.m., and quantum numbers  $J^\pi = 2^+$  (Tables 12.11 and 12.6 in [161]). It corresponds to the level of  $16.1058(7)$  MeV of  $^{12}\text{C}$  and it may be compared

to the mixed by spins  $^{3+5}P_2$  scattering wave with the bound FS and not bound AS. Since, we consider here only triplet components of the WF, we will consider that the  $^3P_2$  resonance is the pure state.

2. The second resonance state has the energy of 675 keV (l.s.), its total width equals 300 keV in c.m. and the moment  $J^\pi = 2^-$  [161]. It corresponds to the level 16.576 MeV and it can be matched to the  $^5S_2$  scattering wave without BSs or ASs. The states with the spin  $S = 2$  are not considered here, because in the experimental cross sections of the proton radiative capture on  $^{11}\text{B}$  to the first excited state this resonance is practically invisible.

The next resonance is at 1.388 MeV, i.e., higher than 1 MeV, so it will not be considered. In the spectrum of  $^{12}\text{C}$  below 1 MeV there are no resonance levels which may be correlated to the  $^3S_1$  scattering resonance [161]. That is why the corresponding phase shifts may be taken close to zero, and, since there are not bound FSs in the  $^3S_1$  wave, so its potential may be equalized to zero [31,150-152].

Among the excited states, as it was said, we will consider only transitions to the first excited state, because only for them there are experimental data [159,163-165]. The first excited state is at 4.43891(31) MeV with the moment  $J^\pi, T = 2^+, 0$  relatively to the GS of  $^{12}\text{C}$  or -11.5183 MeV relatively to the threshold of the  $p^{11}\text{B}$  channel and may be compared to the  $^3P_2$  state of  $^{12}\text{C}$ .

Furthermore, the minimal set of the electromagnetic transitions to the GS and the FES that allow in toto to describe the general behavior of the experimental total cross sections. So far as the  $^3P_0$  level corresponds to the ground state of  $^{12}\text{C}$  the  $E1$  transition from the nonresonance  $^3S_1$  scattering wave with the zero interaction potential to this GS:

$$1. \ ^3S_1 \rightarrow ^3P_0.$$

Besides, it is possible the  $E2$  transition to the GS from the resonance at 162 keV triplet part of the  $^3P_2$  scattering wave:

$$2. \ ^3P_2 \rightarrow ^3P_0.$$

If to consider all states as triplet, then for transitions to the first excited state, on the analogy with the process No.1, the next  $E1$  transition is possible:

$$3. \ ^3S_1 \rightarrow ^3P_2 .$$

As in the previous case for the transition to the GS, the  $E2$  transition to the first excited state from the resonance at 162 keV and the triplet  $^3P_2$  scattering wave is possible:

$$4. \ ^3P_2 \rightarrow ^3P_2 .$$

Let us note that to prove the used further different parameters of the potentials for the BSs and scattering states is possible only by the fact that in the present time it is impossible to obtain the potential of the first excited state with the bound AS, which would lead to the resonance in the  $^3P_2$  scattering wave.

The next values of the masses were used in the given calculations  $m(^{11}\text{B}) = 11.0093052$  amu [137], the proton mass of  $m_p = 1.00727646677$  amu is given in [36].

## 9.2 Interaction potentials

For all  $p^{11}\text{B}$  potentials the Gaussian form of Eq. (9) with point-like Coulomb component was used. Make an example of the potential parameters for the BS and two resonance states of the  $p^{11}\text{B}$  system in  $^{12}\text{C}$ . The following parameters have been found for the resonating  $^3P_2$  wave with the FS and  $J = 2^+$

$$V_{p2} = -24.38058 \text{ MeV}, \quad \alpha_{p2} = 0.025 \text{ fm}^{-2}. \quad (9.1)$$

The resonance energy of level equals  $E = 162.0(1)$  keV (l.s.) and the width of  $0.8(1)$  keV (c.m.), which generally coincide with the experimental data [161]. Note that in this work the proton width of the level equals of  $0.0217(18)$  keV (l.s.) is given in this work. The scattering phase shift is

equal to  $90.0^\circ(1)$  for the resonance energy of  $162.0(1)$  keV (l.s.), and the expression  $\Gamma = 2(d\delta/dE)^{-1}$  was used for the calculation of the resonance level on the scattering phase shift. The shape of the  $^3P_2$  scattering phase shift with this potential is shown in Fig. 9.1 by the solid line.

Here we ought to note that for a while it is not possible to obtain the potential that could lead to the resonance about 0.02 keV. In addition, the basic experimental measurements of the capture cross sections of this reaction were done in the 50÷60<sup>th</sup> years of the last century and, evidently, need improvement on the basis of modern experimental methods and targets.

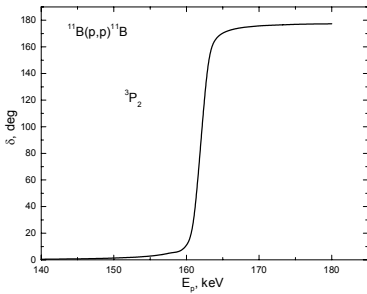


Fig. 9.1. The  $^3P_2$  phase shift of the  $p^{11}\text{B}$  elastic scattering with the resonance at 162 keV.

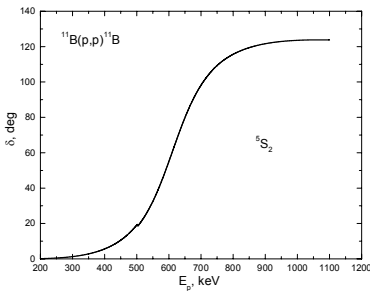


Fig. 9.2. The  $^5S_2$  phase shift of the  $p^{11}\text{B}$  elastic scattering with the resonance at 675 keV.

For this scattering potential we are considering that the FS is bound and AS is not bound and the generalized Levinson theorem is used. It is known that if the potential contains  $N + M$  forbidden and allowed bound states, then it obeys to the generalized Levinson theorem and its phase shift at zero energy starting from  $\pi(N+M)$ , i.e., from  $180^\circ$  in this case [21]. However, in Fig. 9.1 the  $^3P_2$  scattering phase shift is shown from the zero degrees for more customary presentation of the results.

Since, the used model does not allow one evidently to separate the  $^3P$  and  $^5P$  parts of the WF of such potential, the mixed by spin  $P_2$  potential with  $S = 1$  and 2 was obtained above. In all further

calculations of the different  $EJ$  transitions we will use exactly the potential (9.1), which is the same for the  $^3P_2$  and  $^5P_2$  scattering states. Besides, let us remind that at the analysis of the resonance scattering, when there is a resonance at the energies lower than 1.0 MeV the potential is constructed completely unambiguously. At the given number of BSs its depth fix

unambiguously according to the resonance level energy, and the width is completely determined by the width of such resonance. The error of its parameters usually does not exceed the error of the width determination of such level and equals approximately  $3\div 5\%$ . Meanwhile, that goes to the construction of the partial potential according to the scattering phase shifts and to the determination of its parameters according to the resonance in the nucleus spectrum [31,91,151,152].

For the potentials of the nonresonance  $^3P_0$  and  $^3P_1$  scattering waves with FSs it is possible to use parameters

$$V_{P01} = -60.0 \text{ MeV}, \quad \alpha_{P01} = 0.1 \text{ fm}^{-2}, \quad (9.2)$$

which lead to the scattering phase shifts  $1(1)^\circ$  in the energy range from zero to 1.0 MeV. Let us remind that the intercluster potential of the nonresonance scattering processes according to the scattering phase shifts at the given number of BSs, allowed and forbidden in the considered partial wave, also constructs quite unambiguously. The accuracy of the determination of parameters of this potential, in the first place, is connected with the accuracy of the phase shift extracting from the experimental data and can reach to  $20\div 30\%$ . This potential does not contain ambiguities of parameters, because the classification of states according to Young tableaux leads to unambiguously fix the number of the bound states, which absolutely determines its depth, and the width of the potential at the given depth is determined by the shape of the scattering phase shift.

It is difficult to estimate an accuracy of seeking its parameters even in the given number of the BSs at the construction of the nonresonance scattering potential according to data on spectra of nucleus in certain channel, though it is possible, evidently, to hope that it has the value the same as in the previous case. Such potential, as it usually supposed for the energy range up to 1.0 MeV, should give the scattering shift close to zero or gives the taper shape of phase shift, because there are no resonance levels in spectra of nucleus [161].

Even we are not considering here the states with spin  $S=2$ , we nevertheless represent the potential parameters for the second resonance state of the  $p^{11}\text{B}$  system of  $^{12}\text{C}$ . For the potential of the  $^5S_2$  resonance wave without FS with the moment  $J=2^-$  it is possible to use parameters in the



form

$$V_{s2} = -10.9256 \text{ MeV}, \quad \alpha_{s2} = 0.08 \text{ fm}^{-2}, \quad (9.3)$$

which lead to the elastic scattering phase shifts presented in Fig. 9.2. This potential contains the resonance at 675(1) keV (l.s.) with the width of 289(1) keV (c.m.) that is in agreement with the known data [161]. Possibly, this width ought to be slightly less, since in the same work the value for the proton width of 150 keV (l.s.) is given.

Now we will give the potential parameters for the ground and first excited state of  $^{12}\text{C}$  in the  $p^{11}\text{B}$  channel. For the potential corresponding to the  $^3P_0$  GS of  $^{12}\text{C}$  with the bound FS in the  $p^{11}\text{B}$  cluster channel the following parameters were found

$$V_{g.s.} = -142.21387 \text{ MeV}, \quad \alpha_{g.s.} = 0.1 \text{ fm}^{-2}. \quad (9.4)$$

The potential allows one to obtain the value for the mass radius of  $R_m = 2.51 \text{ fm}$ , the charge radius of  $R_{ch} = 2.59 \text{ fm}$ , the binding energy of  $-15.95720 \text{ MeV}$  at an accuracy  $\varepsilon$  of the finite-difference method [154] equals  $10^{-5} \text{ MeV}$  and the asymptotic constant in the dimensionless form (2.10) [38] equals 23.9(2) at the distance range  $7 \div 13 \text{ fm}$ . The error of the numerical constant is determined by its averaging at the noted distance range. For the value of the charge and the mass radius of  $^{11}\text{B}$  the value  $2.406(29) \text{ fm}$  [137] was used, the radius of  $^{12}\text{C}$  equals  $2.4702(22) \text{ fm}$  [137], the charge and the mass radius of proton  $0.8775(51) \text{ fm}$  [36]. The scattering phase shift of such potential does not exceed  $2.0^\circ$  in the energy range up to  $1.0 \text{ MeV}$ .

Because we have not independent results on the AC in the  $p^{11}\text{B}$  channel, the GS potential (9.4) was constructed exclusively from the requirement of the correct description of the nonresonance part of the capture total cross sections that are shown later in Fig. 9.3 by points and squares. These cross sections have a certain experimental error therefore the GS potential parameters have some ambiguity that is connected with this error, which, nevertheless, estimates at the level not more than 10%.

For the potential corresponding to the  $^3P_2$  FES of  $^{12}\text{C}$  with the FS in the  $p^{11}\text{B}$  cluster channel the following parameters were found

$$V_{p2} = -130.61325 \text{ MeV}, \quad \alpha_{p2} = 0.1 \text{ fm}^{-2}. \quad (9.5)$$

Such potential allows one to obtain the value for the mass radius of  $R_m = 2.53 \text{ fm}$ , the charge radius of  $R_{ch} = 2.63 \text{ fm}$ , the binding energy of  $-11.5183 \text{ MeV}$  at an accuracy  $\varepsilon$  of the finite-difference method [154] equals  $10^{-4} \text{ MeV}$  and the asymptotic constant in the dimensionless form (2.10) equals  $16.1(1)$  at the distance range  $7 \div 14 \text{ fm}$ . The scattering phase shift of such potential does not exceed  $1.0^\circ$  in the energy range up to  $1.0 \text{ MeV}$ . Also there are no independent data for the asymptotic constant for this state, therefore the parameters of this potential were obtained from (9.4) by the simple lessening of the depth, at the same geometry, in order to reproduce the binding energy of the first excited state correctly.

We would remind that the parameters of the BS potentials at the given number of the allowed and forbidden states in this partial wave are fixed quite unambiguously according to the binding energy, the radius of nucleus and the asymptotic constant in the considered channel. The accuracy with what the parameters of the BS potential are determined is connected, in first, with the accuracy of the AC, which is usually equals  $10 \div 20\%$ . The accuracy of the experimental determination of the charge radius as a rule is higher and lies at the level  $3 \div 5\%$ . However, as it was said in chapter 2.8, the model calculation errors of such radius might be higher and it will be hardly to estimate their value.

There are no other ambiguities in this potential, because the classification of the states according to Young tableaux allows one to fix the number of BSs, forbidden and allowed in this partial wave, which absolutely determines its depth, and the potential width completely depends from the AC value. In this case, at the unknown AC value of the ground state in the  $p^{11}\text{B}$  channel, the potential parameters error, as it was said above, eventually equals the value about  $10\%$ .

### 9.3 Total cross sections

First, the transitions to the GS, particularly, the  $E1 \ ^3S_1 \rightarrow \ ^3P_0$  process from the  $\ ^3S_1$  scattering wave with zero potential to the  $\ ^3P_0$  GS with potential of (9.4) was considered. The calculated cross section is given by the dashed line in Fig. 9.3 in the energy range  $50 \text{ keV} \div 1.5 \text{ MeV}$ . As it is

seen, it correctly describes the nonresonance part of the experimental data of works [159,163-165] in this energy range. Furthermore, the  $E2$  transition from the  $^3P_2$  resonance wave at 162 keV to the  $^3P_0$  GS of  $^{12}\text{C}$  – dashed line in Fig. 9.3. The summarized total cross section for these two transitions is shown in Fig. 9.3 by the solid line, which practically completely reproduce the value and the form of the experimental capture cross sections up to 1.5 MeV.

At the resonance energy of 162 keV the cross section reaches the value 101  $\mu\text{b}$ , which is considerably larger than the experimentally measured value of 5.5  $\mu\text{b}$ . However the experimental value was obtained at 163 keV, and since the resonance has a small width then the energy variation on 1 keV can lead to the similar mismatch of results. It should to note here that the calculated value of the total cross section at 163 keV is equal to 20  $\mu\text{b}$  – this is also slightly more than the given above experimental value. However, the resonance width for the potential (9.1) used here that equals 0.8 keV, is noticeable more than the given in [161] proton width 0.02 keV. Most probably, just that width disagreement of the resonance in the calculation and in the experiment leads to more slow fall of the calculated cross sections in the resonance range.

Absolutely analogous results are shown in Fig. 9.4 for the astrophysical  $S$ -factor of the considered proton capture reaction on  $^{11}\text{B}$ . The values of the experimental  $S$ -factor for different works were obtained by the recalculation of the total capture cross sections when the masses of particles were used. The value of the astrophysical  $S$ -factor at the range of 30÷100 keV is practically constant and at the average equals 3.5(1) keV·b. Exactly this value can be used as the  $S$ -factor at zero energy.

Pass on to the consideration of the transitions to the FES, which lies at 4.4 MeV relatively the GS of  $^{12}\text{C}$  and first of them is the  $^3S_1 \rightarrow ^3P_2$  process. The calculation results for such transition with the potential of the  $^3P_2$  wave for the FES (9.5) and for the  $^3S_1$  wave potential with zero depth are shown in Fig. 9.5 by the dashed line. As it is seen from these results, the small change of the potential parameters of the bound state from (9.4) for the GS to the (9.5) for the FES allows one correctly to describe the total cross sections of the transition to this excited state at astrophysical and low energies.

The further accounting of the resonance  $E2$  transition  $^3P_2 \rightarrow ^3P_2$  with

potentials (9.1) for scattering and (9.5) for the FES leads to the almost complete explanation of the capture cross section in the resonance range [159,163-165]. The cross section of this transition is shown in Fig. 9.5 by the dotted line, and the summarized capture cross sections taking into account the considered above two processes are shown by the solid line. Furthermore, Fig. 9.6 presents the astrophysical  $S$ -factor of the radiative capture to the first excited state, which corresponds to the cross sections that was shown in Fig. 9.5.

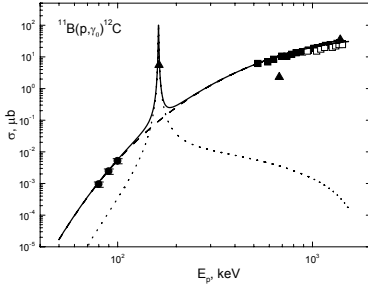


Fig. 9.3. The total cross sections of the proton radiative capture reaction on  $^{11}\text{B}$  to the GS at the energy range  $50 \div 1.5 \cdot 10^3$  keV. Experimental data: black triangle ( $\blacktriangle$ ) – from work [163], points ( $\bullet$ ) – [159], open squares ( $\square$ ) – summed total cross sections from [165], black square ( $\blacksquare$ ) – from [164]. Lines are the calculation results for the different electromagnetic transitions with the potentials, given in the text.

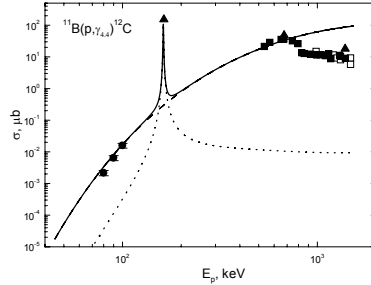


Fig. 9.5. The total cross sections of the proton radiative capture reaction on  $^{11}\text{B}$  to the FES at the energy range  $50 \div 1.5 \cdot 10^3$  keV. Experimental data: the same as in Fig. 9.3. Lines: the same as in Fig. 9.3.

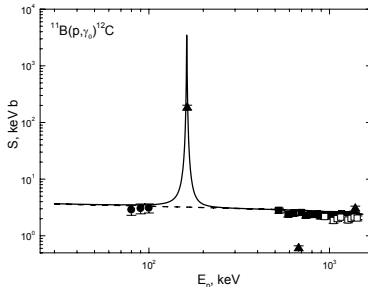


Fig. 9.4. The astrophysical  $S$ -factor of the proton radiative capture reaction on  $^{11}\text{B}$  to the GS at the energy range of  $50 \div 1.5 \cdot 10^3$  keV. Experimental data: the same as in Fig. 9.3. Lines: the same as in Fig. 9.3.

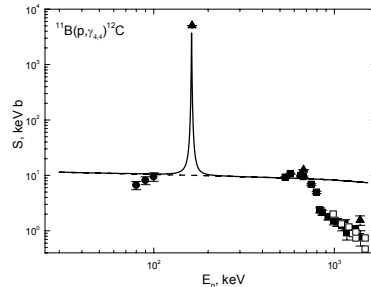


Fig. 9.6. The astrophysical  $S$ -factor of the proton radiative capture reaction on  $^{11}\text{B}$  to the FES at the energy range of  $50 \div 1.5 \cdot 10^3$  keV. Experimental data: the same as in Fig. 9.3. Lines: the same as in Fig. 9.3.

It was demonstrated that quite transparent assumptions on a way of construction of the  $p^{11}\text{B}$  interaction potentials with forbidden states [31,91,151,152] make it possible to reproduce reasonably well available experimental data [159,163-165] for the radiative capture to the GS of  $^{12}\text{C}$  in the energy region from 80 meV up to 1500 keV, as well as claim that the energy dependence of the observed cross sections occurs due to the  $^3S_1 \rightarrow ^3P_0$  and  $^3P_2 \rightarrow ^3P_0$  transitions.

The quality of description the total cross section and the astrophysical  $S$ -factor for the capture on the FES of  $^{12}\text{C}$  in the  $p^{11}\text{B}$  channel is slightly worse, but here we have taken into account only processes for the triplet states. However, in this case there are some transitions between states with spin  $S=2$ , which can slightly change the situation with the description of the experimental data. Particularly, it is possible the transition from the resonance  $^5S_2$  scattering wave at 675 keV to the corresponding WF component of the first exciting state, which ought to lead to the peak in cross sections at this energy.

### **Conclusion**

Thereby, the MPCM with potentials that generally coherent with spectrum of the resonance levels and containing forbidden states in some partial waves allows one to correctly reproduce the behavior of the experimental cross sections of the proton capture on  $^{11}\text{B}$  to the GS in the wide energy range. Meanwhile, the potentials of the GS and the FES are coordinated with the basic characteristics of  $^{12}\text{C}$  in the  $p^{11}\text{B}$  channel, including the binding energy and the charge radius [166]. However, it is necessary to note once more that since we do not know the asymptotic constants for the GS and the FES, then the results of such calculations, evidently, can consider as preliminary. On the other hand, as it was seen earlier, the quality of the description of the capture total cross sections in the different systems is quite agree with the value of the asymptotic constant in the considered channels. Therefore, the obtained results allow one to estimate the value of the asymptotic constant for the ground and the first excited states of  $^{12}\text{C}$  in the  $p^{11}\text{B}$  channel.

# 10. RADIATIVE PROTON CAPTURE ON $^{12}\text{C}$

---

---

## *Introduction*

In this section we will consider the  $p^{12}\text{C}$  system and the process of proton radiative capture on  $^{12}\text{C}$  at astrophysical energies. The new measurement of differential cross sections of the elastic  $p^{12}\text{C}$  scattering at energies from 200 keV up to 1.1 MeV (c.m.) within the range of  $10^\circ\div 170^\circ$  with 10% errors was carried out in works [28]. Furthermore, the standard phase shift analysis made and the potential of the  $S$  state of the  $p^{12}\text{C}$  system was reconstructed in this paper on the basis of these measurements [89], and then the astrophysical  $S$ -factor at the energies down to 20 keV was considered in the frame of modified potential cluster model.

Before we start describing the obtained results, we would like to note that this process is the first thermonuclear reaction of the CNO cycle which took place at a later stage of stellar evolution, when partial hydrogen burning occurred. As the hydrogen is burning, the core of the star starts appreciably compressing, which results in the increase in pressure and temperature in the star and along with the proton-proton cycle the next chain of thermonuclear processes trigger, called CNO cycle.

### **10.1. Differential cross sections**

Upon examination of the elastic scattering in the system of particles with spins 0 and 1/2 we take into account spin-orbital splitting of phase shifts that takes part in nuclear systems of the  $\text{N}^4\text{He}$ ,  $^3\text{H}^4\text{He}$ , and  $p^{12}\text{C}$  type. In this case elastic scattering of nuclear particles is completely described by two independent spin amplitudes ( $A$  and  $B$ ) and the cross section in the next form [46]

$$\frac{d\sigma(\theta)}{d\Omega} = |A(\theta)|^2 + |B(\theta)|^2, \quad (10.1)$$

where

$$A(\theta) = f_c(\theta) + \frac{1}{2ik} \sum_{L=0}^{\infty} \{(L+1)S_L^+ + LS_L^- - (2L+1)\} \exp(2i\sigma_L) P_L^1(\cos\theta) ,$$

$$B(\theta) = \frac{1}{2ik} \sum_{L=0}^{\infty} (S_L^+ - S_L^-) \exp(2i\sigma_L) P_L^1(\cos\theta) .$$
(10.2)

Here,  $S_L^{\pm} = \eta_L^{\pm} \exp(2i\delta_L^{\pm})$  is the scattering matrix,  $\eta_L^{\pm}$  are the inelasticity parameters, the signs “ $\pm$ ” correspond to the total angular momentum of the system  $J = L \pm 1/2$ ,  $f_c$  is the Coulomb amplitude represented as

$$f_c(\theta) = - \left( \frac{\eta}{2k \sin^2(\theta/2)} \right) \exp \{ i\eta \ln[\sin^{-2}(\theta/2)] + 2i\sigma_0 \} ,$$

$P_n^m(x)$  are the associated Legendre polynomials,  $\eta$  is the Coulomb parameter,  $\mu$  is the reduced mass,  $k$  is the wave number of relative particle motion,  $k^2 = \frac{2\mu E}{\hbar^2}$ , and  $E$  is the energy of colliding particles in the center of mass system.

Vector polarization in elastic scattering of such particles can be expressed in terms of amplitudes  $A$  and  $B$  [46]

$$P(\theta) = \frac{2 \operatorname{Im}(AB^*)}{|A|^2 + |B|^2} .$$
(10.3)

Developing definition for the  $B(\Theta)$  amplitude (10.2) we obtain the next expression

$$\operatorname{Re} B = \frac{1}{2k} \sum_{L=0}^{\infty} [a \sin(2\sigma_L) + b \cos(2\sigma_L)] P_L^1(x) ,$$

$$\operatorname{Im} B = \frac{1}{2k} \sum_{L=0}^{\infty} [b \sin(2\sigma_L) - a \cos(2\sigma_L)] P_L^1(x) .$$

Where

$$a = \eta_L^+ \cos(2\delta_L^+) - \eta_L^- \cos(2\delta_L^-) ,$$

$$b = \eta_L^+ \sin(2\delta_L^+) - \eta_L^- \sin(2\delta_L^-) .$$

One can find the next notation [167] for  $A(\Theta)$  amplitude by the similar way

$$\text{Re } A = \text{Re } f_c + \frac{1}{2k} \sum_{L=0}^{\infty} [c \sin(2\sigma_L) + d \cos(2\sigma_L)] P_L(x) ,$$

$$\text{Im } A = \text{Im } f_c + \frac{1}{2k} \sum_{L=0}^{\infty} [d \sin(2\sigma_L) - c \cos(2\sigma_L)] P_L(x) ,$$

where

$$c = (L+1)\eta_L^+ \cos(2\delta_L^+) + L\eta_L^- \cos(2\delta_L^-) - (2L+1) ,$$

$$d = (L+1)\eta_L^+ \sin(2\delta_L^+) + L\eta_L^- \sin(2\delta_L^-) .$$

For the total elastic scattering cross section, the following expression can be obtained [46]

$$\sigma_s = \frac{\pi}{k^2} \sum_L \left[ (L+1) |1 - S_L^+|^2 + L |1 - S_L^-|^2 \right] \quad (10.4)$$

or

$$\sigma_s = \frac{4\pi}{k^2} \sum_L \left\{ (L+1) [\eta_L^+ \sin \delta_L^+]^2 + L [\eta_L^- \sin \delta_L^-]^2 \right\} .$$

These expressions are used later for carrying out the phase shift analysis at the energy up to 1.1 MeV [168].



## 10.2. Control of the computer program

The whole text of our computer program for calculation of the total and differential cross sections of the elastic scattering of particles with half-integral spin, which was used for the applicable phase shift analysis, was tested using elastic scattering in the  $p^4\text{He}$  system. Here we present just one variant of test calculation for the  $p^4\text{He}$  scattering in comparison with the data of [169], in which phase shift analysis for an energy of 9.89 MeV was performed, the positive  $D$  phase shifts were obtained, and the following averaged value over all points was obtained:  $\chi^2 = 0.60$ .

In the analysis of [169], 22 points for cross sections from [170] at an energy of 9.954 MeV were used (it was not indicated in [169] which particular 22 points out of the 24 given in [169] have been used) and several points for polarizations from [169,171]. In the latter case, it is likely that ten points for the following eight angles were used:  $46.5^\circ$ ,  $55.9^\circ$ ,  $56.2^\circ$ ,  $73.5^\circ$ ,  $89.7^\circ$ ,  $99.8^\circ$ ,  $114.3^\circ$ , and  $128.3^\circ$  at energies of 9.89, 9.84 and 9.82 MeV. Phase shifts from [169] are given in Table 10.1, and the average  $\chi^2_\sigma$  for differential cross sections using our program, including 24 points from [170] (and energy of 9.954 MeV) with these phase shifts, is equal to 0.586. For ten experimental points for polarization from [169,171] at 9.82–9.89 MeV and eight scattering angles with phase shifts from [169],  $\chi^2_p = 0.589$  can be obtained (for an energy of 9.954 MeV).

**Table 10.1. Phase shifts of the elastic  $p^4\text{He}$  scattering from [169]**

$E$ (MeV)	$S_0$ (deg)	$P_{3/2}$ (deg)	$P_{1/2}$ (deg)	$D_{5/2}$ (deg)	$D_{3/2}$ (deg)
9.954	119.3 $\begin{smallmatrix} +2.0 \\ -1.8 \end{smallmatrix}$	112.4 $\begin{smallmatrix} +3.5 \\ -5.2 \end{smallmatrix}$	65.7 $\begin{smallmatrix} +2.7 \\ -3.2 \end{smallmatrix}$	5.3 $\begin{smallmatrix} +1.6 \\ -2.5 \end{smallmatrix}$	3.7 $\begin{smallmatrix} +1.6 \\ -2.8 \end{smallmatrix}$

If  $\chi^2$  is averaged over all points ( $24 + 10 = 34$ ), i.e., a more general expression is used

$$\chi^2 = \frac{1}{(N_\sigma + N_p)} \left\{ \sum_{i=1}^N \left[ \frac{\sigma_i^t - \sigma_i^e}{\Delta \sigma_i^e} \right]^2 + \sum_{i=1}^N \left[ \frac{P_i^t - P_i^e}{\Delta P_i^e} \right]^2 \right\} = \frac{1}{(N_\sigma + N_p)} \{ \chi_\sigma^2 + \chi_p^2 \}, \quad (10.5)$$

we obtain  $\chi^2 = 0.5875 \approx 0.59$ , which is in good agreement with the results of [169]. Here,  $N_\sigma$  and  $N_P$  are the numbers of points for cross sections (24 points) and polarizations (10 points);  $\sigma^e, P^e, \sigma', P'$  are the experimental and theoretical values of cross sections and polarizations; and  $\Delta\sigma$  and  $\Delta P$  are their errors.

If additional minimization of  $\chi^2$  is performed using our program, for  $\chi^2_\sigma$  we obtain 0.576, for polarizations  $\chi^2_P = 0.561$  and the average  $\chi^2 = 0.572 \approx 0.57$  for the following phase shifts:

$$S_0 = 119.01^\circ, \quad P_{3/2} = 112.25^\circ, \quad P_{1/2} = 65.39^\circ, \quad D_{5/2} = 5.24^\circ, \quad D_{3/2} = 3.63^\circ,$$

which completely fall into the error range given in [169] and are given in Table 10.1. Thus, the developed program makes it possible to obtain results that agree well with the previous analysis.

Furthermore, our program was tested according to the phase shift analysis given in other papers at low energies for the  $p^{12}\text{C}$  system. Earlier the phase shift analysis of excitation functions for the elastic  $p^{12}\text{C}$  scattering was measured in [172] at energies in the range of 400÷1300 keV (l.s.) and angles of  $106^\circ\div 169^\circ$  was performed in [173]; in this paper it was obtained, for example, that for  $E_{\text{l.s.}} = 900$  keV  $S$ -phase shift should be in a range of  $153^\circ\div 154^\circ$ . We obtained a value of  $152.7^\circ$  for the same experimental data. Scattering cross sections were taken from excitation functions [173] at energies of 866÷900 keV. The results of our calculations of  $\sigma_i$  in comparison with experimental data  $\sigma_e$  are given in Table 10.2. The last column of the table gives partial values of  $\chi^2_i$  for each point at 10% errors of experimental cross sections, and a value of 0.11 was obtained for  $\chi^2$  averaged over all experimental points.

At an energy of 751 keV (l.s.), in [173] the values in an interval of  $155^\circ\div 157^\circ$  were obtained for the  $S$  phase shift. The results we obtained for this energy are given in Table 10.3. The data for cross sections was taken from excitation functions in an energy range of 749÷754 keV, and the value of  $156.8^\circ$  was found for the  $S$  phase shift with the average  $\chi^2 = 0.30$ . Thus, our program yielded phase shifts coinciding with the results of analysis performed based on excitation function from [173] for two energies of the elastic  $p^{12}\text{C}$  scattering.

**Table 10.2. Comparison of the theoretical and experimental cross sections of the  $p^{12}\text{C}$  elastic scattering at 900 keV**

$\theta^\circ$	$\sigma_e$ (mb/st)	$\sigma_t$ (mb/st)	$\chi^2_i$
106	341	341.5	1.90E-04
127	280	282.1	5.76E-03
148	241	251.2	1.80E-01
169	250	237.5	2.50E-01

**Table 10.3. Comparison of the theoretical and experimental cross sections of the  $p^{12}\text{C}$  elastic scattering at 750 keV**

$\theta^\circ$	$\sigma_e$ (mb/st)	$\sigma_t$ (mb/st)	$\chi^2_i$
106	428	428.3	3.44E-05
127	334	342.8	6.91E-02
148	282	299.1	3.66E-01
169	307	279.9	7.82E-01

### **10.3. Phase shift analysis of $p^{12}\text{C}$ elastic scattering**

The test results presented above agree well with each other; therefore our program was used to perform phase shift analysis [89] of new experimental data on differential cross sections of the  $p^{12}\text{C}$  scattering in an energy range of 230÷1200 keV (l.s.) [28]. The results of analysis are given in Table 10.4 and shown by points in Fig. 10.1 in comparison with data from [173], which is shown by a dashed line. The width of such resonance at the energy 456.8(5) keV equals 31.7(8) keV [174].

Figs. 10.2a,b,c show the experimental differential cross sections in the resonance region near 457 keV in the laboratory system (data points), the results of calculation of these cross sections based on Rutherford formula (dotted curve), and cross sections obtained from

our phase shift analysis (solid line), which takes into account the  $S$  phase shift only. It can be seen from these figures that, in the resonance region, it is impossible to describe the cross section based on the  $S$  phase shift only.

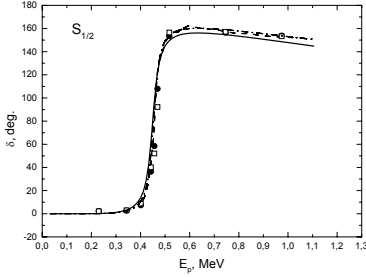
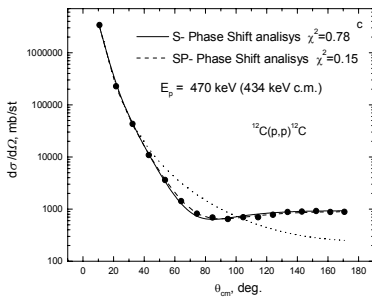
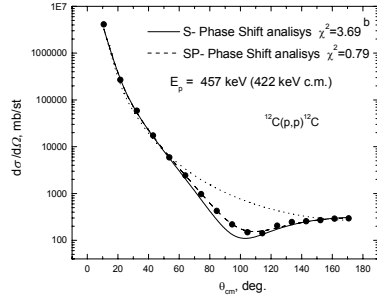
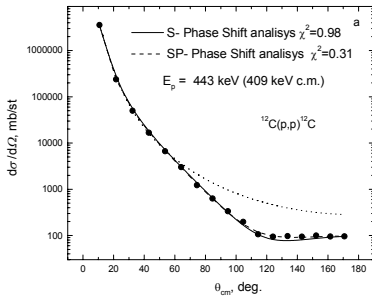


Fig. 10.1. The  $^2S$  phase shift of the  $p^{12}\text{C}$  scattering at low energies. Points show results of the analysis for the  $S$  phase shift taking into account the  $S$  wave only, open squares show results of the analysis for the  $S$  phase shift taking into account the  $S$  and  $P$  waves, and the dashed line shows the results of [173]. Curves show calculations with different potentials.

The  $P$  wave shown in Fig. 10.3 begins to play a noticeable role, and taking this wave into account essentially improves the description of experimental data. The dashed line shows cross sections taking into account the  $S$  and  $P$  waves in phase shift analysis in Fig. 10.2. In particular, at 457 keV (l.s.), the cross sections at this energy are shown in Fig 10.2b and accounting of the  $P$  wave reduces the value of  $\chi^2$  from 3.69 to 0.79.



Figs 10.2a,b,c. Differential cross sections of the  $p^{12}\text{C}$  scattering. The solid line – the phase shift analysis taking account the  $S$  wave only, the dotted – Rutherford scattering, and the dashed line is phase shift analysis taking into account the  $S$  and  $P$  waves, and the data points are from experiment [28].

It can be seen from Fig. 10.3 that, at low energies, the  $P_{1/2}$  phase shift is

higher than  $P_{3/2}$ , but at energies about 1.2 MeV they intersect and at higher

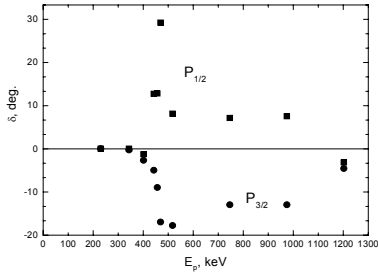


Fig. 10.3.  $^2P$  phase shifts of the  $p^{12}\text{C}$  scattering at low energies. Points show the  $P_{3/2}$  phase shift and squares show the  $P_{1/2}$  phase shift obtained as a result of the phase shift analysis taking into account the  $S$  and  $P$  waves.

energies  $P_{3/2}$  is higher for negative angles [175,176]. The value of the  $S$  phase shift in the case in which the contribution of the  $P$  wave is taken into account practically does not change, its form being shown in Fig. 10.1 by open squares. Taking into account the  $D$  wave in phase shift analysis results in its value of order of  $1^\circ$  in the resonance region and practically does not influence the behavior of calculated differential

cross sections.

**Table 10.4. Results of the phase shift analysis of the  $p^{12}\text{C}$  elastic scattering at low energies taking into account the  $S$  phase shift only**

$E_{cm}$ (keV)	$S_{1/2}$ (deg)	$\chi^2$
213	2.0	1.35
317	2.5	0.31
371	7.2	0.51
409	36.2	0.98
422	58.2	3.69
434	107.8	0.78
478	153.3	2.56
689	156.3	2.79
900	153.6	2.55
1110	149.9	1.77

We ought to note, in the conclusion of this paragraph, that the value  $\hbar^2/m_0 = 41.80159 \text{ MeV fm}^2$ , which is slightly differ than generally used, was employed in this analysis; it was obtained with more contemporary constant values [33].

### 10.4. Astrophysical $S$ -factor

The proton radiative capture on  $^{12}\text{C}$  at low energies is included in the CNO fusion cycle and makes a noticeable contribution to the energy gain of fusion reactions in many stars at later, than pp-chain, stage of their development [58,118] and whereof we previously stated in the introduction. Therefore, let us go to the more detailed consideration of the based characteristics of this reaction at astrophysical energies.

The available experimental data on the  $S$ -factor [34] shows the presence of narrow resonance, with a width of about 32 keV, at an energy of 0.422 MeV (center of mass system), which results in the increase of the  $S$ -factor by two to three orders of magnitude. It is interesting to elucidate the possibility of description of the resonance  $S$ -factor of this reaction based on the modified potential cluster model with forbidden states. These studies are possible, since phase shift analysis of new experimental data [28] on differential cross sections of the elastic  $p^{12}\text{C}$  scattering at astrophysical energies [89] has been performed in previous paragraph, which makes it possible to construct potentials of the  $p^{12}\text{C}$  interaction using found elastic scattering phase shifts.

In the present calculations of the process of the proton radiative capture on  $^{12}\text{C}$  the  $E1(L)$  transition was taken into account, which was conditioned by the orbital part of the electric operator  $Q_{JM}(L)$  [22,26]. The cross sections of the  $E2(L)$  and  $MJ(L)$  transitions and the cross sections depending on the spin part of the  $EJ(S)$  and  $M2(S)$  turned out to be lower by several orders of magnitude. The electric  $E1$  transition in the process of  $p^{12}\text{C} \rightarrow ^{13}\text{N}\gamma$  capture is possible between doublet  $^2S_{1/2}$  and  $^2D_{3/2}$  scattering states and the ground  $^2P_{1/2}$  bound state of  $^{13}\text{N}$  in the  $p^{12}\text{C}$  channel. Therefore, we need potentials for partial waves corresponded to these states.

Before construction of the interaction potentials according to elastic scattering phase shifts, first we consider the classification of orbital states according to Young tableaux for the  $p^{12}\text{C}$  system. We would remind you that possible orbital Young tableaux in a system of particles can be determined as the direct outer product of the orbital tableaux of each subsystem, which in this case yields  $\{1\} \times \{444\} = \{544\}$  and  $\{4441\}$  [123,145]. The first of them is compatible with the orbital angular momentum

$L = 0$  only and is forbidden, since five nucleons cannot be situated in the  $s$ -shell. The second tableau is compatible with orbital angular moments of 1 and 3 [123]; the first one corresponds to the ground bound state of  $^{13}\text{N}$  with  $J = 1/2^-$ . Thus, the potential of the  $^2S$  wave should contain the forbidden bound state, and the  $^2P$  wave possesses an allowed state only at energy of  $-1.9435$  MeV [174].

For calculation of the cross sections of photonuclear processes, the nuclear part of intercluster potential of the  $p^{12}\text{C}$  interaction is represented in general form (2.8) with a point-like Coulomb term. The potential of the  $^2S_{1/2}$  wave was constructed in such a way that the corresponding elastic scattering partial phase shift with pronounced resonance at  $0.457$  MeV (l.s.) is correctly described. The results of phase shift analysis [89] presented above were used here to obtain the  $^2S_{1/2}$  potential of the  $p^{12}\text{C}$  interaction with the forbidden state at the energy  $E_{\text{FS}} = -25.5$  MeV. The parameters of the potential are as follows

$$V_S = -67.75 \text{ MeV}, \quad \alpha_S = 0.125 \text{ fm}^{-2},$$

the calculation results of the  $^2S_{1/2}$  phase shift with this potential are shown in Fig. 10.1 by the solid line.

The potential of the ground  $^2P_{1/2}$  state should correctly reproduce the binding energy of  $^{13}\text{N}$  in the  $p^{12}\text{C}$  channel equals  $-1.9435$  MeV [174] and reasonably describe the root-mean-square radius, which, evidently, does not exceed much the  $^{13}\text{C}$  radius equals  $2.4628(39)$  fm [174]. Consequently, the following parameters were obtained

$$V_{GS} = -81.698725 \text{ MeV}, \quad \alpha_{GS} = 0.22 \text{ fm}^{-2}. \quad (10.6)$$

A binding energy of  $-1.943500$  MeV and the root-mean-square radius of  $R = 2.54$  fm have been obtained for this potential. For the proton and  $^{12}\text{C}$  nuclear radii the following values were used:  $0.8768(69)$  [36] and  $2.472(15)$  fm [161], respectively. Integers were used for mass values. The behavior of the wave function of bound state at large distances was controlled by using asymptotic constant  $C_w$  (2.10) with the asymptotics in the form of the Whittaker function [26], and its value in an interval of  $5\div 20$  fm turned out to be equal to  $1.96(1)$ .

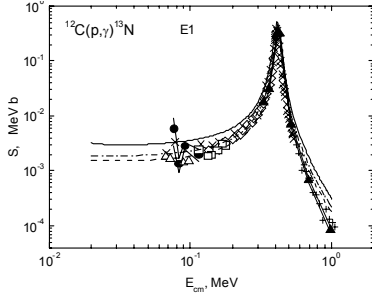


Fig. 10.4. Astrophysical  $S$ -factor of the proton radiative capture on  $^{12}\text{C}$  at low energies. Experimental data denoted by  $\times$ ,  $\bullet$ ,  $\square$ ,  $+$  and  $\Delta$  is taken from survey [34], triangles from [177]. Curves show calculations with different potentials.

The results of calculation of the  $S$ -factor of the proton radiative capture on  $^{12}\text{C}$  with the  $^2P_{1/2}$  and  $^2S_{1/2}$  potentials obtained above for energies from 20 keV to 1.0 MeV are shown in Fig. 10.4 by solid lines in comparison with the experimental data from survey [34] and work [177]. For 25 keV a value of 3.0 keV b has been obtained for the calculated  $S$ -factor, and extrapolation of experimental values of the  $S$ -factor to an energy

of 25 keV yields  $1.45(20)$  and  $1.54^{+15}_{-10}$  keV b [174].

The variant of the  $^2S$  potential presented here is not the only possible way of describing the resonance behavior of the  $S$  phase shift at energies below 1 MeV. Other combinations of bound state and scattering potentials can be found that yield close results for the  $^2S_{1/2}$  phase shift and well describe the value and position of the  $S$ -factor maximum, for example,

$$V_{GS} = -65.8814815 \text{ MeV}, \quad \alpha_{GS} = 0.17 \text{ fm}^{-2}, \quad R_{ch} = 2.58 \text{ fm},$$

$$C_W = 2.30(1), \quad E_{GS} = -1.943500 \text{ MeV},$$

$$V_S = -55.15 \text{ MeV}, \quad \alpha_S = 0.1 \text{ fm}^{-2}.$$

There is a certain correspondence between the parameters of the bound state and the scattering potentials that arises from the requirement of a description of the resonance  $S$  phase shift, the binding energy, and the value of resonance in the  $S$ -factor. The growth of the width of scattering and bound state potentials results in a smoother decrease of the  $S$ -factor at both sides of the resonance. For example, the value of the  $S$ -factor for the above potential at 25 keV is equal to 3.8 keV b.

Other combinations of potentials with a BS potential narrower than in (10.6) can be proposed, for example, with the following parameters



$$V_{GS} = -121.788933 \text{ MeV}, \quad \alpha_{GS} = 0.35 \text{ fm}^{-2}, \quad R_{ch} = 2.49 \text{ fm},$$

$$C_W = 1.50(1), \quad E_{GS} = -1.943500 \text{ MeV},$$

$$V_S = -102.04 \text{ MeV}, \quad \alpha_S = 0.195 \text{ fm}^{-2}. \quad (10.7)$$

These potentials result in a sharper drop of  $S$ -factor at energies near the resonance. The phase shift of potential (10.7) and the behavior of the corresponding  $S$ -factor are shown in Figs. 10.1 and 10.4 by the dash-dotted lines. The scattering potential leads to the resonance energy 457(1) keV with the width of this resonance 36(1) keV that is agree with data [174] not bad. The value of the  $S$ -factor for this combination of potentials at 25 keV is equal to 1.85 keV b, which on the whole agrees with data given in survey [174].

The narrower potential than the BS potential (10.7) is given below

$$V_{GS} = -144.492278 \text{ MeV}, \quad \alpha_{GS} = 0.425 \text{ fm}^{-2}, \quad R_{ch} = 2.47 \text{ fm},$$

$$C_W = 1.36(1), \quad E_{GS} = -1.943500 \text{ MeV}, \quad (10.8)$$

with the same scattering  $V_S$  potential (10.7) results in slight decrease of the  $S$ -factor at the resonance energy, as shown in Fig. 10.4 by the dashed line, and yields  $S(25 \text{ keV}) = 1.52 \text{ keV b}$ , which completely agrees with the data of [174].

The review of asymptotic value constants of the GS of  $^{13}\text{N}$  in the  $p^{12}\text{C}$  channel is given in [177]. It shows their values in the range  $1.43(9) \text{ fm}^{-1/2} - 1.84 \text{ fm}^{-1/2}$ , which leads, after recalculation with  $\sqrt{2k} = 0.7670$ , to the dimensionless quantity of  $1.86 \div 2.40$ .

As one can see from the given above results that with decreasing the width of bound state potentials the asymptotic constant and charge radius of the nucleus also decrease. Evidently, potential (10.8) yields minimum permissible values of these parameters consistent with experimental data, for example, on root-mean-square radius. The known value of the charge radius of  $^{13}\text{C}$  is equal to 2.46 fm [174]; it should not much differ from the radius of  $^{13}\text{N}$ , which turn out to  $^{13}\text{C}$  by  $\beta$ -transition. Thereby, the variant (10.8) of the bound state

potential and the potential (10.7) for scattering states lead to the optimal  $S$ -factor description in the considered energy range and describing with it the resonance  $S$  phase shift of the elastic scattering.

For complementary verification of binding energy calculation the variational method with expansion of the wave function over the non-orthogonal variational Gaussian basis [26] was used; this method yielded energy of 1.943498 MeV on the grid with a dimensionality of 10 in the case of independent parameter variation for the first variant (10.6) of the bound state potential. The asymptotic constant  $C_W$  of the variational WF defined by parameters given in Table 10.5 reaches 1.97(2) at the distances of 5–20 fm, and the residual does not exceed  $10^{-13}$  [26]. The charge radius does not differ from the value obtained by the finite-difference calculation.

**Table 10.5. Variational parameters and expansion coefficients of the radial wave function in the  $p^{12}\text{C}$  system for first variant (10.6) of the bound state potential**

$i$	$\beta_i$	$C_i$
1	4.310731038130567E-001	-2.059674967002619E-001
2	1.110252143696502E-002	-1.539976053334172E-004
3	4.617318488940146E-003	-2.292772895754105E-006
4	5.244199809745243E-002	-1.240687319547592E-002
5	2.431248255158095E-002	-1.909626327101099E-003
6	8.481652230536312 E-000	5.823965673819461E-003
7	1.121588023402944E-001	-5.725546189065398E-002
8	2.309223399000618E-001	-1.886468874357471E-001
9	2.297327380843046 E-000	1.244238759439573E-002
10	3.756772149743554 E+001	3.435757447077250E-003

For variant (10.7) of the bound state potential, the same binding energy, –1.943498 MeV with a residual of  $10^{-14}$ , root-mean-square radius of 2.49 fm, and the asymptotic constant of 1.50(2) in a range of 5–17 fm was obtained using the variational method. The variational parameters and expansion coefficients for the radial wave function of this potential are given in Table 10.6.

**Table 10.6. Variational parameters and expansion coefficients of the radial wave function in the  $p^{12}\text{C}$  system for second variant (10.7) of the bound state potential**

$i$	$\beta_i$	$C_i$
1	1.393662782203888E-002	3.536427343510346E-004
2	1.041704259743847E-001	3.075071412877344E-002
3	4.068236340341411E-001	3.364496084003433E-001
4	3.517787678267637E-002	4.039427231852849E-003
5	2.074448420678197E-001	1.284484754736406E-001
6	7.360025091178769E-001	2.785322894825304E-001
7	3.551046173695889E-000	-1.636661944722212E-002
8	1.5131407009411240E+001	-9.289494991217288E-003
9	9.726024028584802E-001	-1.594107798542716E-002
10	6.634603967502104E-002	8.648073851532037E-003

**Table 10.7. Variational parameters and expansion coefficients of the radial wave function in the  $p^{12}\text{C}$  system for third variant (10.8) of the bound state potential**

$i$	$\beta_i$	$C_i$
1	1.271482702554672E-002	2.219877609724907E-004
2	9.284155511162226E-002	2.240043561912315E-002
3	3.485413978134982E-001	2.407314126671507E-001
4	3.088717918378341E-002	2.494885124596691E-003
5	1.815363020074388E-001	8.792233462610707E-002
6	5.918532693855678E-001	3.652121068403727E-001
7	3.909887088341156E+000	-1.906081640167417E-002
8	1.635608081209650 E+001	-1.111922033874987E-002
9	9.358886757095011E-001	2.314583156796476E-001
10	5.673177540516311E-002	5.956470542991426E-003

Third variant (10.8) of the BS potential in the variational method leads to the binding energy of  $-1.943499$  MeV with a residual of  $10^{-13}$ , the same root-mean-square radius as in finite-difference calculation, and

an asymptotic constant of 1.36(2) in a range of 5÷17 fm. Variational parameters of the radial wave function for this potential are given in Table 10.7.

As we speak repeatedly, the variational energy obtained by the variational method decreases with increasing basis dimensionality and, therefore, yields the upper limit of the true binding energy and the energy from the finite-difference method increases with decreasing step size and increasing number of steps. Therefore, the average value of  $-1.943499(1)$  MeV for the applied methods can be taken as the actual binding energy in this potential. Thus, the accuracy of calculation of the binding energy is about  $\pm 1$  eV. Let us note that in all of these calculations obtained in finite-difference and variational methods the proton mass is taken equal to unity, the mass of  $^{12}\text{C}$  equals 12,  $\hbar^2/m_0 = 41.4686$  MeV fm<sup>2</sup>.

It should be noted that in all calculations the cross section corresponding to the electric  $E1$  transition from the doublet  $^2D_{3/2}$  scattering state to the ground  $^2P_{1/2}$  bound state of  $^{13}\text{N}$  turns out to be lower by four to five orders of magnitude than the cross section of transition from the  $^2S_{1/2}$  scattering state. Therefore, the main contribution into the calculated  $S$ -factor of the process  $p^{12}\text{C} \rightarrow ^{13}\text{N}\gamma$  is made by the  $E1$  transition from the  $^2S$  scattering wave to the ground state of  $^{13}\text{N}$ .

If one will use the expression (3.4) for the  $S$ -factor parametrization, then it is possible to describe the dashed line in Fig. 10.4 in the range 10÷100 keV at the average  $\chi^2 = 0.047$  with the parameters  $S_0 = 1.4258$  keV b and  $S_1 = 0.003738$  keV b keV<sup>-1</sup>.

It is necessary to use quadratic form (3.5) in the range 10÷200 keV. The next values at the average  $\chi^2 = 0.018$  are obtained for its parameters:  $S_0 = 1.4809$  keV b,  $S_1 = -1.4894 \cdot 10^{-4}$  keV b keV<sup>-1</sup> and  $S_2 = 4.0986 \cdot 10^{-5}$  keV b keV<sup>-2</sup>. The 10% errors for calculated values of the  $S$ -factor, as usual, were used for obtaining of  $\chi^2$ . At the second method of parametrization, considered in the paragraph 3.2, we obtain  $S_0 = 1.52$  keV b,  $S_1 = -1.0154 \cdot 10^{-3}$  keV b keV<sup>-1</sup> and  $S_2 = 4.4833 \cdot 10^{-5}$  keV b keV<sup>-2</sup> at  $\chi^2 = 0.0088$ .

## Conclusion

At the end of this paragraph it is necessary to draw attention to this fact

that if shallow potentials of the  $^2S_{1/2}$  wave without a forbidden state are used for the description of the scattering processes, for example, with the following parameters

$$\begin{aligned} V_S &= -15.87 \text{ MeV}, \quad \alpha_S = 0.1 \text{ fm}^{-2}, \\ V_S &= -18.95 \text{ MeV}, \quad \alpha_S = 0.125 \text{ fm}^{-2}, \\ V_S &= -21.91 \text{ MeV}, \quad \alpha_S = 0.15 \text{ fm}^{-2}, \end{aligned} \tag{10.9}$$

it is impossible to correctly reproduce the value of the maximum of  $S$ -factor of radiative capture. It is impossible to describe the absolute value of the  $S$ -factor, which for any variants of scattering potentials (10.9) and bound states turns out to be higher than the experimental maximum by a factor of 2÷3. For all given shallow, potentials of form (10.9) it is possible to reproduce the resonance behavior of the  $^2S_{1/2}$  scattering phase shift. With decreasing width of the  $^2S_{1/2}$  potential, i.e., with increasing  $\alpha$ , the magnitude of the  $S$ -factor maximum increases, and, for example, for the last variant of the  $^2S_{1/2}$  scattering potential in (10.9), it exceeds the experimental value by approximately a factor of 3.

Thus, on the basis of the MPCM and deep  $^2S_{1/2}$  potential with FSs, it is possible to combine the description of the astrophysical  $S$ -factor and  $^2S_{1/2}$  scattering phase shift in a resonance energy region of 0.457 MeV (l.s.) and obtain reasonable values for the charge radius and asymptotic constant. At the same time, shallow scattering potentials do not make it possible to simultaneously describe the  $S$ -factor and  $^2S$  scattering phase shift for any considered combinations of the  $p^{12}\text{C}$  interactions [133].

# **11. S-FACTORS OF THE PROTON CAPTURE ON $^{13}\text{C}$**

---

## ***Introduction***

In this section we continue the study of the astrophysical  $S$ -factors for reactions with protons on light atomic nuclei and will stop on the proton radiative capture on  $^{13}\text{C}$  at astrophysical energies. This process is a part of the CNO thermonuclear cycle, be a second reaction of the radiative capture type (see Table 1.2) and gives an essential contribution to the energy efficiency of thermonuclear processes [1,2,58,178], leading to the burning of the Sun and stars of our Universe [31,179].

Here, as in the previous sections, the modified potential cluster model of light atomic nuclei with the classification of the orbital states according to Young tableaux was used for the calculations of the astrophysical  $S$ -factors. In certain cases, in coupled intercluster interactions such model leads to the bound states forbidden by the Pauli principle [21,22,92]

### **11.1 Phase shift analysis and intercluster potentials**

Before the consideration of the astrophysical  $S$ -factor of the thermonuclear  $^{13}\text{C}(p,\gamma)^{14}\text{N}$  radiative capture reaction using the experimental data obtained in [180,181], the phase shift analysis of the  $p^{13}\text{C}$  elastic scattering at the energies from 250 to 800 keV has been done [182]. The expressions for the differential cross sections of the elastic scattering in the system of two particles with spins 1/2 and 1/2 taking into account the spin-orbital splitting of the states but without singlet-triplet phase mixing [94,183], which can take place in the nuclear systems like  $\text{N}^3\text{He}$ ,  $\text{N}^{13}\text{C}$  etc., are also given in our works [26,182].

One can see that, as the result of the carried out analysis, the singlet  $^1S_0$  phase shift is close to zero (within  $1^\circ\div 3^\circ$ ). Fig. 11.1 shows the form of the triplet  $^3S_1$  phase shift. The triplet  $^3S_1$  phase shift has the pronounced

resonance corresponding to the level  $J^\pi T = 1^- 1$  of  $^{14}\text{N}$  in the  $p^{13}\text{C}$  channel at the energy 0.55 MeV (l.s.) [174]. The width of this resonance has the value 23(1) keV [174] what less than in case of  $p^{12}\text{C}$  scattering [89], and we need for its description the narrow potential without the FS what might lead to the width parameter of the order  $\beta = 2 \div 3 \text{ fm}^{-2}$ .

Let us consider the classification of the orbital states according to the orbital Young tableaux in order to determine the FSs in the  $p^{13}\text{C}$  system [184]. It was shown earlier that the Young's tableau  $\{4441\}$  corresponds to the ground bound state (GS) of  $^{13}\text{N}$  so as for  $^{13}\text{C}$  [22,133]. Let us remind that the possible orbital Young's tableaux in the  $N = n_1 + n_2$  system of particles can be characterized as the direct outer product of the orbital tableaux of each subsystem, and, for the  $p^{13}\text{C}$  system within the  $1p$ -shell, it yields  $\{1\} \times \{4441\} \rightarrow \{5441\} + \{4442\}$  [123]. The first of the obtained tableau is compatible with the orbital moment  $L = 1$  and is forbidden, so far as it could not be five nucleons in the  $s$ -shell, and the second tableau is allowed and is compatible with the orbital moments  $L$  is equal 0 and 2 [123].

Thus, in the  $^3S_1$ -potential there is the only one allowed state, which is not bound for the scattering states, and the  $^3P$  wave has the forbidden state and allowed one at the energy of -7.55063 MeV [174]. However, therefore we have not total tables of products of Young tableaux for systems with the number of particles more than eight [45], which were used by us for the similar calculations [22,31,60,91], so the above-obtained result should be considered only as the qualitative estimation of possible orbital symmetries in the GS of  $^{14}\text{N}$  for the  $p^{13}\text{C}$  channel.

The nuclear part of the intercluster potential of the  $p^{13}\text{C}$  interaction is represented as usual: in the Gaussian form with a point-like Coulomb term, given above. The potential for  $^3S_1$  wave was constructed so as to describe correctly the resonance partial phase shift of the elastic scattering (see Fig. 11.1). Two variants for  $^3S_1$  potential of the  $p^{13}\text{C}$  interaction, without FS were obtained using the results of our phase shift analysis

$$V_S = 265.40 \text{ MeV}, \quad \alpha_S = 3.0 \text{ fm}^{-2}, \quad (11.1)$$

$$V_S = 186.07 \text{ MeV}, \quad \alpha_S = 2.0 \text{ fm}^{-2}. \quad (11.2)$$

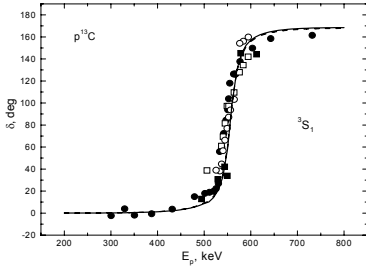


Fig. 11.1. The  ${}^3S_1$  phase shift of the  $p^{13}\text{C}$  elastic scattering at astrophysical energies. Points:  $\bullet$ ,  $\circ$ ,  $\blacksquare$  and  $\square$  – our phase shift analysis based on the data from [180,181]. Lines: solid – the phase shift calculations with potential from (11.1) given in the text, dashed – calculations with potential from (11.2).

The calculation results of the  ${}^3S_1$  phase shift with such potentials practically coincide and are shown in Fig. 11.1 by the solid (11.1) and dashed (11.2) lines. The resonance energy of 558(1) keV with the width of 27(1) keV were obtained for the first potential, and for the second one the energy is equal to 558(1) keV and the width equals 29(1) keV that, in general, is consistent with data [174].

The potential with the FS of the  ${}^3P_1$  bound state should represent correctly the binding energy of  ${}^{14}\text{N}$  with  $J^P T = 1^+ 0$  in the  $p^{13}\text{C}$  channel at -7.55063 MeV [174] as well as describe reasonably the mean square charge radius of  ${}^{14}\text{N}$ , which has the experimental value 2.560(11) fm [174]. As a result, the following parameters were obtained

$$V_{\text{GS}} = 1277.853205 \text{ MeV}, \quad \alpha_{\text{GS}} = 1.5 \text{ fm}^{-2}. \quad (11.3)$$

The potential gives the binding energy equals -7.550630 MeV and the mean square charge radius  $R_{\text{ch}} = 2.37$  fm and the AC of 1.31(1) at the range of 2÷10 fm. The values 0.8768(69) fm [36] and 2.4628(39) fm [174] were used as the radii of the proton and  ${}^{13}\text{C}$ , respectively.

Another variant of the potential of the  ${}^3P_1$  ground state of  ${}^{14}\text{N}$  defined in the  $p^{13}\text{C}$  system presenting as

$$V_{\text{GS}} = 1679.445025 \text{ MeV}, \quad \alpha_{\text{GS}} = 2.0 \text{ fm}^{-2} \quad (11.4)$$

leads to the binding energy of -7.550630 MeV and also gives slightly understated mean square charge radius  $R_{\text{ch}} = 2.36$  fm and the AC of 1.13(1) at the range of 2÷8 fm..

The independent definition of the AC was carried out, for example, in [185], where the value of  $3.74(7) \text{ fm}^{-1/2}$ , which includes the factor  $\sqrt{2k} = 1.080$  and  $\sqrt{7}$ , specified by the identity of nucleons. Recalculations



of these results to the dimensionless value gives the AC equals of 1.31(2) that completely coincided with the calculations for the calculations for the GS potential (11.3).

Let us note that the GS of  $^{14}\text{N}$  could be obtained also on the basis of the singlet  $^1P_1$  state of the  $p^{13}\text{C}$  system. In consequence of which it is a mixture of triplet and the singlet  $P_1$  wave states of the  $p^{13}\text{C}$  channel, and phenomenological, per se, potentials (11.3) and (11.4) correspond evidently to this mixed state. In addition, different states of the  $p^{13}\text{C}$  system, similarly to  $p^7\text{Li}$  [135] and  $p^9\text{Be}$  [150], are mixed by isospin with  $T=0,1$ . Therefore, the  $E1$  transitions with changing of the isospin  $\Delta T=1$  between different levels of  $^{14}\text{N}$  with different  $T$  are possible.

Generally speaking, we have to use only the part of the GS WF, which meets the triplet  $^3P_1$  state, under consideration of the  $E1$  transitions from the  $^3S_1$  scattering wave with  $\Delta T=1$  [31]. However, it is not possible to extract this part on the basis of methods used here, the available experimental data and at the absence of full and accurate classification of BSs according Young tableaux in the present time. Therefore, furthermore we will use “total” GS WF, obtaining under solution of the Schrödinger equation with the potentials (11.3) or (11.4), which contains the contributions of singlet and triplet states. This approach is based on the assumption that the triplet part gives the dominant contribution into the total wave function of the bound state of  $^{14}\text{N}$  in the  $p^{13}\text{C}$  channel.

The variational method [26] is used for an additional control of the accuracy of binding energy calculations of the GS, which even at the grid with the dimension of  $N=10$  and independent variation of the parameters for the first variant of the GS potential (11.3) leads to the energy  $-7.550628$  MeV. The asymptotic constant  $C_w$  of the variational WF, which has parameters listed in Table 11.1, at the range  $2\div 8$  fm equals 1.31(1), residuals are of the order of  $10^{-14}$  [26]. The charge radius does not differ from previous value, obtained earlier in FDM calculations.

Also, the binding energy of  $-7.550628$  MeV with the residuals of the order of  $10^{-13}$ , the radius 2.36 fm, the asymptotic constant 1.12(1) at the region  $2\div 10$  fm were obtained for the second variant of the GS potential (11.4) by the variational method with  $N=10$ . The coefficients and expansion parameters of the radial variational wave function are listed in Table 11.2.

**Table 11.1. The variational coefficients and expansion parameters of the radial WF in the  $p^{13}C$  system for the first variant (11.3) of the BS potential. The normalization coefficient of the wave function in the range  $0 \div 30$  fm equals  $N = 9.99999999996705E-001$**

$i$	$\beta_i$	$C_i$
1	3.435659028770459E - 002	5.549604576612908E - 004
2	7.916144802348336E - 002	8.310251876131318E - 003
3	1.693220678918127E - 001	4.971938301388198E - 002
4	3.501613626660634E - 001	2.059060460963998E - 001
5	7.105562481791941E - 001	7.061698723817919E - 001
6	1.388530019918587	1.912520851394402
7	3.819181085609714	- 8.087112297992904
8	5.771728151810915	- 5.176238924345936
9	23.482380472173390	11.379563256090777E - 002
10	96.327450253114260	5.258601877559056E - 002

**Table 11.2. The variational coefficients and expansion parameters of the radial WF in the  $p^{13}C$  system for the second variant (11.4) of the BS potential. The normalization coefficient of the wave function in the range  $0 \div 30$  fm equals  $N = 9.99999999996705E-001$**

$i$	$\beta_i$	$C_i$
1	4.037610291453870E-002	9.785307431545794E-004
2	9.865755407308111E-002	1.370856960682145E-002
3	2.213739718639349E-001	7.895870172870946E-002
4	4.716934681793400E-001	3.124034843582795E-001
5	9.623149409598139E-001	1.002536390673191
6	1.852140654482041	2.530616591930234
7	4.993108962845088	- 10.761311643622440
8	7.582193499612377	- 7.448842087973955
9	34.992924237340400	1.069695807929516E-001
10	147.448443128141100	5.824678193758300E-002

Let us pay attention to the fact that the variational energy gives the upper limit of the true binding energy at the increasing of the basis dimension. At the same time, the finite-difference energy increases at the decreasing of the step size and increasing of the steps number [22,26,31]. Therefore, it is possible to accept the average value of  $-7.550629(1)$  MeV as the real binding energy in such potential, i.e., the accuracy of the determination of the binding energy by two methods using two different computer programs is at the level of  $\pm 1.0$  eV.

This result well demonstrates the possibilities of the computer programs and numerical calculation methods used here, which provide the absolute accuracy of finding the binding energy in the  $p^{13}\text{C}$  system that equals  $10^{-6}$  MeV, the same as in the  $p^2\text{H}$  channel of  $^3\text{He}$  [60]. Let us note that, for example, it is quite possible to obtain the value of accuracy of  $10^{-8}$  MeV, i.e., 0.01 eV [31] for the energy of the bound state of the  $p^3\text{H}$  on the basis of the same calculation methods [26] and the similar computer programs [3].

## ***11.2 Astrophysical S-factor***

Following to the direct description of the calculation results of the astrophysical  $S$ -factor of the proton radiative capture on  $^{13}\text{C}$ , let us note that earlier we show the possibility of the description of the  $S$ -factor of the proton radiative capture on  $^{12}\text{C}$  on the basis of the MPCM with FSs, which take into account the supermultiplet symmetry of the wave function [31,179]. The results of our phase shift analysis of the  $p^{12}\text{C}$  scattering [89] were used for construction of the intercluster interaction potentials, which describe elastic scattering phase shifts, of the corresponded to these clusters nuclei in free states, correctly. Usually used by us [31,88] classification of orbital states allows one to analyze the structure of intercluster interaction, determine the presence and the number of allowed and forbidden states in intercluster potentials, and so, the number of nodes of the radial WF of the relative cluster motion [120] that is quite unambiguously allows one to define the depth of cluster interaction potentials. On the other hand, the used construction of the intercluster potentials by the resonance phase shifts or by the BS characteristics allows one to determine their width quite unambiguously. Consequently, the interaction potentials of clusters are

constructing more definitely than, for example, the optical model allows to do it.

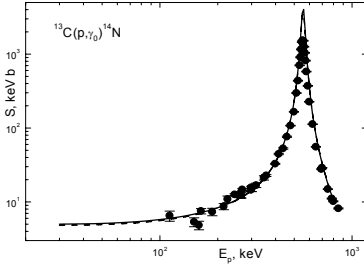


Fig. 11.2. Astrophysical  $S$ -factor of the proton radiative capture on  $^{13}\text{C}$  at low energies. Experimental points (●) are from [186]. Lines: solid – our calculation for the first set of potentials (11.1) and (11.3), dashed line – calculation for the second set of the potentials (11.2) and (11.4).

the  $^3S_1$  resonance scattering state at 0.55 MeV and moments  $J^\pi T = 1^-1$  [174] to the  $^3P_1$  triplet bound state of  $p^{13}\text{C}$  clusters, with the potentials like (11.3) or (11.4). This state corresponds the ground state of  $^{14}\text{N}$  with quantum numbers  $J^\pi T = 1^+0$  in the  $p^{13}\text{C}$  channel, since  $^{13}\text{C}$  has the moments  $J^\pi T = 1/2^-1/2$  [174].

The  $S$ -factor calculations of the radiative proton capture on  $^{13}\text{C}$  to the ground state of  $^{14}\text{N}$  with the above-cited potentials, for the  $^3P_1$  ground state and the  $^3S_1$  resonance scattering wave at the energies below 0.8 MeV, are given in Fig. 11.2 by the solid and dashed lines. The experimental results were taken from work [186], where, evidently, the most recent investigations of this reaction are reported. In the figure - the solid line is the result for combination of the potentials (11.1) and (11.3) and the dashed line for potentials (11.2) and (11.4). The calculation results of  $S$ -factor are very close, since the fact that the phase shifts of two  $^3S_1$  scattering potentials, which are shown in Fig. 11.1, practically coincide.

The calculated astrophysical  $S$ -factor for the first set of the potentials given in (11.1) and (11.3) has practically constant value equals 5.0(1) keV b at the energy range 30÷50 keV. The value 4.8(1) keV b was obtained for the second set of the potentials from (11.2) and (11.4) at the same energies. The fixed up error is obtained by the averaging of the  $S$ -

The available experimental data, of the astrophysical  $S$ -factor of the proton radiative capture on  $^{13}\text{C}$  [34], show the presence of the narrow, with the width about 23(1) keV, resonance at the energy 0.551(1) MeV (l.s.) [174]. It leads to the  $S$ -factor's rise by two-three orders with the full analogy with the  $S$ -factor of the proton capture on  $^{12}\text{C}$  [133]. Such form of the  $S$ -factor can be obtained due to the  $E1$  transition, with the spin change  $\Delta T = 1$ , from

factor value over the above noted energy range.

The known extrapolations of the experimental measurements of the  $S$ -factor to zero energy, and in some works to the energy 25 keV, lead to the values  $7.0 \pm 1.5$  keV b [34],  $6.0 \pm 0.8$  keV b [174,180] and  $7.7 \pm 1.0$  keV b [186]. For transition to the ground state of  $^{14}\text{N}$ , the extrapolations of the different data lead to the next values: 5.25 keV b [186], on the basis of data [186] in work [187] was obtained  $5.16 \pm 0.72$  keV b; the value of  $5.36 \pm 0.71$  keV b was obtained in [188]. The value of 5.5 keV b was suggested in measurements [189]; work [190] gives the value for the  $S$ -factor at zero energy of 5.06 keV b. All these results, in whole, quite agree with the obtained here calculated values.

Note that here, as earlier in the systems  $p^{12}\text{C}$  [89,133] or  $^4\text{H}^{12}\text{C}$  [31,179,191] we did not take into account possible forbidden orbital tableaux of  $^{13}\text{C}$  [22,88]. This situation is connected with the absence of product tables of Young tableaux for number of particles more than 8 and similar [45] and, as it was said earlier, the classification of FSs and ASs for the  $p^{13}\text{C}$  system in  $^{14}\text{N}$  has simply qualitative character. However, as we can see from the given above results, even so qualitative classification of the states according to Young tableaux and supposition about the structure of the total WF of the nucleus allows one to obtain the potentials that lead to the acceptable description of the available experimental data on the astrophysical  $S$ -factor of the proton radiative capture on  $^{13}\text{C}$  at low and astrophysical energies.

If to use the expression (3.4) for parameterization of the  $S$ -factors, then it is possible to describe the solid line in Fig. 11.2 in the range  $30 \div 200$  keV at the average  $\chi^2 = 0.11$  using the parameters  $S_0 = 4.1339$  keV b and  $S_1 = 0.01844$  keV b keV $^{-1}$ . The next values will be obtained  $S_0 = 4.9186$  keV b,  $S_1 = -3.3635 \cdot 10^{-6}$  keV b keV $^{-1}$  and  $S_2 = 8.5159 \cdot 10^{-5}$  keV b keV $^{-2}$  when we will use the quadratic parametrization of the form (3.5). The 10% errors are used for determination  $\chi^2$  of the calculated values of the  $S$ -factor. If for 10 keV we will use the  $S$ -factor value equals 5.0 keV b, then for parameters will be obtained  $S_0 = 4.9301$  keV b,  $S_1 = -3.3635 \cdot 10^{-6}$  keV b keV $^{-1}$  and  $S_2 = 8.4640 \cdot 10^{-5}$  keV b keV $^{-2}$  at  $\chi^2 = 0.0012$  at the range of  $10 \div 200$  keV. At the second method of parameterization we obtain the next:  $S_0 = 5.0$  keV b,  $S_1 = -3.3635 \cdot 10^{-6}$  keV b keV $^{-1}$  and  $S_2 = 8.1472 \cdot 10^{-5}$  keV b keV $^{-2}$  at  $\chi^2 = 0.0078$  at the range of  $10 \div 200$  keV.

## **Conclusion**

Thereby, on the basis of the simple MPCM, deep and narrow  $^3S_1$  potential without FSs, the width of which is determined by the width of the resonance, in the large it is possible to obtain the acceptable description of the astrophysical  $S$ -factor of the proton radiative capture on  $^{13}\text{C}$  to the ground  $^3P_1$  state of  $^{14}\text{N}$ , considered in the cluster  $p^{13}\text{C}$  channel and the description of the scattering phase shift  $^3S_1$  in the resonance energy range 0.55 MeV (l.s.) obtained as a result of the phase shift analysis. That is to say, the completely acceptable results in the description of the astrophysical  $S$ -factor of the radiative proton capture on  $^{13}\text{C}$  at the energy range from 30 to 800 keV are obtained for both considered variants of the  $p^{13}\text{C}$  intercluster potentials. The  $S$ -factor value is practically constant at energies 30–50 keV, thereby determines its value for the extrapolation to zero energy.

The obtained results confirm [31,179] once again that only at the quite accurate determination of the resonance elastic scattering phase shifts from the experimental data on the differential cross section it is possible to parametrize reliable intercluster scattering potentials and to obtain, on their basis, the calculation characteristics of nuclei and nuclear processes. The resonance shape of certain partial phase shift and analysis of the structure of the FSs and ASs at the given orbital moment allows one to determine quite unambiguous parameters of such partial potential. In addition, the potentials of the intercluster potentials of the bound states in certain partial wave taking into account the classification of the FSs according to the known characteristics of the GS of nuclei (binding energy, root-mean-square radius, asymptotic constant) are fixed quite definitely.

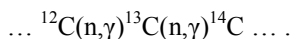


# **12. RADIATIVE PROTON CAPTURE ON $^{14}\text{C}$**

---

## ***Introduction***

Recently, for example in [192], it was supposed that baryon number fluctuations in the early Universe lead to the formation of high-density proton-rich and low-density neutron-rich regions. This might be the result of the nucleosynthesis of elements with mass  $A \geq 12$  in the neutron-rich regions of the early Universe [193,194]. The special interest  $^{14}\text{C}$  nucleus represents [195], which is produced by successive neutron capture on  $^{12}\text{C}$  of the form [196]



$^{14}\text{C}$  has a half-life about 5700 years and is stable on the time scale of the Big-Bang nucleosynthesis. Therefore the synthesis of elements with mass  $\geq 14$  depends on the rate of the neutron, alpha, and proton capture reactions on  $^{14}\text{C}$ . Because the cross section for neutron capture on  $^{14}\text{C}$  at thermal energies is very small ( $\sigma \leq 1 \mu\text{b}$ , [197]) and it is located at the level of  $5\div 15 \mu\text{b}$  in the region of  $100\div 1000 \text{ keV}$ , it is assumed [193] that the alpha capture reaction is dominant. However, the proton capture on  $^{14}\text{C}$  might be of equal importance, because it depends on the proton concentration and density of their distribution in certain regions of the early Universe [195].

Note furthermore that the results of new studies of the reaction  $^{14}\text{C}(p,\gamma)^{15}\text{N}$  in the nonresonance energy range [195] lead to the cross sections that higher on the order and more than the cross sections obtained earlier in [32]. It allows one to obtain higher rate of the  $^{14}\text{C}(p,\gamma)^{15}\text{N}$  reaction at lower temperatures, notably, lower than  $0.3T_9$ , that is essentially rise the role of this reaction for synthesis of heavier elements in the low energy range at the different stages of formation and development our



Universe [193].

Therefore, in continuing to study the processes of radiative capture [31,91,151,152], we will consider the  $p^{14}\text{C} \rightarrow ^{15}\text{N}\gamma$  reaction within the framework of the MPCM at low energies. The potentials of intercluster interactions for scattering processes of the initial particles are constructed based on the reproduction of the elastic scattering phase shifts taking into account their resonance behavior or based on the structure of spectra of resonance states for the final nucleus in the initial channel. The intercluster potentials are constructed based on the description both of the binding energies of these particles in the final nucleus and of certain basic characteristics of these states for the bound state or the ground state of nuclei, formed as a result of the capture reaction in the cluster channel, which coincide with the initial particles. For example, the charged radius and the asymptotic constant are considered in the considered cluster channel [31,91,151,152].

### ***12.1 Classification of Young tableaux and structure of cluster states***

We will suppose that for  $^{14}\text{C}$  (or  $^{14}\text{N}$ ) it is possible to assume the orbital Young tableau in the form  $\{4442\}$  [21,123]; therefore, for the  $p^{14}\text{C}$  system, we have  $\{1\} \times \{4442\} \rightarrow \{5442\} + \{4443\}$  in the frame of  $1p$ -shell [21,123,198]. The first of the obtained tableaux is compatible with orbital moments  $L = 0$ , and 2, and is forbidden because it contains five nucleons in the  $s$ -shell. The second tableau is allowed and is compatible with orbital moments  $L = 1$  [123]. Higher values of the orbital moments are not used in the calculation and are not taken into account here.

Thus, by limiting our consideration to only the lowest partial waves with orbital moment  $L = 0, 1, 2$  it could be said that for the  $n^{14}\text{C}$  system in the potential of the  $^2S_{1/2}$  wave there is only forbidden bound state. For the  $^2P_{1/2}$  wave there is only AS which corresponds to the GS of  $^{15}\text{N}$  with  $J^\pi = 1/2^-$  and is at the binding energy of the  $p^{14}\text{C}$  system of  $-10.2074$  MeV (c.m.) [174]. Let us note that for the ground state of  $^{14}\text{C}$  the moments have the values  $J^\pi, T = 0^+, 1$ , and for  $^{15}\text{N}$  it is known that  $J^\pi, T = 1/2^-, 1/2$  [174]. In this case we have not total tables of products of Young tableaux for system with the particles more than eight [45], which were used by us earlier for the

similar calculations [31,91,151,152,198,199]. Therefore, the result obtained above must be considered only as a qualitative estimation of possible orbital symmetries for BSs, allowed or forbidden in  $^{15}\text{N}$  for the considering  $p^{14}\text{C}$  channel.

Now let us consider the whole spectrum of resonance states in the  $p^{14}\text{C}$  system, i.e., states at positive energies. There are no resonance levels at the energies lower than 1 MeV in the spectra of  $^{15}\text{N}$  for the  $p^{14}\text{C}$  channel, which would have the width value more than 1 keV. Only at 1.5 MeV (l.s.) the very wide resonance at  $J^\pi = 1/2^+$  with the width of 405 keV (c.m.) is observed. Therefore, the  $^2S_{1/2}$  potential with the FS that describes this resonance will be constructed. The potentials of the  $^2P$  scattering waves can be equalized to zero, because they have no resonances and FSs.

Since, the GS of  $^{15}\text{N}$  in the  $p^{14}\text{C}$  channel is the  $^2P_{1/2}$  wave, therefore it is possible to consider the  $E1$  transition from the resonance  $^2S_{1/2}$  scattering wave at 1.5 MeV to the doublet  $^2P_{1/2}$  GS of  $^{15}\text{N}$ :

$$1. \quad ^2S_{1/2} \rightarrow ^2P_{1/2} .$$

The  $M1$  transitions to the GS from the doublet  $^2P$  scattering waves with potentials simply equal to zero are possible in principle, because they have not resonances, bound FSs or ASs:

$$2. \quad \begin{matrix} ^2P_{1/2} \rightarrow ^2P_{1/2} \\ ^2P_{3/2} \rightarrow ^2P_{1/2} \end{matrix} .$$

For the first process one needs to use the same potential in the continuous and discrete spectrum, therefore its cross section at the  $M1$  transition will be equal to zero due to the orthogonality of wave functions.

And also the  $E1$  transition from the  $^2D_{3/2}$  scattering wave with the bound FS to the  $^2P_{1/2}$  GS:

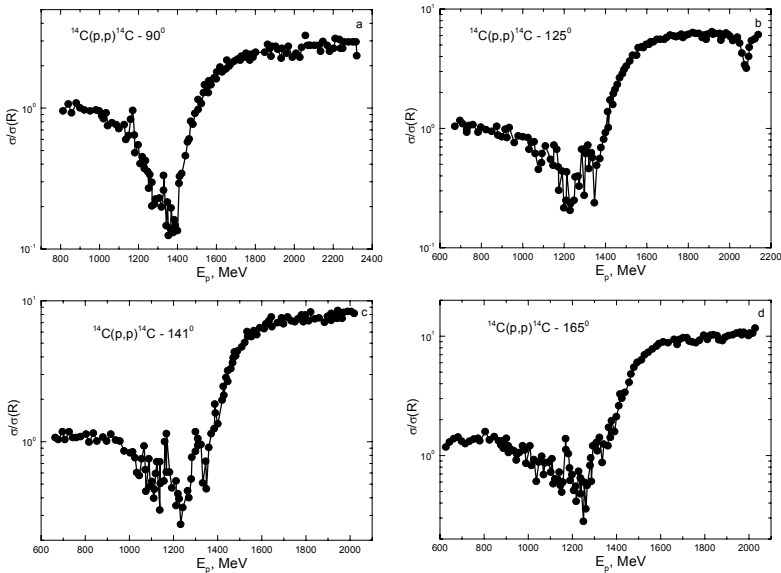
$$3. \quad ^2D_{3/2} \rightarrow ^2P_{1/2} .$$

However, as it was obtained later as a result of our calculations, the transition 3 and the second reaction from 2 lead to the very small as compared

with the 1<sup>st</sup> process total capture cross sections. Therefore, furthermore we study only one reaction No.1 with the proton capture on  $^{14}\text{C}$  from the  $^2S_{1/2}$  wave to the  $^2P_{1/2}$  GS of  $^{15}\text{N}$ , which is considered in the  $p^{14}\text{C}$  channel.

### 12.2 Phase shift analysis of the $p^{14}\text{C}$ elastic scattering

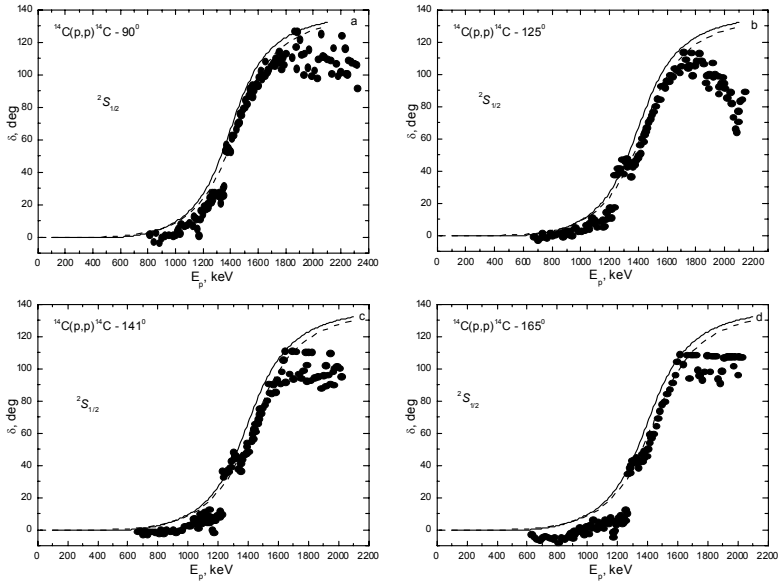
Let us consider furthermore the possibility to carry out the phase shift analysis for cross sections of the  $p^{14}\text{C}$  elastic scattering. The excitation functions of the  $p^{14}\text{C}$  elastic scattering from [200], measured at  $90^\circ$ ,  $125^\circ$ ,  $141^\circ$  and  $165^\circ$  in the energy range from 0.6 to 2.3 MeV (l.s.), are shown in Figs. 12.1 by dots. These data are used by us further for carrying out of the phase shift analysis and extracting the resonance form of the  $^2S_{1/2}$  scattering phase at 1.5 MeV. The results of the present analysis are shown in Figs. 12.2 by dots, and the solid lines in Fig. 12.1 show cross sections calculated with the obtained scattering phase shifts [201].



Figs. 12.1. The excitation functions in the elastic  $p^{14}\text{C}$  scattering in the range of the  $^2S_{1/2}$  resonance [200]. The solid line – their approximation on the basis of the obtained scattering phase shifts.

About 120 first points, cited in work [200], in the stated above energy

range were used in this analysis. In addition, it was obtained that for description of the cross sections in the excitation functions, at least at the energies up to  $2.2 \div 2.3$  MeV, there is no need to take into account  $^2P$  or  $^2D$  scattering waves. Since only one point in the cross sections of excitation functions is considered for each energy and angle, therefore the value of  $\chi^2$  at all energies and angles usually lays at the level  $10^{-2} \div 10^{-10}$  and taking into account another partial scattering phase shifts already does not lead to its decrease.



Figs. 12.2. The  $^2S_{1/2}$  elastic phase shift of the  $p^{14}\text{C}$  scattering at low energies, obtained on the basis of the excitation functions, shown in Figs. 12.1. Points – results of our phase shift analysis, carried out on the basis of data from [200], lines – calculation of the phase shift with the potentials given in the text.

The resonance energy, as it is seen in Fig. 12.2, obtained from the excitation function at  $90^\circ$  is at the interval of  $1535 \div 1562$  keV for which the phase shift value lays within limits of  $87^\circ \div 93^\circ$  with the value of  $90^\circ$  at of 1554 keV. The resonance energy obtained from the excitation function at  $125^\circ$  is at the interval of  $1551 \div 1575$  keV for which the phase shift value lays within limits of  $84^\circ \div 93^\circ$ . The resonance energy obtained from the excitation function at  $141^\circ$  is at the interval of  $1534 \div 1611$  keV for which the phase

shift value lays within limits of  $84^\circ \div 90^\circ$  with the value of  $90^\circ$  at 1534, 1564 and 1611 keV. The resonance energy obtained from the excitation function at  $165^\circ$  is at the interval of 1544÷1563 keV for which the phase shift value lays within limits of  $87^\circ \div 91^\circ$ . For so noticeable scatter of values, it can be said only that the resonance phase shift value equals  $90^\circ$  lays within limits of 1534÷1611 that is, in general, agree with data [33], where the resonance energy value of 1509 keV is given.

Let us note that work [200] mentions that the detailed analysis of the resonances, including 1.5 MeV, was not carried out, because it was done earlier in works [202] on the basis of the proton capture reaction on  $^{14}\text{C}$ . Here, as one can see from the results of the phase shift analysis, the resonance energy at 1.5 MeV slightly overestimated relatively results [202]. However, as it was seen in Fig. 12.1, the data spread on cross sections in excitation functions is too large for clear conclusion about the energy of resonance.

Apparently, the additional and more modern measurements of the elastic scattering cross sections are required, in order to on the basis of these data to perform more unambiguous conclusions about the resonance energy in the  $^2S_{1/2}$  phase shift at 1.5 MeV. The difference between obtained here and in work [202] energies of this resonance of 63 keV does not play principle role in the large, because it is clear were it is located. However, this difference will affect on the description of the experimental data of the radiative capture cross section.

### **12.3 Interaction potentials and total capture cross sections**

In the previous paragraph the phase shift analysis of the elastic  $p^{14}\text{C}$  scattering at astrophysical energies was carried out, its results are given in work [201], and now turn to the analysis of the obtained scattering potentials and determine the GS potential of  $^{15}\text{N}$  in the  $p^{14}\text{C}$  channel.

For description of the obtained  $^2S_{1/2}$  scattering phase in the phase shift analysis it is possible to use simple Gaussian potential of the form (2.8) with the bound FS and parameters

$$V_0 = -5037.0 \text{ MeV}, \quad \alpha = 12.0 \text{ fm}^{-2}, \quad (12.1)$$

which lead to the scattering phase shifts with the resonance at 1500 keV (l.s.) and with the width of 530 keV (c.m.) that is in a good agreement with the available experimental data [174]. In this work in Table 15.11 the value of 1509(4) keV (l.s.) with the total width  $404.9 \pm 6.3$  keV (c.m.) and with the proton width  $400.9 \pm 6.3$  keV. The potential parameters (12.1) were chosen so that generally correct describe the resonance data just from work [174], which were obtained earlier in works [202].

The phase shift of this potential is shown in Figs. 12.2 by the solid lines and at the resonance energy reaches the value of 1500 keV at  $90(1)^\circ$ . The energy behavior of the scattering phase shift of this potential correctly describes obtained in the phase shift analysis scattering phases in whole, taking into account the shift of the resonance energy approximately at  $60\text{--}70$  keV relative to results [174,202]. The calculated phase shift line for this potential is parallel to points, obtained in our phase shift analysis, for all four scattering angles.

For more accurate description of the obtained data in the phase shift analysis the next potential is needed

$$V_0 = -5035.5 \text{ MeV}, \quad \alpha = 12.0 \text{ fm}^{-2}. \quad (12.2)$$

It leads to the resonance energy of 1550 keV, its width of 575 keV, and the calculation results of the  $^2S_{1/2}$  phase shift are shown in all Figs.12.2 by the dashed line. As one can see this line appreciably better reproduce results of the carried out here phase shift analysis.

As it was said before, all potentials of the  $P$  scattering waves can be equalized to zero, because they does not contain FSs. Such potentials will lead to the phase shifts that also equal to zero. There are two resonance levels in spectra of  $^{15}\text{N}$ , which can be referred to  $P$  waves in the  $p^{14}\text{C}$  channel. Notably, one of them lays approximately at 0.53 MeV and has the moment  $J^\pi = 3/2^-$ . The second lies approximately at the energy 1.16 MeV and has  $J^\pi = 1/2^-$ . But their widths of 0.2 keV and  $8(3)$  keV correspondingly, are so small (see Table 15.11 in work [174]) that it is impossible to construct corresponding potentials according these data [201].

It should be noted over again that the potential of the  $^2S_{1/2}$  wave is constructed completely unambiguously, if the number of FSs is given (in

this case, it is equal to unit), according to the known energy of the resonance level in spectra of any nucleus [198] and its width. In other words, it is not possible to find another combination of the parameters  $V$  and  $\alpha$ , which could be possible to describe the resonance energy of level and its width correctly. The depth of such potential unambiguously determines the resonance location, i.e., resonance energy of the level, and its width  $\gamma$  specifies the certain width of this resonance state [60,151,198], which has to correspond to experimental observable values [174].

In this case, for the correct reproduction of the resonance width at 1509 keV, it will be necessary to decrease the width of potential increasing the  $\gamma$  parameter. Only in this case it is possible to obtain more correct resonance width of the order of 400 keV. However, as it will be shown furthermore, the experimental data on the proton radiative capture on  $^{14}\text{C}$  at energy region of 1÷2 MeV are simply absent in the present time. Therefore, there is no point to search more accurate potential in the present time for the correct description of the width of such resonance.

For the  $^2P_{1/2}$  GS potential of  $^{15}\text{N}$  without FSs in the cluster  $p^{14}\text{C}$  channel the following parameters were found

$$V_0 = -221.529718 \text{ MeV}, \quad \alpha = 0.6 \text{ fm}^{-2}. \quad (12.3)$$

It allows to find the value of  $R_m = 2.52 \text{ fm}$  for the mass radius, the value of  $R_{ch} = 2.47 \text{ fm}$  for the charge radius, the binding energy of -10.207400 MeV at the accuracy of the finite-difference method [154] of  $10^{-6} \text{ MeV}$ . The phase shift of such potential decreases smoothly and at 2 MeV approximately equals  $179^\circ$ , and for the asymptotic constant in the dimensionless form the value of 1.80(1) was obtained at the distance interval 3÷10 fm. The mentioned AC error is obtained by its averaging over the given distance interval. Note once more that we failed in finding AC data in this channel, obtained in other works by independent methods.

The value of 2.56(5) fm [174] was used for radius of  $^{14}\text{C}$ , for radius of  $^{15}\text{N}$  it is known the value of 2.612(9) fm [174], the proton radius is equal to 0.8775(51) [36]. In the given calculations the next mass value was used -  $m(^{14}\text{C}) = 14.003242 \text{ amu}$  [137], and for the mass of  $^{15}\text{N}$  the value  $m(^{15}\text{N}) = 15.000108 \text{ amu}$  [137] was used.

Going to the description of the obtained results, let us note that the experimental data for total cross section of the proton radiative capture on  $^{14}\text{C}$  to the GS of  $^{15}\text{N}$  or for the astrophysical  $S$ -factor were measured in work [195] for the energy range 260-740 keV – these results are shown by squares in Figs. 12.3 and 12.4 and in numerical form were taken by us from the data base [137]. There are no other measurements of the total cross sections of this reaction. For the description of the available data the capture cross section to the GS with the potential (12.3) to the  $E1$  transition from the resonance  $^2S$  scattering wave with potential (12.1), i.e., described above process No.1, was considered. Other transitions give a small contribution, and, since there is experimental data in the resonance region they are not considered.

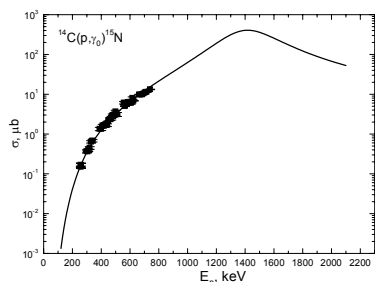


Fig. 12.3. The total cross section of the proton capture on  $^{14}\text{C}$  to the GS of  $^{15}\text{N}$ . The experimental data are from work [195].

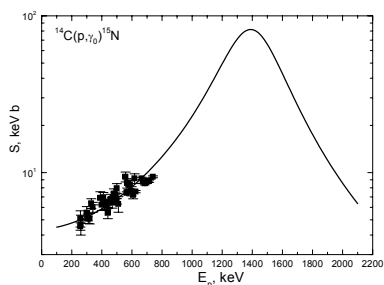


Fig. 12.4. The astrophysical  $S$ -factor of the radiative proton capture on  $^{14}\text{C}$  to the GS of  $^{15}\text{N}$ . The experimental data are from work [195].

The calculation results of the total cross section and the astrophysical  $S$ -factor are shown in Figs. 12.3 and 12.4 by the solid lines, respectively. They practically completely describe the experimental data at all measured in [195] energies. Meanwhile, it is good to see that in Fig. 12.4 the calculated line is in the band of experimental errors and ambiguities of available measurements from [195]. The value of the calculated  $S$ -factor remains almost constant and equals 4.5(1) keV b in the region of low energies, notably 100-140 keV. Apparently, just that very value can be considered as the  $S$ -factor at zero energy for the considered here proton radiative capture reaction on  $^{14}\text{C}$ .

It should be noted here that if scattering potential (12.1) was constructed exclusively based on the characteristics of the resonance at 1.5



MeV, then because of the absence of the AC value in the  $p^{14}\text{C}$  channel the GS potential (12.3) is determined so that to describe available experimental data of the total capture cross sections at low energies [195] to the best advantage. However, this potential leads to the quite reasonable radius value of  $^{15}\text{N}$ , and the AC value obtained with it could be used further for comparison with the results of other works. Moreover, the studies of such capture reactions in the used model allow one to extract the AC value, though its accuracy hardly exceeds 10-20%. Although, the accuracy of obtaining such constant from other experimental data by the independent methods, evidently, also not more than 10% [185] – this error usually caused by the average error of such experiments.

The calculated values of the  $S$ -factor at the resonance energy also can be used in future for comparison with modern measurements of this reaction. But the measurement spread on the  $S$ -factor [195] and the experimental errors of these measurements [195], for example, in the considered energy range reach 20-30%. Therefore, the calculation accuracy of the maximum  $S$ -factor value, which in these calculations equals 81-82 keV b at  $E_p=1390\text{keV}$ , will be approximately the same, although the phase shift resonance of potential (12.1) is at 1500 keV.

### **Conclusion**

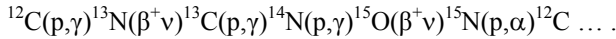
Thereby, the measured cross sections or the astrophysical  $S$ -factor of the proton capture reaction on  $^{14}\text{C}$  are succeeded to correctly describe in the frame of the MPCM on the basis only of the  $E1$  transition from the resonance  $^2S_{1/2}$  scattering wave with FS to the  $^2P_{1/2}$  GS without FS of  $^{15}\text{N}$ , considered in the two-body  $p^{14}\text{C}$  channel. The potentials of the intercluster interactions in the continuous spectrum are constructed on the basis of the description of the scattering phase shifts at astrophysical energies, and BSs on the basis of reproduction by them main characteristics of such states – in this case it is binding energy and charge radius. The carrying out in future more detailed measurements of total cross sections of this reaction, especially, in the resonance region at 1.5 MeV allows one to draw, apparently, more concrete conclusions about the quality of description of the considered cross sections of the reaction of the proton capture on  $^{14}\text{C}$  in the framework of the MPCM [203].

# **13. RADIATIVE PROTON CAPTURE ON $^{15}\text{N}$**

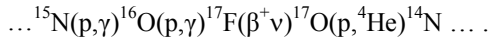
---

## ***Introduction***

Continuing the study of the radiative proton capture reactions on light atomic nuclei, which are the part of different thermonuclear processes [1], let us stop on the  $p^{15}\text{N} \rightarrow ^{16}\text{O}\gamma$  capture reaction at astrophysical energies. This process is a part of basic chain of thermonuclear reactions of the CNO cycle [1], which determine the formation of the Sun and stars at early stages of their evolution [1,178]



This chain has alternative reaction channel, which begins from the last reaction of the proton interaction with  $^{15}\text{N}$  [204]



Furthermore, the calculations of the total cross sections of this reaction in the frame of the MPCM with FSs and classification of the orbital states according to Young tableaux, given in paragraph 2.5. The principles given in paragraph 2.8 are used for the construction of the interaction potentials.

### ***13.1 Interaction potentials and structure of states***

We would remind the classification of cluster states for the  $p^{15}\text{N}$  system that was in detail considered [n [205]. In this case we have  $\{1\} \times \{4443\} \rightarrow \{5443\} + \{4444\}$  [21]. The first of the obtained tableaux compatible with the orbital moments  $L = 1, 3$  and is forbidden as it contains five cells in the first row, and the second tableau is allowed and compatible with the orbital moment  $L = 0$  [123]. Thereby, if to limit by the consideration of only lowest

partial waves with orbital moment, it could be said that there is bound forbidden state in the  $P$  wave potential, and the  $S$  wave has no forbidden state. Exactly this structure of BSs, FS, or ASs will be used further for construction of the intercluster interaction potentials in continuous and discrete spectrum.

Examine now the presence of the resonance states in the considered cluster system of  $^{16}\text{O}$ , which are at the positive energies, i.e., above the  $p^{15}\text{N}$  channel threshold. In this system there are two resonances at energies up to 1.1 MeV, which can be compared to  $^3S_1$  wave of the  $p^{15}\text{N}$  elastic scattering, and there are three such resonances:

1. The first resonance is at the energy of 335(4) keV with the total width of 110(4) keV (l.s.) and has the moment  $J^\pi, T = 1^-, 0$  (see Table 16.22 in [206]) – it can be caused by the triplet  $^3S_1$  scattering state.

2. The second resonance is at the energy of 710(7) keV with the width of 40(40) keV (l.s.) and has the moment  $J^\pi, T = 0^-, 1$ . It can be caused by the  $^1S_0$  scattering state. However, one doesn't evidently observe the resonance peak in the capture cross section.

3. The third resonance is at the energy of 1028(10) keV with the total width of 140(10) keV (l.s.) and has the moment  $J^\pi, T = 1^-, 1$  (see Table 16.22 in [206]) – it also can be caused by the triplet  $^3S_1$  scattering state.

For two necessary resonance levels we have the next energies in the center-of-mass system:

1. The first resonance is at the energy of 312(2) keV with the width of 91(6) keV – it corresponds to the ES of  $^{16}\text{O}$  at the energy of 12.440(2) MeV.

2. The third resonance is at the energy of 962(8) keV with the width of 130(5) keV – it corresponds to the ES of  $^{16}\text{O}$  at the energy of 13.090(8) MeV (see Table 16.13 in [206]).

We do not consider the second resonance, because, as it was mentioned, it does not give obvious contribution to the total radiative capture cross sections. There are two resonance at energies 430 keV and 897 keV with moments  $J^\pi, T = 2^-, 0$  and  $J^\pi, T = 2^-, 1$ , respectively, which

can be compared to the  $^3D_2$  scattering waves. However, (see Table 16.22 in work [206]) their total widths have the value low than 1.5 keV and such resonances we will not consider also. In addition, there is the resonance with  $J = 2^+$  [206] at the energy 1.050(150) MeV in spectrum of  $^{16}\text{O}$ , which can be compare with the  $^3P_2$  level, however there is not the value of the width for it. The next resonance with  $J = 1^+$  and the width of 68(3) keV, which can be compare with the  $^3P_1$  wave lies above 1.5 MeV [206] and we will not consider it also.

Consequently, at first we considered the  $E1$  transitions for description of the total cross section of the proton radiative capture on  $^{15}\text{N}$  to the GS, as in previous works [31,150-152]. We have considered the energy range up to 1.5 MeV and transition from the resonance  $^3S_1$  scattering wave without bound FSs to the triplet  $^3P_0$  GS of the  $p^{15}\text{N}$  system in  $^{16}\text{O}$  with one bound FS:

$$1. \ ^3S_1 \rightarrow ^3P_0 .$$

We would remind you that the total moment of  $^{15}\text{N}$  equals  $J^\pi, T = 1/2^-, 1/2$  [174], and for  $^{16}\text{O}$  it equals  $J^\pi, T = 0^+, 0$  [206].

At carrying out the calculations of the total cross sections of the radiative capture the nuclear part of the intercluster potential of the  $p^{15}\text{N}$  interaction is presented in the Gaussian form, as usual [31,150-152]. Immediately note that for the potential of the resonance  $^3S_1$  scattering wave without FSs two potentials were obtained, which correspond to two resonances of different width at different energies of 335 keV and 1028 keV. The parameters of the first potential

$$V_{S1} = -1.0857 \text{ MeV}, \quad \alpha_{S1} = 0.003 \text{ fm}^{-2} \quad (13.1)$$

lead to the resonance energy of 335.0(1) keV and its width of 138(1) keV (l.s.), and the scattering phase shift is shown in Fig. 13.1 by the solid line. The relative accuracy of calculation of the  $^3S_1$  scattering phase in these calculations is equal to  $10^{-3}$  or 0.1% and for the resonance energy of 335 keV this potential leads to the value of the phase shift of 90.0(1)°.

The next parameters were obtained for the second potential of the  $^3S_1$  wave

$$V_{S2} = -105.059 \text{ MeV}, \quad \alpha_{S2} = 1.0 \text{ fm}^{-2}. \quad (13.2)$$

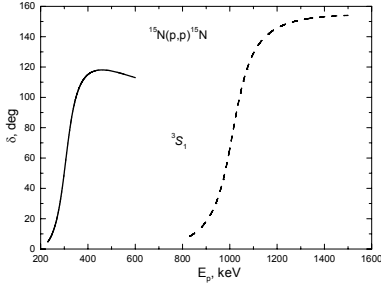


Fig. 13.1. The phase shifts of the  $p^{15}\text{N}$  elastic scattering in the  $^3S_1$  wave

This potential leads to the resonance at 1028.0(5) keV and its width is equal to 140(1) keV (l.s.), and the scattering phase shift is shown in Fig. 13.1 by the dashed line – for resonance energy this potential also leads to the phase shift value of 90.0(1)°.

Here, we must draw attention [31,150-152] that the potential with the given number of BSs is constructed completely unambiguously using the energy values of the resonance level in spectra of  $^{16}\text{O}$  and its width. It is impossible to find other parameters  $V_0$  and  $\alpha$ , which can be able correctly reproduce the level resonance energy and its width, if the specified number of BSs, FSs or ASs are given, which in this case equals zero. The depth of this potential unambiguously determines the location of the resonance, i.e., the level resonance energy  $E_r$ , and its width gives specific width  $\Gamma_r$  of this resonance state. The error of parameters of such potential is determined by the measurement error of the level  $E_r$  and its width  $\Gamma_r$  [31,150-152].

However, we must note that it is impossible, for the present, to construct the unified  $^3S_1$  potential, which would contain two, noted above, resonances with different energies and widths. Therefore, the calculated total cross section for these resonances will consist of two parts – the first with the potential (13.1) and the second for the interaction (13.2), also both of these parts are the same  $E1$  transition from the  $^3S_1$  scattering wave to the  $^3P_0$  GS of  $^{16}\text{O}$ .

There are no resonance levels with  $J = 0^+, 1^+, 2^+$  and widths more than 10 keV (see Table 16.22 in work [206]) in the spectra of the elastic  $p^{15}\text{N}$  scattering at the energies up to 1.0 MeV. Therefore, it is possible to use the parameter values for the potentials of the  $^3P$  scattering waves with one

bound FS based on the assumption of their nonresonance nature and that in the considered energy range, i.e., up to 1.0 MeV, their phase shifts are equal to zero. The next parameters were obtained for such potentials

$$V_p = -14.4 \text{ MeV}, \quad \alpha_p = 0.025 \text{ fm}^{-2}. \quad (13.3)$$

The calculation of the  $^3P$  phase shifts with this potential at the energy up to 1.5 MeV leads to their values from  $180^\circ$  at 0.0 MeV to  $179^\circ$  at 1.5 MeV.

Furthermore, we will construct the potential with bound FS of the  $^3P_0$  state, which has to correctly reproduce the binding energy of the GS of  $^{16}\text{O}$  with  $J^\pi T = 0^+0$  in the  $p^{15}\text{N}$  channel at -12.1276 MeV [206] and reasonably describe the mean square radius of  $^{16}\text{O}$ , which experimental value equals 2.710(15) fm [206], when the experimental radius of  $^{15}\text{N}$  equals 2.612(9) fm [174]. Consequently, the next parameters for the potential of the GS of  $^{16}\text{O}$  in the  $p^{15}\text{N}$  channel were obtained

$$V_{\text{g.s.}} = -1057.99470 \text{ MeV}, \quad \alpha_{\text{g.s.}} = 1.2 \text{ fm}^{-2}. \quad (13.4)$$

The potential leads to the binding energy of -12.12760 MeV at the FDM accuracy of  $10^{-5}$  MeV, the mean square charged radius of 2.52 fm and the mass radius of 2.57 fm. The value of 1.94(1) at the range of 2÷10 fm was obtained for the AC, written in the dimensionless form [38]. The error of the constant is determined by its averaging over the noted above range interval. The phase shift of this potential is in the range from  $180^\circ$  to  $179^\circ$  at the energy up to 1.5 MeV.

The value of  $192(26) \text{ fm}^{-1}$  for this AC is given in [207] that after division on the spectrofactor value of 2.1 and the antisymmetrization coefficient of 16 [208] gives  $5.71(77) \text{ fm}^{-1}$  or  $2.39(88) \text{ fm}^{-1/2}$ . Its recalculation to the dimensionless value at  $\sqrt{2k_0} = 1.22$  gives 1.96(72) – this value is in a good agreement with the constant obtained above. The recalculation of the AC to the dimensionless value is needed because another definition of the AC was used in these works, which differs from using here by factor  $\sqrt{2k_0}$ . In addition, the AC from [207] contains the spectrofactor equals, evidently, 2.1 and the antisymmetrization coefficient,

obtained in review [40].

Give here the second variant of the GS potential with the similar parameters, but slightly another AC

$$V_{\text{g.s.}} = 976.85193 \text{ MeV}, \quad \alpha_{\text{g.s.}} = 1.1 \text{ fm}^{-2}. \quad (13.5)$$

It leads to the same binding energy, does not change the values of mean square charged and mass radii, and for the AC in the dimensionless form [38] at the range of 2÷9 fm the value of 2.05(1) was obtained. The phase shift of this potential at the energy up to 1.5 MeV lies at the same interval of values as for the potential (13.4).

Earlier it was shown once and again in [31,150-152,179,198] that the additional control of calculation of the binding energy of GS or BS on the basis of the variational method (VM) [154] leads to the results coinciding with the FDM with the given determination accuracy of the binding energy of two-cluster system, therefore here we already not used the VM for the verification of this binding energy.

### **13.2 The total proton capture cross sections on $^{15}\text{N}$**

Going to the direct consideration of the results of the  $M1$  and the  $E1$  transitions to the GS of  $^{16}\text{O}$ , note that we succeeded [209-211] to find the experimental data for the total cross section of the process of the proton capture on the  $^{15}\text{N}$  in the energy range from 80 keV up to 1.5 MeV, which will be considered furthermore – these results are shown in Figs. 13.2a,b. The first part of the cross section of the  $E1$  transition  $^3S_1 \rightarrow ^3P_0$  to the GS, calculated with the potentials of the scattering state (13.1) and the GS (13.4), is shown in Fig. 13.2a by the dashed line. The dotted line shows the cross section of the  $E1$  transition for the scattering potential (13.1) and the GS (13.4).

In addition, we considered the  $M1$  transition of the form:

$$2. \quad ^3P_1 \rightarrow ^3P_0$$

with the potentials of the scattering state (13.3) and the GS (13.4). The

results of these calculations are shown in Fig. 13.2a by the dot-dashed line and the total summed cross section for the referred above capture processes to the ground state is shown by the solid line. The  $S$ -factor is equal to  $39.50(5)$  keV b and practically constant at the energy range of  $50\div60$  keV.

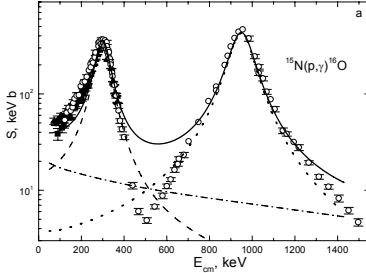


Fig. 13.2a. The astrophysical  $S$ -factor of the proton radiative capture on  $^{15}\text{N}$  to the GS. The experimental data:  $\blacktriangle$  – from [209],  $\blacksquare$  – from [210],  $\circ$  – from [211]. Lines – the calculation of the total cross sections for transitions to the GS (13.4).

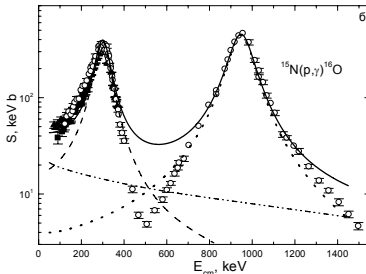


Fig. 13.2b. The same as in Fig. 13.2a. Lines – the calculation of the total cross sections for transitions to the GS (13.5).

The similar calculations are given in Fig. 13.2b for the GS potential (13.5); these results differ from the previous one only in the low energy range. This potential of the GS leads to the  $S$ -factor values of  $43.35(5)$  keV b at the energy range of  $50\div60$  keV. The values of the  $S$ -factor at these energies, owing to their weak changes, can be considered, evidently, as the  $S(0)$ -factor for zero energy.

It can be noted that if the parameters of the resonance  $^3S_1$  potential are fixed according to the resonance of phase shift relatively unambiguously and for the bound state they are chosen on the basis of the description of the bound state characteristics, therefore for the  $^3P_1$  potential (13.3) with the FS which leads to zero scattering phases, another

parameter values are possible. However, while there are not results on the phase shift analysis on the elastic scattering in the  $p^{15}\text{N}$  system, we can not do unambiguous conclusions about the shape and depth of such scattering potential.

In addition, the medium-energy region, where the minimum of cross sections at 500 keV is observed, is described badly. It is connected with the inefficient abrupt decrease of the cross section after the first resonance at the energy above 400 keV (the dashed line in Figs. 13.2a,b) and with the inefficient abrupt rising of it before the second resonance at the energies up to  $600\div650$  keV (the dotted line in Figs. 13.2a,b). It is also connected with the



value of the cross section for the  $M1$  transition, which is, for this energy region, more than minimal experimental value of 4.9 keV b at 507 keV [211]. And here, evidently, the results of the phase shift analysis of angular distribution of the elastic  $p^{15}\text{N}$  scattering are needed for the construction of the correct potentials of two resonances in the  $^3S_1$  wave.

### **Conclusion**

Thereby, the intercluster potentials of the bound state, constructed on the basis of the quite obvious requirements for description of the binding energy, the mean square radii of  $^{16}\text{O}$  and the AC values in the  $p^{15}\text{N}$  channel, and also the scattering potentials describing the resonances allow one to reproduce generally correctly the available experimental data for the total cross sections of the proton radiative capture on  $^{15}\text{N}$  at low energies [209-211]. Meanwhile, all  $p^{15}\text{N}$  potentials using here are constructed on the basis of the given above classification of the FSs and the ASs according to Young tableaux [205].

However, it is difficult to do defined and final conclusions if there are no results on the phase shift analysis, carried out on the basis of differential cross sections of the  $p^{15}\text{N}$  elastic scattering. Such data are needed, approximately, in the range of 0.3÷1.5 MeV, however the results at the energies lower 1 MeV are absent up to now. Meanwhile, the available data on the differential cross sections [212] were obtained in the form of excitation function only at two angles and only above the energy of 0.97 MeV. Therefore, furthermore it is desirable to carry out the detailed measurement of the differential cross sections of the elastic scattering in the energy range from 0.1÷0.3 MeV up to 1.3÷1.5 MeV. Such data have to contain angular distributions in the range of two resonances at 335 keV and 1028 keV [206] at angles from 30° to 170°.

# **14. ASTROPHYSICAL $S$ -FACTORS OF THE RADIATIVE CAPTURE IN THE $^3\text{He}^4\text{He}$ , $^3\text{H}^4\text{He}$ AND $^2\text{H}^4\text{He}$ SYSTEMS**

---



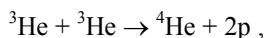
---

## ***Introduction***

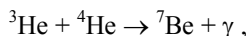
In this section the astrophysical  $S$ -factors of radiative capture processes of  $^4\text{He}(^3\text{He}, \gamma)^7\text{Be}$  down to 15 keV,  $^4\text{He}(^3\text{H}, \gamma)^7\text{Li}$  and  $^4\text{He}(^2\text{H}, \gamma)^6\text{Li}$  reactions down to 5 keV were considered in the frame of the modified potential cluster model with classification of orbital states according to Young tableaux [213] and refined potential parameters of the ground states for  $^7\text{Be}$ ,  $^7\text{Li}$  and  $^6\text{Li}$  in the  $^3\text{He}^4\text{He}$ ,  $^3\text{H}^4\text{He}$  and  $^2\text{H}^4\text{He}$  cluster models with forbidden states.

The radiative capture reaction  $^4\text{He}(^3\text{He}, \gamma)^7\text{Be}$  at superlow energies has a undeniable interest for nuclear astrophysics, since it is included in the proton-proton fusion chain, and new experimental data on the astrophysical  $S$ -factors of this process at energies as low as 90 keV and data on the radiative capture reaction  $^4\text{He}(^3\text{H}, \gamma)^7\text{Li}$  down to 50 keV appeared recently.

The proton-proton chain may be completed by the following process with a probability of 69% [118] (according to [214] this probability equals 86%)



or the reaction, considered here, involving the prestellar  $^4\text{He}$ , (see, for example, [8])



the probability of which is 31% [118] (according to [214] the probability of

this channel equals approximately 14%). Moreover, radiative capture reactions  ${}^4\text{He}({}^3\text{He}, \gamma){}^7\text{Be}$  and  ${}^4\text{He}({}^2\text{H}, \gamma){}^6\text{Li}$  may have played a certain role in prestellar nucleosynthesis after the Big Bang, when the temperature of the Universe decreased to the value of  $0.3T_9$  [215] ( $T_9 = 10^9$  K).

### **14.1 Potentials and scattering phase shifts**

It was shown in [213] that orbital states in the  ${}^3\text{He}^4\text{He}$ ,  ${}^3\text{H}^4\text{He}$  and  ${}^2\text{H}^4\text{He}$  systems for  ${}^7\text{Be}$ ,  ${}^7\text{Li}$  and  ${}^6\text{Li}$  nuclei, unlike lighter cluster systems as  $\text{p}^2\text{H}$  or  $\text{p}^3\text{H}$  [60,92,120], are pure according to Young tableaux. Therefore, nuclear potentials of form (2.8) with the parameters obtained based on elastic scattering phase shifts and a spherical Coulomb term [46] can be directly used for examination of the characteristics of the bound states of these nuclei in the potential cluster model. Agreement of the obtained results with experimental data depends mainly on the degree of clusterization of such nuclei in the considered cluster channels. Since the clusterization probability for these nuclei is relatively high [213], it should be expected that the results of calculations should on the whole agree with the available experimental data.

The parameters of the Gaussian interaction potentials for cluster states in  ${}^7\text{Li}$ ,  ${}^7\text{Be}$  and  ${}^6\text{Li}$  nuclei that are pure according to Young tableaux obtained earlier in [216,217] are given in Table 14.1, and the interactions in the  ${}^3\text{H}^4\text{He}$  and  ${}^3\text{He}^4\text{He}$  systems differed by the Coulomb term only. Table 14.1 also presents the energies of bound forbidden states for the  ${}^2\text{H}^4\text{He}$  channel of  ${}^6\text{Li}$  and the  ${}^3\text{H}^4\text{He}$  system, which slightly differ from the corresponding values for  ${}^3\text{He}^4\text{He}$  interactions. In the  $S$  wave for the  ${}^3\text{He}^4\text{He}$  and  ${}^3\text{H}^4\text{He}$  systems these bound states correspond to forbidden Young tableaux  $\{7\}$  and  $\{52\}$ , in the  $P$  wave of tableau  $\{61\}$  for an allowed bound state with the Young tableau  $\{43\}$ , and the  $D$  wave has the forbidden state with tableau  $\{52\}$  [22]. For the  ${}^2\text{H}^4\text{He}$  system, the  $S$  wave contains the forbidden bound state with tableau  $\{6\}$  and allowed bound state with  $\{42\}$ , and in the  $P$  wave the state with tableau  $\{51\}$  is forbidden [22].

The quality of description of scattering phase shifts is demonstrated in Figs. 14.1, 14.2 and 14.3a,b,c; these figures also show experimental data from [218,219] for the  ${}^3\text{He}^4\text{He}$ -, [219,220] for the  ${}^3\text{H}^4\text{He}$ -, and [221-224] for the  ${}^2\text{H}^4\text{He}$  elastic scattering. The shown errors are due to inaccuracies of

determination of phase shifts using figures from [218,219].

**Table 14.1. Potential parameters of the elastic  ${}^3\text{H}^4\text{He}$ ,  ${}^3\text{He}^4\text{He}$  and  ${}^2\text{He}^4\text{He}$  scattering and energies of corresponding forbidden bound states [216,217]. The potential width parameter for the  ${}^3\text{H}^4\text{He}$  and  ${}^3\text{He}^4\text{He}$  systems is  $\alpha = 0.15747 \text{ fm}^{-2}$ , and the Coulomb radius  $R_{\text{Coul}} = 3.095 \text{ fm}$ .  $R_{\text{Coul}} = 0$  for potentials of the  ${}^2\text{He}^4\text{He}$  system**

${}^7\text{Li}$ and ${}^7\text{Be}$			${}^6\text{Li}$			
$2S+1L_J$	$V_0$ (MeV)	$E_{FS}$ ( ${}^7\text{Li}$ ) (MeV)	$2S+1L_J$	$V_0$ (MeV)	$\alpha$ ( $\text{fm}^{-2}$ )	$E_{FS}$ (MeV)
${}^2S_{1/2}$	-67.5	-36.0, -7.4	${}^3S_1$	-76.12	0.2	-33.2
${}^2P_{1/2}$	-81.92	-27.5	${}^3P_0$	-68.0	0.22	-7.0
${}^2P_{3/2}$	-83.83	-28.4	${}^3P_1$	-79.0	0.22	-11.7
${}^2D_{3/2}$	-66.0	-2.9	${}^3P_2$	-85.0	0.22	-14.5
${}^2D_{5/2}$	-69.0	-4.1	${}^3D_1$	-63.0	0.19	—
				(-45.0)	(0.15)	
$F_{5/2}$	-75.9	—	${}^3D_2$	-69.0	0.19	—
				(-52.0)	(0.15)	
$F_{7/2}$	-84.8	—	${}^3D_3$	-80.88	0.19	—

For the  ${}^3\text{He}^4\text{He}$  and  ${}^3\text{H}^4\text{He}$  systems, only the  $S$  scattering phase shifts are presented, since as it will be shown below, exactly transitions from the  $S$  waves to the ground and the first excited bound states of  ${}^7\text{Be}$  and  ${}^7\text{Li}$  make a dominant contribution to the radiative capture  $S$ -factor. It can be seen from Figs. 14.1, 14.2, and 14.3a that the calculated  $S$  phase shifts for the elastic  ${}^3\text{H}^4\text{He}$ ,  ${}^3\text{He}^4\text{He}$  and  ${}^2\text{H}^4\text{He}$  scattering quite well describe the known results of the phase shift analysis at low energies up to 10 MeV.

Fig. 14.3b shows that the data on the  $P$  phase shifts of the  ${}^2\text{H}^4\text{He}$  scattering from different papers strongly differs; therefore, it is possible to construct the  $P$  potential only approximately; however, on the whole they describe phase shifts at low energies, representing a certain compromise between the results of different phase shift analyses. For energy below 1 MeV, i.e., in the region of determination of the  $S$ -factors, the results of

calculation of all  $P$  phase shifts slightly differ and are close to zero.

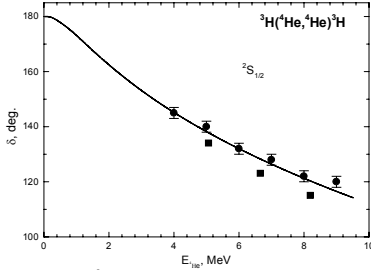


Fig. 14.1.  $^2S_{1/2}$  phase shift of the elastic  $^3\text{H}^4\text{He}$  scattering at low energies. Experimental data from [219] is shown by filled circles and data from [220] by filled squares.

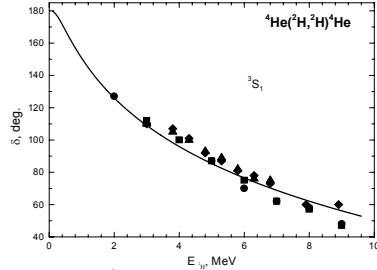


Fig. 14.3a.  $^3S_1$  phase shift of the elastic  $^2\text{H}^4\text{He}$  scattering at low energies. Experimental data from [221] is shown by filled circles, [222] filled squares, [223] filled triangles, and [224] filled rhombs. Curve is the result with obtained potentials (see text).

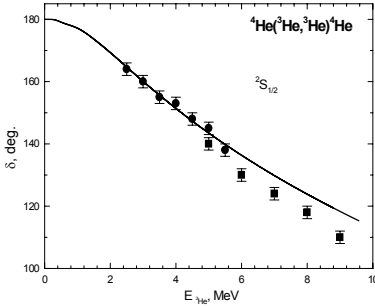


Fig. 14.2.  $^2S_{1/2}$  phase shift of the elastic  $^3\text{He}^4\text{He}$  scattering at low energies. Experimental data from [218] is shown by filled circles and data from [219] by filled squares. Curve is the result with obtained potentials (see text).

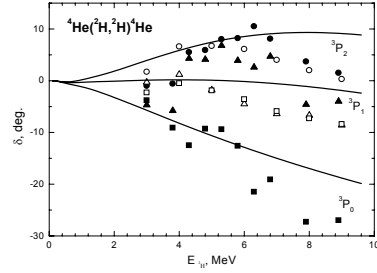


Fig. 14.3b.  $^3P$  phase shift of the elastic  $^2\text{H}^4\text{He}$  scattering at low energies. Experimental data from [222] is shown by open circles  $P_2$ , open triangles  $-P_1$ , and open squares  $-P_0$ ; data from [224]: points  $-P_2$ , triangles  $-P_1$ , and squares  $-P_0$ . Curves are the results with obtained potentials (see text).

In Fig. 14.3c dashed lines show the results of calculation of the  $^3D_1$  and  $^3D_2$  phase shifts of the  $^2\text{H}^4\text{He}$  scattering obtained using the changed potentials, the parameters of which are given in Table 14.1. These potentials somewhat better describe the behavior of the available experimental data, especially at the energies higher than 5 MeV.

It should be note that all  $S$  scattering phase shifts at zero energy are shown in Figs. 14.1, 14.2 and 14.3a beginning from a value of  $180^\circ$ ,

although in the presence of two bound (allowed or forbidden) states in all systems, according to the generalized Levinson theorem [213], they should begin from  $360^\circ$ . Figure 9.3b shows the  $P$  phase shifts of the  ${}^2\text{H}^4\text{He}$  scattering at zero energy beginning from  $0^\circ$ , although, in the presence of a bound forbidden state with tableau  $\{51\}$ , they should be counted from  $180^\circ$ .

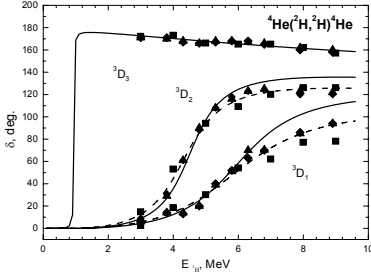


Fig. 14.3c.  ${}^3D$  phase shifts of the elastic  ${}^2\text{H}^4\text{He}$  scattering at low energies.

Experimental data from [222] is shown by filled squares, [223] filled triangles, and [223] filled rhombs. Curves are the results with obtained potentials (see text).

the  ${}^2\text{H}^4\text{He}$  were determined first of all based on correct description of binding energy [21]. In the latter case, it is possible to reproduce not only the binding energy, but also to correctly reproduce the behavior of the  $S$  phase shift of elastic scattering at low energies (Fig. 14.3a). It should be noted that all results were obtained without taking into account tensor forces [225].

## 14.2 New variants of potentials

In the framework of this approach, the good agreement of calculations with different experimental data was obtained for both electromagnetic processes and the main characteristics of bound states of many light nuclei in cluster channels [22]. However, for example, the binding energy of  ${}^7\text{Li}$  in the  ${}^3\text{H}^4\text{He}$  channel with  $J = 3/2^-$ , as well as other systems, was really determined with an accuracy of several kiloelectronvolts; therefore, the accuracy of calculation of the  $S$ -factor of the radiative capture even at 10 keV turned out to be relatively low.

Therefore, in [134] the main calculated characteristics of bound states

Then intercluster interactions thus matched with scattering phase shifts were used for calculation of different characteristics of the ground states of  ${}^7\text{Li}$ ,  ${}^7\text{Be}$ , and  ${}^6\text{Li}$  and electromagnetic processes in these nuclei, and clusters were matched with corresponding properties of free nuclei [21,216]. The parameters of the potentials of the ground states in the  $P$  wave for the  ${}^3\text{He}^4\text{He}$  and  ${}^3\text{H}^4\text{He}$  systems, and the  $S$  wave for

for  ${}^7\text{Li}$ ,  ${}^7\text{Be}$ , and  ${}^6\text{Li}$  nuclei in the  ${}^3\text{H}^4\text{He}$ ,  ${}^3\text{He}^4\text{He}$ , and  ${}^2\text{H}^4\text{He}$  channels have been refined. For this purpose the parameters of the potentials for bound states have been refined, the calculated energy levels completely describe the experimental values [124]. In other words, the potential parameters were chosen in such a way that experimental energy levels were described with maximal possible accuracy. If the experimental binding energy [124] was known with accuracy to the fourth place, for example,  $-1.4743$  MeV, it was assumed that it could be represented with six places,  $-1.474300$  MeV. The energies of the bound levels of the considered nuclei for the given potentials were calculated using the finite-difference method [26] with an accuracy no worse than  $10^{-6}$  MeV. It will be shown below that the actual accuracy of determination of the binding energy in all systems using two different methods turned out to be on the order of  $\pm 1$  eV and the largest error was probably introduced by the variational method of expansion of the wave function over the non-orthogonal Gaussian basis and independent parameter variation [26].

The necessary change of the parameters of the  ${}^3\text{H}^4\text{He}$  and  ${}^3\text{He}^4\text{He}$  potentials required for more accurate description of the channel energies is given in Table 14.2. The slight change of parameters of the  ${}^3\text{H}^4\text{He}$ ,  ${}^3\text{He}^4\text{He}$  and  ${}^2\text{H}^4\text{He}$  potentials with respect to results [22,88] and Table 14.1 practically does not influence the behavior of the scattering phase shifts. However, this change makes it possible to maximally accurately reproduce energy levels in cluster channels, which plays an essential role in calculation of  $S$ -factors for energies of the order of  $1\div 10$  keV.

**Table 9.2. Refined potential parameters of the  ${}^3\text{H}^4\text{He}$ ,  ${}^3\text{He}^4\text{He}$  and  ${}^2\text{H}^4\text{He}$  interactions; energy levels; and charge radii of  ${}^7\text{Li}$ ,  ${}^7\text{Be}$  and  ${}^6\text{Li}$  nuclei calculated with these potentials. The parameter  $\alpha$  for  ${}^3\text{H}^4\text{He}$  and  ${}^3\text{He}^4\text{He}$  systems is  $0.15747\text{ fm}^{-2}$ , and  $R_{\text{Coul}} = 3.095\text{ fm}$ . For  ${}^2\text{H}^4\text{He}$  scattering, it is assumed that  $R_{\text{Coul}} = 0\text{ fm}$**

${}^7\text{Li}$				${}^7\text{Be}$		
$2S+I$ $L$	$V_0$ (MeV)	$E$ (MeV)	$\langle r^2 \rangle^{1/2}$ (fm)	$V_0$ (MeV)	$E$ (MeV)	$\langle r^2 \rangle^{1/2}$ (fm)
${}^2P_{3/2}$	-83.616808	-2.467000	2.46	-83.589554	-1.586600	2.64
${}^2P_{1/2}$	-81.708413	-1.990390	2.50	-81.815179	-1.160820	2.69

<sup>6</sup> Li				
<sup>2S+1</sup> L J	V <sub>0</sub> (MeV)	α (fm <sup>-2</sup> )	E (MeV)	<r <sup>2</sup> > <sup>1/2</sup> (fm)
<sup>3</sup> S <sub>1</sub>	-75.8469155	0.2	-1.474300	2.65

The potential widths in Tables 14.1, 14.2 were chosen from the condition of description of charge radii and asymptotic constants [134]. Table 14.2 presents the results of calculation of the charge radii of considered nuclei in the cluster channels. For finding the charge radius of the nucleus, cluster radii given in [36,72,124] were used; the values of these radii, together with the energies of the bound states in cluster channels and cluster masses, are given in Tables 3.2 and 14.3. In the case of availability of several experimental results, the averaged value, shown in Tables 3.2, was used.

**Table 14.3. Experimental data on charge radii and binding energies [36,72,124]**

Nucleus	Radius (fm)	Binding energy (MeV)
<sup>6</sup> Li	2.51(10)	$E(^4\text{He}^2\text{H}) = -1.4743$
<sup>7</sup> Li	2.35(10)	$E(^4\text{He}^3\text{H}) = -2.467 (3/2^-); -1.99039 (1/2^-)$
<sup>7</sup> Be	—	$E(^4\text{He}^3\text{He}) = -1.5866 (3/2^-); -1.16082 (1/2^-)$

It can be seen from Table 14.2 that the root-mean-square charge radius of <sup>7</sup>Li turns out to be somewhat larger than the experimental value (see Table 14.3). This may be due to existing experimental uncertainty of cluster radii (Table 3.2) which reaches ±5% of the average value and can change the radius of <sup>7</sup>Li by approximately 0.05 fm. In addition, it follows from three-body [49] and RGM calculations (see, for example, [226]) that the deuteron cluster in <sup>6</sup>Li is compressed by approximately a factor of 1.2÷1.4, and this deformation was not taken into account in our examination of <sup>6</sup>Li in the cluster <sup>2</sup>H<sup>4</sup>He model. This makes it possible to explain the somewhat overestimated <sup>6</sup>Li radius obtained in our calculations [22,88,134]. Thus, both for energy levels that are currently accurately



reproduced and for charge radii, rather acceptable agreement with experimental data were obtained with the application of refined potentials.

For examination of the stability of the “tail” of the wave function of the ground and first excited bound states at large distances, the asymptotic constant  $C_w$  in form (2.10) has been used. As a result, for ground states of  $^7\text{Be}$ ,  $^7\text{Li}$ , and  $^6\text{Li}$  nuclei, in the considered channels, the following values were obtained: 5.03(1), 3.92(1), and 3.22(1), respectively. For the first excited states of  $^7\text{Be}$  and  $^7\text{Li}$  nuclei, in this model the following values were found: 4.64(1) and 3.43(1). The error given in brackets is determined by averaging the constant for nuclei with  $A = 7$  obtained in calculation on an interval of  $6 \div 16$  fm and for  $^6\text{Li}$  at an interval of  $5 \div 19$  fm.

In [49], based on a three-body  $np^4\text{He}$  model for the asymptotic constant of the ground  $S$  state of  $^6\text{Li}$  in the  $^2\text{H}^4\text{He}$  channel, a value of 2.71 was obtained. A value of 2.93(15) was found in [227] from the phase shift analysis of the elastic  $^2\text{H}^4\text{He}$  scattering. In [228] values from 2.09 to 3.54 were obtained for different types of the  $NN$  and  $N\alpha$  interaction using recalculation to the dimensionless quantity at  $k_0 = 0.308 \text{ fm}^{-1}$ . In this paper references to experimental data varying from 2.29(25) to 2.96(14) are also given [228]. At the earlier work [40] the value of 3.04 is given, which was obtained using recalculation to the dimensionless quantity too. If the asymptotic  $^2\text{H}^4\text{He}$  constant is determined from common exponential asymptotics, i.e., without taking into account Coulomb effects, the following value is obtained in the model used here for an interval of  $4 \div 12$  fm: 1.9(2). The following values are known for this case: from 1.5 to 2.8 [229] and 2.15(5) [38,74]. In [40] a survey of asymptotic and vertex constants, including those for the  $^2\text{H}^4\text{He}$  channel, was presented and it was noted that the values of these constants, depending on the presence or absence of Coulomb effects, can differ by several times. The real change of asymptotic constant in the above results comes to approximately  $1.5 \div 2.0$ .

For the ground state of the  $^3\text{H}^4\text{He}$  system in  $^7\text{Li}$ , for example in [230], with Whittaker asymptotics taking into account Coulomb (2.10), using recalculation to the dimensionless quantity with  $k_0 = 0.453 \text{ fm}^{-1}$ , the values of asymptotic constant of the ground state is equal to 3.87(16) and asymptotic constant of the first excited state 3.22(15) was obtained. The value 3.73(26) for the GS was found in [231] after using recalculation to the dimensionless quantity, that is quite agree with our results.

The value of 5.66(16) that is slightly more than our calculated value, is proposed for the ground state of  ${}^7\text{Be}$  in the  ${}^3\text{He}^4\text{He}$  channel in [232] on the base of different experimental data after using recalculation to the dimensionless quantity with  $k_0 = 0.363 \text{ fm}^{-1}$ . The value 4.66(15) is given for the first excited state, that is in a good agreement with the value obtained here. Note that, for example in work [233], the values in an interval of  $3.5 \div 4.6$  were obtained for the constant of the ground state of  ${}^7\text{Be}$  in the  ${}^3\text{He}^4\text{He}$  channel after using recalculation to the dimensionless quantity.

### 14.3 Results of variational calculations

The variational method [26] was used to control the accuracy of determination of the binding energy in the considered cluster systems; in the  ${}^3\text{H}^4\text{He}$  channel, this method made it possible, even for dimensionality of non-orthogonal Gaussian basis equals 10 and independent parameter variation, to obtain a binding energy of  $-2.466998 \text{ MeV}$ . Therefore, as was mentioned earlier, for the actual binding energy in this potential, an average value of  $-2.466999(1) \text{ MeV}$  can be taken.

The parameters of expansion of the radial intercluster variational wave function of the form (2.9) for the  ${}^3\text{H}^4\text{He}$  system are given in Table 9.4. The asymptotic constant at distances of  $6 \div 16 \text{ fm}$  was on a level of 3.93(3), and the residual did not exceed the value of  $3 \times 10^{-12}$  [26]. For the first excited state in this channel, the energy of  $-1.990374 \text{ MeV}$  was obtained. The parameters of the corresponding wave function are also given in Table 14.4. The asymptotic constant on an interval of  $6 \div 20 \text{ fm}$  turned out to be equal to 3.40(5), and the residual was equal to  $4 \times 10^{-13}$ .

**Table 14.4. Parameters and expansion coefficients of the variational wave functions of  ${}^7\text{Li}$  in the  ${}^3\text{H}^4\text{He}$  model for the potential from Table 14.2.**

${}^7\text{Li} ({}^3\text{H}^4\text{He}) J = 3/2^-$ Normalization coefficient of wave function in an interval of $0 \div 25 \text{ fm}$ is equal to $N = 9.99999999992\text{E}-001$		
$i$	$\beta_i$	$C_i$
1	6.567905679421632E-001	4.270672892119584E-001

2	1.849427298619411E-002	-6.326508826973404E-004
3	1.729324040753008E-001	-2.047665503330138E-001
4	4.173925751998056E-002	-1.032337189461229E-002
5	8.818471551829664E-002	-6.301223045259621E-002
6	4.503350223878621E-001	6.962475101962766E-001
7	9.210585557350788E-001	2.076348167318741E-002
8	2.000570770210328	1.488688664230068E-003
9	2.925234985697186	-1.124699482527892E-003
10	3.981951253509630	3.797289741762020E-004
<p style="text-align: center;"><b><math>{}^7\text{Li}({}^3\text{H}^4\text{He}) J = 1/2^-</math></b>  <b>Normalization coefficient of wave function in an interval</b>  <b>of 0÷25 fm is equal to <math>N = 9.999999994\text{E}-001</math></b></p>		
<b><math>i</math></b>	<b><math>\beta_i</math></b>	<b><math>C_i</math></b>
1	3.767783843541890E-001	4.630588198830661E-001
2	3.862289845123266E-002	-1.122717538276013E-002
3	1.902467043551489E-001	-2.185424962074149E-001
4	1.465702154047247E-002	-4.355239784992325E-004
5	9.174545622012323E-002	-7.860947071320935E-002
6	8.478055592043516E-001	-5.602419628674884E-001
7	6.512974681188465E-001	1.017849119474616
8	1.401572634787409	57.704730892399640
9	1.405534176137368	-58.402969632676760
10	1.569682720436807	9.151457061882704E-001

For the binding energy in the  ${}^3\text{He}^4\text{He}$  channel and for the same basis dimensionality, a value of -1.586598 MeV was obtained; the coefficients of expansion of the WF are given in Table 14.5. It follows from these results that the mean binding energy in this potential can be taken equal to -1.586699(1) MeV. The asymptotic constant in a range of 6÷15 fm is preserved at a level of 5.01(4), and the residual does not exceed  $5 \times 10^{-13}$ . For the first excited state, the energy of -1.160801 MeV was obtained; the parameters of the wave function are also given in Table 9.5. The

asymptotic constant at an interval of 6÷14 fm is equal to 4.64(4), and the residual did not exceed  $5 \times 10^{-12}$ .

**Table 14.5. Parameters and expansion coefficients of the variational wave functions of  ${}^7\text{Be}$  in the  ${}^3\text{He}{}^4\text{He}$  model for the potential from Table 14.2.**

${}^7\text{Be} ({}^3\text{He}{}^4\text{He}) J = 3/2^-$ Normalization coefficient of wave function in an interval of 0÷25 fm is equal to $N = 9.999999995\text{E}-001$		
$i$	$\beta_i$	$C_i$
1	7.592678086347688E-001	4.226683168050651E-001
2	1.764646518442939E-002	-9.297447488403448E-004
3	1.713620418679277E-001	-1.913577297864284E-001
4	4.166190335743666E-002	-1.157464906616252E-002
5	8.829356096205253E-002	-6.210954724479718E-002
6	4.566882349965201E-001	7.725352747968277E-001
7	1.263871984172901	-7.575809619184885E-001
8	1.358053110884124	7.836457309371079E-001
9	1.741955980844547	-1.277551712466414E-001
10	2.379459759640717	1.446300395173141E-002
${}^7\text{Be} ({}^3\text{He}{}^4\text{He}) J = 1/2^-$ Normalization coefficient of wave function in an interval of 0÷25 fm is equal to $N = 9.99999998\text{E}-001$		
$i$	$\beta_i$	$C_i$
1	3.857719633413334E-001	4.891511738383773E-001
2	3.862289845123266E-002	-1.229249560611409E-002
3	1.881845128735454E-001	-2.002401467853206E-001
4	1.465702154047247E-002	-7.752125472489987E-004
5	9.174545622012323E-002	-7.680363457361430E-002
6	8.478055592043516E-001	-3.264723437643782E-001
7	6.512974681188465E-001	8.230628856230295E-001

8	1.401572634787409	21.258288548024340
9	1.405534176137368	−21.437482795337960
10	1.569682720436807	2.883954334066227E−001

In the  ${}^2\text{H}^4\text{He}$  channel, the variational method yields the energy of  $-1.474298$  MeV and the mean binding energy for this potential is of  $-1.474299(1)$  MeV. The asymptotic constant in an interval of 6–20 fm is equal to 3.23(3), the residual is no higher than  $7 \times 10^{-13}$ , and the parameters of expansion of the variational wave function are given in Table 14.6.

**Table 14.6. Parameters and expansion coefficients of the variational wave functions of  ${}^6\text{Li}$  in the  ${}^2\text{H}^4\text{He}$  model for the potential from Table 14.2.**

${}^6\text{Li} ({}^2\text{H}^4\text{He}) J = 1^+$ Normalization coefficient of wave function in an interval of 0÷25 fm is equal to $N = 9.99999865\text{E}−001$		
$i$	$\beta_i$	$C_i$
1	9.437818606389059E−003	5.095342831090755E−003
2	2.339033265895747E−002	3.991949900002217E−002
3	5.360473343158653E−002	1.164934149242748E−001
4	1.140512295822141E−001	2.165501771045687E−001
5	2.076705835662333E−001	1.831336962855912E−001
6	3.702254820081791E−001	−6.350857624465279E−001
7	2.848601430685521	2.165544802826948E−002
8	5.859924777191484E−001	−7.358532868463539E−001
9	82.336677993239830	5.086893578426774E−003
10	12.344385769445580	1.002621348014230E−002

Thus, the difference in the binding energy of the ground states of all systems found using two methods does not exceed  $\pm 1$  eV and the asymptotic constants in these ranges of distances and error margins completely coincide. For all the considered systems, the values of charge radii obtained using two different methods also coincide within two digits.

These results demonstrate good agreement of wave functions of bound states of all considered nuclei obtained using two different methods in an interval from  $5\div 6$  to  $16\div 20$  fm.

#### 14.4. Astrophysical *S*-factor

Earlier total cross sections of photoprocesses and the astrophysical *S*-factors for the  $^2\text{H}^4\text{He}$ ,  $^3\text{H}^4\text{He}$  and  $^3\text{He}^4\text{He}$  systems were calculated in a cluster model [234] similar to that applied here and also in the frame of the RGM [235]. For interaction potentials with forbidden states, the total photodisintegration cross sections in the  $^2\text{H}^4\text{He}$  cluster channel of  $^6\text{Li}$  were calculated based on three-body wave functions of the ground state [236]. The total cross sections of photoprocesses for  $^6\text{Li}$  and  $^7\text{Li}$  nuclei in two-cluster models with forbidden states were calculated in [216] based on Gaussian potentials matched with elastic scattering phase shifts of corresponded particles.

In relation with publication of new experimental data, we consider the astrophysical *S*-factors of the radiative capture of  $^4\text{He}(^3\text{He}, \gamma)^7\text{Be}$ ,  $^4\text{He}(^3\text{H}, \gamma)^7\text{Li}$  and  $^4\text{He}(^2\text{H}, \gamma)^6\text{Li}$  reactions at energies as low as possible in the framework of the potential cluster model [216,217] and specified potentials of ground states of  $^7\text{Li}$ ,  $^7\text{Be}$ , and  $^6\text{Li}$  nuclei (Table 14.2). Only the *E1* transitions were taken into account in calculations for the  $^3\text{H}^4\text{He}$  and  $^3\text{He}^4\text{He}$  systems, since the contributions of the *E2* and *M1* transitions are lower by two to three orders of magnitude [88]. In these systems only the *E1* transitions between the ground  $P_{3/2}$  state of  $^7\text{Li}$ ,  $^7\text{Be}$ , and  $S_{1/2}$ ,  $D_{3/2}$ ,  $D_{5/2}$  scattering states and between the first excited bound  $P_{1/2}$  state and  $S_{1/2}$ ,  $D_{3/2}$  scattering states are possible.

For the radiative capture in the  $^2\text{H}^4\text{He}$  channel of  $^6\text{Li}$  the *E1* transitions from  $^3P$  scattering phase shifts to the ground bound  $^3S$  state of  $^6\text{Li}$  and the *E2* transitions from the  $^3D$  scattering waves to the ground state are possible. The main contribution to the *E2* transition at low energies is made by the  $^3D_3$  wave with a resonance at 0.71 MeV and the *E1* transition turns out to be strongly suppressed due to the cluster factor  $A_{\mu}(K)$  given in (2.5); therefore, the cross section of the radiative capture process is mainly determined by the *E2* transition. It was shown earlier [88] that, at the lowest energies of the order of  $100\div 150$  keV, the contribution of the *E1*

transition becomes prevailing; therefore, it will be shown below that it is the  $E1$  process that determines the behavior of the astrophysical  $S$ -factor in this energy region.

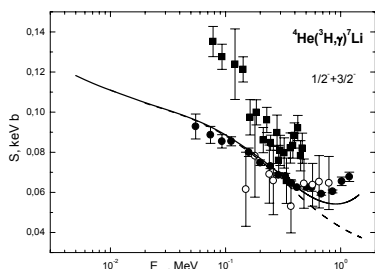


Fig. 14.4. Astrophysical  $S$ -factor of the radiative  ${}^4\text{He}({}^3\text{H}, \gamma){}^7\text{Li}$  capture. Filled circles show experimental data [237], open circles [238], and filled squares [239]. Lines show results of calculation with parameters of ground state potentials from Table 14.2.

The results of calculation of the astrophysical  $S$ -factors of radiative capture of  ${}^4\text{He}({}^3\text{H}, \gamma){}^7\text{Li}$  reaction at energies down to 5 keV are shown in Fig. 14.4 by a solid line. Experimental data is taken from [237,238]; in the first of them the results for energies down to 55 keV are presented. The value of the  $S$ -factor at 10 keV turned out to be equal to 111.0 eV b; the value extracted from experiment for zero energy was equal to 106.7(4) eV b

[237]. Earlier results [238] yield 64 eV b; however, these data contains such large errors that they are extrapolated by a straight line.

There exist other data, which result in the following values at zero energy: 140(20) [239] and 100(20) eV b [34]. Note that results of [239] shown in Fig. 14.4 by squares disagree with later measurements [237] and have relatively large errors. Among theoretical calculations, results of cluster model [234] can be noted; in this model the value of the  $S$ -factor equals 100 eV b was obtained at zero energy, in the resonating group method, 98(6) eV b [235], and in recent paper [230]  $S(0) = 97.4(10)$  eV b.

If only transitions from the  $S$  scattering wave to the ground and first excited bound  $P$  states are taken into account, at 10 keV we obtain 110.8 eV b, which practically does not differ from that presented above. The results of calculation of the  $S$ -factor in this case are shown in Fig. 9.4 by a dashed line; they differ from the previous results only at energies above 0.3 MeV.

Thus, the results of our calculation of the  $S$ -factor of  ${}^4\text{He}({}^3\text{H}, \gamma){}^7\text{Li}$  radiative capture quite well describe experimental data [237] at energies below 0.5 MeV and result in the  $S$ -factor at 10 keV, which is in reasonable agreement with extrapolation of this experiment to zero energy. It should be noted that our previous calculations for this  $S$ -factor resulted in 87 eV b

[88]. This difference may be related with the properties of the bound state potential used in calculations that yielded the binding energy with accuracy to several keV [88].

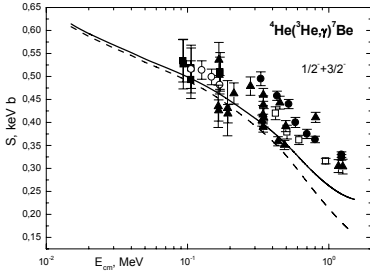


Fig. 14.5. Astrophysical  $S$ -factor of the radiative  ${}^4\text{He}({}^3\text{He}, \gamma){}^7\text{Be}$  capture. Filled circles show experimental data [240], filled squares [241], open circles [242], open squares [243], and filled triangles [244]. Lines show results of calculation with parameters of GS potentials from Table 14.2.

0.593 keV b. For comparison we present the results of extrapolation of experimental data to zero energy: 0.54(9) [34], 0.550(12) [245], 0.595(18) [240], 0.560(17) [241], 0.550(17) [242], and 0.567(18) keV b [246]. In the cluster model [234], the following value was obtained for this  $S$ -factor: 0.56 keV b, and in the resonating group method [235] 0.5(3) keV b. Recently, it was obtained, in [232] based on analysis of different experimental data, that  $S(0) = 0.610(37)$  keV b and  $S(23 \text{ keV}) = 0.599(36)$  keV b, which well agrees with the value found here.

If transitions from the  $S$  scattering waves to the ground and first excited bound states only are considered, similarly to the previous nuclear system, at 20 keV we obtain 0.587 keV b, which slightly differs from the above value. The calculated  $S$ -factor for this case is shown in Fig. 14.5 by the dashed line, which slightly differs from the previous results obtained taking into account transitions from the  $S$  and  $D$  waves.

It can be seen from results obtained not long ago that the value of the  $S$ -factor at zero energy can be in the range of  $0.54 \div 0.65$  keV b and our calculated value falls in this interval. The form of the  $S$ -factor at energies below 0.5 MeV agrees well with data [244], and at lower energies it describes new data [241,242]. Note that our previous calculations of the  ${}^3\text{H}^4\text{He}$   $S$ -factor yielded 0.47 keV b [88]. The difference of this value from

The results of calculation of the astrophysical  $S$ -factor of the  ${}^4\text{He}({}^3\text{He}, \gamma){}^7\text{Be}$  capture at energies down to 15 keV are shown in Fig. 14.5 by a solid line. Experimental data has been taken from [240-244]. The calculated curve at energy below 200 keV best agrees with results [241,242] obtained recently, and partially with data [244] at energies below 0.5 MeV. For energy of 20 keV, our calculation yields an  $S$ -factor of



the new results can also be connected with the imperfection of the ground state potential used in [88].

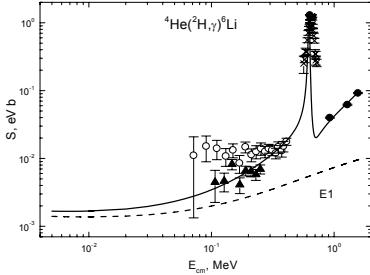


Fig. 14.6. Astrophysical  $S$ -factor of the radiative  ${}^4\text{He}({}^2\text{He}, \gamma){}^6\text{Li}$  capture. Filled circles show experimental data [247], crosses [248], and open circles [249], and triangles – [185,250]. The dashed line shows contribution of  $E1$  process for transition to the ground state from the  $P$  scattering wave. The solid line shows the total  $S(E1+E2)$  – factor.

$S$ -factor determined by the  $E1$  and  $E2$  transitions, a value of  $1.67(1) \times 10^{-3}$  eV b or  $1.67(1)$  eV mb was obtained. The contribution of the  $E1$  transition in this energy region is defining and comes to  $1.39(1)$  eV mb. Obviously, it is the  $E1$  transition that makes the main contribution to the astrophysical  $S$ -factor at low energies. The mentioned errors of the  $S$ -factor are determined by averaging over this energy interval. Unlike the systems considered above, this  $S$ -factor is practically constant in this energy region. Note that our previous calculations of the  $S$ -factor of the radiative  ${}^4\text{He}({}^2\text{He}, \gamma){}^6\text{Li}$  capture led to the value  $1.5$  eV mb [22]. This difference from the obtained here value  $1.67(1)$  eV mb is also caused by the approximate character of the used earlier potential of the bound state, which was able to obtain the binding energy only with an accuracy down to few keV [88].

The results of extrapolation of experimental data given in [34] at 10 keV yield  $1.6(1)$  eV mb, which well agrees with the value that we obtained. However, if data from [249] that allows linear extrapolation are so extrapolated, an average value of  $13$  eV mb can be obtained, which is higher by almost one order of magnitude. At the same time, more modern data on the  $S$ -factor [185,250] more exactly determined its behavior at lowest energies, having a good agreement with our results.

The following value was obtained in theoretical calculations of [228] for

The results of the  $S$ -factor calculation for the  ${}^4\text{He}({}^2\text{He}, \gamma){}^6\text{Li}$  capture reaction are shown in Fig. 14.6 by the solid line, and the contribution of the  $E1$  transition is shown by the dashed line. Experimental data is taken from [185,247-250]; the results of the last but one paper were determined from figures presented in [34]. As it is seen from Fig. 14.6, the calculation results are in better agreement with data [185,250] at low energies. In a range of  $5 \div 10$  keV for the total calculated

the  $S$ -factor at zero energy: 1.2(1) eV mb, which corresponds to an asymptotic constant of 3.06, and the constant extracted from experimental data [227,250] is equal to 2.96(14). However, the asymptotic constant obtained in calculations in which the  $S$ -factor is determined varies in a range of 2.1÷3.5 and, therefore, the  $S$ -factor can have values that differ by a factor of 2. As a result, the uncertainty of experimental data and theoretical results does not make it possible, still, to arrive at a fixed and final conclusion on the value of the  $S$ -factor of  ${}^4\text{He}({}^2\text{He}, \gamma){}^6\text{Li}$  radiative capture at zero energy and its behavior in the region below the resonance. Although the results [185,250] show quite exactly its behavior at the lowest energies.

### 14.5. Variation two-body program

Now let us briefly stop at the description of the variational method and computer program, since earlier almost always the given results were obtained by this method. More detailed description of this method can be found in our work [26]. The wave functions in matrix elements for the ground and the resonance states can be presented in the form of expansion according to Gaussian basis of (2.9), which are obtained by the variational method for bound states or by the approximation by Gaussians of numerical wave functions of the resonance levels [251].

The matrix eigenvalue problem [252] is solved for determination of the spectrum of eigen energies and wave functions in the standard variational method at the expansion of the WF according to orthogonal basis

$$\sum_i (H_{ij} - EI_{ij})C_i = 0 ,$$

where  $H$  – symmetrical matrix of the Hamiltonian,  $I$  – unit matrix,  $E$  – eigenvalues and  $C$  – eigenvectors of the problem.

In this case, at the nonorthogonal Gaussian basis we are leading to the generalized matrix problem of the type (2.13) [253]. At usage the WF of the type (2.9) it is easy to find expressions for all two-body matrix elements [253].

$$H_{ij} = T_{ij} + V_{ij} + \langle i | Z_1 Z_2 / r | j \rangle + \langle i | \hbar^2 L(L+1) / 2\mu r^2 | j \rangle ,$$

$$N_0 = [\sum_i C_i C_j L_{ij}]^{-1/2},$$

$$T_{ij} = -\frac{\hbar^2}{2\mu} \frac{\sqrt{\pi}(2L-1)!!}{2^{L+1}\beta_{ij}^{L+1/2}} \left\{ L(2L+1) - L^2 - \frac{\alpha_i \alpha_j (2L+1)(2L+3)}{\beta_{ij}^2} \right\},$$

$$V_{ij} = \int V(r) r^{2L+2} \exp(-\beta_{ij} r^2) dr,$$

$$L_{ij} = \frac{\sqrt{\pi}(2L+1)!!}{2^{L+2}\beta_{ij}^{L+3/2}},$$

$$\langle i | Z_1 Z_2 / r | j \rangle = \frac{Z_1 Z_2 L!}{2\beta_{ij}^{L+1}},$$

$$\langle i | \hbar^2 L(L+1)/2\mu r^2 | j \rangle = \frac{\sqrt{\pi}(2L-1)!!}{2^{L+1}\beta_{ij}^{L+1/2}} \frac{L(L+1)\hbar^2}{2\mu},$$

where  $\beta_{ij} = \beta_i + \beta_j$  – parameters of expansion of the WF. The matrix element of the potential  $V_{ij}$  is determined in the analytical form in the case of the Gaussian potential of the intercluster interaction of (2.8)

$$V_{ij} = V_0 \frac{\sqrt{\pi}(2L+1)!!}{2^{L+2}(\beta_{ij} + \alpha)^{L+3/2}},$$

where  $\alpha$  – parameter of the potential depth.

Let us present now the text of the computer program for realization of this method with independent variation of the parameters using the Fortran-90 language. The description of the majority of the parameters and potentials are given in the text of the program itself.

### **PROGRAM AL\_3H\_\_SOB**

```
! VARIATIONAL PROGRAMM OF SEARCHING THE BINDING
!ENERGY
USE MSIMSL
IMPLICIT REAL(8) (A - Z)
```

```

INTEGER I,J,K,LO,NV,NI,NP,NF,LK
DIMENSION XP(0:100)
!,XPN(0:100)
!DIMENSION E2(0:100)
!DIMENSION FU(0:10240000)
DIMENSION C0(0:100),CW0(0:100),CW(0:100)
!,ALA(0:100)
COMMON /A/
B44,B23,B11,B33,A11,PM,B55,S22,S44,C22,LO,S11,LK,RC,PI,C11,C33,
B22
COMMON /B/
T(0:100,0:100),VC(0:100,0:100),VN(0:100,0:100),VK(0:100,0:100),RN,R
N1,F1(0:10240000)
COMMON /C/ EP,PNC,PVC,HC,EPP
COMMON /D/ AA(0:100,0:100)
COMMON /F/
AL1(0:100,0:100),C(0:100,0:100),B(0:100,0:100),AD(0:100,0:100),AL(0:
100,0:100),Y(0:100),AN(0:100),D(0:100),X(0:100),SV(0:100),H(0:100,0:1
00)
COMMON /G/ FF(0:10240000)
! ***** INITIAL VALUES *****
Z1=2.0D - 000 ; ! Masses and charges of clusters
Z2=1.0D - 000
Z=Z1+Z2
AM1=4.001506179127D - 000; ! AL
AM2=3.0155007134D - 000; ! 3H
!AM2=3.0149322473D - 000; ! 3HE
R01=1.67D - 000 ; ! Radiuses of clusters
R02=1.73D - 000
RK11=1.67D - 000 ; ! Radiuses of clusters
RK22=1.73D - 000
AM=AM1+AM2 ; ! Input constants
PM=AM1*AM2/AM
GK=3.44476D - 002*Z1*Z2*PM
A11=20.7343D - 000
A22=1.4399750D - 000*Z1*Z2

```

```

P1=4.0D - 000*ATAN(1.0D - 000)
NF=1000 ; ! Number of step of calculation of function
R00=25.0D - 000
HFF=R00/NF ; ! Step of calculation of function
NFF=NF/100
NP=10 ; ! Dimension of basis
NI=1 ; ! Number of iterations
NV=0 ; ! = 0 - without minimization, = 1 - with minimization according
to energy
EP=1.0D - 015 ; ! Search precision of energy
EPP=1.0D - 015 ; ! Search precision of null of determinant
HC=0.001230D - 000 ; ! Look of null of determinant
PNC= - 2.7D - 000 ; ! Lower value of energy for searching !of the null
of determinant !
PVC= - 0.0001D - 000 ; ! Upper value of energy for searching !of the null
of determinant !
PHN=0.000123450D - 000 ; ! Step of parameters !alpha
! ***** PARAMETERS OF POTENTIALS *****
V0= - 83.616808D - 000;! RCU=3.095 R0=0.15747 E= - 2.467000 -
!CW=3.92(2) RCH=2.46(1.67,1.73) RMAS=2.50
RN=0.15747D - 000
LO=1
RC=3.095D - 000
V1=0.0D - 000
RN1=1.0D - 000
! **** INITIAL ALPHA PARAMETERS*****
NPP=NP
OPEN (1,FILE='ALFA.DAT')
DO I=1,NPP
READ(1,*) I,XP(I)
PRINT *,I,XP(I)
ENDDO
CLOSE(1)
PRINT *
! ***** INITIAL CONSTANTS *****
C11=LO+1.50D - 000

```

```

C22=LO+0.50D - 000
PI=DSQRT(P1)
C33=LO+1.0D - 000
N11=2*LO+3
S44=1.0D - 000
DO K=1,N11,2
S44=S44*K
ENDDO
LK=LO*LO
S11=S44/(2.0D - 000*LO+3.0D - 000)
S22=S11/(2.0D - 000*LO+1.0D - 000)
R1=1.0D - 000
DO K=1,LO
R1=R1*K
ENDDO
B11=PI*S11/(2.0D - 000** (LO+2.0D - 000))
B22=B11*V0
B23=B11*V1
B33=1.0D - 000*LO*(LO+1.0D - 000)*PI*S22/(2.0D - 000** (LO+1.0D -
000))
B44=A22*R1/2.0D - 000
B55=PI/(2.0D - 000** (LO+1.0D - 000))
! ***  SEARCHING OF THE WF !PARAMETERS AND BINDING
ENERGY ***
CALL VARMIN(PHN,NP,NI,XP,EP,BIND,NV)
! *****  NUCLEAR CHARACTERISTICS *****
PRINT *, '----- -- ENERGIES ----- -- '
PRINT *, '                      E = ', BIND
PRINT *, '----- ALPHA ----- '
DO I=1,NP
PRINT *, I, XP(I)
ENDDO
! *****  EIGENVECTORS *****
CALL SVV(BIND,NP,XP)
! *****  NORMALIZATION OF VECTORS *****
A111: DO I=1,NP

```

```

DO J=1,NP
AL(I,J)=PI*S11/(2.0D - 000***(LO+2)*(XP(I)+XP(J))**C11)
ENDDO
ENDDO A111
S=0.0D - 000
B111: DO I=1,NP
DO J=1,NP
S=S+SV(I)*SV(J)*AL(I,J)
ENDDO
ENDDO B111
ANOR=1.0D - 000/SQRT(S)
PRINT *, '                VECTORS                '
DO I=1,NP
SV(I)=ANOR*SV(I)
PRINT *,I,SV(I)
ENDDO
! ***** CALCULATION OF THE WF *****
FFFF=0.0D - 000
DO I=0,NF
R=HFF*I
S=0.0D - 000
DO J=1,NP
RRR=R**2.0D - 000*XP(J)
IF (RRR>50) GOTO 9182
S=S+SV(J)*EXP( - RRR)
9182 ENDDO
FF(I)=R**(LO+1)*S
ENDDO
IF (FFFF==0.0D - 000) GOTO 246
PRINT ' R                F(R)'
DO I=0,NF,NFF
R=I*HFF
PRINT *,R
PRINT *,FF(I)
ENDDO
246 CONTINUE

```

```

! **** CHECK OF NORMALIZATION *****
DO I=0,NF
R=I*HFF
F1(I)=FF(I)**2
ENDDO
CALL SIM(F1,NF,HFF,SII)
PRINT *,'          NOR = ',SII
! ***** ASYMPTOTIC CONSTANTS *****
SKS=(ABS(BIND)*PM/A11)
SS=SQRT(ABS(SKS))
SQQ=SQRT(2.*SS)
GGG=GK/SS
M1=NF/4
M3=NF/20
M2=NF
PRINT *,'      R      C0      CW0      CW'
K=0
DO I=M1,M2,M3
K=K+1
R=I*HFF
CALL ASIMP(R,SKS,GK,LO,I,C01,CW01,CW1)
C0(K)=C01
CW0(K)=CW01
CW(K)=CW1
WRITE(*,1) R,C01,CW01,CW1
ENDDO
1 FORMAT(3X,4(F10.5))
! ***** RADIUS OF NUCLEUS *****
SS=0.0D - 000
DO I=1,NP
DO J=1,NP
SS=SS+SV(I)*SV(J)/(XP(I)+XP(J))**(LO+2.5)
ENDDO
ENDDO
RR=PI*S44*SS/2.0D - 000**(LO+3)
RRR=SQRT(RR)

```



```

RCH=AM1*R01**2.0D      -      000/AM+AM2*R02**2.0D      -
000/AM+AM1*AM2*RR/AM**2
RZ=Z1/Z*RK11**2      +      Z2/Z*RK22**2      +
(((Z1*AM2**2+Z2*AM1**2)/AM**2)/Z)*RR
PRINT *, '      RM = , RZ = ',SQRT(RCH),SQRT(RZ)
PRINT *, '----- - - ENERGIES ----- - - '
PRINT *, '      E = ',BIND
! ***** SAVE TO FILE *****
PRINT *, 'SAVE???'
READ *
OPEN (1,FILE='ALFA.DAT')
DO I=1,NP
WRITE(1,*) I,XP(I)
ENDDO
CLOSE(1)
OPEN (1,FILE='SV.DAT')
DO I=1,NP
WRITE(1,*) I,SV(I)
ENDDO
WRITE(1,*)
WRITE(1,*) 'E = ',BIND
CLOSE(1)
END
SUBROUTINE VARMIN(PHN,NP,NI,XP,EP,AMIN,NV)
IMPLICIT REAL(8) (A - Z)
INTEGER I,NV,NI,NP,NN
DIMENSION XPN(0:100),XP(0:100)
! ***** SEARCHING OF MINIMUM *****
DO I=1,NP
XPN(I)=XP(I)
ENDDO
NN=1
PH=PHN
CALL DETNUL(XPN,NP,ALAA)
BB=ALAA
IF (NV==0) GOTO 3012

```

```

A111: DO I=1,NI
NN=0
GOTO 1119
1159 XPN(NN)=XPN(NN) - PH*XP(NN)
1119 NN=NN+1
IN=0
2229 A=BB
XPN(NN)=XPN(NN)+PH*XP(NN)
IF (XP(NN)<0.0D - 000) GOTO 1159
IN=IN+1
CALL DETNUL(XPN,NP,ALAA)
BB=ALAA
PRINT *,NN,XPN(NN),ALAA
IF (BB<A) GOTO 2229
C=A
XPN(NN)=XPN(NN) - PH*XP(NN)
IF (IN>1) GOTO 3339
PH= - PH
GOTO 5559
3339 IF (ABS(C - BB)<EP) GOTO 4449
PH=PH*0.50D - 000
5559 BB=C
GOTO 2229
4449 PH=PHN
IF (NN<NP) GOTO 1119
PH=PHN*1.0D - 000
AMIN=BB
ENDDO A111
3012 AMIN=BB
DO I=1,NP
XP(I)=XPN(I)
ENDDO
END
SUBROUTINE MAT(XP,NP)
IMPLICIT REAL(8) (A - Z)
INTEGER I,NP,NFF,LO,LK

```

```

DIMENSION XP(0:100)
COMMON /A/
B44,B23,B11,B33,A11,PM,B55,S22,S44,C22,LO,S11,LK,RCC,PI,C11,C3
3,B22
COMMON /B/
T(0:100,0:100),VC(0:100,0:100),VN(0:100,0:100),VK(0:100,0:100),RN,R
N1,F1(0:10240000)
COMMON /F/
AL1(0:100,0:100),C(0:100,0:100),B(0:100,0:100),AD(0:100,0:100),AL(0:
100,0:100),Y(0:100),AN(0:100),D(0:100),X(0:100),SV(0:100),H(0:100,0:1
00)
! ***** MATRIX CALCULATION *****
A111: DO KK=1,NP
B111: DO JJ=1,NP
ALL=XP(KK)+XP(JJ)
T(KK,JJ)= - B55*(LO*S11 - LK*S22 -
XP(KK)*XP(JJ)*S44/ALL**2)/ALL**C22
SF=1.0D - 000
SS1=1.0D - 000
IF (RCC==0.0D - 000) GOTO 7654
PF=RCC*DSQRT(ALL)
NFF=200
HF=PF/NFF
IF (PF>3.0D - 000) GOTO 9765
DO I=0,NFF
XX=HF*I
F1(I)=DEXP( - XX**2)
ENDDO
CALL SIM(F1,NFF,HF,SI)
SF=SI*2.0D - 000/PI
9765 ALR=DSQRT(ALL)*RCC
ALR2=ALR**2
EX=DEXP( - ALR2)
SS=PI*(9.0D - 000*ALR - 15.0D - 000/(2.0D - 000*ALR))*SF
SS1=(15.0D - 000*EX+SS)/(8.0D - 000*ALR2)
7654 VK(KK,JJ)=B44/ALL**C33*SS1

```

```

VN(KK,JJ)=B22/(ALL+RN)**C11
VN(KK,JJ)=VN(KK,JJ)+B23/(ALL+RN1)**C11
VC(KK,JJ)=B33/ALL**C22
H(KK,JJ)=(A11/PM)*(T(KK,JJ)+VC(KK,JJ))+VN(KK,JJ)+VK(KK,JJ)
AL1(KK,JJ)=B11/ALL**C11
H(JJ,KK)=H(KK,JJ)
AL1(JJ,KK)=AL1(KK,JJ)
ENDDO B111
ENDDO A111
END
SUBROUTINE DETNUL(XP,NP,ALA)
IMPLICIT REAL(8) (A - Z)
INTEGER NP
COMMON /C/ EP,PNC,PVC,HC,EPP
DIMENSION XP(0:100)
! SEARCHING OF THE NULL OF DETERMINANT
! —— FORMING OF THE MATRIX —— - -
CALL MAT(XP,NP)
! -SEARCHING OF THE NULL OF DETERMINANT
A2=PNC
B2=PNC+HC
CALL DETER(A2,D12,NP)
51 CALL DETER(B2,D11,NP)
IF (D12*D11>0.0D - 000) GOTO 4
44 A3=A2
B3=B2
11 C3=(A3+B3)/2.0D - 000
IF (ABS(A3 - B3)<EPP) GOTO 151
CALL DETER(C3,F2,NP)
IF (D12*F2>0.0D - 000) GOTO 14
B3=C3
D11=F2
GOTO 15
14 A3=C3
D12=F2
15 IF (ABS(F2)>EPP) GOTO 11

```

```

151 ALA=C3
GOTO 7
4 IF (ABS(D11*D12)<EPP) GOTO 44
A2=A2+HC
B2=B2+HC
D12=D11
IF (B2 - PVC<0.010D - 000) GOTO 51
7 END
SUBROUTINE DETER(ALL,DET,NP)
IMPLICIT REAL(8) (A - Z)
INTEGER NP,I,J
COMMON /F/ AL1(0:100,0:100), C(0:100,0:100),
B(0:100,0:100),AD(0:100,0:100),AL(0:100,0:100),Y(0:100),
AN(0:100),D(0:100),X(0:100),SV(0:100),H(0:100,0:100)
! ***** CALCULATION OF THE ! MATRIX DETERMINANT
*****
DO I=1,NP
DO J=1,NP
AL(I,J)=(H(I,J) - ALL*AL1(I,J))
B(I,J)=0.0D - 000
C(I,J)=0.0D - 000
ENDDO
ENDDO
CALL TRIAN(AL,B,C,DET,NP)
END
SUBROUTINE SVV(ALL,NP,XP)
IMPLICIT REAL(8) (A - Z)
INTEGER NP,I,J,K
COMMON /F/
AL1(0:100,0:100),C(0:100,0:100),B(0:100,0:100),AD(0:100,0:100),AL(0:
100,0:100),Y(0:100),AN(0:100),D(0:100),X(0:100),SV(0:100),H(0:100,0:1
00)
DIMENSION XP(0:100)
! ***** EIGENVECTORS *****
! —— - - FORMING OF THE MATRIX —— - -
CALL MAT(XP,NP)

```

```

! --- -- PREPARATION OF THE MATRIX ----- -
DO I=1, NP
DO J=1, NP
AL(I,J)=(H(I,J) - ALL*AL1(I,J))
B(I,J)=0.0D - 000
C(I,J)=0.0D - 000
ENDDO
ENDDO
DO I=1, NP - 1
DO J=1, NP - 1
AD(I,J)=AL(I,J)
ENDDO
ENDDO
DO I=1,NP - 1
D(I)= - AL(I,NP)
ENDDO
NP=NP - 1
CALL TRIAN(AD,B,C,DET,NP)
! - - - - - CALCULATION OF THE VECTORS - - - - -
Y(1)=D(1)/B(1,1)
DO I=2, NP
S=0.0D - 000
DO K=1, I - 1
S=S+B(I,K)*Y(K)
ENDDO
Y(I)=(D(I) - S)/B(I,I)
ENDDO
X(NP)=Y(NP)
DO I=NP - 1,1, - 1
S=0.0D - 000
DO K=I+1,NP
S=S+C(I,K)*X(K)
ENDDO
X(I)=Y(I) - S
ENDDO
DO I=1, NP

```

```

SV(I)=X(I)
ENDDO
NP=NP+1
SV(NP)=1
S=0.0D - 000
DO I=1, NP
S=S+SV(I)**2
ENDDO
DO I=1, NP
SV(I)=SV(I)/SQRT(S)
ENDDO
! --- - - CALCULATION OF RESIDUALS -----
DO I=1, NP
S=0.0D - 000
SS=0.0D - 000
DO J=1, NP
S=S+H(I,J)*SV(J)
SS=SS+ALL*AL1(I,J)*SV(J)
ENDDO
AN(I)=S - SS
ENDDO
PRINT *, '                H*SV - LA*L*SV=0'
DO I=1, NP
PRINT *, I, AN(I)
ENDDO
END
SUBROUTINE TRIAN(AD,B,C,DET,NP)
IMPLICIT REAL(8) (A - Z)
INTEGER NP,I,J
COMMON /D/ AA(0:100,0:100)
DIMENSION B(0:100,0:100),C(0:100,0:100),AD(0:100,0:100)
! EXPANSION OF MATRIX TO THE TRIANGULAR MATRIXES
AD=B*C
DO I=1,NP
C(I,I)=1.0D - 000
B(I,1)=AD(I,1)

```

```

C(1,I)=AD(1,I)/B(1,1)
ENDDO
DO I=2, NP
DO J=2, NP
S=0.0D - 000
IF (J>I) GOTO 551
DO K=1, I - 1
S=S+B(I,K)*C(K,J)
ENDDO
B(I,J)=AD(I,J) - S
GOTO 552
551 S=0.0D - 000
DO K=1, I - 1
S=S+B(I,K)*C(K,J)
ENDDO
C(I,J)=(AD(I,J) - S)/B(I,I)
552 ENDDO
ENDDO
S=1.0D - 000
DO K=1, NP
S=S*B(K,K)
ENDDO
DET=S
! - - - - - CALCULATION OF RESIDUALS - - - - -
GOTO 578
SS=0.0D - 000
DO I=1, NP
DO J=1, NP
S=0.0D - 000
DO K=1, NP
S=S+B(I,K)*C(K,J)
ENDDO
AA(I,J)=S - AD(I,J)
SS=SS+AA(I,J)
ENDDO
ENDDO

```



```

PRINT *, '                                N = AD - B*C = 0'
DO I=1, NP
DO J=1, NP
PRINT *,AD(I,J),AA(I,J)
ENDDO
ENDDO
578 END

SUBROUTINE WW(SK,L,GK,R,WH)
IMPLICIT REAL(8) (A - Z)
INTEGER I,L,NN
DIMENSION F(0:1000000)
! ***** WHITTAKER FUNCTION *****
SS=DSQRT(ABS(SK))
AA=GK/SS
BB=L
ZZ=1.0D - 000+AA+BB
GAM=DGAMMA(ZZ)
RR=R
CC=2.0D - 000*RR*SS
NN=30000
HH=0.001D - 000
DO I=0, NN
TT=HH*I
F(I)=TT**(AA+BB)*(1.0D - 000+TT/CC)**(BB - AA)*DEXP( - TT)
ENDDO
CALL SIM(F,NN,HH,SI)
WH=SI*DEXP( - CC/2.0D - 000)/(CC**AA*GAM)
END

SUBROUTINE SIM(V,N,H,SI)
IMPLICIT REAL(8) (A - Z)
INTEGER I,J,N
! ***** INTEGRAL OVER SIMPSON *****
DIMENSION V(0:10240000)
A=0.0D - 000
B=0.0D - 000
DO I=1,N - 1,2

```

```

B=B+V(I)
ENDDO
DO J=2,N - 2, 2
A=A+V(J)
ENDDO
SI=H*(V(0)+V(N)+2.0D - 000*A+4.0D - 000*B)/3.0D - 000
END
SUBROUTINE ASIMP(R,SK,GK,L,N,C0,CW0,CW)
IMPLICIT REAL(8) (A - Z)
INTEGER L,N
COMMON /G/ FF(0:10240000)
! ***** ASYMPTOTIC CONSTANT *****
SS=SQRT(ABS(SK))
SQ=SQRT(2.0D - 000*SS)
GG=GK/SS
CALL WW(SK,L,GK,R,WWW)
CW=FF(N)/WWW/SQ
C0=FF(N)/(EXP( - SS*R)*SQ)
CW0=C0*(R*SS*2.0D - 000)**GG
END

```

Now we will do the control calculation on this program for the  ${}^4\text{He}^3\text{H}$  system with the same values of the variational parameters  $\beta$ , which are listed above in Table 14.4.

#### BETTA

1	6.567905679421632E - 001
2	1.849427298619411E - 002
3	1.729324040753008E - 001
4	4.173925751998056E - 002
5	8.818471551829664E - 002
6	4.503350223878621E - 001
7	9.210585557350788E - 001
8	2.000570770210328E +000
9	2.925234985697186E +000
10	3.981951253509630E +000

$$H*SV - LA*L*SV=0$$

- 1 1.443289932012704E - 015
- 2 2.842170943040401E - 014
- 3 3.019806626980426E - 014
- 4 4.973799150320701E - 014
- 5 2.486899575160351E - 014
- 6 2.831068712794149E - 015
- 7 1.887379141862766E - 015
- 8 4.718447854656915E - 016
- 9 2.775557561562891E - 016
- 10 3.122793690302217E - 012

### VECTORS

- 1 4.270672897023774E - 001
- 2 - 6.326508827916876E - 004
- 3 - 2.047665503209801E - 001
- 4 - 1.032337189382823E - 002
- 5 - 6.301223045637849E - 002
- 6 6.962475100484991E - 001
- 7 2.076348108196292E - 002
- 8 1.488689730498523E - 003
- 9 - 1.124701190142763E - 003
- 10 3.797299221855067E - 004

$$N = 9.99999999917769E - 001$$

$R$	$C_0$	$C_{w0}$	$C_w$
6.25000	- 3.17695	- 5.00114	- 3.91393
7.50000	- 2.92688	- 4.83283	- 3.91798
8.75000	- 2.73971	- 4.71016	- 3.92041
10.00000	- 2.59384	- 4.61811	- 3.92311
11.25000	- 2.46513	- 4.52645	- 3.90849
12.50000	- 2.36455	- 4.46326	- 3.90566
13.75000	- 2.30063	- 4.45237	- 3.93964
15.00000	- 2.24363	- 4.44216	- 3.96770
16.25000	- 2.14262	- 4.33204	- 3.90062

17.50000	- 1.96194	- 4.04448	- 3.66720
18.75000	- 1.70026	- 3.56895	- 3.25584
20.00000	- 1.38590	- 2.95868	- 2.71369
21.25000	- 1.06010	- 2.29936	- 2.11909
22.50000	- .76060	- 1.67464	- 1.54998
23.75000	- .51202	- 1.14341	- 1.06238
25.00000	- .32355	- .73229	- .68278

$$RM = , \quad RZ = 2.50 , \quad 2.46$$

ENERGY

$$E = - 2.466997950$$

Here some other values of eigenvectors are given, than it was listed in Table 14.4, it is connected with use of other calculation accuracy and really does not influence on the shape of WF that is seen from the value of its normalization  $N$ .

### **Conclusion**

Thereby, on the basis of classification of the orbital states according to Young tableaux it is possible to construct interaction potentials of clusters, which directly describe either elastic scattering phase shifts or basic characteristics of bound states of nuclei in the corresponding cluster channels. It is possible, as opposed to lighter systems [60,107], due to the absence of the Young tableaux mixing in bound states and due to the big degree of clusterization of such nuclei in the cluster  ${}^3\text{He}{}^4\text{He}$ ,  ${}^3\text{H}{}^4\text{He}$  and  ${}^2\text{H}{}^4\text{He}$  channels [21,213]. Consequently, the considered potential cluster model allows one to describe the last experimental data on the astrophysical  $S$ -factors of the radiative capture reactions  ${}^4\text{He}({}^3\text{He}, \gamma){}^7\text{Be}$  and  ${}^4\text{He}({}^3\text{H}, \gamma){}^7\text{Li}$  at low energies and gives their values at zero energies that quite conform, in the limit of experimental ambiguities, with the available experimental data. As concerns the  ${}^2\text{H}{}^4\text{He}$  system in  ${}^6\text{Li}$ , in the present time there are no enough accurate experimental data for the astrophysical  $S$ -factor of the radiative capture reaction  ${}^4\text{He}({}^2\text{H}, \gamma){}^6\text{Li}$  at low energies. They are necessary even though at the range of  $70\div 500$  keV, but with smaller

than in work [249] errors. The obtaining of these data allows one to do more concrete conclusions about the shape and the value of the  $S$ -factor at low and zero energy [134].

# **15. THE $^{12}\text{C}(^4\text{He},\gamma)^{16}\text{O}$ RADIATIVE CAPTURE REACTION**

---

## ***Introduction***

Now let us consider the process of  $^{12}\text{C}(^4\text{He},\gamma)^{16}\text{O}$  radiative capture which, along with triple helium capture, is present in the chain of fusion reactions at the hot stage of star formation when the temperature inside the star is hundreds of millions of Kelvin [254]. At such a high temperature, the interacting particles have sufficient energy to considerably increase the probability of penetration of the Coulomb barrier to the region of strong interaction and, therefore, for increasing the contribution of this reaction to the total energy balance of the star.

The considered reaction results in the formation of the stable  $^{16}\text{O}$  nucleus, which is an intermediate link in the process of formation of heavier elements, for example, in the reactions  $^{16}\text{O}(^4\text{He},\gamma)^{20}\text{Ne}$  and  $^{20}\text{Ne}(^4\text{He},\gamma)^{24}\text{Mg}$ , etc. [2,118]. Therefore, knowledge of the cross section of this reaction and its energy dependence is important for nuclear astrophysics. However, great uncertainties in accurate determination of the reaction rate for the  $^{12}\text{C}(^4\text{He},\gamma)^{16}\text{O}$  process existed for a long time, and a relatively short time ago new experimental data in an energy range of 1.9÷4.9 MeV [255] appeared that have comparatively high precision and probably eliminate most of these uncertainties.

In this section we present the results of the phase shift analysis of the elastic  $^4\text{He}^{12}\text{C}$  scattering at low energies that we performed. Note that in different nuclear systems, depending on the energy of colliding particles, the number of parameters of the multivariate variational problem formulated for the search of scattering phase shifts can vary from 1÷2 to 20÷40 [89,256]. Then the found elastic scattering phase shifts will be used to construct potentials of the  $^4\text{He}^{12}\text{C}$  interaction in

continuous spectrum, which provide a correct description of the obtained scattering phase shifts and energies of bound states of  $^{16}\text{O}$  under assumption of the  $^4\text{He}^{12}\text{C}$  cluster configuration. Finally, the modified potential cluster model will be used to study the possibility of description of the astrophysical  $S$ -factor of the  $^{12}\text{C}(^4\text{He},\gamma)^{16}\text{O}$  radiative capture at low energies.

### 15.1 Differential cross sections

In the case of elastic scattering of nonidentity particles with zero spin, the expression for the cross section takes the simplest form [46]

$$\frac{d\sigma(\theta)}{d\Omega} = |f(\theta)|^2, \quad (15.1)$$

where the total scattering amplitude  $f(\theta)$  is represented as the sum of the Coulomb  $f_c(\theta)$  and nuclear  $f_N(\theta)$  amplitudes

$$f(\theta) = f_c(\theta) + f_N(\theta),$$

which are expressed in terms of nuclear ( $\delta_L \rightarrow \delta_L + i\Delta_L$ ) and Coulomb ( $\sigma_L$ ) scattering phase shifts; the form of these amplitudes is given in Section 5. We have the next form for the total cross section of the elastic scattering at  $f_c = 0$

$$\sigma_s = \frac{\pi}{k^2} \sum_L \left[ (2L+1) \left( |1 - S_L|^2 \right) \right] = \frac{4\pi}{k^2} \sum_L (2L+1) \eta_L^2 \sin^2 \delta_L.$$

Summation in this expression carries out over all possible  $L$  and till the certain  $L_{\max}$ , which can be equal to the values from  $1 \div 3$  to  $5 \div 6$  due to the energy of  $\alpha$ -particles.

### 15.2 Phase shift analysis

Let us present the results of the phase shift analysis obtained for the

$^4\text{He}^{12}\text{C}$  elastic scattering in the region from 1.5 to 6.5 MeV. Earlier the phase shift analysis of the differential cross sections at energies of 2.5÷5 MeV was performed in [257]. The potential description of such scattering phase shifts based on potentials with forbidden states was performed in [258]. Furthermore, in [259] very thorough phase shift analysis of experimental data for 49 energies from 1.5 to 6.5 MeV was performed. We used this data to perform our phase shift analysis at energies of 1.466, 1.973, 2.073, 2.870, 3.371, 4.851, 5.799 and 6.458 MeV. The results of our analysis are given in Tables 15.1÷15.8, together with the average values of  $\chi^2$ , in comparison with tabulated data from [259]. Furthermore, the spectrum of resonance levels observed in the elastic  $^4\text{He}^{12}\text{C}$  scattering [260] was given in Table 15.9.

**Table 15.1. Results of phase shift analysis of the  $^4\text{He}^{12}\text{C}$  elastic scattering and their comparison with data [259] at 1.466 MeV**

$E_{l.s.} = 1.466 \text{ MeV } (\chi^2 = 0.055)$		
$L$	$\delta^\circ (\text{our})$	$\delta^\circ [\text{259}]$
0	-0.2	$0.5 \pm 1.0$
1	-0.4	$-0.1 \pm 1.0$
2	-1.1	$-0.8 \pm 1.0$

**Table 15.2. Results of phase shift analysis of the  $^4\text{He}^{12}\text{C}$  elastic scattering and their comparison with data [259] at 1.973 MeV**

$E_{l.s.} = 1.973 \text{ MeV } (\chi^2 = 0.077)$		
$L$	$\delta^\circ (\text{our})$	$\delta^\circ [\text{259}]$
0	-2.6	$-0.5 \pm 1.0$
1	0.0	$0.9 \pm 1.7$
2	-1.2	$-0.1 \pm 1.3$

**Table 15.3. Results of phase shift analysis of the  $^4\text{He}^{12}\text{C}$  elastic scattering and their comparison with data [259] at 2.073 MeV**

$E_{l.s.} = 2.073 \text{ MeV } (\chi^2 = 0.029)$		
$L$	$\delta^\circ (\text{our})$	$\delta^\circ [\text{259}]$
0	-1.2	$0 \pm 0.8$
1	-0.1	$0.1 \pm 1.2$
2	-1.1	$-0.6 \pm 0.9$

**Table 15.4. Results of phase shift analysis of the  $^4\text{He}^{12}\text{C}$  elastic scattering and their comparison with data [259] at 2.870 MeV**

$E_{l.s.} = 2.87 \text{ MeV } (\chi^2 = 0.038)$		
$L$	$\delta^\circ (\text{our})$	$\delta^\circ [\text{259}]$
0	-3.1	$-2.1 \pm 1.1$
1	21.3	$22.0 \pm 2.1$
2	0.0	$0.4 \pm 0.9$
3	0.5	$1.0 \pm 0.5$



**Table 15.5. Results of phase shift analysis of the  $^4\text{He}^{12}\text{C}$  elastic scattering and their comparison with data [259] at 3.371 MeV**

$E_{l.s.} = 3.371 \text{ MeV } (\chi^2 = 0.31)$		
$L$	$\delta^\circ$ (our)	$\delta^\circ$ [259]
0	169.4	—
1	103.4	103.7 $\pm$ 1.7
2	-1.7	0.0 $\pm$ 0.7
3	0.2	0.8 $\pm$ 0.6

**Table 15.6. Results of phase shift analysis of the  $^4\text{He}^{12}\text{C}$  elastic scattering and their comparison with data [259] at 4.851 MeV**

$E_{l.s.} = 4.851 \text{ MeV } (\chi^2 = 0.26)$		
$L$	$\delta^\circ$ (our)	$\delta^\circ$ [259]
0	164.2	164 $\pm$ 1.1
1	128.4	129.5 $\pm$ 0.9
2	177.1	178.8 $\pm$ 0.9
3	15.5	16.4 $\pm$ 0.8
4	176.9	177.2 $\pm$ 0.8
5	-0.3	0.5 $\pm$ 0.5

**Table 15.7. Results of phase shift analysis of the  $^4\text{He}^{12}\text{C}$  elastic scattering and their comparison with data [259] at 5.799 MeV**

$E_{l.s.} = 5.799 \text{ MeV } (\chi^2 = 0.37)$		
$L$	$\text{Re}\delta^\circ$ (our)	$\text{Re}\delta^\circ$ [259]
0	162.2	—
1	128.2	—
2	83.2	82.3 $\pm$ 0.6
3	86.0	—
4	173.8	175.3 $\pm$ 0.7
5	-1.0	0.2 $\pm$ 0.4

**Table 15.8. Results of phase shift analysis of the  $^4\text{He}^{12}\text{C}$  elastic scattering and their comparison with data [259] at 6.458 MeV**

$E_{l.s.} = 6.458 \text{ MeV } (\chi^2 = 0.41)$		
$L$	$\delta^\circ$ (our)	$\delta^\circ$ [259]
0	151.2	153 $\pm$ 2.5
1	115.8	119.4 $\pm$ 2.1
2	172.2	172.2 $\pm$ 1.9
3	120.8	122.0 $\pm$ 2.4
4	176.4	179.1 $\pm$ 1.2
5	0.8	2.2 $\pm$ 0.8
6	0.1	0.4 $\pm$ 0.4

It can be seen from these tables that the energy of the  $^4\text{He}^{12}\text{C}$  scattering of 3.371 MeV corresponds to a level of 3.324 MeV with a width of 480 $\pm$ 20 keV. Although in tables from [259] the phase shift for the  $S$  wave is not given (it is a blank cell in Table 15.5) for this energy, our phase shift analysis based on real scattering phase shifts makes it possible to determine this phase shift, which is presented in Table 15.5

with  $\chi^2 = 0.31$  and 10% errors of determination of experimental data from the figure in [259].

The energy of 5.799 MeV exactly corresponds to a level of  $5.809 \pm 18$  MeV, and the tables in [259] do not contain the values of scattering phase shifts for some partial waves (blank cells in Table 15.7). In our phase shift analysis, it is possible to describe the differential scattering cross sections with the average  $\chi^2 = 0.37$  and find all partial phase shifts.

**Table 15.9. Level spectrum of  $^{16}\text{O}$  in the elastic  $^4\text{He}^{12}\text{C}$  scattering with the isospin  $T = 0$  [260]. Here,  $J^\pi$  is the total angular momentum and parity,  $E_{L.s.}$  is the energy of incident  $\alpha$ -particle, and  $\Gamma_{c.m.}$  is the level width**

$E_{L.s.}$ (MeV)	$J^\pi$	$\Gamma_{c.m.}$ (keV)
3.324	$1^-$	$480 \pm 20$
$3.5770 \pm 0.5$	$2^+$	$0.625 \pm 0.1$
4.259	$4^+$	$27 \pm 3$
$5.245 \pm 8$	$4^+$	$0.28 \pm 0.05$
5.47	$0^+$	2500
$5.809 \pm 18$	$2^+$	$73 \pm 5$
$5.92 \pm 20$	$3^-$	$800 \pm 100$
$6.518 \pm 10$	$0^+$	$1.5 \pm 0.5$
$7.043 \pm 4$	$1^-$	$99 \pm 7$

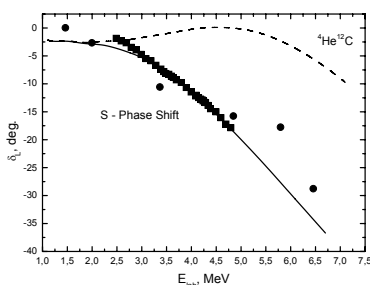


Fig. 15.1. The  $S$  phase shift of the elastic  $^4\text{He}^{12}\text{C}$  scattering. Squares show data of [257]. Points show our results [261] obtained by using data from [259]. Curves show results of calculations with found potentials.

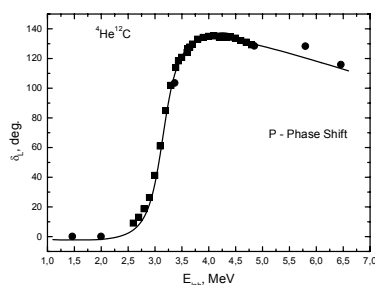


Fig. 15.2. The  $P$  phase shift of the elastic  $^4\text{He}^{12}\text{C}$  scattering. Conventional signs are the same as in Fig. 15.1.

Other non-resonance energies (2.870, 4.851, and 6.458 MeV) are described by phase shifts that coincide with data from [259] within phase shift errors given in [259] and with account of possible 10% errors of our determination of experimental data from figures in [259]. The first three energy values of 1.466, 1.973 and 2.073 MeV, in essence, are compatible with zero values of nuclear phase shifts and correspond to pure Coulomb, i.e., Rutherford, scattering.

The slight differences in scattering phase shifts obtained here and in work [259], may be caused by the different values of constants and particle masses that are used in such analysis. For example, exact values of particle masses [36] or their integer values can be used and the constant  $\hbar^2/m$  can be taken equal, for example, to 41.47 or, more accurately, 41.4686 MeV fm<sup>2</sup>. We estimate the accuracy of phase shift determination in the performed phase shift analysis based on data from [259] to be on a level of  $1^\circ \div 2^\circ$ .

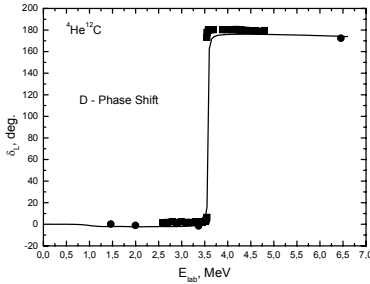


Fig. 15.3. The *D* phase shift of the elastic  ${}^4\text{He}^{12}\text{C}$  scattering. Conventional signs are the same as in Fig. 15.1.

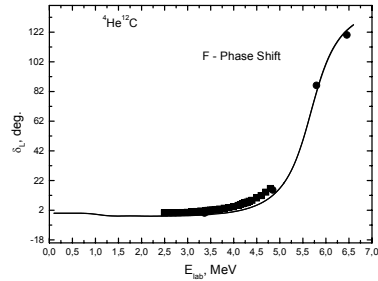


Fig. 15.4. The *F* phase shift of the elastic  ${}^4\text{He}^{12}\text{C}$  scattering. Conventional signs are the same as in Fig. 15.1.

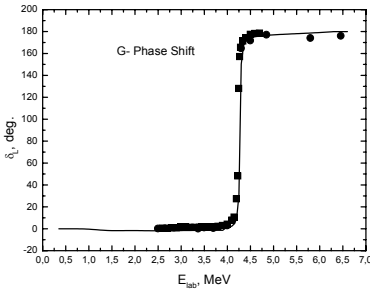


Fig. 15.5. The *G* phase shift of the elastic  ${}^4\text{He}^{12}\text{C}$  scattering. Conventional signs are the same as in Fig. 15.1.

Figures 15.1÷15.5 show the comparison of results of our phase shift analysis [261] carried out by using experimental data from [259] (points)

and phase shift analysis from [257] (squares). It can be seen from Tables 15.1÷15.8 and Figs. 15.1÷15.5 that the obtained phase shifts practically coincide with the results of [259] but somewhat differ from data of [257], especially as regards the  $S$  wave. Generally, it is clear, because the analysis [257] was done in the beginning of 60<sup>th</sup>, when there were no computing technique practically and the software only begin to develop, but work [259] was done in the end of 80<sup>th</sup> at highly developed computer and software systems.

### ***15.3 Description of the scattering phase shifts in the potential model***

Before going to construction of the potentials, let us first consider the classification of orbital states of the  ${}^4\text{He}{}^{12}\text{C}$  system which makes it possible to determine the total number of forbidden states in the  $S$  wave interaction. The potentials obtained as a result can be used further for calculation of the astrophysical  $S$ -factors of the capture reaction  ${}^{12}\text{C}({}^4\text{He},\gamma){}^{16}\text{O}$  [34].

Possible orbital Young tableaux of the  ${}^4\text{He}{}^{12}\text{C}$  system are defined by the Littlewood's theorem [123], which in this case yields  $\{444\} \times \{4\} = \{844\} + \{754\} + \{7441\} + \{664\} + \{655\} + \{6442\} + \{6541\} + \{5551\} + \{5542\} + \{5443\} + \{4444\}$  [258]. Young tableaux  $\{4\}$  and  $\{444\}$  correspond to  ${}^4\text{He}$  and  ${}^{12}\text{C}$  nuclei in the ground state. According to rules [123], the conclusion can be drawn that only the Young tableau  $\{4444\}$  is Pauli-allowed for  ${}^{16}\text{O}$ , all other orbital configurations are forbidden. In particular, all possible configurations in which the first row contains a number larger than four cells cannot exist, since the  $s$ -shell cannot contain more than four nucleons.

Orbital angular moments corresponding to different Young tableaux can be determined using Elliott's rule [123]. Consequently, we find that the states of  ${}^{16}\text{O}$  with the angular moment  $L = 0$  in the  ${}^4\text{He}{}^{12}\text{C}$  system correspond to the following orbital tableaux:  $\{4444\}$ ,  $\{5551\}$ ,  $\{664\}$ ,  $\{844\}$ , and  $\{6442\}$ . This result can be used for determination of the number of bound forbidden states in the potential of the ground state. Since in the ground state only symmetry  $\{4444\}$  is allowed, and the other four Young tableaux are forbidden, the potential of the  ${}^4\text{He}{}^{12}\text{C}$  interaction should have four bound forbidden states and one allowed bound state [258].

$^{16}\text{O}$  $^4\text{He}^{12}\text{C}$	G	$4^+$	3.19
	D	$2^+$	2.69
	P	$1^+$	2.46
	1P	$1^-$	-0.045
	1D	$2^+$	-0.245
	1F	$3^+$	-1.032
	2S	$0^+$	-1.113
	1S	$0^+$	-7.162

Fig. 15.6. Level spectrum of  $^{16}\text{O}$ .

Earlier in [258] the parameters of potential of form (2.8) with spherical Coulomb interaction [46] and  $R_{\text{Coul.}} = 3.55$  fm for the ground state of the  $^4\text{He}^{12}\text{C}$  system of  $^{16}\text{O}$  have been obtained. This potential was constructed based on the requirement of description of such characteristics as binding energy, charge radius, Coulomb form factor at small transferred moments and probabilities

of electromagnetic transitions between bound levels.

Then in [262] the parameters of potential of the ground 1S state [201] were specified (see Fig. 15.6) for  $^{16}\text{O}$  in the  $^4\text{He}^{12}\text{C}$  channel and, for the same Coulomb radius, it was obtained that

$$V_{1S} = -256.845472 \text{ MeV}, \quad \alpha = 0.189 \text{ fm}^{-2}. \quad (15.2)$$

The finite-difference method [26] on the basis of the computer programs was used for obtaining a binding energy of  $-7.161950$  MeV for this potential compared to an experimental value of  $-7.16195$  MeV [260] and a charge radius of  $2.705$  fm for the  $^4\text{He}$  radius of  $1.671(14)$  fm [72] and the  $^{12}\text{C}$  radius of  $2.4829(19)$  fm [161]. The experimental value of the  $^{16}\text{O}$  radius is equal to  $2.710(15)$  fm [260]. This potential has forbidden states at four energies  $-37.6$ ,  $-80.8$ ,  $-134.5$ , and  $-197.2$  MeV according to the classification of forbidden and allowed states.

For the potential of the first excited 2S level with an experimental energy of  $-1.113$  MeV [260] that is correctly reproduced by this potential, more accurate parameters were obtained

$$V_{2S} = -143.1092 \text{ MeV}, \quad \alpha = 0.111 \text{ fm}^{-2}.$$

This potential leads to the energies of FSs at  $-16.9$ ,  $-40.5$ ,  $-70.6$  and  $-106.1$  MeV.

For the 1F state of  $^{16}\text{O}$  in the  $^4\text{He}^{12}\text{C}$  channel, the following parameters have been obtained

$$V_{1F} = -191.4447 \text{ MeV}, \quad \alpha = 0.277 \text{ fm}^{-2}.$$

The potential yields energy of the bound state of  $-1.032 \text{ MeV}$ , which agrees with data [260] and contains one forbidden bound state at the energy of  $-38.3 \text{ MeV}$ .

For the parameters of the bound state potential in the  $1D$  wave shown in Fig. 15.6, the following was obtained

$$V_{1D} = -90.3803 \text{ MeV}, \quad \alpha = 0.1 \text{ fm}^{-2}.$$

This results in energy of the bound level of  $-0.245 \text{ MeV}$ , in complete agreement with data of [260] and contains two forbidden bound states at  $-14.0$  and  $-34.3 \text{ MeV}$ .

At the refinement of parameters of the bound state potential in the  $1P$  wave (Fig. 15.6), the following values were obtained [262]

$$V_{1P} = -161.2665 \text{ MeV}, \quad \alpha = 0.16 \text{ fm}^{-2}.$$

This potential exactly reproduces the energy of the bound state of  $-0.045 \text{ MeV}$  and has three forbidden states at  $-20.4$ ,  $-52.0$ , and  $-92.5 \text{ MeV}$ .

The following energy was obtained using the variational method with expansion of the wave function over the non-orthogonal Gaussian basis with the basis dimensionality  $N=8$  for the ground  $1S$  state of  ${}^{16}\text{O}$  with potential parameters (15.2):  $-7.16194 \text{ MeV}$ , i.e., lower by approximately  $10 \text{ eV}$  than the experimental value. The parameters of the variational wave function of relative cluster motion in the ground state of  ${}^{16}\text{O}$  of form (2.9) are given in Table 15.10.

**Table 15.10. Variational parameters and expansion coefficients of the radial wave function of the bound state of the  ${}^4\text{He}^{12}\text{C}$  system for potential (15.2). Normalization of the wave function with these coefficients in an interval of  $0\div 25 \text{ fm}$  is  $N = 1.0000000000000735$**

$i$	$\beta_i$	$C_i$
1	8.763690790288099E-002	-1.911450719348557E-001
2	1.866025286442256E-001	-2.207934474863762

3	4.827753981321283E-001	28.389690447396200
4	8.199789461942612E-001	-96.796133806414110
5	1.201089178851195	117.191836404848400
6	1.811929119752430	-48.033080106666700
7	2.549438805955688	-8.312967983049469E-001
8	6.019066491886866	2.748007062675085E-003

A value of 2.697 fm was obtained for the charge radius; this value is just slightly smaller than the result of finite-difference calculation. However, it should be noted that it is as of yet impossible to construct a wave function with large basis dimensionality  $N$ , as was usually done for lighter cluster systems (see, e.g., [60]); therefore, the values of this wave function already for  $R > 7.5$  fm decrease more rapidly than it follows from asymptotics (2.10). If this wave function is used, it should be matched with the asymptotic expression at distances of an order of 7.0–7.5 fm. Only a basis dimensionality of 10 or higher can provide correct asymptotics of the variational wave function at distances of the order of 10–15 fm [60].

The potential of the ground  $1S$  state does not result in the correct  $S$  scattering phase shift, as shown in Fig. 15.6 by the dashed line. In order to describe the phase shifts obtained from the phase shift analysis, it is necessary to change its depth and take

$$V_0 = -155 \text{ MeV}, \quad \alpha = 0.189 \text{ fm}^{-2}$$

with the same Coulomb radius. The results of calculation of the  $S$  phase shift with this potential are shown in Fig. 15.6 by the solid line. The potential also contains four bound forbidden states at energies of -1.3, -25.1, -61.5, and -107.7 MeV; it can be seen from Fig. 10.6 that this potential reasonably describes the  $S$  phase shift obtained in [257].

For the  $P$ ,  $D$ ,  $F$  and  $G$  scattering waves the interaction potentials different from potentials of bound states were obtained. The parameters of these potentials and energies of forbidden states (units in MeV) ( $R_{\text{Coul}} = 3.55$  fm) are as follows

$$V_P = -145.0 \text{ MeV}, \quad \alpha_P = 0.160 \text{ fm}^{-2}, \quad \text{FSs: } -13.6, -42.1, -79.7;$$

$$V_D = -435.25 \text{ MeV}, \quad \alpha_D = 0.592 \text{ fm}^{-2}, \quad \text{FSs: } -61.9; -167.0;$$

$$V_F = -73.4 \text{ MeV}, \quad \alpha_F = 0.125 \text{ fm}^{-2}, \quad \text{FSs: } -7.5;$$

$$V_G = -55.55 \text{ MeV}, \quad \alpha_G = 0.1 \text{ fm}^{-2}, \quad \text{FSs: no.}$$

The results of the phase shift calculation for these potentials are shown in Figs. 15.7÷15.10 by the solid lines, and, evidently, they give a correct general behavior of the experimental scattering phase shifts.

Thus, the potentials of the  ${}^4\text{He}^{12}\text{C}$  interaction for scattering states and discrete levels have been obtained that correctly describe elastic scattering phase shifts and channel state energies. The difference of potentials describing scattering phase shifts from potentials describing characteristics of the bound states can be explained by the small contribution of the considered channel in the bound states of  ${}^{16}\text{O}$ . It is possible that the simple cluster  ${}^4\text{He}^{12}\text{C}$  model of  ${}^{16}\text{O}$ , unlike lighter nuclei [88], is incapable of complete description of different characteristics of  ${}^{16}\text{O}$  in the  ${}^4\text{He}^{12}\text{C}$  channel and scattering processes on the basis of unified potentials.

### 15.4 Astrophysical *S*-factor

Let us consider the astrophysical *S*-factor of the radiative capture reaction  ${}^{12}\text{C}({}^4\text{He}, \gamma){}^{16}\text{O}$  at energies from 0.3 to 4.0 MeV based on the modified potential cluster model and compare it with the results of new experimental data from [255]. It is assumed that experimental data obtained below 2.5 MeV are due to the *E1* transition [255]. However, in the considered model, this transition is possible only due to the difference of the particle masses from corresponding integer values. The results of calculation of the *S*-factor of this transition turned out to be lower by two to three orders of magnitude than the experimental data, although the obtained *S*-factor has a correct form due to the resonance behavior of the *P* scattering phase shift [258].

Thus, the model under consideration cannot correctly describe experimental data based on the *E1* process. However, in the framework of the MPCM with FSs, these data are reasonably described based on the *E2* transitions from different partial scattering waves to the ground bound state



and some excited bound levels of  $^{16}\text{O}$  shown in Fig. 15.6. These results can be of particular interest from the point of view of demonstration of the general capabilities of the modified potential cluster model if the presence of the  $E2$  processes in the considered radiative capture at low energies is assumed.

Therefore, below we consider the  $E2$  transitions only; the first of these transitions is the transition from the  $D$  scattering wave to the ground bound  $1S$  state of  $^{16}\text{O}$ . This process results in the  $S$ -factor shown in Fig. 15.7 by the dash-dotted line. The obtained  $S$ -factor reasonably explains the experiment at energies from 0.9 to 3.0 MeV but does not describe the resonance at 2.46 MeV, since this resonance is due to the behavior of the  $P$  scattering phase shift in this energy region. At energies from 2.5 to 3.0 MeV, the calculated  $S$ -factor on the whole represents the position and height of the peak due to the resonance in the  $D$  scattering wave at an energy of 2.69 MeV, but the level width is somewhat larger than the experimental one. This indicates insufficiently high growth of the calculated  $D$  scattering phase shift in the resonance region at 2.69 MeV.

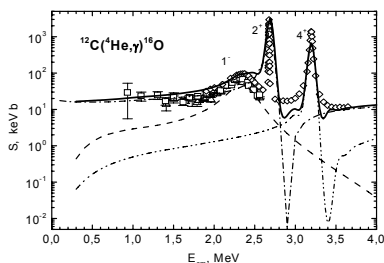


Fig. 15.7. Astrophysical  $S$ -factor of the radiative capture  $^{12}\text{C}(^4\text{He}, \gamma)^{16}\text{O}$ . Squares show experimental data from review [34], open triangles from [263,264], and open rhombs [255]. Curves show calculations of the  $S$ -factor for different  $E2$  transitions.

If it is assumed that the experiment includes transitions to the  $1P$  level, then the  $E2$  process from the  $P$  scattering wave to the bound  $1P$  state of  $^{16}\text{O}$  at energy of  $-0.045$  MeV (Fig. 15.6) can be considered. The results of this calculation shown in Fig. 15.7 by a dashed line quite well reproduce the form of the resonance at 2.46 MeV.

The double-dash-dotted line shows the results of the calculation of possible  $E2$  transition from the  $G$  scattering wave to the  $1D$  bound state, which correctly reproduces the position and width of maximum of  $4^+$  resonance but its value turns out to be lower by approximately a factor of 2 than the experimental value. It should be noted that we did not succeed in finding the parameters of the potential for the  $G$  wave such that the value of the  $S$ -factor at  $4^+$  resonance energy was described correctly. If we will use potentials with another number of forbidden states, then, for the  $G$  wave

with one FS

$$V_G = -110.7 \text{ MeV}, \quad \alpha_G = 0.127 \text{ fm}^{-2}, \quad \text{FS: } -13.6 \text{ MeV}$$

or two FS

$$V_G = -222.4 \text{ MeV}, \quad \alpha_G = 0.127 \text{ fm}^{-2}, \quad \text{FS: } -42.8; -14.6 \text{ MeV},$$

the calculated peak magnitude of  $4^+$  resonance appreciably noticeably decreases, and, then reduction of the number of FSs in the bound  $1D$  state to one

$$V_D = -254.8 \text{ MeV}, \quad \alpha_D = 0.592 \text{ fm}^{-2}, \quad \text{FS: } -57.0 \text{ MeV}$$

or generally without FSs

$$V_D = -57.7833 \text{ MeV}, \quad \alpha_D = 0.1 \text{ fm}^{-2}$$

does not lead to the essential rising of the  $S$ -factor in the range of the  $4^+$  resonance.

The solid line in Fig. 15.7 shows the sum of all three  $E2$  transitions, which, on the whole, describes the experimental behavior of the astrophysical  $S$ -factor at energies from 0.9 to 4.0 MeV. Our calculated  $S$ -factor at 300 keV caused by the  $E2$  process with transition from the  $D$  wave to the ground state of the nucleus turns out to be equal to 16.0 keV b, and at 100 keV its value is somewhat higher: 17.5 keV b. However, these results are noticeably lower than the known data for 300 keV, which result, for example, in  $S_{E1} = 101(17)$  keV b and  $S_{E2} = 42(^{+16}_{-23})$  keV b [231],  $S_{E1} = 79(21)$  keV b or 82(26) keV b [265] and  $S_{E2} = 120(60)$  keV b [34]. In the method of generator coordinates [266] taking into account different cluster configurations, the following values were obtained for 300 keV:  $S_{E1} = 160$  keV b and  $S_{E2} = 70$  keV b. It can be seen that all of these results and our calculations strongly differ between each other.

However, it does not directly follow from the experimental data shown in Fig. 15.7 that, at energies below 1 MeV, the  $S$ -factor experiences sharp

growth and at 300 keV it has a value of order of 100 keV b. In a range of 1.1÷1.8 MeV, the  $S$ -factor is in an interval of 16÷25 keV b with errors from 3 to 7 keV b, and at 0.9 MeV it has a value of  $29 \pm 23$  keV b [34].

### **Conclusion**

Thus, the qualitative analysis of the number of forbidden and allowed states in the intercluster interactions of the  ${}^4\text{He}{}^{12}\text{C}$  system makes it possible to obtain a certain partial potentials matched with the elastic scattering phase shifts and bound state energies of  ${}^{16}\text{O}$ . These potentials, at certain assumptions, lead to the acceptable description of the available data on the astrophysical  $S$ -factor of the radiative capture  ${}^{12}\text{C}({}^4\text{He},\gamma){}^{16}\text{O}$  at energies from 0.9 to 4.0 MeV based on the contribution of the  $E2$  transitions only.

However, it must be noted that the given above number of FSs in the potentials of different partial waves, instead of the  $S$  wave, determines only on the basis of the general tendency of their decreasing at the increasing of the orbital moment  $L$ . Therefore, the number of such FSs can not consider as final and uniquely determined.

# CONCLUSION

---

*A certain nuclear model, which can describe the available experimental data, for example, astrophysical  $S$ -factors of a thermonuclear reaction within the energy range for which they are obtained, may also claim to predict correctly the behavior of the  $S$ -factor at ultralow energies – the range for which the experimental measurements are absent now [31].*

Thus, on the basis of the modified potential cluster model there have been considered the astrophysical  $S$ -factors of the radiative capture reactions in the next cluster systems:  $p^2\text{H}$ ,  $p^3\text{H}$ ,  $p^6\text{Li}$ ,  $p^7\text{Li}$ ,  $p^9\text{Be}$ ,  $p^{10}\text{B}$ ,  $p^{11}\text{B}$ ,  $p^{12}\text{C}$ ,  $p^{13}\text{C}$ ,  $p^{14}\text{C}$ ,  $p^{15}\text{N}$ ,  $^2\text{H}^4\text{He}$ ,  $^3\text{H}^4\text{He}$ ,  $^3\text{He}^4\text{He}$  and  $^4\text{He}^{12}\text{C}$ . For construction of the potentials of interactions between clusters in some considered systems the phase shift analysis of the available experimental data on elastic scattering at astrophysical energies was performed. Then on the basis of the descriptions of obtained or available in literature phase shifts corresponding intercluster interaction potentials were constructed within the framework of forbidden states concept in multinucleon system consisting of two subsystems the interaction between which is described, as it is supposed, by a local potential. And for each partial wave an individual Gaussian - type potential differing from the potentials for other partial waves was obtained.

For cluster systems pure by Young tableaux orbital states, the nuclear potential was obtained from the description of the elastic scattering phase shifts. Furthermore, then it is used for description of the properties of the ground bound states of these nuclei. And it is assumed that the nucleus consists of two fragments the internal properties of which coincide with the properties of corresponding nuclei in a free state. Such a situation takes place with a high likelihood in the  $^2\text{H}^4\text{He}$ ,  $^3\text{H}^4\text{He}$ ,  $^3\text{He}^4\text{He}$  systems due to a strongly pronounced clusterization of  $^6\text{Li}$ ,  $^7\text{Li}$ , and  $^7\text{Be}$  nuclei in the channels under consideration.

In the  $p^2H$ ,  $p^3H$ ,  $p^6Li$ ,  $p^7Li$ ,  $p^9Be$  and, evidently,  $p^{10}B$  systems the situation is more difficult due to mixing of orbital states in isospin or Young tableaux. For the above mentioned systems, except  $p^7Li$ , two orbital symmetries with different Young tableaux are allowed in the continuous spectrum in states with the minimum spin. While for the bound ground states of these systems only one of two such systems is allowed [29]. Therefore, it is impossible to construct the potential for the bound states of clusters on the basis of experimental data description according to elastic scattering phases without the preliminary separation of phases in accordance with the Young tableaux. The method of separation of orbital states and potentials of the scattering processes according to Young tableaux is demonstrated on the example of the  $p^2H$  and  $p^3H$  systems.

Classification of states according to the orbital Young tableaux allows one to determine the presence and the number of Pauli forbidden states, allows one to fix the number of wave function nodes of relative cluster motion, and establishes a definite depth of the interaction potential. Thus, the discrete ambiguity of the potential depth that characterized to the optical model [46] is avoided. The form of each partial scattering phase shift as a function of energy is very sensitive to the width of the potential with the forbidden states, which is used to get rid of the continuous ambiguity of the potential, which is also characteristic of the usual optical model [46].

Therefore, all the parameters of scattering potentials in the considered MPCM are fixed quite unambiguously as compared to the general optical model. In addition, the obtained potentials of intercluster interactions pure by permutation symmetry and isospin or containing forbidden states allow describing correctly the main characteristics of the bound state of the nucleus as a system of two fragments – clusters. The formalism worked out for obtaining intercluster potentials [21,22] is used here for the description of nuclear reactions of photocapture in the considered systems. It is clearly that the operator of electromagnetic transition for the processes of radiative capture, as opposed to other nuclear reactions mediated by strong interactions, is well known. Moreover, in photocapture reaction there is no interaction in the final state, while the interaction in the initial state is taken into account quite correctly on the basis of the well-developed potential approach. Therefore, at the theoretical description of the considered

reactions it is quite possible to expect the quantitative agreement between the experiments their total cross sections too, that was demonstrated in this book.

Therefore, it is not a surprise that within the considered cluster model it was possible to predict the energy dependence of the  $S$ -factor of the proton radiative capture on  $^3\text{H}$  in the energy range from 50 to 700 keV by taking into account only the  $E1$  transition. On the basis of experimental data for energies beyond 700 keV we managed to calculate about 15 years ago the  $S$ -factor for the energies down to 10 keV [93]. As it was shown in chapter 4, the results of those calculations reproduce the new data on the  $S$ -factor [105] in the wide energy range from 50 keV to 5 MeV. In addition, the predictions as to the behavior of the  $S$ -factor of the proton radiative capture on  $^2\text{H}$  at energies down to 10 keV [30] made within the considered here MPCM. At the time of the publication of work [30], we knew only the experimental data for the energies above 150÷200 keV. The calculations that we have done in this work were in a good agreement with the results [67,68] which appeared much later for the energy range from 50 keV to 150÷200keV and results [69] at energies down to 10 keV.

The cluster interaction potentials given here may also be used for theoretical description of other nuclear processes at low energies involving the same particles. However, as it has been shown above, the reliable results for the intercluster potentials and, consequently, for the characteristics of nuclear processes calculated on their basis can be obtained only if the phase shifts of the elastic scattering are accurately determined in the experiment. Unfortunately, at present time for the majority of lightest nuclear systems the elastic scattering phase shifts are found with significant errors reaching sometimes 20÷30%.

In this connection the problem to raise the accuracy of experimental measurements of elastic scattering of light nuclei at astrophysical energies and to perform a more accurate phase shift analysis becomes exclusively urgent. The increase in the accuracy will allow making more definite conclusions regarding the mechanisms and conditions of thermonuclear reactions, as well as better understanding their nature in general [3,31,60,91,151,152,198].



# APPENDIX 1

## Calculation methods for Coulomb and Whittaker functions

---

### Coulomb functions

Consider on the calculation methods of the Coulomb scattering wave functions, whose regular  $F_L(\eta, \rho)$  and irregular  $G_L(\eta, \rho)$  parts are the linearly independent solutions of the radial Schrödinger equation only with the Coulomb potential for the scattering states having the form [79]

$$\chi_L''(\rho) + \left(1 - \frac{2\eta}{\rho} - \frac{L(L+1)}{\rho^2}\right) \chi_L(\rho) = 0, \quad ,$$

where  $\chi_L = F_L(\eta, \rho)$  or  $G_L(\eta, \rho)$ ,  $\rho = kr$ , and  $\eta = \frac{\mu Z_1 Z_2}{\hbar^2 k}$  is the Coulomb parameter. Wronskians of such functions have the forms [267]

$$W_1 = F_L' G_L - F_L G_L' = 1, \quad ,$$

$$W_2 = F_{L-1} G_L - F_L G_{L-1} = \frac{L}{\sqrt{\eta^2 + L^2}}.$$

The recurrent relations between them write down as

$$L[(L+1)^2 + \eta^2]^{1/2} u_{L+1} = (2L+1) \left[ \eta + \frac{L(L+1)}{\rho} \right] u_L - (L+1)[L^2 + \eta^2]^{1/2} u_{L-1}, \quad ,$$

$$(L+1)u_L' = \left[ \frac{(L+1)^2}{\rho} + \eta \right] u_L - [(L+1)^2 + \eta^2]^{1/2} u_{L+1}, \quad ,$$

$$L u_L' = [L^2 + \eta^2]^{1/2} u_{L-1} - \left[ \frac{L^2}{\rho} + \eta \right] u_L, \quad ,$$



where  $u_L = F_L(\eta, \rho)$  or  $G_L(\eta, \rho)$ .

The asymptotic of these functions at  $\rho \rightarrow \infty$  may be represented as [268]

$$F_L = \sin(\rho - \eta \ln 2\rho - \pi L / 2 + \sigma_L),$$

$$G_L = \cos(\rho - \eta \ln 2\rho - \pi L / 2 + \sigma_L).$$

There are a number of methods and approximations for calculation of the Coulomb scattering wave functions [269-275]. However, only recently the quick convergent representation, that allowed get their values with high accuracy and in a wide diapason of variables, with the small computing time was appeared [43,44].

In this method the Coulomb functions are represented as infinite continued fractions [276]

$$f_L = F'_L / F_L = b_0 + \frac{a_1}{b_1 + \frac{a_2}{b_2 + \frac{a_3}{b_3 + \dots}}},$$

where

$$b_0 = (L + 1)/\rho + \eta/(L + 1),$$

$$b_n = [2(L + n) + 1][(L + n)(L + n + 1) + \eta\rho],$$

$$a_1 = -\rho[(L + 1)^2 + \eta^2](L + 2)/(L + 1),$$

$$a_n = -\rho^2[(L + n)^2 + \eta^2][(L + n)^2 - 1]$$

and

$$P_L + iQ_L = \frac{G'_L + iF'_L}{G_L + iF_L} = \frac{i}{\rho} \left( b_0 + \frac{a_1}{b_1 + \frac{a_2}{b_2 + \frac{a_3}{b_3 + \dots}}} \right),$$

where

$$b_0 = \rho - \eta, \quad b_n = 2(b_0 + in),$$

$$a_n = -\eta^2 + n(n-1) - L(L+1) + i\eta(2n-1).$$

Using the given expressions it is possible to obtain the connection between Coulomb functions and their products [44,277]

$$F'_L = f_L F_L,$$

$$G_L = (F'_L - P_L F_L) / Q_L = (f_L - P_L) F_L / Q_L,$$

$$G'_L = P_L G_L - Q_L F_L = [P_L(f_L - P_L) / Q_L - Q_L] F_L.$$

Such calculation method is applicable in region at  $\rho \geq \eta + \sqrt{\eta^2 + L(L+1)}$ , i.e., for  $L=0$  we have  $\rho > 2\eta$ , and it easy allows to get the high accuracy due to the quick convergence of continued fractions [44]. Since the Coulomb parameter  $\eta$  is of order to one and the moment  $L$  is always possible to set as zero, then this method gives the good results starting from  $\rho > 2$ . It is possible to get the values of Coulomb functions for any  $\rho$  and for  $L > 0$  from the recurrent relations.

Thereby, setting any magnitude of  $F_L$  at point  $\rho$  it is possible to find all of other functions and their derivatives accurate within constant factor that determines from the Wronskians. Calculation of the Coulomb functions by usage of given formulas and comprising them with the table data [267] leads to the result that it is easy get the correct value with eight-nine accuracy of order if  $\rho$  satisfies the condition marked above.

The text of the computing program for the Coulomb functions calculating is given below. This program has been written down by the Fortran-90 language for the PS-4 system. Here:

Q – the Coulomb parameter,

LM – the moment of a given partial wave,

R – the distance from a centre where the Coulomb functions are calculating,

F and G – the Coulomb functions,

W – Wronskian, determining the accuracy of Coulomb functions calculation at the given distance.

EP = 1.0D-015 – calculation accuracy of Coulomb functions.

### **SUBROUTINE CULFUN(LM,R,Q,F,G,W)**

! \*\*\*\* Subprogram for calculation of Coulomb functions \*\*\*\*

IMPLICIT REAL(8) (A - Z)

INTEGER L,K,LL,LM

EP=1.0D-15; L=0; F0=1.0D0

GK=Q\*Q

GR=Q\*R

RK=R\*R

B01=(L+1)/R+Q/(L+1)

K=1

BK=(2\*L+3)\*((L+1)\*(L+2)+GR)

AK= - R\*((L+1)\*\*2+GK)/(L+1)\*(L+2)

DK=1.0D0/BK

DEHK=AK\*DK

S=B01+DEHK

15 K=K+1

AK= - RK\*((L+K)\*\*2 - 1.0D0)\*((L+K)\*\*2+GK)

BK=(2\*L+2\*K+1)\*((L+K)\*(L+K+1)+GR)

DK=1.0D0/(DK\*AK+BK)

IF (DK>0.0D0) GOTO 35

25 F0= - F0

35 DEHK=(BK\*DK - 1.0D0)\*DEHK

S=S+DEHK

```

IF (ABS(DEHK)>EP) GOTO 15
FL=S
K=1
RMG=R - Q
LL=L*(L+1)
CK= - GK - LL
DK=Q
GKK=2.0D0*RMG
HK=2.0D0
AA1=GKK*GKK+HK*HK
PBK=GKK/AA1
RBK= - HK/AA1
AOMEK=CK*PBK - DK*RBK
EPSK=CK*RBK+DK*PBK
PB=RMG+AOMEK
QB=EPSK
52 K=K+1
CK= - GK - LL+K*(K - 1.0D0)
DK=Q*(2.0D0*K - 1.0D0)
HK=2.0D0*K
FI=CK*PBK - DK*RBK+GKK
PSI=PBK*DK+RBK*CK+HK
AA2=FI*FI+PSI*PSI
PBK=FI/AA2
RBK= - PSI/AA2
VK=GKK*PBK - HK*RBK
WK=GKK*RBK+HK*PBK
OM=AOMEK
EPK=EPSK
AOMEK=VK*OM - WK*EPK - OM
EPSK=VK*EPK+WK*OM - EPK
PB=PB+AOMEK
QB=QB+EPSK
IF (( ABS(AOMEK)+ABS(EPSK) )>EP) GOTO 52
PL= - QB/R
QL=PB/R

```

```

G0=(FL - PL)*F0/QL
G0P=(PL*(FL - PL)/QL - QL)*F0
F0P=FL*F0
ALFA=1.0D0/( (ABS(F0P*G0 - F0*G0P))**0.5 )
G=ALFA*G0
GP=ALFA*G0P
F=ALFA*F0
FP=ALFA*F0P
W=1.0D0 - FP*G+F*GP
IF (LM==0) GOTO 123
AA=(1.0D0+Q**2)**0.5
BB=1.0D0/R+Q
F1=(BB*F - FP)/AA
G1=(BB*G - GP)/AA
WW1=F*G1 - F1*G - 1.0D0/(Q**2+1.0D0)**0.5
IF (LM==1) GOTO 234
DO L=1,LM - 1
AA=((L+1)**2+Q**2)**0.5
BB=(L+1)**2/R+Q
CC=(2*L+1)*(Q+L*(L+1)/R)
DD=(L+1)*(L**2+Q**2)**0.5
F2=(CC*F1 - DD*F)/L/AA
G2=(CC*G1 - DD*G)/L/AA
WW2=F1*G2 - F2*G1 - (L+1)/(Q**2+(L+1)**2)**0.5
F=F1; G=G1; F1=F2; G1=G2
ENDDO
234 F=F1; G=G1
123 CONTINUE
END

```

The calculation results of Coulomb functions for  $\eta = 1$  and  $L = 0$  control and their comparing with the table data [267] are given in table A.1.1. We see that now the correct results are getting for  $\rho = kr = 1$ . The magnitude of Wronskian represented as  $W_0 - 1$  is not larger  $10^{-15}$  for any  $\rho \geq 1$ .

**Table A1.1 The Coulomb functions**

$\rho$	$F_0$ (Our calculation)	$F_0$ [267]	$G_0$ (Our calculation)	$G_0$ [267]
1	2.275262105105590E-001	0.22753	2.043097162103547	2.0431
5	6.849374120059441E-001	0.68494	-8.98414359092021E-001	-0.89841
10	4.775608158625742E-001	0.47756	9.428742426537808E-001	0.94287
15	-9.787895837822600E-001	-0.97879	3.404637385301291E-001	0.34046
20	-3.292255362657541E-001	-0.32923	-9.72428398697120E-001	-0.97243

**Whittaker functions**

The Whittaker function is the solution of the Schrödinger equation without nuclear potential for the forbidden states [267]

$$\frac{d^2 W(\mu, \nu, z)}{dz^2} - \left( \frac{1}{4} - \frac{\nu}{z} - \frac{1/4 - \mu^2}{z^2} \right) W(\mu, \nu, z) = 0,$$

that is possible leads to the standard Schrödinger equation

$$\frac{d^2 \chi(k, L, r)}{dr^2} - \left( k^2 + \frac{g}{r} + \frac{L(L+1)}{r^2} \right) \chi(k, L, r) = 0,$$

where  $g = \frac{2\mu Z_1 Z_2}{\hbar^2} = 2k\eta$ ,  $\eta = \frac{\mu Z_1 Z_2}{k\hbar^2}$  – the Coulomb parameter,  $z = 2kr$ ,

$$\nu = -\frac{g}{2k} = -\eta \text{ and } \mu = L + 1/2.$$

For finding the numerical magnitudes of the Whittaker function its integral representation is used frequently

$$W(\mu, \nu, z) = \frac{z^\nu e^{-z/2}}{\Gamma(1/2 - \nu + \mu)} \int_0^\infty t^{\mu-\nu-1/2} (1+t/z)^{\mu+\nu-1/2} e^{-t} dt,$$

that may be transformed to the form

$$W_{-\eta L+1/2}(z) = W(L+1/2, -\eta, z) = \frac{z^{-\eta} e^{-z/2}}{\Gamma(L+\eta+1)} \int t^{L+\eta} (1+t/z)^{L-\eta} e^{-t} dt$$

It is easy to see that at  $L = 1$  and  $\eta = 1$  the integral marked above reduces into  $I(3)$  that cancels with denominator. As the result we get the simple expression

$$W(1 + \frac{1}{2}, -1, z) = \frac{e^{-z/2}}{z}.$$

It could be used furthermore for the control of correctness the Whittaker function calculation at the arbitrary  $z$ , remembering that  $L = 1$ ,  $\eta = 1$  and  $z = 2kr$

The program for the Whittaker function calculation under its integral representation [267] is given below. Here:

$$A = \frac{\mu Z_1 Z_2}{k \hbar^2} = G/k \text{ is the Coulomb parameter,}$$

$$G = \frac{\mu Z_1 Z_2}{\hbar^2}, \quad k^2 = \frac{2\mu E}{\hbar^2} = \frac{2\mu E}{41.4686} - \text{wave number in fm}^2,$$

$E$  – energy in MeV,

$\mu$  – reduced mass in amu,

$X$  – distance from the center equals  $r$  in fm,

$Z = 2kr$  – dimensionless variable,

$L$  – orbital moment.

## PROGRAM UNIT

IMPLICIT REAL(8) (A - Z)

INTEGER L

L=1

SK=1.0D - 000

GK=1.0D - 000

DO X=1,20

CALL WW(SK,L,GK,X,WH)

W=DEXP( - X\*SK)/2.0D - 000/X/SK

PRINT\*, X,WH,W

ENDDO

**END**

**SUBROUTINE WW(SK,L,GK,RR,WH)**

IMPLICIT REAL(8) (A - Z)

DIMENSION VV(0:100000)

INTEGER NN,L,NNN,I

SS=(ABS(SK))\*\*0.5

AA=GK/SS

BB=L

ZZ=1.0D - 000+AA+BB

AAA=1.0D - 000/ZZ

NNN=1000000

DO I=1,NNN

AAA=AAA\*I/(ZZ+I)

ENDDO

GAM=AAA\*NNN\*\*ZZ

CC=2.0D - 000\*RR\*SS

NN=10000

HH=0.0050D - 000

DO I=0,NN

TT=HH\*I

VV(I)=TT\*\*((AA+BB)\*(1.0D - 000+TT/CC))\*\*((BB - AA)\*EXP( - TT))

ENDDO

CALL SIMP(VV,HH,NN,SI)

WH=SI\*EXP( - CC/2.0D - 000)/(CC\*\*AA\*GAM)

**END**

**SUBROUTINE SIMP(V,H,N,S)**

IMPLICIT REAL(8) (A - Z)

DIMENSION V(0:10240000)

INTEGER N,II,JJ

A=0.0D - 000; B=0.0D - 000

A111: DO II=1,N - 1,2

B=B+V(II)

ENDDO A111

B111: DO JJ=2,N - 2,2

A=A+V(JJ)



END DO B111

$$S=H*(V(0)+V(N)+2.0D - 000*A+4.0D - 000*B)/3.0D - 000$$

END

The calculation results of the Whittaker function at  $\eta = 1$  and  $k = 1$  for the different orbital moments  $L$  and its exact values  $W_{\text{ex}}$  at  $L = 1$  and  $\eta = 1$  are given below.

R	W(L = 0)	
1.0000000000000000	1.020290079327840E - 001	
2.0000000000000000	2.363196623576423E - 002	
3.0000000000000000	6.392391215042637E - 003	
4.0000000000000000	1.863857863268692E - 003	
5.0000000000000000	5.684597929937536E - 004	
6.0000000000000000	1.786848627416934E - 004	
7.0000000000000000	5.739835037958716E - 005	
8.0000000000000000	1.874246806441706E - 005	
9.0000000000000000	6.199016558901119E - 006	
10.0000000000000000	2.071563699444139E - 006	
11.0000000000000000	6.981628624614050E - 007	
12.0000000000000000	2.369723360890071E - 007	
13.0000000000000000	8.092018511054453E - 008	
14.0000000000000000	2.777589770610260E - 008	
15.0000000000000000	9.577168790058733E - 009	
16.0000000000000000	3.315309238772864E - 009	
17.0000000000000000	1.151676608740117E - 009	
18.0000000000000000	4.013201009814541E - 010	
19.0000000000000000	1.402378280368625E - 010	
20.0000000000000000	4.912856187198094E - 011	
R	W(L = 1)	W <sub>ex</sub> (L = 1)
1.0000000000000000	1.839408242280025E-001	1.839397205857212E - 001
2.0000000000000000	3.383402381280602E-002	3.383382080915318E - 002
3.0000000000000000	8.297894515224235E-003	8.297844727977325E - 003
4.0000000000000000	2.289468597870201E-003	2.289454861091772E - 003
5.0000000000000000	6.737987426912442E-004	6.737946999085467E - 004

6.0000000000000000	2.065639207693961E-004	2.065626813888632E - 004
7.0000000000000000	6.513481691899502E-005	6.513442611103688E - 005
8.0000000000000000	2.096654004284359E-005	2.096641424390699E - 005
9.0000000000000000	6.856141363786637E-006	6.856100227037754E - 006
10.0000000000000000	2.270010108152015E-006	2.269996488124243E - 006
11.0000000000000000	7.591727727640804E-007	7.591682177384391E - 007
12.0000000000000000	2.560103841139389E-007	2.560088480553421E - 007
13.0000000000000000	8.693626803869737E - 008	8.693574642234824E - 008
14.0000000000000000	2.969763243906337E - 008	2.969745425369885E - 008
15.0000000000000000	1.019680519741103E - 008	1.019674401672753E - 008
16.0000000000000000	3.516745310397776E - 009	3.516724209976847E - 009
17.0000000000000000	1.217636046617811E - 009	1.217628740819167E - 009
18.0000000000000000	4.230575312477445E - 010	4.230549929086842E - 010
19.0000000000000000	1.474428961693802E - 010	1.474420115141386E - 010
20.0000000000000000	5.152914973511605E - 011	5.152884056096395E - 011

From this table we see that at  $L = \eta = 1$  the coincidence with exact function magnitudes with the relative error  $10^{-5}$  of order take place. Under usage the lower accuracy of  $NNN = 1000$  and  $NN = 1000$  with  $HH = 0.015$  this error is about  $6 \cdot 10^{-3}$  or 0.6%.



# APPENDIX 2

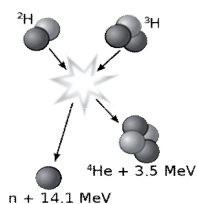
## Basic astrophysical terms and concepts

---

### Nuclear astrophysics

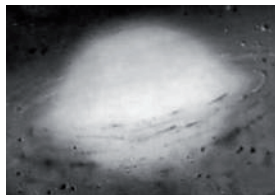
New field of modern astrophysics, which studies the role of microcosm processes in the cosmic phenomena, is the nuclear astrophysics. The subject of nuclear astrophysics are the nuclear processes (thermonuclear reactions) in stars, protostars, and other cosmic objects that lead to the release of energy and to the formation of different chemical elements [7,9].

### Thermonuclear fusion reaction



The nuclear reaction at ultrahigh energies. In order to the thermonuclear reaction (fusion reaction) will be carried out the charged atomic nuclei at their collision must to overcome the force of electrostatic repulsion, and for this they ought to have higher kinetic energy. If to suppose that the kinetic energy of nuclei is determined by their thermal motion, then it can be said that the big temperature [7,9] is necessary for start of the fusion reaction. Therefore, such nuclear reaction is titled “thermonuclear” – depending on temperature. The scheme of this reaction for the  ${}^2\text{H}{}^3\text{H}$  fusion is shown in the figure above.

### Protostar



The star at the final stage of its formation, up to the moment of the burning of thermonuclear reactions (proton-proton cycle) in its center. After this stage the compression of the protostar is finishing and it becomes the stable star of the main sequence [7,9].

## Star

Hot sphere of ionized gas or plasma, heating up due to the nuclear energy (thermonuclear reactions) and retaining in the relative stable state by the gravity forces. Our Sun is the typical example of the star. Large groups of stars form galaxies [7,9].

## Sun

Gas or more specifically plasma ball – sphere. The Sun radius equals  $R_{\odot} = 6,96 \cdot 10^{10}$  cm, i.e., about 109 times more than equatorial radius of the Earth; mass of the Sun is  $M_{\odot} = 1,99 \cdot 10^{33}$  g, i.e., 333000 times more than the mass of the Earth. About 99,9% of the mass of the solar system concentrates in the Sun. The average density of solar material equals  $1,4 \text{ g/cm}^3$  that is 0,256 of the average density of the Earth.



The solar material consists of the 73% mass of hydrogen, 25% mass of helium and about 2% of other elements. The Sun radiation power – its luminosity is  $L_{\odot} \approx 3,86 \cdot 10^{33}$  erg/sec or  $3,86 \cdot 10^{26}$  watt, effective temperature of the surface is  $T_{\text{eff}} = 5780$  K.

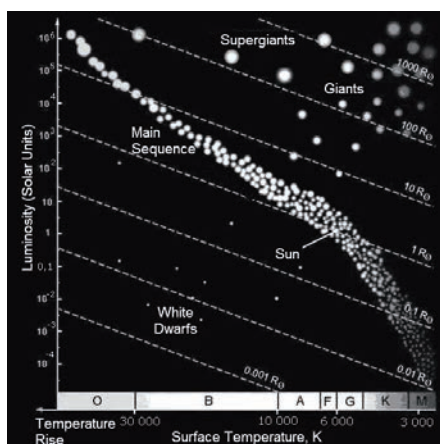
The Sun has relation to stars – Dwarfs so the spectral class G2V. In the diagramme spectrum-luminosity diagram or in the Hertzsprung-Russell diagram it is situated in the middle part of the Main sequence, where the stationar stars lie and they practically do not change their luminosity during many of billions years [7,9].

## Main sequence

The Main sequence crosses the Hertzsprung-Russell diagram diagonally from the upper left corner (high luminosities, early-type stars) to the lower right corner (low luminosities, late-type stars). The position of stars at the Hertzsprung-Russell diagram depends on the mass, the chemical composition and the processes of energy output in their depths.

Stars of the Main sequence have the same energy source (thermonuclear reaction of hydrogen burning or, so called, proton-proton thermonuclear cycle), so their luminosity and temperature (and consequently their position on the Main sequence) are formed essentially by the mass. The most massive stars with  $m \approx 50m_{\odot}$  lie at the upper (left) part of the Main sequence, and with the forwarding downwards on the Main sequence the masses of stars decrease down to  $m \approx 0.08m_{\odot}$  [7,9].

### Hertzsprung-Russell diagram



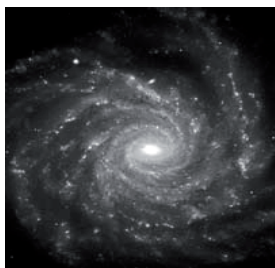
The Hertzsprung-Russell diagram is showing the relationship between the stars' absolute magnitudes or luminosities versus their spectral types or classifications and effective temperatures. Unexpected result is the fact that stars on this diagram hasn't random position but form well discernible sections. The diagram is used for classification

of the stars and corresponds to the modern ideas about star evolution. The diagram gives the possibility (although not so exactly) to find absolutely value according to the spectral class.

The existence of the Main sequence is connected with the fact that the burning stage of the matter equals  $\sim 90\%$  of evolution time of the majority of stars: burning-out of the hydrogen in central parts of the star leads to the formation of the isothermal helium core, transformation to the Red Giant stage and to the departure of the star from the Main sequence. Relatively brief evolution of the Red Giants leads to the dependence from their masses and to the formation of White dwarfs, neutron stars or black holes [7,9].

### Galaxy

The giant star system consisting of billions stars like our Sun. The large



amount of matter in the form of gas-dust clouds and different types of radiation contain in it. Diameter of our galaxy is about  $40 \text{ kpc} = 40000 \text{ parsec}$  [7,9].

### **Light-year**

A light-year is defined as the distance that light is travelling in vacuum during 1 tropical year:  $1 \text{ light-year (ly)} = 9.46 \cdot 10^{15} \text{ m} = 9.46 \cdot 10^{12} \text{ km} = 0.307 \text{ pc}$  [9].

### **Parsec**

Another astronomical distance unit is parsec:  $1 \text{ parsec (pc)} = 3.26 \text{ ly} = 206,265 \text{ AU} = 3.086 \cdot 10^{16} \text{ m}$  [9].

### **Astronomical unit**

The mean Earth-Sun distance approximately equals semimajor axis of the Earth's orbit. It is one of the most precisely defined astronomical constants. It is used as a unit for estimation of the distances between bodies in the Solar system. Astronomical unit  $1 \text{ (au)} = 149\,597\,870 \pm 2 \text{ km}$  [9].

### **Red giant**

Red giants are cold stars with  $T \sim 3000 \div 5000 \text{ K}$ , big stars with  $R = (10 \div 200) R_{\odot}$  and high luminosity  $L \sim 10^2 \div 10^4 L_{\odot}$ . They have small inert core consisting in helium and have layerwise source around the core, where the hydrogen is burning, meanwhile such star has very spread convective zone [7,9].

### **White dwarf**

These are stars after evolution process with the mass not more than Chandrasekhar limit (it is an upper bound on the mass of a stable white dwarf star) and without own sources of thermonuclear energy.

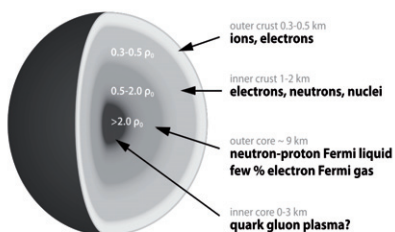
White dwarfs are compact stars with masses comparable with solar mass, radiuses  $\sim 100$  times and luminosities  $\sim 10\,000$  times less than the solar radius and luminosity correspondingly. The density of White dwarfs is equal to  $10^5 \div 10^9$  g/cm<sup>3</sup> that is about one million times greater than the density of general stars of the Main sequence. The number of White dwarfs, from different estimation, equals 3÷10% of stars of our Galaxy [7,9].

White dwarfs come from the compressed and cooling cores of normal stars at the final stage of the evolution releasing the shell. There are not thermonuclear reactions in the White dwarf unlike usual stars and it shines exclusively at the expense of cooling-down [7,9]. If the mass of the White dwarf is more than Chandrasekhar limit it is turning into the neutron star.

## Neutron star

It is astronomic object one of the final products of the star evolution. It consists of the neutron core and thin crust of the degenerate matter with the dominance of iron and nickel nuclei.

Neutron stars have very small diameter (about 20÷30 km); mean density of the substance of this star several times more than the density of an atomic nucleus, which for heavy nuclei at the average equals  $2,8 \cdot 10^{17}$  kg/m<sup>3</sup>.



Masses of the majority of neutron stars are close to 1,4 solar masses, which is equal to the value of the Chandrasekhar limit [7,9]. If the mass of neutron star exceeds the Oppenheimer-Volkoff limit it

turns into the Black hole.

## Black hole

It is the space-time region where the gravitational attraction so high that it is impossible to leave it even for objects that move with the speed, which is equal to the speed of light. The boundary around this region is called event horizon, and its characteristic dimension – gravitational radius. In the



simplest case of spherically symmetric black hole, it is equal to the Schwarzschild radius  $r_s = \frac{2GM}{c^2}$ , where  $c$  is the speed of light,  $M$  – mass of a body,  $G$  – gravitational constant. Theoretically, the possibility of the existence certain exact solutions of the Einstein equations [7,9].

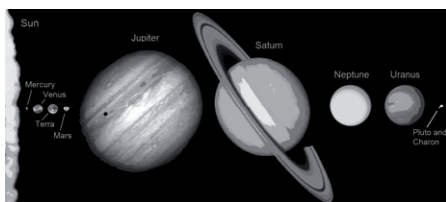
### Chandrasekhar limit

The Chandrasekhar limit is a critical mass of the White dwarf star where the gravitational equilibrium is supporting by the pressure of the degenerate electron gas. The value of this mass is slightly depends on the chemical composition of the White dwarf and lays in the interval  $M = 1.38 \div 1.44 m_\odot$  [7,9].

### Oppenheimer-Volkoff limit

The upper limit of mass of the neutron star, when pressure of the degenerate neutron gas already could not compensate the gravitational forces that leads it to the collapse into the black hole. Simultaneously, the Oppenheimer-Volkoff limit is the lower limit of the black hole masses that formed during the star evolution. The modern (2008 year) estimations of the Oppenheimer-Volkoff limit lies within the frame of  $2.5 \div 3$  solar masses  $m_\odot$  [7,9].

### Planet

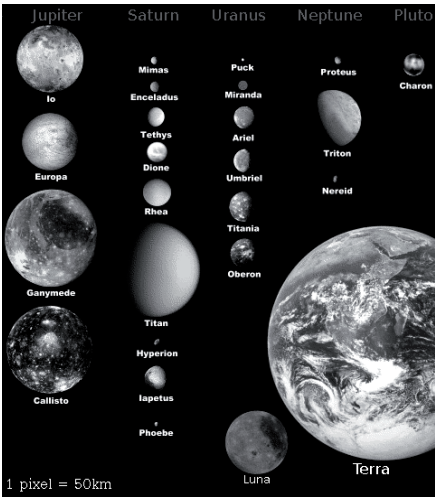


It is celestial body orbiting the Sun (or any star) in their gravitational field and shines by reflected solar light. The mass of such planet is not enough to cause the specific nuclear that

can flow in stellar interiors. Nuclear reactions can not be burned in interiors of planets with a mass less than  $0.1$  solar mass  $m_\odot$  [7,9].

Satellite

It is celestial body circulating on the certain trajectory (orbit) around other object (for example, planet) in the space, under the influence of gravity.



There are natural and non-natural satellites. Almost all planets of our Solar System have natural satellites [7,9].

History of the Universe, the Sun and the Earth

It is considered that the singularity of the Universe was 20 billions years ago [7,9,118,278] (although, according to modern data, it was about 14 billions years ago – see the next table). The data that given here and in the next table slightly differ – they are taken from different sources.

Time	Epoch	Event	Time from the present moment, years
0	Singularity	The Big Bang	20 bn
$10^{-43}$ sec	Planck time	Particle production	20 bn

	interval		
$10^{-6}$ sec	Hadronic era	Annihilation of proton-antiprotonic pairs	20 bn
1 sec	Leptonic era	Annihilation of electron-positronic pairs	20 bn
1 min	Radiation era	Nuclear fusion of helium and deuterium	20 bn
1 week		Thermalization of radiation in this era	20 bn
10000 years	Era of substance	The substance becomes dominate in the Universe	20 bn
300000 years		The Universe clears for radiation	19.7 bn
1-2 bn years		Beginning of the formation of galaxies	18-19 bn
3 bn years		Formation of the galactic clusters	17 bn
4 bn years		Compression of our protogalaxy	16 bn
4.1 bn years		Formation of the first stars	15.9 bn
5 bn years		Birth of quasars, star formation	15 bn
10 bn years		Star formation	10 bn
15.2 bn years		Formation of the interstellar cloud originating the Solar System	4.8 bn
15.3 bn years		Compression of the protosolar nebula	4.7 bn
15.4 bn years		Formation of the planets, hardening of rocks	4.6 bn
16.1 bn years	Archaeozoic era	Formation of the oldest terrestrial rocks	3.9 bn
17 bn years		Origin of the microorganism	3 bn
18 bn years	Proterozoic era	Formation of the rich	2 bn

		oxygen atmosphere	
19 bn years	Paleozoic era	Origin of the macroscopic forms	1 bn
19.4 bn years		Earliest fossils	600 million
19.55 bn years		The first plants on the earth	450 million
19.6 bn years		Fishes	400 million
19.75 bn years	Mesozoic era	Conifers, formation of mountains	250 million
19.8 bn years		Reptiles	200 million
19.85 bn years	Tertiary era	Dinosaurs, continental drift	150 million
19.95 bn years		First mammalia	50 million
20 bn years		Human (Homo sapiens)	2 million

### Characteristics of the Universe

Basic, and more modern than in the previous table, characteristics of the Universe and certain stages of its evolution [2,7,9] are shown below

t = 0		The Big Bang. Birth of the Universe $\rho(\text{g/cm}^3) = \frac{5 \times 10^5}{t^2(\text{sec})}, \quad T(\text{K}) = \frac{10^{10}}{\sqrt{t(\text{sec})}}$
t = $10^{-43}$ sec		Quantum gravitation era. Strings $\rho = 10^{90} \text{ g/cm}^3, \quad T = 10^{32} \text{ K}$
t = $10^{-35}$ sec		Quark-gluon medium $\rho = 10^{75} \text{ g/cm}^3, \quad T = 10^{28} \text{ K}$

t = 1 microsecond		Quarks are associated into neutrons and protons $\rho = 10^{17} \text{ g/cm}^3$ , $T = 6 \times 10^{12} \text{ K}$
t = 100 sec		Formation of prestellar 4He $\rho = 50 \text{ g/cm}^3$ , $T = 10^9 \text{ K}$
t = 380,000 years		Formation of neutral atoms $\rho = 0.5 \times 10^{-20} \text{ g/cm}^3$ , $T = 3 \times 10^3 \text{ K}$
t = $10^8$ years	EARLIEST STARS	Hydrogen burning in stars $\rho = 10^2 \text{ g/cm}^3$ , $T = 2 \times 10^6 \text{ K}$ Helium burning in stars $\rho = 10^3 \text{ g/cm}^3$ , $T = 2 \times 10^8 \text{ K}$ Carbon burning in stars $\rho = 10^5 \text{ g/cm}^3$ , $T = 8 \times 10^8 \text{ K}$ Oxygen burning in stars $\rho = 10^5 \div 10^6 \text{ g/cm}^3$ , $T = 2 \times 10^9 \text{ K}$ Silicon burning in stars $\rho = 10^6 \text{ g/cm}^3$ , $T = (3 \div 5) \times 10^9 \text{ K}$
t = 13.7 billions of years		Modern Universe $\rho = 10^{-30} \text{ g/cm}^3$ , $T = 2.73 \text{ K}$

# REFERENCES

---

1. Barnes, C. A.; Clayton, D. D.; Schramm, D. N.; *Essays in Nuclear Astrophysics* Presented to William A. Fowler; Publisher: Cambridge University Press, Cambridge, UK, 1982; pp 562.
2. Kapitonov, I. M.; Ishkhanov, B. S.; Tutyn', I. A. *Nucleosynthesis in the Universe*; Publisher: Librokom, Moscow, 2009, (in Russian); <http://nuclphys.sinp.msu.ru/lect/index.html>; Peacock, J. A. *Cosmological Physics*; Publisher: Cambridge University Press, Cambridge, UK, 1999.
3. Dubovichenko S.B. Selected method for nuclear astrophysics Third Edition, corrected and added. Germany, Saarbrucken: Lambert Academy Publ. GmbH&Co. KG. 2014. 661p.
4. Gorbunov, D. S.; Rubakov, V. A. *Introduction to theory of early Universe. Theory of hot Big Bang*; Publisher: Singapore, N.J. Hackensack, World Scientific, 2011.
5. Zasov, A. V.; Postnov, K. A. *General astrophysics*; Publisher: Fryazino, Moscow, 2006, pp 496 (in Russian); Postnov, K. A. *Lectures on general astrophysics for physicists*; <http://www.astronet.ru:8101/db/msg/1170612/index.html> (in Russian).
6. Shklovskii, I. S. *Stars: birth, life and death*; Publisher: San Francisco, W.H. Freeman, 1978.
7. <http://ru.wikipedia.org>
8. Zel'dovich, Ya. B.; Novikov, I. D. *Structure and Evolution of the Universe*; Publisher: University of Chicago Press, L. Fishbone, 1983.
9. <http://astronet.ru>
10. Gulyaev, S. A.; Zhukovski V. M.; Komov S. V. *World system*; <http://detc.usu.ru/assets/ansci0011/general/index.html>.
11. Epelbaum E, Glockle W., Meissner U.G. The two-nucleon system at next-to-next-to-next-to-leading order // Nucl. Phys. 2005. V. A747. P. 362-424; Epelbaum E. et al. Three-nucleon forces from chiral effective field theory // Phys. Rev. 2002. V. C66. P. 064001.1–064001.17; Epelbaum E. Four-nucleon force using the method of unitary transformation // Eur. Phys. J. 2007. V. A34. P. 197-214.

12. Faddeev, L. D. Scattering theory for system of three particles // *Zh. Eksp. Teor. Fiz.* 1960, vol. 39, 1459-1467.
13. Yakubovskii, O. A. About integral equations in scattering theory for N particles // *Yad. Fiz.* 1967, vol. 5, 1312-1320.
14. Grassberger P. and Sandhas W. Systematical treatment of the non-relativistic N-particle scattering problem // *Nucl. Phys.* 1967. V. B2. P. 181-206; Alt E.O., Grassberger, P. and Sandhas W. Systematical and practical treatment of the few-body problem // JINR Report No. E4-6688. Dubna. 1972.
15. Deltuva A., Fonseca A.C. Four-body calculation of proton- $^3\text{He}$  scattering // *Phys. Rev. Lett.* 2007. V. 98 . P. 162502.1–162502.4; Deltuva A., Fonseca A.C. Ab initio four-body calculation of n- $^3\text{He}$ , p- $^3\text{H}$ , and d-d scattering // *Phys. Rev.* 2007. V. C76. P. 021001.1 –0211001.4.
16. Lazauskas R. Elastic proton scattering on tritium below the n- $^3\text{He}$  threshold // *Phys. Rev.* 2009. V. C79. P. 054007.1–054007.5.
17. Tang Y.C., Lemere M., Thompson D.R. Resonating-group method for nuclear many-body problems // *Phys. Rep.* 1978. V. 47. P. 167-223.
18. Navratil P., Vary J.P., and Barrett B.R. Properties of  $^{12}\text{C}$  in the ab initio nuclear shell model // *Phys. Rev. Lett.* 2000. V. 84. P. 5728-5731.
19. Quaglioni S. and Navratil P. Ab initio many-body calculations of n- $^3\text{H}$ , n- $^4\text{He}$ , p- $^3,^4\text{He}$ , and n- $^{10}\text{Be}$  scattering // *Phys. Rev. Lett.* 2008. V. 101. P. 092501-1-092501-4.
20. Kievsky A., Viviany M., Rosati S. Polarization observables in p-d elastic scattering below 30 MeV // *Phys. Rev.* 2001. V. C64. P. 024002-1-024002-18.
21. Nemets, O. F.; Neudatchin, V. G.; Rudchik, A. T.; Smirnov, Y. F.; Tchuvil'sky, Yu. M. *Nucleon Association in Atomic Nuclei and the Nuclear Reactions of the Many Nucleons Transfers*; Publisher: Naukova dumka, Kiev, 1988, pp 488 (in Russian).
22. Dubovichenko, S. B. *Property of light atomic nuclei in potential cluster models*; Publisher: Daneker, Almaty, Kazakhstan, 2004; pp 248 (in Russian); <http://xxx.lanl.gov/abs/1006.4944>.
23. Zaguskii, V. L. *Guide on numerical methods of solution of equations*; Publisher: Fiz. Mat. Lit, Moscow, 1960; pp 215.
24. Melent'ev, P. V. *Approximate calculus*; Publisher: Fiz. Mat. Lit, Moscow, 1962; pp 387.

25. Demidovich, B. P.; Maron, I. F. *Foundation of calculus mathematics*; Publisher: Nauka, Moscow, 1966; pp 664.
26. Dubovichenko, S. B. *Calculation methods of the nuclear characteristics*; Publisher: Complex, Almaty, Kazakhstan, 2006; pp 311 (in Russian); <http://xxx.lanl.gov/abs/1006.4947>.
27. Baktybaev M.K. et al. The scattering of protons from  ${}^6\text{Li}$  and  ${}^7\text{Li}$  nuclei // The Fourth Eurasian Conference “Nuclear Science and its Application”. October 31-November 3. Baku. Azerbaijan. 2006. P. 62; Burtebaev N. et al. The new experimental data on the elastic scattering of protons from  ${}^6\text{Li}$ ,  ${}^7\text{Li}$ ,  ${}^{16}\text{O}$  and  ${}^{27}\text{Al}$  nuclei // Book of Abstracts the Fifth Eurasian Conference on “Nuclear Science and its Application”. October 14-17. Ankara. Turkey. 2008. P. 40.
28. Zazulin D.M. et al. Scattering of protons from  ${}^{12}\text{C}$  // The Sixth International conference “Modern Problems of Nuclear Physics” September 19-22. Tashkent. Uzbekistan. 2006. P. 127; Baktybaev M.K. et al. Elastic scattering of protons from  ${}^{12}\text{C}$ ,  ${}^{16}\text{O}$  and  ${}^{27}\text{Al}$  // The 4<sup>th</sup> Eurasia Conf. “Nucl. Sci. and its Appl.” Baku. Azerbaijan. 2006. P. 56.
29. Neudatchin V.G. et al. Generalized potential-model description of mutual scattering of the lightest  $p+d$ ,  $d+{}^3\text{He}$  nuclei and the corresponding photonuclear reactions // *Phys. Rev.* 1992. V. C45. P. 1512-1527.
30. Dubovichenko, S. B. Analysis of photonuclear processes in the  $\text{N}^2\text{H}$  and  ${}^2\text{H}^3\text{He}$  systems on the basis of cluster models for potentials with forbidden states // *Phys. Atom. Nucl.* 1995, vol. 58, 1174-1180.
31. Dubovichenko S.B., Uzikov Yu.N. Astrophysical S-factors of reactions with light nuclei // *Physics of Particles and Nuclei* 2011. V.42. №2. P.251-301; Dubovichenko S.B., Dzhazairov-Kakhramanov A.V. Astrophysical S-factors of proton radiative capture in thermonuclear reactions in the Stars and the Universe. // *The Big Bang: Theory, Assumptions and Problems*. NOVA Sci. Pub. New-York. USA. 2011. P.1-60.
32. Fowler W.A., Caughlan G.R., Zimmerman B.A. Thermonuclear reaction rates. II // *Ann. Rev. Astr. Astrophys.* 1975. V. 13. P. 69-112.
33. Mohr P.J., Taylor B.N. CODATA recommended values of the fundamental physical constants: 2002 // *Rev. Mod. Phys.* 2005. V. 77(1). P. 1-107.
34. Angulo C. et al. A compilation of charged-particle induced



thermonuclear reaction rates // Nucl. Phys. 1999. V. A656. P. 3-183.

35. Varshalovich, D. A.; Moskalev, A. N.; Khersonskii, V. K. *Quantum Theory of Angular Momentum*; Publisher: World Scientific, Singapore, 1989.

36. [http://physics.nist.gov/cgi-bin/cuu/Value?mud|search\\_for=atomnuc!](http://physics.nist.gov/cgi-bin/cuu/Value?mud|search_for=atomnuc!)

37. Eisenberg, J. M.; Greiner, W. *Excitation mechanisms of the nucleus*; Publisher: North Holland, Amsterdam, 1976, pp 421.

38. Plattner G.R., Viollier R.D. Coupling constants of commonly used nuclear probes // Nucl. Phys. 1981. V. A365. P. 8-12.

39. Mukhamedzhanov A.M., Tribble R. E. Connection between asymptotic normalization coefficients, sub threshold bound states, and resonances // Phys. Rev. 1999. V. C59. P. 3418-3424.

40. Blokhintsev, L. D.; Borbey, I.; Dolinskii, E. I. Nuclear vertex constants // *Fiz. Elem. Chastits Atom. Yadra* 1977, vol. 8, 1189-1254 [*Sov. J. Part. Nucl.* 1977, vol. 8, 485].

41. Marchuk, G. I.; Kolesov, V. E. *Application of Numerical Methods to Neutron Cross-Section Calculations*; Publisher: Atomizdat, Moscow, 1970, pp 304 (in Russian).

42. Abramowitz, I. G. et al. *Reference mathematical library. Mathematical analysis, Differentiation and integration*; Publisher: Fiz. Mat. Lit., Moscow, 1961, pp 350 (in Russian).

43. Barnet A. et al. Coulomb wave function for all real  $\eta$  and  $\rho$  // Comput. Phys. Comm. 1974. V. 8. P. 377-395.

44. Dubovichenko, S. B.; Chechin, L. M. Calculation methods of Coulomb functions and scattering phase shifts // *Bulletin of KazNPU Phys.-Math.* (Kazakhstan) 2003, vol. 1(7), 115-122.

45. Itzykson C., Nauenberg M. Unitary groups: Representations and decompositions // Rev. Mod. Phys. 1966. V. 38. P. 95-101.

46. Hodgson, P. E. *The Optical Model of Elastic Scattering*; Publisher: Clarendon Press, Oxford, 1963, pp 211.

47. Dubovichenko, S. B. Phase shift analysis of the  $^4\text{He}^4\text{He}$  elastic scattering at 40-50 MeV // *Phys. Atom. Nucl.* 2008, vol. 71, 65-74.

48. Dubovichenko, S. B.; Takibaev, N. Zh.; Chechin, L. M. *Physical processes in deep and near space*; Publisher: Daik-Press, Almaty, 2008, pp 228; <http://xxx.lanl.gov/abs/1012.1705>.

49. Kukulin V.I. et al. Detailed study of the cluster structure of light

nuclei in a three-body model: (I). Ground state of  ${}^6\text{Li}$  // Nucl. Phys. 1984. V. A417. P. 128-156.

50. Skornyakov, L. A. *Reference mathematical library. General algebra*; Publisher: Nauka, Moscow, 1990, pp 591 (in Russian).

51. Popov, B. A.; Tesler, G. S. *Computer calculation of functions*; Publisher: Naukova Dumka, Kiev, 1984, pp 598 (in Russian).

52. Korn, G.; Korn, T. *Reference book on mathematics*; Publisher: Mir, Moscow, 1974, pp 832 (in Russian).]

53. Dubovichenko, S. B.; Chechin, L. M. Methods of solution of the generalized eigenvalue problem // *Bulletin of KazNPU Phys.-Math.* (Kazakhstan) 2003, vol. 1(7), 110-115; Dubovichenko, S. B. Some methods of solution nuclear physics problems on the binding states // *Bulletin of KazNU Ser. Phys.* (Kazakhstan) 2008, vol. 1, 49-58.

54. Dubovichenko, S. B. Alternative method of solution the generalized matrix eigenvalue problem // *Izv. NAN RK Ser. Fiz.-Math.* (Kazakhstan) 2007, vol. 4, 52-55.

55. Mikhlin, S. G.; Smolitskii, Kh. L. *Approximate methods of solution of differential and integral equations*; Publisher: Nauka, Moscow, 1965, pp 383 (in Russian).

56. Dubovichenko, S. B.; Chechin, L. M. Modern methods of programming actual physical problems // *Materials of the Conference "Modern problems and tasks of Informatization in the Kazakhstan"*, October 6-10, Almaty, Kazakhstan; 2004, p. 358-390.

57. Blatt, J. M.; Weisskopf, V. F. *Theoretical nuclear physics*; Publisher: John Wiley and Sons Inc., New York, 1952, pp 864 [Publisher: IL, Moscow, 1954, pp 658 (in Russian)].

58. Fowler, W. A. *Experimental and Theoretical Nuclear Astrophysics: the Quest for the Original of the Elements*; Nobel Lecture, Stockholm, 8 Dec. 1983; Fowler, W. A. *Uspehi Fiz. Nauk* 1985, vol. 145, 441-488.

59. Snover K.A. // Solar p-p chain and the  ${}^7\text{Be}(p,\gamma){}^8\text{B}$  S-factor // University of Washington, CEPRA. NDM03. 1/6/2008.

60. Dubovichenko S.B., Dzhazairov-Kakhramanov A.V. Astrophysical S-factor of the radiative  $p^2\text{H}$  capture // *Euro. Phys. Jour.* 2009. V. A39. № 2, P. 139-143.

61. Schiavilla R., Pandaripande V.R., Wiringa R.B. Momentum distributions in A=3 and 4 nuclei // Nucl. Phys. 1986. V. A449. P. 219-242.

62. Uzikov Yu.N. Backward elastic  $p^3\text{He}$  scattering and high momentum components of  $^3\text{He}$  wave function // *Phys. Rev.* 1998. V. C58. P. 36-39.
63. Uzikov Yu.N. and Haidenbauer J.  $^3\text{He}$  structure and mechanism of  $p^3\text{He}$  elastic scattering // *Phys. Rev.* 2003. V. C68. P. 014001-1-014001-6.
64. Schmelzbach P. et al. Phase shift analysis of  $p^2\text{H}$  elastic scattering // *Nucl. Phys.* 1972. V. A197. P. 273-289; Arvieux J. Analyse en dephasages des sections efficaces et polarisations dans la diffusion elastique  $p^2\text{H}$  // *Nucl. Phys.* 1967. V. A102. P. 513-528; Chauvin J., Arvieux J. Phase shift analysis of spin correlation coefficients in  $p^2\text{H}$  scattering // *Nucl. Phys.* 1975. V. A247. P. 347-358; Huttel E. et al. Phase shift analysis of  $p^2\text{H}$  elastic scattering below break-up threshold // *Nucl. Phys.* 1983. V. A406. P. 443-455.
65. Dubovichenko, S. B.; Dzhazairov-Kakhramanov, A. V. Potential description of the processes of Nd, dd, N $\alpha$  and d $\tau$  elastic scattering // *Sov. J. Nucl. Phys.* 1990, vol. 51, 971-980.
66. Griffiths G.M., Larson E.A., Robertson L.P. The capture of proton by deuteron // *Can. J. Phys.* 1962. V. 40. P. 402-411.
67. Ma L. et al. Measurements of  $^1\text{H}(d \rightarrow, \gamma)^3\text{He}$  and  $^2\text{H}(p \rightarrow, \gamma)^3\text{He}$  at very low energies // *Phys. Rev.* 1997. V. C55. P. 588-596.
68. Schimd G.J. et al. The  $^2\text{H}(p \rightarrow, \gamma)^3\text{He}$  and  $^1\text{H}(d \rightarrow, \gamma)^3\text{He}$  reactions below 80 keV // *Phys. Rev.* 1997. V. C56. P. 2565-2681.
69. Casella C. et al. First measurement of the  $d(p, \gamma)^3\text{He}$  cross section down to the solar Gamow peak // *Nucl. Phys.* 2002. V. A706. P. 203-216.
70. Dubovichenko, S. B. Astrophysical  $S$ -factor of the proton radiative capture on  $^2\text{H}$  at low energies // *Rep. Nat. Acad. Sci. RK* (Kazakhstan) 2008, vol. 3, 33-38.
71. Tilley D.R., Weller H.R., Hasan H.H. Energy Levels of Light Nuclei  $A = 3$  // *Nucl. Phys.* 1987. V. A474. P. 1-60.
72. Tilley D.R., Weller H.R., Hale G.M. Energy levels of light nuclei  $A = 4$  // *Nucl. Phys.* 1992. V. A541. P. 1-157.
73. Kirzhnits, D. A. Is deuteron contained inside triton? // *Pis'ma Zh. Eksp. Teor. Fiz.* 1978, vol. 28, 479-481 [*JETP Letters* 1978, vol. 28, 444-446].
74. Bornard M. et al. Coupling constants for several light nuclei from a dispersion analysis of nucleon and deuteron scattering amplitudes // *Nucl.*

Phys. 1978. V. A294. P. 492-512.

75. Plattner G.R., Bornard M., Viollier R.D. Accurate determination of the  $^3\text{He-pd}$  and  $^3\text{He-pd}^*$  coupling constants // *Phys. Rev. Lett.* 1977. V. 39. P. 127-130.

76. Lim T.K. Normalization of the tail of the trinucleon wave function // *Phys. Rev. Lett.* 1973. V. 30. P. 709-710.

77. Kievsky A. et al. The three-nucleon system near the N-d threshold // *Phys. Lett.* 1997. V. B406. P. 292-296.

78. Ayer Z. et al. Determination of the asymptotic D- to S-state ratio for  $^3\text{He}$  via  $(d, ^3\text{He})$  reactions // *Phys. Rev.* 1995. V. C52. P. 2851-2858.

79. Mott, N. F.; Massey, H. S. W. The theory of atomic collisions; Publisher: Oxford Univ. Press, London, 1965, pp 858 [Publisher: Mir, Moscow, 1969, pp 756 (in Russian)].

80. Schimid G.J. et al. Effects of Non-nucleonic Degrees of Freedom in the  $D(p \rightarrow \gamma)^3\text{He}$  and  $p(d \rightarrow \gamma)^3\text{He}$  Reactions // *Phys. Rev. Lett.* 1996. V. 76. P. 3088-3091.

81. Schimid G.J. et al. Polarized proton capture by deuterium and the  $^2\text{H}(p, \gamma)^3\text{He}$  astrophysical S-factor // *Phys. Rev.* 1995. V. 52. P. R1732-R1735.

82. Viviani M., Schiavilla. R., Kievsky A. Theoretical study of the radiative capture reactions  $^2\text{H}(n, \gamma)^3\text{H}$  and  $^2\text{H}(p, \gamma)^3\text{He}$  at low energies // *Phys. Rev.* 1996. V. C54. P. 534-553.

83. Warren J.B. et al. Photodisintegration of  $^3\text{He}$  near the Threshold // *Phys. Rev.* 1963. V. 132. P. 1691-1692.

84. Berman B.L., Koester L.J., Smith J.H. Photodisintegration of  $^3\text{He}$  // *Phys. Rev.* 1964. V. 133. P. B117-B129.

85. Fetisov V.N., Gorbunov A.N., Varfolomeev A.T. Nuclear photo effect on three-particle nuclei // *Nucl. Phys.* 1965. V. 71. P. 305-342.

86. Ticcioni G. et al. The two-body photodisintegration of  $^3\text{He}$  // *Phys. Lett.* 1973. V. B46. P. 369-371.

87. Geller K.N., Muirhead E.G., Cohen L.D. The  $^2\text{H}(p, \gamma)^3\text{He}$  reaction at the breakup threshold // *Nucl. Phys.* 1967. V. A96. P. 397-400.

88. Dubovichenko, S. B., Dzhazairov-Kakhramanov, A. V. Electromagnetic effects in light nuclei in the frame of potential cluster model // *Phys. Part. Nucl.* 1997, vol. 28, 615-641.

89. Dubovichenko S.B. Phase shift  $p^{12}\text{C}$  analysis at astrophysical

energies // *Rus. Phys. J.* 2008. V.51. P.1136-1143.

90. Dubovichenko S.B. Contribution of the  $M1$  process to the astrophysical  $S$ -factor of the  $p^2H$  radiative capture // *Russian Physics Journal* 2011. V.54. P.157-164.

91. Dubovichenko S.B. Contribution of the  $M1$  process to the astrophysical  $S$ -factor of the  $p^2H$  radiative capture // *Russian Physics Journal* 2011. V.54. P.157-164.

92. Dubovichenko, S. B.; Neudatchin, V. G.; Sakharuk, A. A.; Smirnov, Yu. F. Generalized potential description of interaction light nuclei  $p^3H$  and  $p^3He$  // *Izv. Akad. Nauk SSSR Ser. Fiz.* 1990, vol. 54, 911-916; Neudatchin V.G., Sakharuk A.A., Dubovichenko S.B. Photodisintegration of  $^4He$  and supermultiplet potential model of cluster-cluster interaction // *Few Body Systems.* 1995. V. 18. P. 159-172.

93. Dubovichenko S.B. Photonuclear processes in channels  $p^3H$  and  $n^3He$  of  $^4He$  nucleus in potential cluster models // *Phys. Atom. Nuc.* 1995. V. 58. P. 1295-1302.

94. Tombrello T.A. Phase shift analysis for  $^3He(p,p)^3He$  // *Phys. Rev.* 1965. V. 138. P. B40-B47.

95. Yoshino Y. et al. Phase shift of  $p^3He$  scattering at low energies // *Prog. Theor. Phys.* 2000. V. 103. P. 107-125.

96. McSherry D.H., Baker S.D.  $^3He$  polarization measurements and phase shifts for  $p^3He$  elastic scattering // *Phys. Rev.* 1970. V. C1. P. 888-892.

97. Drigo L., Pisent G. Analysis of the  $p^3He$  low energy interaction // *Nuovo Cim.* 1967. V. BLI. P. 419-436.

98. Szaloky G., Seiler F. Phase shift analysis of  $^3He(p, p)^3He$  elastic scattering // *Nucl. Phys.* 1978. V. A303. P. 57-66.

99. Tombrello T.A. et al. The scattering of protons from  $^3He$  // *Nucl. Phys.* 1962. V. 39. P. 541-550.

100. McIntosh J.S., Gluckstern R.L., Sack S. Proton triton interaction // *Phys. Rev.* 1952. V. 88. P. 752-759.

101. Frank R.M., Gammel J.L. Elastic scattering of proton by  $^3He$  and  $^3H$  // *Phys. Rev.* 1955. V. 99. P. 1406-1410.

102. Kankowsky R. et al. Elastic scattering of polarized protons on tritons between 4 and 12 MeV // *Nucl. Phys.* 1976. V. A263. P. 29-46.

103. Berg H. et al. Differential cross section, analyzing power and

phase shifts for  $p^3\text{He}$  elastic scattering below 1.0 MeV // Nucl. Phys. 1980. V. A334. P. 21-34; Kavanagh R.W., Parker P.D. He+p elastic scattering below 1 MeV // Phys. Rev. 1966. V. 143. P. 779-782; Morrow L., Haeberli W. Proton polarization in  $p^3\text{He}$  elastic scattering between 4 and 11 MeV // Nucl. Phys. 1969. V. A126. P. 225-232.

104. Arkatov, Yu. M. et al. Study of the reaction  $^4\text{He}(\gamma, p)^3\text{H}$  at the maximal energy of gamma radiation 120 MeV // *Yad. Fiz.* 1970, vol. 12, 227-233 [*Sov. J. Nucl. Phys.* 1971, vol. 12, 123].

105. Hahn K. et al.  $^3\text{H}(p, \gamma)^4\text{He}$  cross section // Phys. Rev. 1995. V. C51. P. 1624-1632.

106. Canon R. et al.  $^3\text{H}(p, \gamma)^4\text{He}$  reaction below  $E_p = 80$  keV // Phys. Rev. 2002. V. C65. P. 044008.1-044008.7.

107. Dubovichenko, S. B. Astrophysical  $S$ -factors of the proton radiative capture on  $^3\text{H}$  at low energies // *Izv. NAN RK Ser. Fiz.-Mat.* (Kazakhstan) 2008, vol. 4, P. 89-92; Dubovichenko S.B., Dzhazairov-Kakhramanov A.V. Astrophysical  $S$ -factors of the  $p^2\text{H}$  and  $p^3\text{H}$  radiative capture at low energies // *Uz. J. Phys.* 2008. V. 10. No. 6. P. 364-370.

108. Lim T.K.  $^3\text{He}$ -n vertex constant and structure of  $^4\text{He}$  // Phys. Lett. 1975. V. B55. P. 252-254; Lim T.K. Normalization of the  $p$ - $^3\text{H}$  and  $n$ - $^3\text{He}$  tails of  $^4\text{He}$  and the  $^4\text{He}$  charge form factor // Phys. Lett. 1973. V. B44. P. 341-342.

109. Gibson B.F. Electromagnetic disintegration of the  $A = 3$  and  $A = 4$  nuclei // Nucl. Phys. 1981. V. A353. P. 85-98.

110. Dubovichenko, S. B. Astrophysical  $S$ -factor of the radiative  $p^2\text{H}$  and  $p^3\text{H}$  capture // *Rus. Phys. J.* 2009, vol. 52, 294-300.

111. Perry J.E., Bame S.J.  $^3\text{H}(p, \gamma)^4\text{He}$  reaction // Phys. Rev. 1955. V. 99. P. 1368-1375.

112. Balestra F. et al. Photodisintegration of  $^4\text{He}$  in Giant-Resonance Region // *Nuo. Cim.* 1977. V. 38A. P. 145-166.

113. Meyerhof W. et al.  $^3\text{He}(p, \gamma)^4\text{He}$  reaction from 3 to 18 MeV // Nucl. Phys. 1970. V. A148. P. 211-224.

114. Feldman G. et al.  $^3\text{H}(p, \gamma)^4\text{He}$  reaction and the  $(\gamma, p)/(\gamma, n)$  ratio in  $^4\text{He}$  // Phys. Rev. 1990. V. C42. P. R1167- R1170.

115. Dubovichenko S.B. Astrophysical  $S$ -factors for radiative proton capture by  $^3\text{H}$  and  $^7\text{Li}$  nuclei // *Physics of Atomic Nuclei* 2011. V.74. P. 358-370.

116. Dubovichenko, S. B. Astrophysical  $S$ -factor of radiative  $p^6\text{Li}$  capture at low energies // *Rus. Phys. J.* 2010, vol. 53, P. 743-749.
117. Skill M. et al. Differential cross section and analyzing power for elastic scattering of protons on  $^6\text{Li}$  below 2.2 MeV // *Nucl. Phys.* 1995. V. A581. P. 93-106.
118. <http://nuclphys.sinp.msu.ru/nuclsynt>
119. Dubovichenko, S. B.; Dzhazairov-Kakhramanov, A. V.; Sakharuk, A. A. Potential description of the elastic  $N^6\text{Li}$  and  $\alpha t$  scattering // *Phys. Atom. Nucl.* 1993, vol. 56, 1044-1053.
120. Neudatchin, V. G.; Sakharuk, A. A.; Smirnov, Yu. F. Generalized potential description of the interaction of lightest clusters – scattering and photonuclear reactions // *Sov. J. Part. Nucl.* 1992, vol. 23, 210; Neudatchin, V. G.; Struzhko, B. G.; Lebedev, V. M. Supermultiplet potential interaction model of lightest and unified description of different nuclear reactions // *Phys. Part. Nucl.* 2005, vol. 36, 468-497.
121. Petitjean C., Brown L., Seyler R. Polarization and phase shifts in  $^6\text{Li}(p,p)^6\text{Li}$  from 0.5 to 5.6 MeV // *Nucl. Phys.* 1969. V. A129. P. 209-219.
122. Dubovichenko, S. B.; Zazulin, D. M. Phase analysis of elastic  $p^6\text{Li}$  scattering at astrophysical energies // *Rus. Phys. J.* 2010, vol. 53, 458-464.
123. Neudatchin, V. G.; Smirnov, Yu. F. *Nucleon associations in light nuclei*; Publisher: Nauka, Moscow, RU, 1969; pp 414 (in Russian).
124. Tilley D.R. et al. Energy levels of light nuclei  $A=5,6,7$  // *Nucl. Phys.* 2002. V. A708. P. 3-163.
125. Nollett K.M., Wiringa R.B. Asymptotic normalization coefficients from ab initio calculations // arXiv:1102.1787v3 [nucl-th] 14 Apr 2011.
126. Switkowski Z.E. et al. Cross section of the reaction  $^6\text{Li}(p,\gamma)^7\text{Be}$  // *Nucl. Phys.* 1979. V. A331. P. 50-60; Bruss R. et al. Astrophysical  $S$ -factors for the radiative capture reaction  $^6\text{Li}(p,\gamma)^7\text{Be}$  at low energies // Proc. 2nd Intern. Symposium on Nuclear Astrophysics. Nuclei in the Cosmos. Karlsruhe. Germany. 6-10 July. 1992. Kappeler F., Wisshak K., Eds. IOP Publishing Ltd. Bristol. England. 1993. P. 169.
127. Arai K., Baye D., Descouvemont P. Microscopic study of the  $^6\text{Li}(p, \gamma)^7\text{Be}$  and  $^6\text{Li}(p, \alpha)^3\text{He}$  reactions // *Nucl. Phys.* 2002. V. A699. P. 963-975.
128. Prior R. M. et al. Energy dependence of the astrophysical  $S$ -factor for the  $^6\text{Li}(p,\gamma)^7\text{Be}$  reaction // *Phys. Rev.* 2004. V. C70. P. 055801-055809.

129. Burker F.C. Neutron and proton capture by  ${}^6\text{Li}$  // *Austr. J. Phys.* 1980. V. 33. P. 159-176.
130. Cecil F.E. et al. Radiative capture of protons by light nuclei at low energies // *Nucl. Phys.* 1992. V. A539. P. 75-96.
131. Dubovichenko, S. B.; Dzhazairov-Kakhramanov, A. V. Astrophysical  $S$ -factor for the proton radiative capture on  ${}^6\text{Li}$  // *Rep. Nat. Acad. Sci. RK (Kazakhstan)* 2009, vol. 6, 41-45.
132. Dubovichenko S.B., Burtebaev N., Zazulin D.M., Kerimkulov Zh. K., Amar A.S.A. Astrophysical  $S$ -factor for the radiative-capture reaction  $p{}^6\text{Li} \rightarrow {}^7\text{Be}\gamma$  // *Phys. Atom. Nucl.* 2011. V. 74. P. 984-1000.
133. Dubovichenko, S. B., Dzhazairov-Kakhramanov, A. V. Astrophysical  $S$ -factor for  $p{}^{12}\text{C} \rightarrow {}^{13}\text{N}\gamma$  radiative capture // *Rus. Phys. J.* 2009, vol. 52, 833-840.
134. Dubovichenko, S. B. Astrophysical  $S$ -factors of radiative  ${}^3\text{He}{}^4\text{He}$ ,  ${}^3\text{H}{}^4\text{He}$ , and  ${}^2\text{H}{}^4\text{He}$  capture // *Phys. Atom. Nucl.* 2010, vol. 73, 1526-1538.
135. Dubovichenko, S. B. Astrophysical  $S$ -factors of  $p{}^7\text{Li} \rightarrow {}^8\text{Be}\gamma$  capture at low energies // *Rus. Phys. J.* 2010, vol. 53, 1254-1263; Dubovichenko, S. B. et al. Astrophysical  $S$ -factor of the proton radiative capture on  ${}^7\text{Li}$  // *Izv. NAN RK Ser. Fiz.-Mat.* (Kazakhstan) 2010, No. 4, 32-36.
136. Tilley D.R. et al. Energy level of light nuclei.  $A = 8, 9, 10$  // *Nucl. Phys.* 2004. V. A745. P. 155-363.
137. <http://cdfc.sinp.msu.ru>
138. Warters W.D., Fowler W.A., Lauritsen C.C. The elastic scattering of proton by Lithium // *Phys. Rev.* 1953, V. 91, P. 917-921.
139. Brown L. et al. Polarization and phase shifts in  ${}^7\text{Li}(p,p){}^7\text{Li}$  from 0.4 to 2.5 MeV and the structure of  ${}^8\text{Be}$  // *Nucl. Phys.* 1973. V. A206. P. 353-373.
140. Zahnow D. et al. The  $S$ -factor of  ${}^7\text{Li}(p,\gamma){}^8\text{Be}$  and consequences for  $S$ -extrapolation in  ${}^7\text{Be}(p,\gamma_0){}^8\text{B}$  // *Z. Phys.* 1995. V. A351. P. 229-236.
141. Avotina, M. P.; Zolotavin, A. V. *Moments of ground and excited states of nuclei*; Publisher: Atomizdat, Moscow, 1979, pp 522 (in Russian).
142. Godwin M.A. et al.  ${}^7\text{Li}(p,\gamma){}^8\text{Be}$  reaction at  $E_p = 80.0$  keV // *Phys. Rev.* 1997. V. C56. P. 1605-1612.
143. Spraker M. et al. Slope of the astrophysical  $S$ -factor for the  ${}^7\text{Li}(p,\gamma){}^8\text{Be}$  reaction // *Phys. Rev.* 1999. V. C61. P. 015802-015808.



144. Zahn D. et al. Thermonuclear reaction rates of  ${}^9\text{Be}(p,\gamma){}^{10}\text{B}$  // Nucl. Phys. 1996. V. A589. P. 95-105.
145. Bohr, A.; Mottelson, B. R. *Nuclear structure Vol. I Single particle motion*; Publisher: World Scientific Pub Co Inc, Singapore, 1998 [Publisher: Mir, Moscow, 1971, pp 456 (in Russian)].
146. Ajzenberg - Selove F. Energy level of light nuclei  $A = 5 - 10$  // Nucl. Phys. 1988. V. A490. P. 1-225.
147. Wulf E.A. et al. Astrophysical S-factors for the  ${}^9\text{Be}(p,\gamma){}^{10}\text{B}$  reaction // Phys. Rev. 1998. V. C58, P. 517-523.
148. Sattarov A. et al. Astrophysical S-factors for  ${}^9\text{Be}(p,\gamma){}^{10}\text{B}$  // Phys. Rev. 1999. V. C60. P. 035801-035808.
149. Mukhamedzhanov A.M. et al. Asymptotic normalization coefficient for  ${}^{10}\text{B} \rightarrow {}^9\text{Be} + p$  // Phys. Rev. 1999. V. C56. P. 1302-1312.
150. Dubovichenko, S. B. Astrophysical S-factors of the radiative  $p^9\text{Be}$  capture. // *Rus. Phys. J.*, 2011, vol. 54, № 7. P. 814-821.
151. Dubovichenko S.B., Dzhazairov-Kakhramanov A.V. The  ${}^7\text{Li}(n,\gamma){}^8\text{Li}$  radiative capture at astrophysical energies // *Ann. der Phys.* 2012. V.524. P.850-861.
152. Dubovichenko S.B., Dzhazairov-Kakhramanov A.V. Neutron radiative capture by  ${}^2\text{H}$ ,  ${}^6\text{Li}$ ,  ${}^7\text{Li}$ ,  ${}^{12}\text{C}$ ,  ${}^{13}\text{C}$ ,  ${}^{14}\text{C}$  and  ${}^{14}\text{N}$  at astrophysical energies // Book: *The Universe Evolution. Astrophysical and Nuclear Aspects*. New-York, NOVA Sci. Publ. 2013. P.49-108.
153. Kelley J.H. et al. Energy level of light nuclei  $A = 11$  // Nucl. Phys. 2012. V.A880. P.88-195.
154. Dubovichenko S.B. Calculation method of the nuclear characteristics. Nuclear and thermonuclear processes. Second edition, revised and updated. Saarbrucken, Germany: Lambert Acad. Publ. GmbH&Co. KG. 2012. 425p.; [https://www.lap-publishing.com/catalog/details //store/ru/book/978-3-659-21137-9/metody-rascheta-yadernyh-kharacteristic](https://www.lap-publishing.com/catalog/details//store/ru/book/978-3-659-21137-9/metody-rascheta-yadernyh-kharacteristic). (in Russian).
155. Artemov S.V. et al. Estimates of the astrophysical S-factors for proton radiative capture by  ${}^{10}\text{B}$  and  ${}^{24}\text{Mg}$  nuclei using the ancs from proton transfer reactions // *Int. Jour. Mod. Phys.* 2010. V.E19. P.1102-1108.
156. Wiescher M. et al.  ${}^{11}\text{C}$  level structure via the  ${}^{10}\text{B}(p,\gamma)$  reaction // Phys. Rev. 1983. V.C28. P.1431-1442.
157. Tonchev A.P. et al. The  ${}^{10}\text{B}(p,\gamma){}^{11}\text{C}$  reaction at astrophysically

relevant energies // Phys. Rev. 2003. V.C68. P.045803(1-12).

158. Dubovichenko S.B., Adilbekov D.N., Tkachenko A.S. Radiative proton capture on  $^{10}\text{B}$  // Bul. NAS (Kazakhstan) Ser. Phys.-Mat. 2014. №3. (In press).

159. Kelley J.H. et al. The  $^{11}\text{B}(p \rightarrow \gamma)^{12}\text{C}$  reaction below 100 keV // Phys. Rev. 2000. V.C62. P.025803(1-6).

160. Anderson B.D. et al. A new determination of the partial widths of the 16.11 MeV state in  $^{12}\text{C}$  // Nucl. Phys. 1974. V.A233. P.286-296.

161. Ajzenberg-Selove F. Energy level of light nuclei  $A=11,12$  // Nucl. Phys. 1990. V.A506. P.1-158.

162. Cecil F.E. et al. Radiative capture of protons by light nuclei at low energies // Nucl. Phys. 1992. V.A539. P.75-96.

163. Huus T., Day R.B. The Gamma Radiation from  $^{11}\text{B}$  Bombarded by Protons // Phys. Rev. 1953. V.91. P.599-605.

164. Segel R.E., Hanna S.S., Allas R.G. States in  $^{12}\text{C}$  Between 16.4 and 19.6 MeV // Phys. Rev. 1965. V.139. P.B818-B830.

165. Allas R.G. et al. Radiative capture of protons by  $^{11}\text{B}$  and the giant dipole resonance in  $^{12}\text{C}$  // Nucl. Phys. 1964. V.58. P.122-144.

166. Dubovichenko S.B. Astrophysical proton capture by  $^{11}\text{B}$  nucleus // Rus. Phys. J. 2014. (In press).

167. Dubovichenko S.B. Program of searching phase shifts of elastic scattering of nuclear particles with spin of  $1/2$  // *Bulletin of KazNTU*. 2004. No.3. P. 137-144 (Kazakhstan).

168. Dubovichenko S.B., et al. Phase shift analysis of differential cross sections of the  $p^{12}\text{C}$  elastic scattering at astrophysical energies // Bul. NAS (Kazakhstan) Ser. Phys.-Mat. 2007. №6. P. 58-67.

169. Jahns M.F., Bernstein E.M. Polarization in  $p\alpha$  scattering // Phys. Rev. 1967. V. 162. P. 871-877.

170. Barnard A., Jones C., Well J. Elastic scattering of 2-11 MeV proton by  $^4\text{He}$  // Nucl. Phys. 1964. V. 50. P. 604-620.

171. Brown R.I., Haeberli W., Saladin J.X. Polarization in the scattering of protons by  $\alpha$  particles // Nucl. Phys. 1963. V. 47. P. 212-213.

172. Jackson H.L. et al. The  $^{12}\text{C}(p,p)^{12}\text{C}$  differential cross section // Phys. Rev. 1953. V. 89. P. 365-369.

173. Jackson H.L. et al. The excited states of the  $^{13}\text{N}$  nucleus // Phys. Rev. 1953. V. 89. P. 370-374.

174. Ajzenberg-Selove F. Energy levels of light nuclei  $A = 13, 14, 15$  // Nucl. Phys. 1991. V. A523. P. 1-116.
175. Moss S.J., Haeberli W. The polarization of protons scattered by Carbon // Nucl. Phys. 1965. V. 72. P. 417-435.
176. Barnard A.C.L. et al. Cross section as a function of angle and complex phase shifts for the scattering of protons from  $^{12}\text{C}$  // Nucl. Phys. 1966. V. 86. P. 130-144.
177. Burtebaev N. et al. New measurements of the astrophysical S-factor for  $^{12}\text{C}(p,\gamma)^{13}\text{N}$  reaction at low energies and the asymptotic normalization coefficient (nuclear vertex constant) for  $p+^{12}\text{C} \rightarrow ^{13}\text{N}$  reaction // Phys. Rev. 2008. V. C78. P. 035802-035813.
178. Adelberger E.G. et al. Solar fusion cross sections. II. The pp chain and CNO cycles // Rev. Mod. Phys. 2011. V. 83. P. 195-245.
179. Dubovichenko S.B. Thermonuclear processes of the Universe. Second edition. The Series "Kazakhstan space research" V.7. Kazakhstan, Almaty, A-tri, 2011, 402p.; <http://arxiv.org/abs/1012.0877>; <http://nuclphys.sinp.msu.ru/thpu/index.html>
180. Hebbard D.F., Vogl J.L. Elastic scattering and radiative capture of protons by  $\text{C}^{13}$  // Nucl. Phys. 1960. V. 21, P. 652-675.
181. Galster W. et al. Target and detection techniques for the  $^{13}\text{N}(p,\gamma)^{14}\text{O}$  reaction using radioactive ion beams:  $^{13}\text{C}(p,\gamma)^{14}\text{N}$  reaction as a test case // Phys. Rev. 1991. V. C44. P. 2776-2787.
182. Dubovichenko S.B. Phase shift analysis for elastic  $p^{13}\text{C}$  scattering at astrophysical energies // Phys. Atom. Nucl. 2012, vol. 75, 314-319.
183. Clegg T. et al. The elastic scattering of protons from  $^3\text{He}$  from 4.5 to 11.5 MeV // Nucl. Phys. 1964. V.50. P.621-628.
184. Dubovichenko S.B. Astrophysical S-factor for the radiative-capture reaction  $p^{13}\text{C} \rightarrow ^{14}\text{N}\gamma$  // Phys. Atom. Nucl. 2012, vol. 75, 196-203.
185. Yarmukhamedov R. et al. Asymptotic normalization coefficients for  $A+a \rightarrow B$  and the R-matrix method of analysis of nuclear-astrophysical radiative capture  $A(a,\gamma)B$  reactions// Uzbek. J. Phys. 2010. V. 12. №4-6. P. 233-247.
186. King J.D. et al. Cross section and astrophysical S-factor for the  $^{13}\text{C}(p,\gamma)^{14}\text{N}$  reaction // Nucl. Phys. 1994. V. A567. P. 354-376.
187. Mukhamedzhanov A.M. et al. Asymptotic normalization coefficients from proton transfer reactions and astrophysical S factors for

the CNO  $^{13}\text{C}(p,\gamma)^{14}\text{N}$  radiative capture process // Nucl. Phys. 2003. V. A725. P. 279-294.

188. Mukhamedzhanov A.M. et al. Astrophysical S factor for  $^{13}\text{C}(p,\gamma)^{14}\text{N}$  and asymptotic normalization coefficients // Phys. Rev. 2002. V. C66. P. 027602-1–027602-4.

189. Caughlan G.R., Fowler W.A. Thermonuclear reaction rates V // At. Data Nucl. Data Tables 1988. V. 40. P. 283-334.

190. Artemov S.V. et al. Nuclear Asymptotic Normalization Coefficients for  $^{14}\text{N} \rightarrow ^{13}\text{C} + p$  Configurations and Astrophysical S Factor for Radiative Proton Capture // Phys. Atom. Nucl. 2008. V. 71. P. 998-1011.

191. Dubovichenko S.B., Dzhazairov-Kakhramanov A.V. Astrophysical reaction of the  $^{12}\text{C}(^4\text{He},\gamma)^{16}\text{O}$  capture at low energies // *Izv. Ros. Acad. Nauk, Ser. Fiz.* 2011, vol. 75, 1614-1620.

192. Applegate J.H. and Hogan C.J. Relics of cosmic quark condensation // Phys. Rev. 1985. V.D31. P.3037-3045.

193. Applegate J.H., Hogan C.J. and Scherer R.J. Codmological quantum chromodynamics, neutron diffusion, and the production of primordial heavy elements // *Astrophys. J.* 1988. V.329. P.572-579.

194. Malaney R.A. and Fowler W.A. Late-time neutron diffusion and nucleosynthesis in a post-QCD inhomogeneous  $\Omega=1$  Universe // *Astrophys. J.* 1988. V.333. P.14-20.

195. Gorres J. et al. Proton capture on  $^{14}\text{C}$  and its astrophysical implications // Nucl. Phys. 1990. V.A517. P.329-339.

196. Heil M. et al. The  $(n,\gamma)$  cross section of  $^7\text{Li}$  // *Astrophys. Jour.* 1998. V.507. P.997-1002; Guimaraes V. and Bertulani C.A. Light radioactive nuclei capture reactions with phenomenological potential models // arXiv:0912.0221v1 [nucl-th] 1 Dec 2009; Masayuki Igashira, Toshiro Ohsaki Neutron capture nucleosynthesis in the Universe // *Sci. Tech. Adv. Materials* 2004. V.5. P.567-573; Nagai Y. et al. Fast neutron capture reactions in nuclear astrophysics // *Hyperfine Interactions* 1996. V.103. P.43-48; Liu Z.H. et al. Asymptotic normalization coefficients and neutron halo of the excited states in  $^{12}\text{B}$  and  $^{13}\text{C}$  // Phys. Rev. 2001. V.C64. P.034312(1- 5); Horvath A. et al. Cross section for the astrophysical  $^{14}\text{C}(n,\gamma)^{15}\text{C}$  reaction via the inverse reaction // *Astrophys. Jour.* 2002. V.570. P.926-933.

197. Yaffe L. and Stevens W.H. The reaction  $^{14}\text{C}(n,\gamma)^{15}\text{C}$  // Phys. Rev. 1950. V.79. P.893-893.
198. Dubovichenko S.B. Neutron capture by light nuclei at astrophysical energies // Phys. Part. Nucl. 2013. V.44. P.803-847; Dubovichenko S.B., Dzhazairov-Kakhramanov A.V., Burkova N.A. Neutron radiative capture by  $^2\text{H}$ ,  $^6\text{Li}$ ,  $^7\text{Li}$ ,  $^{12}\text{C}$  and  $^{13}\text{C}$  at astrophysical energies // Int. J. Mod. Phys. 2013. V.E22. P.1350028(1-52); Dubovichenko S.B., Dzhazairov-Kakhramanov A.V., Afanasyeva N.V. Neutron radiative capture by  $^9\text{Be}$ ,  $^{14}\text{C}$ ,  $^{14}\text{N}$ ,  $^{15}\text{N}$  and  $^{16}\text{O}$  at astrophysical energies // Int. J. Mod. Phys. 2013. V.E22. P.1350075(1-53).
199. Dubovichenko S.B. Light nuclei and nuclear astrophysics. Second Edition, corrected and enlarged, Lambert Academy Publ. GmbH&Co. KG., Saarbrucken. 2013. 320p.
200. Henderson J.D. et al. Capture and elastic scattering of proton be  $^{14}\text{C}$  // Phys. Rev. 1968. V.172. P.1058-1062.
201. Dubovichenko S.B., Dzhazairov-Kakhramanov A.V. Phase shifts analysis of  $p^{14}\text{C}$  scattering at energy  $^2S_{1/2}$  resonance // Rus. Phys. J. 2014. (In press).
202. Bartholomew G.A. et al. Capture radiation and neutrons from the bombardment of  $^{14}\text{C}$  with protons // Can. Jour. Phys. 1955. V. 33(8). P.441-456; Bartholomew G.A. et al. Note on the  $T = 3/2$  State in  $^{15}\text{N}$  // Can. Jour. Phys. 1956. V. 34. P.147.
203. Dubovichenko S.B. et al. Astrophysical  $S$ -factor  $p^{14}\text{C}$  radiative capture at low energies // Rus. Phys. J. 2014. (In press); Dubovichenko S.B. et al. Astrophysical  $S$ -factor of the radiative proton capture on  $^{14}\text{C}$  at low energies // arXiv:1402.5236v1 [nucl-th].]
204. Rolfs C. et al. Proton capture by  $^{15}\text{N}$  at stellar energies // Nucl. Phys. 1974. V.A235. P.450-459.
205. Dubovichenko S.B. et al. Radiative  $p^{15}\text{N}$  capture in the astrophysical energy region // Rus. Phys. J. 2014. (In press).
206. Ajzenberg-Selove F. Energy levels of light nuclei  $A=16,17$  // Nucl. Phys. 1993. V.A564. P.1-183.
207. Mukhamedzhanov A.M., Cognata M.L., and Kroha V. Astrophysical  $S$  factor for the  $^{15}\text{N}(p,\gamma)^{16}\text{O}$  reaction // Phys. Rev. 2011. V.C83. P.044604(1-11).
208. Mukhamedzhanov A.M. // Private Communication 2013.

209. Caciolli A. et al. Revision of the  $^{15}\text{N}(p,\gamma)^{16}\text{O}$  reaction rate and oxygen abundance in H-burning zones // arXiv:1107.4514v1 [astro-ph.SR] 22 Jul 2011.
210. Bemmerer D. et al. Direct measurement of the  $^{15}\text{N}(p,\gamma)^{16}\text{O}$  total cross section at novae energies // *Jour. Phys.* 2009. V.G36. P.045202(1-10).
211. LeBlanc P.J. et al. Constraining the  $S$  factor of  $^{15}\text{N}(p,\gamma)^{16}\text{O}$  at astrophysical energies // *Phys. Rev.* 2010. V.C82. P.055804(1-10).
212. Bashkin S., Carlson R.R., Douglas R.A. Cross Sections for Elastic Scattering and Reactions Due to Protons on  $^{15}\text{N}$  // *Phys. Rev.* 1958. V.114. P.1543-1551.
213. Kukulin, V. I.; Neudatchin; V. G. Smirnov, Yu. F. Interaction of the compound particles and Pauli principle // *Sov. J. Part. Nucl.* 1979, vol. 10, 1006.
214. Imbriani G. Underground laboratory studies of pp and CNO some astrophysical consequences LUNA // Third European Summer School on Experimental Nuclear Astrophysics. October 2-9. 2005. Catania. Sicily. Italy.
215. Caciolli A. et al. Ultra-sensitive in-beam  $\gamma$ -ray spectroscopy for nuclear astrophysics at LUNA // *Eur. Phys. J.* 2009. V. A39. P. 179-186.
216. Dubovichenko, S. B.; Dzhazairov-Kakhramanov, A. V. Photoprocesses on  $^7\text{Li}$  and  $^7\text{Be}$  nuclei in the cluster model for potentials with the forbidden states // *Phys. Atom. Nucl.* 1995, vol. 58, 579-585; Dubovichenko, S. B.; Dzhazairov-Kakhramanov, A. V. Photoprocesses on  $^6\text{Li}$  in the cluster models for potentials with the forbidden states // *Phys. Atom. Nucl.* 1995, vol. 58, 788-795.
217. Dubovichenko, S. B.; Dzhazairov-Kakhramanov, A. V. Potential description of the lithium cluster channels // *Phys. Atom. Nucl.* 1993, vol. 56, 195-202; Dubovichenko, S. B.; Dzhazairov-Kakhramanov, A. V. Coulomb formfactors of lithium nuclei in the cluster model on the basis of potentials with the forbidden states // *Phys. Atom. Nucl.* 1994, vol. 57, 733-740.
218. Barnard A.C., Jones C.M., Phillips G.C. The scattering of  $^3\text{He}$  by  $^4\text{He}$  // *Nucl. Phys.* 1964. V. 50. P. 629-640.
219. Spiger R., Tombrello T.A. Scattering of  $\text{He}^3$  by  $\text{He}^4$  and of  $\text{He}^4$  by Tritium // *Phys. Rev.* 1967. V. 163. P. 964-984.
220. Ivanovich M., Young P.G., Ohlsen G.G. Elastic scattering of the

several hydrogen and helium isotopes from tritium // Nucl. Phys. 1968. V. A110. P. 441-462.

221. McIntyre L.C., Haeberli W. Phase shifts analysis of d- $\alpha$  scattering // Nucl. Phys. 1967. V. A91. P. 382-398.

222. Keller L.G., Haeberli W. Vector polarization measurements and phase shift analysis for d- $\alpha$  scattering between 3 and 11 MeV // Nucl. Phys. 1979. V. A156. P. 465-476.

223. Gruebler W. et al. Phase shift analysis of d- $\alpha$  elastic scattering between 3 and 17 MeV // Nucl. Phys. 1975. V. A242. P. 265-284.

224. Schmelzbach P.A. et al. Phase shift analysis of d- $\alpha$  elastic scattering // Nucl. Phys. 1972. V. A184. P. 193-213.

225. Dubovichenko, S. B. Tensor  $^2\text{H}^4\text{He}$  interactions in the potential cluster model with the forbidden states // *Phys. Atom. Nucl.* 1998, vol. 61, 162-168.

226. Mertelmeir T., Hofmann H.M. Consistent cluster model description of the electromagnetic properties of lithium and beryllium nuclei // Nucl. Phys. 1986. V.A459. P.387-416.

227. Blokhintsev L.D. et al. Determination of the  $^6\text{Li}(\alpha+d)$  vertex constant (asymptotic coefficient) from the  $^4\text{He}+d$  phase-shift analysis // Phys. Rev. 1993. V. C48. P. 2390-2394.

228. Blokhintsev, L. D. et al. The calculation of nuclear vertex constants for the virtual disintegration  $^6\text{Li} \rightarrow \alpha+d$  in the three-body model and its application for description of the astrophysical nuclear reaction  $d(\alpha,\gamma)^6\text{Li}$  at lowest energies // *Yad. Fiz.* 2006, vol. 69, 456-466.

229. Lim T.K. The  $^6\text{Li}-\alpha-d$  vertex constant // Phys. Lett. 1975. V. B56. P. 321-324.

230. Igamov S.B., Yarmukhamedov R. Modified two-body potential approach to the peripheral direct capture astrophysical  $a+A \rightarrow B+\gamma$  reaction and asymptotic normalization coefficients // Nucl. Phys. 2007. V. A781. P. 247-276.

231. Brune C.R. et al. Sub-Coulomb  $\alpha$  transfers on  $^{12}\text{C}$  and the  $^{12}\text{C}(\alpha,\gamma)^{16}\text{O}$  S-factor // Phys. Rev. Lett. 1999. V. 83. P. 4025-4028.

232. Igamov S.B., Tursunmakhatov K.I., Yarmukhamedov R. Determination of the  $^3\text{He}+\alpha$  to  $^7\text{Be}$  asymp. normalization coefficients (nucl. vertex constants) and their application for extrapolation of the  $^3\text{He}(\alpha,\gamma)^7\text{Be}$

astrophysical S-factors to the solar energy region // arXiv:0905.2026v4 [nucl-th] 6 Jan. 2010. 28p.

233. Blokhintsev, L. D. et al. Determination of nuclear vertex constants for the vertex  ${}^7\text{Be} \rightarrow {}^3\text{He}{}^4\text{He}$  with the help of N/D-equations and calculation of the astrophysical S-factor for the reaction  ${}^4\text{He}({}^3\text{He},\gamma){}^7\text{Be}$  // *Izv. Ros. Acad. Nauk, Ser. Fiz.* 2008, vol. 72, 321-326.

234. Langanke K. Microscopic potential model studies of light nuclear capture reactions // *Nucl. Phys.* 1986. V. A457. P. 351-366.

235. Kajino T. The  ${}^3\text{He}(\alpha, \gamma){}^7\text{Be}$  and  ${}^3\text{He}(\alpha, \gamma){}^7\text{Li}$  reactions at astrophysical energies // *Nucl. Phys.* 1986. V. A460. P. 559-580.

236. Burkova N.A. et al. Is it possible to observe an isoscalar E1-multipole in  ${}^6\text{Li}\gamma\alpha$  reactions? // *Phys. Lett.* 1990. V. B248. P. 15-20.

237. Brune C.R., Kavanagh R.W. Rolf C.  ${}^3\text{H}(\alpha,\gamma){}^7\text{Li}$  reaction at low energies // *Phys. Rev.* 1994. V. C50. P. 2205-2218.

238. Griffiths G.M. et al. The  ${}^3\text{H}({}^4\text{He},\gamma){}^7\text{Li}$  reactions // *Can. J. Phys.* 1961. V. 39. P. 1397-1403.

239. Schroder U. et al. Astrophysical S-factor of  ${}^3\text{H}(\alpha,\gamma){}^7\text{Li}$  // *Phys. Lett.* 1987. V. B192. P. 55-58.

240. Brown T.A.D. et al.  ${}^3\text{He} + {}^4\text{He} \rightarrow {}^7\text{Be}$  astrophysical S-factor // *Phys. Rev.* 2007. V. C76. P. 055801.1-055801.12; arXiv:0710.1279v4 [nucl-ex] 5 Nov. 2007.

241. Confortola F. et al. Astrophysical S-factor of the  ${}^3\text{He}(\alpha,\gamma){}^7\text{Be}$  reaction measured at low energy via detection of prompt and delayed  $\gamma$  rays // *Phys. Rev.* 2007. V. C75. P. 065803; arXiv:0705.2151v1 [nucl-ex] 15 May 2007.

242. Gyurky G. et al.  ${}^3\text{He}(\alpha,\gamma){}^7\text{Be}$  cross section at low energies // *Phys. Rev.* 2007. V. C75. P. 035805-035813.

243. Singh N. et al. New Precision Measurement of the  ${}^3\text{He}({}^4\text{He},\gamma){}^7\text{Be}$  cross section // *Phys. Rev. Lett.* 2004. V. 93. P. 262503-262507.

244. Osborn J.L. et al. Low-energy behavior of the  ${}^3\text{He}(\alpha, \gamma){}^7\text{Be}$  cross section // *Nucl. Phys.* 1984. V. A419. P. 115-132.

245. Bemmerer D. et al. Activation measurement of the  ${}^3\text{He}(\alpha,\gamma){}^7\text{Be}$  cross section at low energy // *Phys. Rev. Lett.* 2006. V. 97. P. 122502-122507; arXiv:nucl-ex/0609013v1 11 Sep. 2006.

246. Costantini H. The  ${}^3\text{He}(\alpha,\gamma){}^7\text{Be}$  S-factor at solar energies: the



prompt experiment at LUNA // arXiv:0809.5269v1 [nucl-ex] 30 Sep. 2008.

247. Robertson R.C. et al. Observation of the Capture Reaction  ${}^2\text{H}(\alpha, \gamma){}^6\text{Li}$  and Its Role in Production of  ${}^6\text{Li}$  in the Big Bang // *Phys. Rev. Lett.* 1981. V. 47. P. 1867-1870.

248. Mohr P. et al. Direct capture in the  $3^+$  resonance of  ${}^2\text{H}(\alpha, \gamma){}^6\text{Li}$  // *Phys. Rev.* 1994. V. C50. P. 1543-1549.

249. Kiener J. et al. Measurements of the Coulomb dissociation cross section of 156 MeV  ${}^6\text{Li}$  projectiles at extremely low relative fragment energies of astrophysical interest // *Phys. Rev.* 1991. V. C44. P. 2195-2208.

250. Igamov S.B., Yarmukhamedov R. Triple-differential cross section of the  ${}^{208}\text{Pb}({}^6\text{Li}, \alpha d){}^{208}\text{Pb}$  Coulomb breakup and astrophysical S-factor of the  $d(\alpha, \gamma){}^6\text{Li}$  reaction at extremely low energies // *Nucl. Phys.* 2000. V. A673. P. 509-525.

251. Kukulin, V. I., Neudachin V. G., Smirnov Yu. F., Al Hovari R. Pauli principle role in formation of the optical potentials // *Izv. Acad. Nauk SSSR, Ser. Fiz.* 1974, vol. 38, 2123-2128.

252. Voevodin V. V., Kuznetsov Yu. A. *Reference mathematical library. Matrices and calculus*. Publisher: Fiz. Math. Lit., Moscow, 1984, pp 318.

253. Dubovichenko, S. B.; Chechin, L. M. Variational calculation methods of Schrödinger equation // *Bulletin of ASU Phys.-Math. Ser.* (Kazakhstan) 2003, vol. 2(8), 50-58.

254. Salpeter E.E. Nuclear reactions in stars // *Phys. Rev.* 1957. V. 107. P. 516-525; Salpeter E.E. Nuclear Reactions in stars without hydrogen // *Astrophys. Jour.* 1952. V. 115. P. 326; Rolfs C. Nuclear reactions in stars far below the Coulomb barrier // *Progress in Particle and Nuclear Physics* 2007. V. 59. P. 43.

255. Schurmann D. et al First direct measurement of the total cross-section of  ${}^{12}\text{C}(\alpha, \gamma){}^{16}\text{O}$  // *Eur. Phys. J.* 2005. V.A26. P.301-305; ArXiv: nucl-ex/0511050v1. 29 Nov. 2005.

256. Dubovichenko, S. B. Phase shift analysis of the  ${}^4\text{He}{}^4\text{He}$  scattering at 40-50 MeV // *Rus. Phys. J.* 2007, vol. 50, P. 605-611.

257. Jones C.M. et al. The scattering of alpha particles from  ${}^{12}\text{C}$  // *Nucl. Phys.* 1962. V. 37. P. 1-9.

258. Dubovichenko, S. B. Photonuclear processes in the  ${}^4\text{He}{}^{12}\text{C}$  channel of the  ${}^{16}\text{O}$  nucleus in potential cluster model // *Phys. Atom. Nucl.*

1996, vol. 59, P. 421-427.

259. Plaga R. et al. The scattering of alpha particles from  $^{12}\text{C}$  and the  $^{12}\text{C}(\alpha, \gamma)^{16}\text{O}$  stellar reaction rate // Nucl. Phys. 1987. V. A465. P. 291-316.

260. Tilley D. R., Weller H. R., Cheves C. M. Energy levels of light nuclei  $A = 16, 17$  // Nucl. Phys. 1993. V. A564. P. 1-183.

261. Dubovichenko, S. B., Burtebaev N. T., Dzhazairov-Kakhramanov, A. V., Zazulin D. M. Phase analysis and potential description of elastic  $^4\text{He}^{12}\text{C}$  scattering at low energies // *Rus. Phys. J.* 2009, vol. 52, 715-724; Dubovichenko, S. B. et al. Phase shift analysis of the elastic  $^4\text{He}^{12}\text{C}$  scattering at energies 1.5-6.5 MeV // *Rep. Nat. Acad. Sci. RK* (Kazakhstan) 2008, vol. 6, 24-32.

262. Dubovichenko, S. B.; Dzhazairov-Kakhramanov, A. V. *Rep. Nat. Acad. Sci. RK* (Kazakhstan) 2009, vol. 3, 30-36.; Dubovichenko, S. B.; Dzhazairov-Kakhramanov, A. V. Astrophysical S-factor of  $^4\text{He}^{12}\text{C}$  capture // *Izv. RAN. Ser. Fiz.* (Russia) 2011, vol. 75, 1517-1522.

263. Kettner K.U. et al. The  $^4\text{He}(^{12}\text{C}, \gamma)^{16}\text{O}$  reaction at stellar energies // *Z. Phys.* 1982. V. A308. P. 73-94.

264. Dyer P., Barnes C.A. The  $^{12}\text{C}(\alpha, \gamma)^{16}\text{O}$  reaction and stellar helium burning // Nucl. Phys. 1974. V. A233. P. 495-520.

265. Asuma R.E. et al. Constraints on the low-energies E1 cross section of  $^{12}\text{C}(\alpha, \gamma)^{16}\text{O}$  from the  $\beta$ -delayed  $\alpha$  spectrum of  $^{16}\text{N}$  // *Phys. Rev.* 1994. V. C50. P. 1194-1215.

266. Descouvemont P., Baye D.  $^{12}\text{C}(\alpha, \gamma)^{16}\text{O}$  reaction in a multiconfiguration microscopic model // *Phys. Rev.* 1987. V. C36. P. 1249-1255.

267. Abramowitz, M. *Reference book on special functions*; Publisher: Nauka, Moscow, 1979, pp 830 (in Russian).

268. Luke, Yu. L. *Mathematical functions and their approximations*; Publisher: Academic Press, New York, 1975 [Mir, Moscow, 1980, pp 608 (in Russian)].

269. Melkanoff M.A. Fortran program for elastic scattering analysis with nuclear optical model // Univ. California Pres. Berkley. Los Angeles. 1961. 116p.

270. Lutz H.F., Karvelis M.D. Numerical calculation of coulomb wave functions for repulsive coulomb fields // Nucl. Phys. 1963. V. 43. P. 31-44.

271. Melkanoff M. Nuclear optical model calculations // *Meth. in*

Comput. Phys. Acad. Press. N-Y. 1966. V. 6. P. 1-80.

272. Gody W.J., Hillstrom K.E. Chebyshev approximations for the coulomb phase shifts // Meth. Comput. 1970. V. 111. P. 671-677.

273. Smith W.R. Nuclear penetrability and phase shift subroutine // Usics Communs. 1969. V. 1. P. 106-112.

274. Froberg C.E. Numerical treatment of Coulomb wave functions // Rev. Mod. Phys. 1955. V. 27. P. 399-411.

275. Abramowitz M. Tables of Coulomb wave function. V.1. Washington. N.B.S. 1952. 141p.

276. Danilov, V. L. et al. *Reference mathematical library. Mathematical analysis. Functions, limits and continued fractions*; Publisher: Fiz. Mat. Lit., Moscow, 1961, pp 439 (in Russian).

277. Kuznetsov, D. S. *Special functions*; Publisher: Vysshaya Shkola, Moscow, 1965, pp 272 (in Russian).

278. <http://phys.bsu.edu.ru/resource/nphys/spargalka/038.htm>





**More  
Books!** 



**yes**  
**I want morebooks!**

Buy your books fast and straightforward online - at one of the world's fastest growing online book stores! Environmentally sound due to Print-on-Demand technologies.

Buy your books online at  
**[www.get-morebooks.com](http://www.get-morebooks.com)**

---

Kaufen Sie Ihre Bücher schnell und unkompliziert online – auf einer der am schnellsten wachsenden Buchhandelsplattformen weltweit!  
Dank Print-On-Demand umwelt- und ressourcenschonend produziert.

Bücher schneller online kaufen  
**[www.morebooks.de](http://www.morebooks.de)**

OmniScriptum Marketing DEU GmbH  
Heinrich-Böcking-Str. 6-8  
D - 66121 Saarbrücken  
Telefax: +49 681 93 81 567-9

[info@omniscrptum.com](mailto:info@omniscrptum.com)  
[www.omniscrptum.com](http://www.omniscrptum.com)

OMNIScriptum









